Seismic Hazard Assessment Update for the Yankee Doodle Tailings Impoundment Site, Butte, Montana

Final Report

Submitted to:

Knight Piesold Ltd.
750 West Pender, Suite 1400
Vancouver, BC V6C 2T8

Prepared by:

Linda Al Atik and Nick Gregor

March 17, 2021

Table of Contents

List of Tables

List of Figures

1. INTRODUCTION

In 2016, a seismic hazard assessment study was performed for the Yankee Doodle Tailings Impoundment site (YDTI, latitude 46.034°N and longitude 112.504°W) in Butte, Montana. The 2016 study, documented in Al Atik and Gregor (2016), consisted of performing probabilistic and deterministic seismic hazard analyses for the YDTI site for a reference site class B/C with average shear-wave velocity in the top 30 m of the profile (V_{S30}) of 760 m/sec. Horizontal and vertical design response spectra were developed for the site along with corresponding design time histories. In addition, a fault displacement hazard analysis was performed for the Continental fault intersecting the YDTI footprint. Estimates of average and maximum fault displacements were estimated using an informed deterministic approach for the Maximum Credible Earthquake (MCE) scenarios on the Continental fault. Given the relatively poor characterization of the Continental fault and its impact on the ground motion and fault displacement results at the YDTI site, Al Atik and Gregor (2016) recommended that a fault study be carried out to determine if the Continental fault is indeed active and to provide a better characterization of this fault.

In 2021, Lettis Consultants International Inc. (LCI) was engaged by Montana Resources, LLP to evaluate the Quaternary activity of the Continental and Rocker faults and provide a seismic source characterization for these faults for use in seismic hazard analysis. Following the conclusion of the LCI study and the documentation of their findings in LCI (2021a, b) reports, the seismic hazard assessment and fault displacement analysis for the YDTI site are updated to incorporate changes to the seismic source characterization and ground motion characterization models. This report describes the study update conducted as part of engineering design work that Knight Piesold (KP) is performing to support a permit application for an impoundment raise. Results from this study are expected to be used as input to the downstream embankment stability analyses.

The seismic hazard study update is performed for the same site location as the 2016 study (latitude 46.034°N and longitude 112.504°W) for the reference site condition with V_{S30} of 760 m/sec as well as for a site-specific V_{S30} of 420 m/sec. A site location map is shown in Figure 1-1 and the project site layout is shown in Figure 1-2. The scope of work presented in this report includes the following tasks:

1. Perform a literature review to update the relevant seismic sources and ground-motion models for the site.

2. Conduct a probabilistic seismic hazard analysis (PSHA) for the site using the updated seismic source model and ground-motion models.

3. Conduct a deterministic seismic hazard analysis (DSHA) for the maximum credible earthquake (MCE) scenario on fault sources located in close proximity to the site.

4. Develop site-specific horizontal acceleration response spectra for earthquake ground motions covering the entire range of natural periods of vibration from 0.01 to 10 sec. Response spectra are provided for the following hazard levels:
   - DSHA 50th and 84th percentile horizontal response spectra for the MCE scenarios
   - PSHA uniform hazard spectra (UHS) for return periods of 475, 1,000, 2,475, and 10,000 years

5. Develop vertical response spectra for the horizontal spectra obtained in (4).

6. Perform a deterministic fault displacement analysis to evaluate the net average and maximum surface displacement that may occur along the Continental fault.

7. Select and spectrally modify recorded ground-motion time series to be compatible with the design horizontal and vertical response spectra obtained from the previous steps for the MCE median and 84th percentile deterministic spectra and the 1,000-year return period probabilistic target spectra for V_{S30} of 760 m/sec.

The next chapters of this report start with an overview of the 2016 study and then describe the inputs, methodology, and results obtained for the tasks listed above for this study update. Sensitivity analyses are presented to evaluate the incremental impact of the changes in the seismic source characterization and ground motion characterization models on the hazard results compared to the 2016 results. The selection and development of design time histories are addressed in the last section of this report.

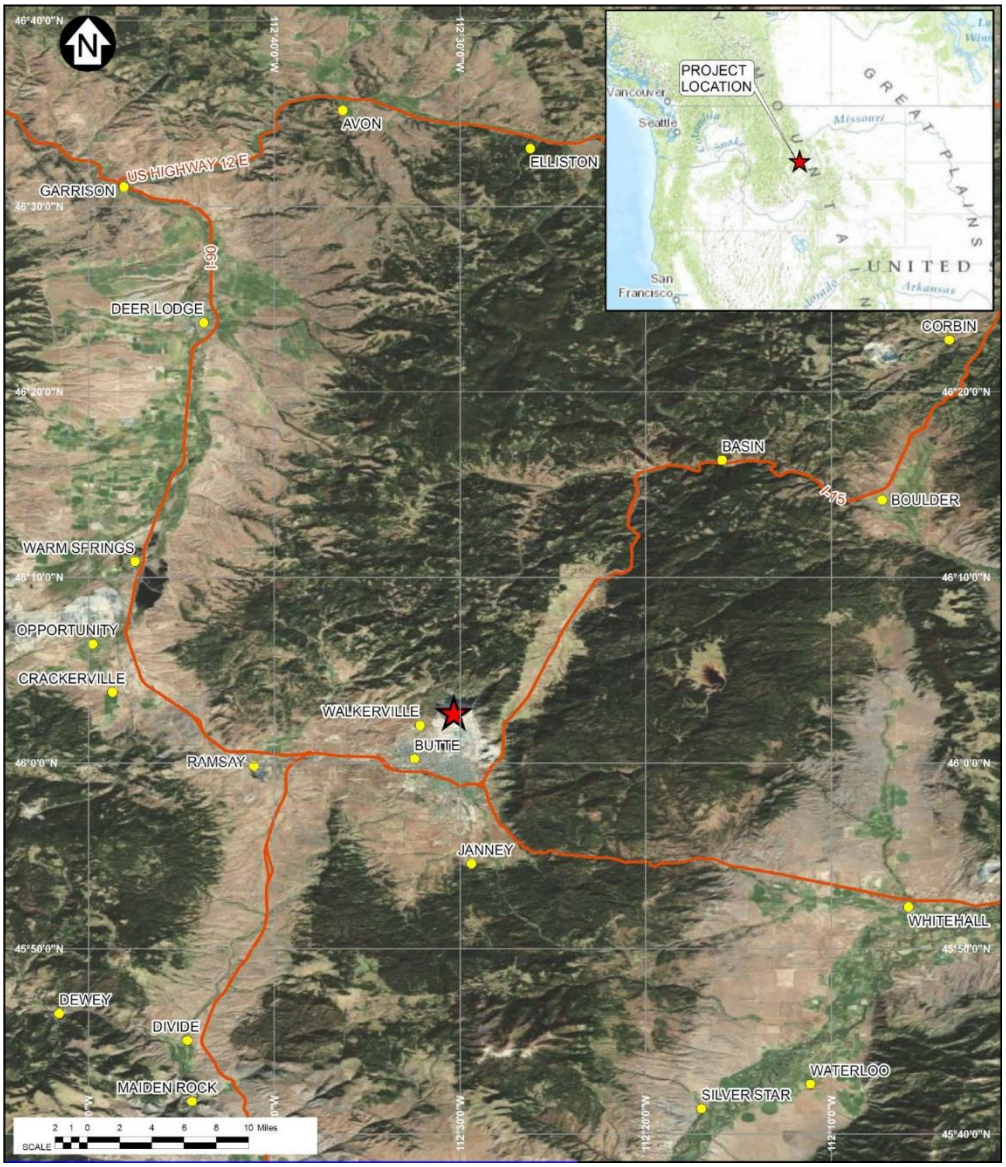

Figure 1-1. Site location map (source: KP 2015)

Figure 1-2. Project site layout (source: KP 2020)

2. OVERVIEW OF AL ATIK AND GREGOR (2016) STUDY

The seismic source characterization (SSC) used in the Al Atik and Gregor (2016) PSHA for the YDTI site was based on the source model developed as part of the 2014 National Seismic Hazard Maps (NSHMs) (Petersen et al. 2014) with updates to incorporate fault sources located in the vicinity of the site based on Wong et al. (2005). This SSC model consisted of a seismicity-based background model with parameters listed in Table 3-1 of Al Atik and Gregor (2016) and fault sources with parameters listed in Tables 3-2 to 3-5 of that report. The closest faults to the YDTI site were the Continental and the Rocker faults with closest distance to the site of 1.2 and 8.54 km, respectively. The source parameters of the Continental and the Rocker faults were based on the Wong et al. (2005) study and are listed in Table 2-1. Al Atik and Gregor (2016) noted that the Continental and Rocker faults were poorly constrained and recommended a study of these faults to improve their characterization given their proximity to the site.

The ground-motion characterization (GMC) model used in Al Atik and Gregor (2016) consisted of the five NGA-West2 ground motion prediction equations (GMPEs): Abrahamson et al. (2014) (ASK14), Boore et al. (2014) (BSSA14), Campbell and Bozorgnia (2014) (CB14), Chiou and Youngs (2014) (CY14), and Idriss (2014) (Id14) used along with the epistemic uncertainty in the median prediction model of Al Atik and Youngs (2014). In addition to the NGA-West2 GMPEs, the stochastic-based GMPE of Wong et al. (2005) was included in the logic tree as shown in Figure 2-1. The Wong et al. (2005) model was used only for the median prediction and was assigned the aleatory variability standard deviation model of ASK14. The Wong et al. (2005) model and the NGA-West2 GMPEs were assigned weights of one third and two thirds, respectively, as shown in Figure 2-1.

The PSHA was conducted using the SSC and GMC source models described in this section for V_{S30} of 760 m/sec and uniform hazard spectra (UHS) were calculated for the 475, 1000, 2,475, and 10,000-year return periods. Deaggrgeation of the hazard results at these return periods and for peak ground acceleration (PGA) and spectral periods of 0.2 and 1 sec showed that, for the return periods of 2,475 years and shorter, the hazard was attributed to the background seismicity. For the 10,000-year return period, equal contribution from the gridded background seismicity and the Continental fault was observed. For the deterministic hazard analysis, the logic tree shown in Figure 2-1 was used to calculate the median and 84th percentile response spectra for MCE scenarios on the Continental fault with **M** 6.5 and rupture distances (Rrup) of 1.2 and 0.1 km. Design probabilistic and deterministic horizontal spectra obtained in the 2016 study are listed in Table 2-2 and shown in Figure 2-2. Because of the low slip rate on the Continental fault and the fact that the 84th percentile deterministic response spectra were consistent with approximately the 100,000-year return period spectrum, the use of the median deterministic design spectrum was recommended over the 84th percentile spectrum. Given the horizontal spectra shown in Figure 2-2, corresponding vertical design spectra were computed using the empirical vertical-to-horizontal ratio (V/H) model of Gulerce and Abrahamson (2011).

In addition to the ground-motion characterization, estimates of displacement on the Continental fault were provided in Al Atik and Gregor (2016). Primary displacement estimates were calculated based on a deterministic fault displacement analysis that accounted for the uncertainty in the MCE scenario magnitude as well as the uncertainty in the displacement prediction equations (DPE). Median and 84th percentile average and maximum displacement estimates were calculated and are listed in Table 2-3.

Estimates of off-fault distributed deformation or secondary or triggered deformation that may occur on adjacent faults were not considered.

Table 2-1. Source parameters of the Continental and Rocker faults used in the Al Atik and Gregor (2016) study. Weights are given in parentheses. Both faults have a normal style of faulting and zero depth to top of rupture.

Fault Name	Closest Distance to Site (km)	b-value	Mmin	Recurrence Model	Slip Rate (mm/yr)	Mmax	Dip (degrees)	Fault Thickness (km)	Fault Length (km)
Continental fault	1.2	0.8	5.00	Y & C	0.020 (0.6)	6.5 (0.6)	70 W	15 (0.6)	18.2
					0.005 (0.2)	6.2 (0.2)		12 (0.2)	
					0.120 (0.2)	6.8 (0.2)		18 (0.2)	
Rocker fault	8.5	0.8	5.00	Y & C	0.020 (0.6)	7.0 (0.6)	55 W (0.6)	15 (0.6)	43.5
					0.005 (0.2)	6.7 (0.2)	30 W (0.2)	12 (0.2)	
					0.120 (0.2)	7.3 (0.2)	70 W (0.2)	18 (0.2)	

Table 2-2. Horizontal design spectra for the YDTI site for V_{S30} of 760 m/sec in the Al Atik and Gregor (2016) study.

	UHS PSA (g)				Deterministic PSA (g) Rrup = 1.2 km		Deterministic PSA (g) Rrup = 0.1 km	
Period (sec)	475 yr	1,000 yr	2,475 yr	10,000 yr	Median	84th Percentile	Median	84th Percentile
0.01/PGA	0.083	0.124	0.197	0.372	0.416	0.779	0.447	0.837
0.02	0.085	0.128	0.204	0.388	0.443	0.830	0.472	0.885
0.03	0.095	0.142	0.227	0.434	0.505	0.951	0.539	1.015
0.05	0.122	0.185	0.295	0.562	0.652	1.234	0.694	1.314
0.075	0.156	0.238	0.386	0.739	0.815	1.561	0.864	1.654
0.1	0.177	0.269	0.434	0.834	0.892	1.723	0.942	1.820
0.15	0.191	0.287	0.461	0.884	0.908	1.779	0.955	1.870
0.2	0.183	0.274	0.439	0.843	0.867	1.698	0.912	1.786
0.3	0.154	0.228	0.360	0.678	0.715	1.411	0.752	1.484
0.4	0.128	0.187	0.290	0.543	0.589	1.173	0.622	1.238
0.5	0.109	0.158	0.244	0.455	0.490	0.986	0.518	1.043
0.75	0.076	0.110	0.168	0.311	0.335	0.687	0.355	0.729
1	0.057	0.082	0.125	0.231	0.247	0.513	0.264	0.548
1.5	0.037	0.055	0.083	0.150	0.153	0.321	0.165	0.344
2	0.027	0.040	0.061	0.110	0.104	0.219	0.112	0.236
3	0.017	0.025	0.039	0.072	0.064	0.133	0.069	0.145
4	0.013	0.019	0.028	0.053	0.041	0.086	0.045	0.094
5	0.011	0.015	0.023	0.042	0.030	0.061	0.033	0.068
7.5	0.006	0.009	0.013	0.022	0.013	0.026	0.014	0.029
10	0.003	0.005	0.008	0.014	0.007	0.015	0.008	0.016

Table 2-3. Surface fault displacement hazard results on the Continental fault.

Exceedance	Percentile	Average Displacement (m)	Maximum Displacement (m)
0.50	50	0.51	0.74
0.16	84	1.44	2.07

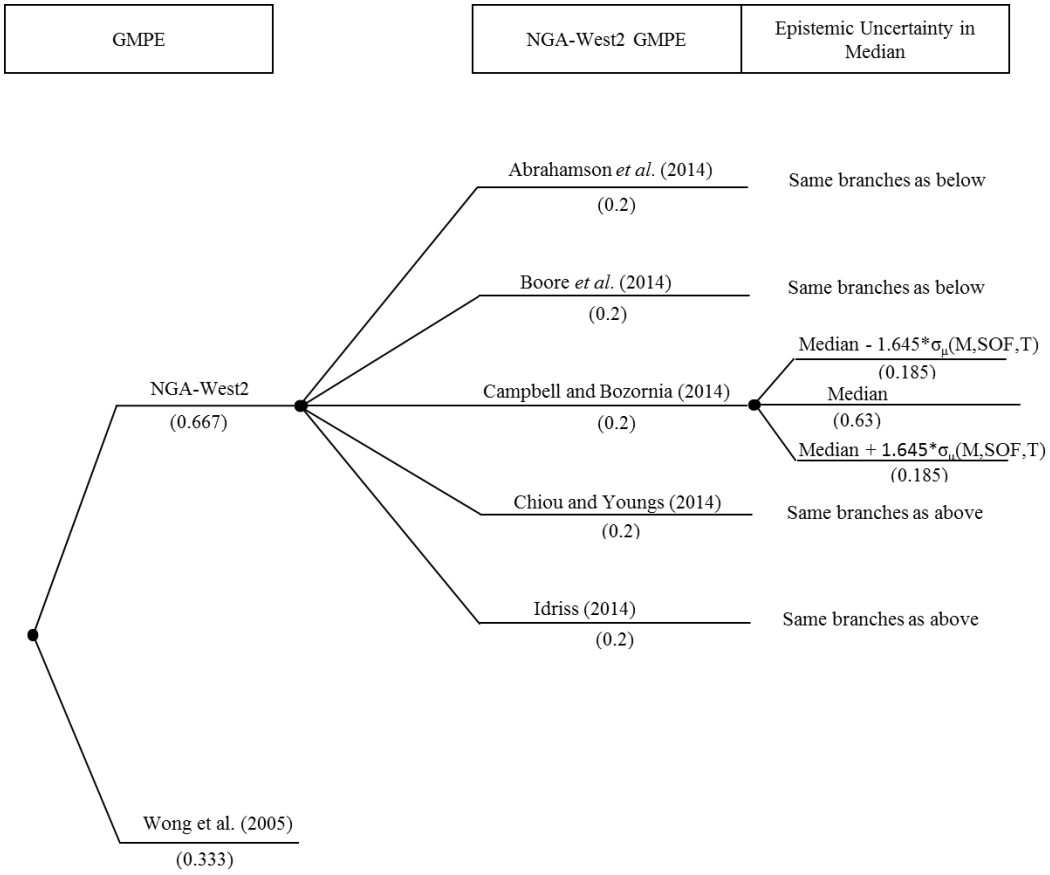

Figure 2-1. Logic tree for the median ground-motion model used in the Al Atik and Gregor (2016) study. σ_μ refers to the additional epistemic uncertainty in LN units based on Al Atik and Youngs (2014). M refers to magnitude, SOF to style-of-faulting, and T to spectral period.

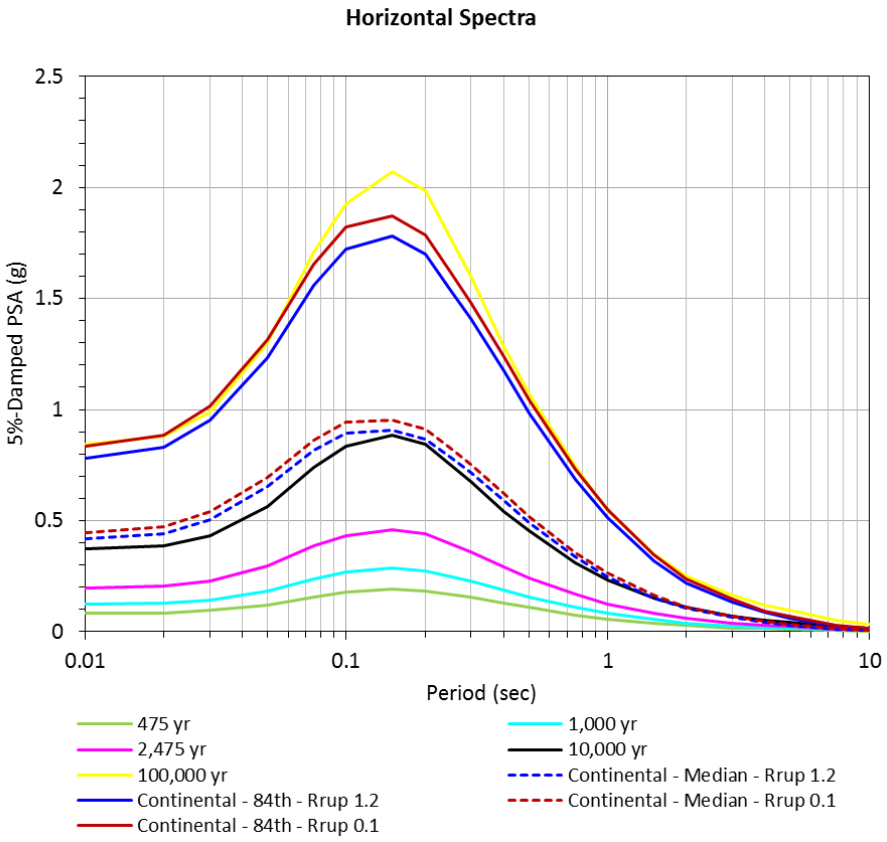

Figure 2-2. Comparison of the UHS (475, 1,000, 2,475, 10,000, and 100,000 years return period) to the median and 84th percentile deterministic response spectra for the MCE scenarios on the Continental fault at the YDTI site with V_{S30} of 760 m/sec in the Al Atik and Gregor (2016) study.

3. SEISMIC SOURCE CHARACTERIZATION

The YDTI site is located in southwestern Montana in the northern margin of the Basin and Range province as shown in Figure 3-1. A detailed discussion on the seismotectonic setting of the site region is provided in LCI (2021a) and a brief summary of that discussion is given here. Quaternary faulting in Southwest Montana has been attributed to the Basin and Range style extension and the migration of the Yellowstone hotspot. Seismicity in western Montana is largely concentrated within the Centennial Tectonic Belt (CTB), the Northern Interseismic Mountain Belt (NIMB), and the Yellowstone areas. Focal mechanism records of events near Butte, Montana, indicate the predominance of normal faulting with a component of minor strike-slip deformation. The two largest historic events in the region are the **M** 7.5 1959 Hebgen Lake earthquake and the **M** 7.3 Borah Peak earthquake in Idaho. Both earthquakes are associated with normal faulting and occurred north of the Snake River Plain. More recent moderate magnitude earthquakes in the region include the **M** 5.3 1999 Red Rock Valley earthquake, the **M** 5.6 2005 Dillon earthquake, and the **M** 5.8 2005 Lincoln earthquake.

For this study update of the PSHA for the YDTI site, both the seismicity-based background sources and fault sources are updated. The seismicity-based background sources are based on the 2018 update to the NSHMs (Petersen et al., 2020). For fault sources, the characterization of the Continental-Elk Park fault and the Rocker fault is based on the LCI (2021a, b) fault study. A detailed description of the seismicity-based background sources and fault sources is provided in the next subsections.

3.1 Seismicity-Based Background Model

The seismicity-based background model used for this study update is based on the smooth gridded seismicity model developed by Petersen et al. (2020) as part of the 2018 update to the NSHMs. Similar to the 2014 NSHMs, this gridded seismicity model consists of two source types: extensional and compressional regime sources. The parameters of the background model used in this study are listed in Table 3-1. The closest rupture distance from the individual grid points contained within the sources to the site is included in the table. The b-value, activity rate, and maximum earthquake magnitude describe the modeled magnitude recurrence within each individual source zone. On a log scale, the b-value is the slope of the Gutenberg-Richter distribution, relating the number of earthquakes in a given area over a fixed period of time to the magnitude of those earthquakes. Higher b-values, for example, lead to models that generate more small magnitude earthquakes with respect to larger magnitude earthquakes. The activity rate for the background sources implemented in this study is defined as the annual rate of earthquakes greater than or equal to a minimum magnitude of 5.0 [N(**M**>5)]. The maximum magnitude (Mmax) defines the upper truncation point for the magnitude recurrence models. The lower truncation point is defined by the minimum **M** 5 for the background model used in the PSHA. The rates of different sized-earthquakes are based on a truncated exponential magnitude-frequency distribution.

The updated seismicity-based background model in Petersen et al. (2020) is based on the development of an updated composite, uniform, moment magnitude seismicity catalog for western North America which included earthquakes through April 2018. A b-value of 0.8 is used for the background sources similar to the 2014 NSHMs gridded seismicity model. To smooth the gridded rates, fixed-kernel and adaptive-kernel smoothing methods are used with weights of 0.6 and 0.4, respectively. Similar to the

background model in the 2016 study, two alternative Mmax values are selected for the background model: **M** 7.45 and **M** 7.95 with weights of 0.9 and 0.1, respectively. For the extensional regime source, normal and strike-slip style of faulting are used with weights of 0.67 and 0.33, respectively. For the compressional regime source, reverse and strike-slip style of faulting are used with weights of 0.67 and 0.33, respectively. Table 3-1 indicates a decrease in the activity rates of the background model in this study compared to those used in the 2016 study.

Figures 3-2 and 3-3 show contour plots of the seismicity rate (a-value) for the extensional and compressional regime background sources, respectively, with respect to the YDTI site location. Each figure shows the a-value contours for the fixed and the adaptive smoothing methods. For the extensional regime source zone, Figure 3-2 indicates that the fixed smoothing method results in a large area of higher seismicity towards the northwest of the YDTI site. The adaptive smoothing method results in more concentrated clusters of higher seismicity. Figure 3-3 shows that the seismicity associated with the compressional regime source zone is relatively low with the site located in an area of zero a-value for the fixed smoothing case. Figures 3-2 and 3-3 indicate that the smoothed gridded seismicity shows some spatial differences compared to the background source model contour plots in Al Atik and Gregor (2016).

Table 3-1. Source parameters of the seismicity-based background sources based on Petersen et al. (2020). Weights of alternatives are given in brackets. Magnitude recurrence model is the truncated exponential model. Top of rupture is at 2 km, dip angle is 45 degrees, and seismogenic thickness is 15 km.

Source	Source Name	Smoothing	Closest Rupture Distance to Site (km)	b-value	Mmin	Activity Rate - N(M>Mmin)	Mmax	Sense of Slip
WUSExt	Extensional Regime	Fixed [0.6]	5.1	0.8	5.00	0.4954	7.45 [0.9]	Strike-Slip [0.33]
							7.95 [0.1]	Normal [0.67]
		Adaptive [0.4]	5.1	0.8	5.00	0.5396	7.45 [0.9]	Strike-Slip [0.33]
							7.95 [0.1]	Normal [0.67]
WUSCmp	Compressional Regime	Fixed [0.6]	102.6	0.8	5.00	0.0096	7.45 [0.9]	Strike-Slip [0.33]
							7.95 [0.1]	Reverse [0.67]
		Adaptive [0.4]	5.1	0.8	5.00	0.0124	7.45 [0.9]	Strike-Slip [0.33]
							7.95 [0.1]	Reverse [0.67]

The seismicity-based background model used in this study update is based on the U.S. Geological Survey (USGS) catalog (Mueller, 2019) including earthquakes that occurred through April 2018. A search for additional earthquakes that occurred in the site region since April 2018 was performed as part of this study to evaluate recent seismicity and the potential need to update the recurrence models of the seismicity-based background sources. Specifically, the ANSS seismicity catalog database was searched (https://earthquake.usgs.gov/earthquakes/search/) for events with magnitudes 2.5 and larger since May 01, 2018, and through October 24, 2021. The geographical limits of the search are from -115.5 to -109.5 degrees longitude and 43 to 49 degrees latitude. This search resulted in a total of 1,480

earthquakes including dependent events, with a largest **M** of 6.5 for the March 31, 2020, Stanley, Idaho earthquake.

The new seismicity catalog (since May 2018) is then processed to convert the various magnitude scales to uniform moment magnitude following the magnitude-scaling relationships in the Mid-Columbia PSHA report (JBA, 2012). Following the same approach that was used by the USGS, dependent events are identified based on Gardner and Knopoff (1974). The resulting declustered catalog for events since May 1, 2018, consists of 154 events with 3 earthquakes having magnitude greater than 4. These events are plotted in Figure 3-4. A total of 41 earthquakes occurred since May 1, 2018, within 100 km of the YDTI site with a largest **M** 4.2 earthquake at 89.5 km from the site. The closest event is an **M** 2.9 earthquake at a distance of 40.9 km from the site.

Next, the recurrence parameters of the truncated exponential model listed in Table 3-1 are evaluated in light of the additional 154 earthquakes that occurred since April 2018. Given the predominance of the extensional regime in the site region, the magnitude-recurrence models of the extensional source with fixed and adaptive smoothing models are evaluated. For this source, the cumulative number of earthquakes is estimated for the completeness period of the catalog for the different magnitude ranges by adding the observed number of earthquakes in the declustered catalog since April 2018 to the number of earthquakes predicted using the a- and b-values listed in Table 3-1 for the truncated exponential model. The western US completeness model in Mueller (2019) for areas outside of California is: **M** 4+ since 1963, **M** 5+ since 1930, and **M** 6+ since 1850. Using the periods of completeness for the different magnitude intervals, the cumulative annual rates of events are calculated and compared to the truncated exponential magnitude-recurrence model. Figure 3-5 shows this comparison for the extensional regime source for the fixed and adaptive smoothing models and indicates that the addition of the recent observed seismicity does not change the extensional regime magnitude-recurrence models used in this study.

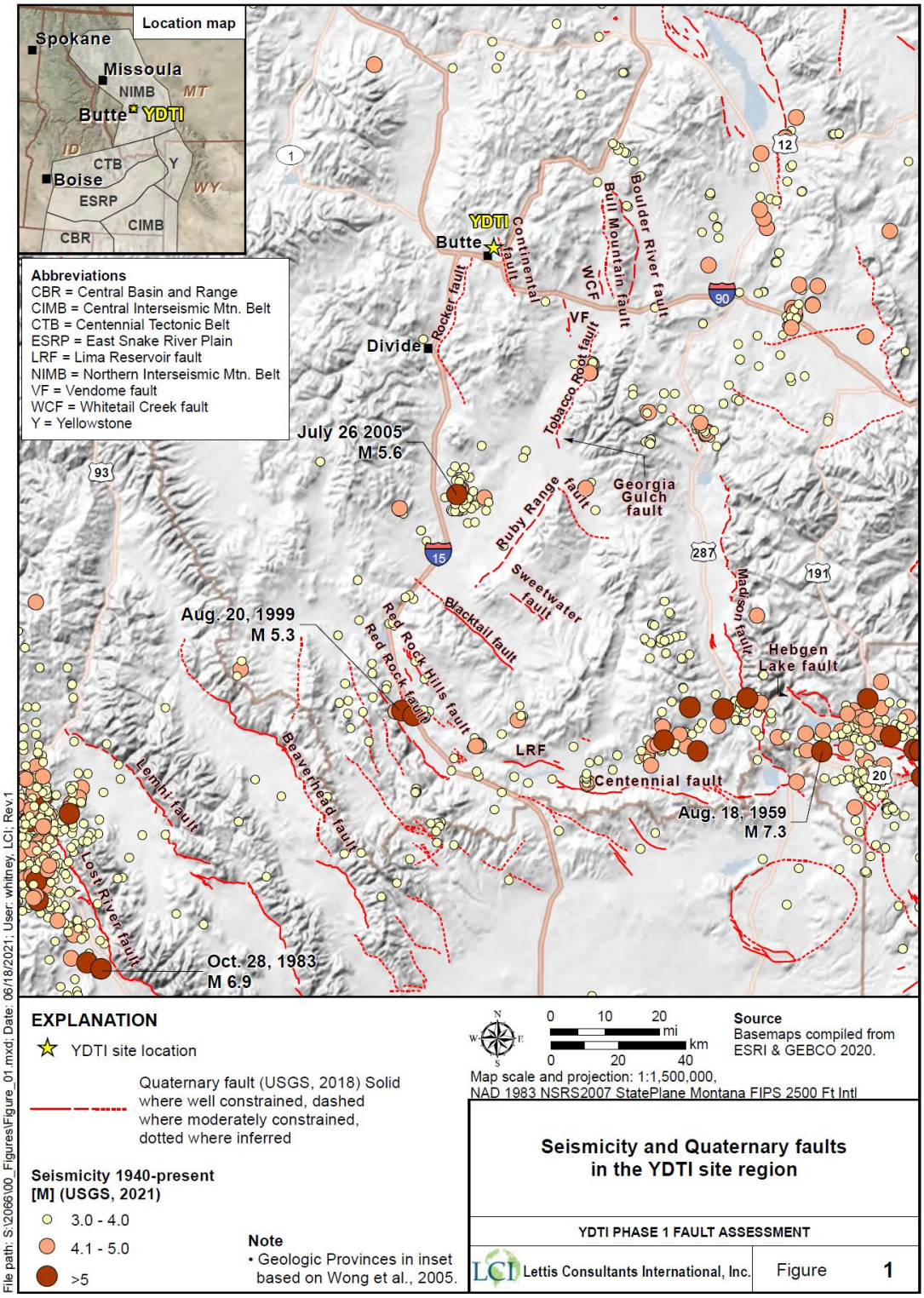

Figure 3-1. Seismicity and Quaternary faults in the YDTI site region (source: LCI 2021a).

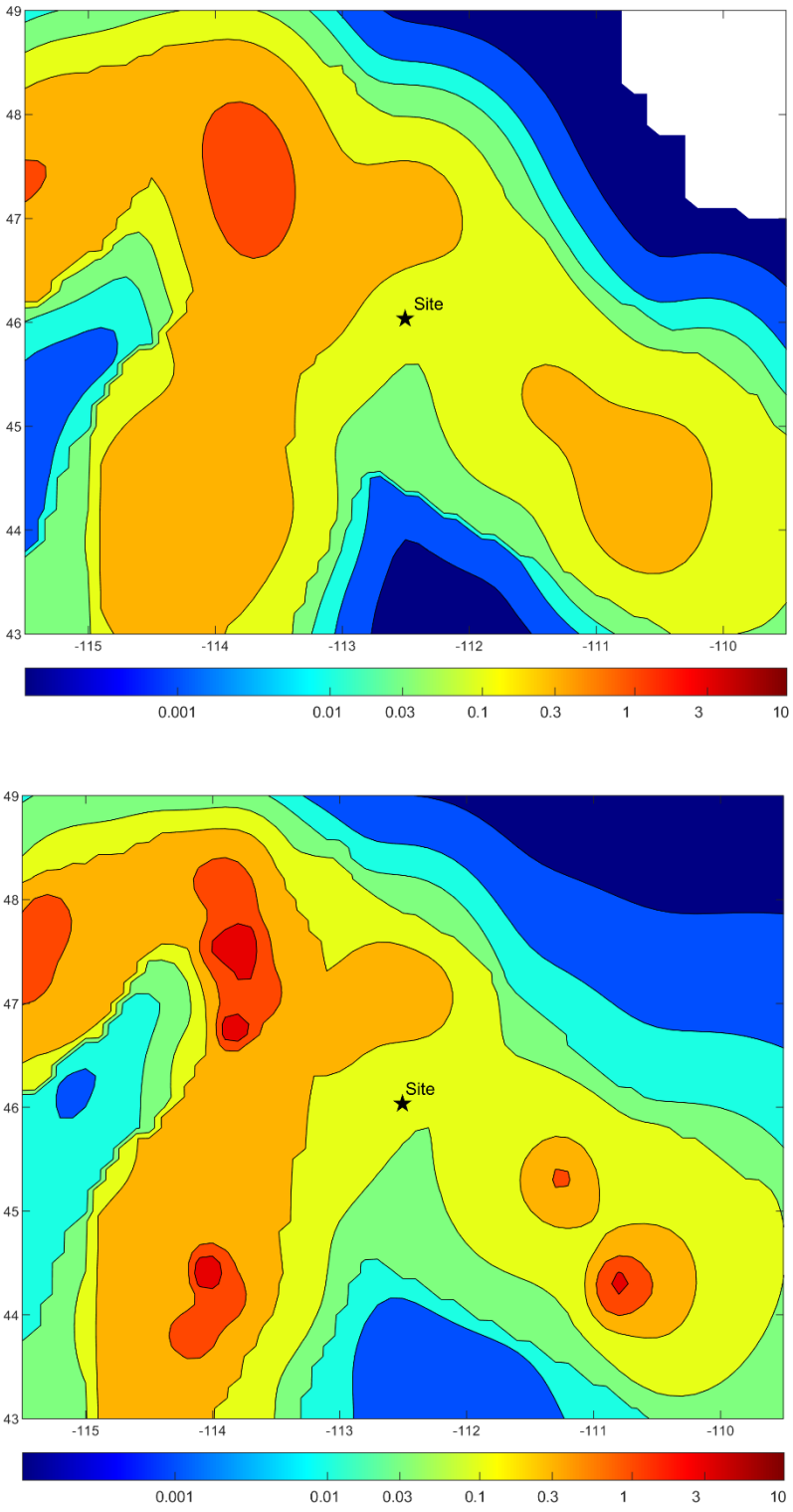

Figure 3-2. Seismicity rate (a-value) contour plots for the extensional regime background source for the fixed smoothing method (top) and adaptive smoothing method (bottom).

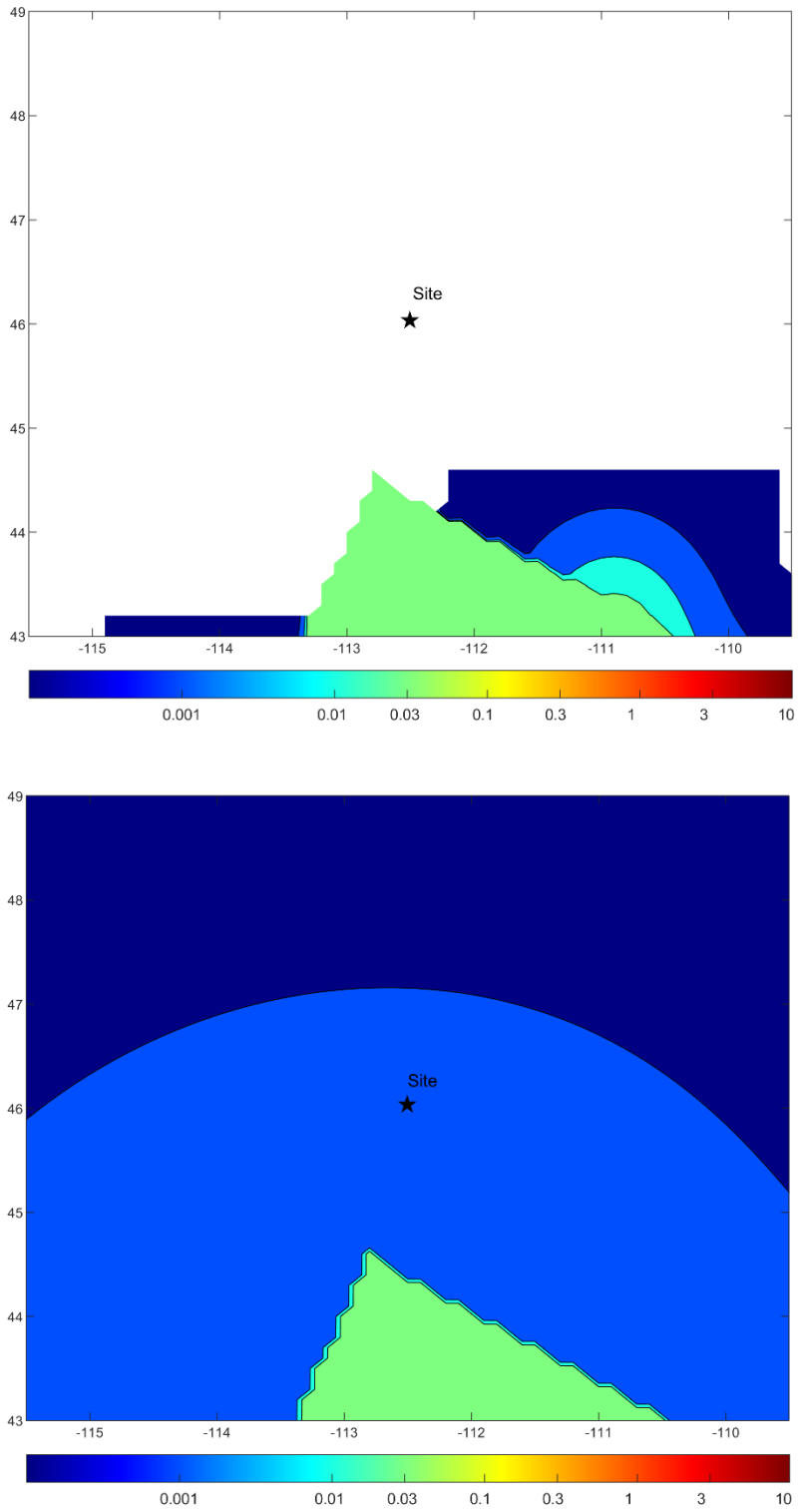

Figure 3-3. Seismicity rate (a-value) contour plots for the compressional regime background source for the fixed smoothing method (top) and adaptive smoothing method (bottom).

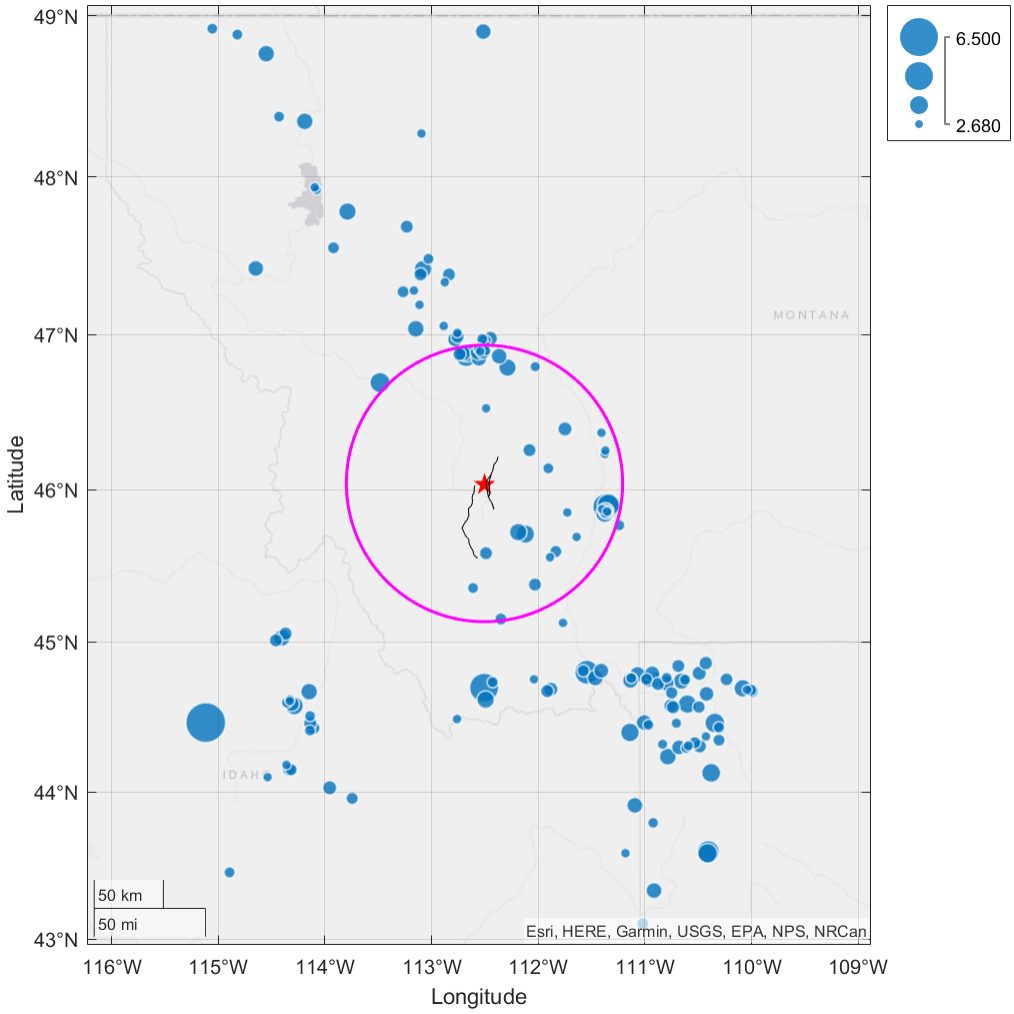

Figure 3-4. Seismicity map showing the declustered earthquakes since May 1, 2018, around the YDTI site (red pentagon). The magenta circle shows the seismicity within 100 km radius of the site. The rocker, Continental, Elk Park, and East Ridge faults are shown in black.

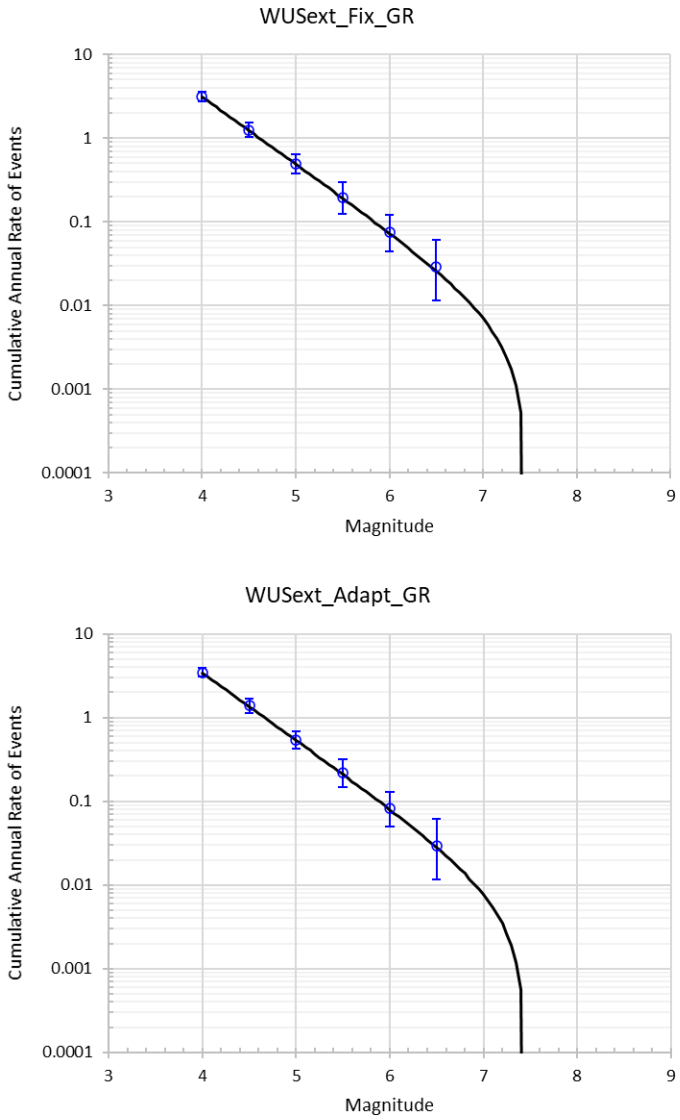

Figure 3-5. Comparison of the truncated exponential recurrence model for fixed (top) and adaptive (bottom) smoothing for the extensional regime source to the recurrence rates obtained from adding the recent observed seismicity (2018 to 2021) to the model.

3.2 Continental-Elk Park and Rocker Faults

LCI (2021a) performed a Phase 1 geologic assessment of the Continental and Rocker faults using a combination of literature review and data compilation, expert interviews, geomorphic analyses, field reconnaissance, and site mapping. This study provided invaluable information regarding the evidence of Quaternary activity on the Continental, Rocker, and surrounding faults as well as the seismic characterization of these faults for implementation in the PSHA update for the YDTI site. Figure 3-6 shows the various fault sections that are part of the LCI (2021a) study: Continental, Rocker, East Ridge, Klepper, and Elk Park faults. A key finding of this study is that there is strong geologic and geomorphic

evidence of Quaternary activity on the Continental fault and limited evidence of activity on the Rocker fault. Other key findings from LCI (2021a) are summarized below:

- The Continental fault is Quaternary active with estimated length of 25.7 km. This estimated length is greater than the 18.2 km length used in Al Atik and Gregor (2016) resulting in larger characteristic magnitude on this fault compared the best estimate of characteristic magnitude of 6.5 used in Al Atik and Gregor (2016).
- The East Ridge fault (a fault strand parallel to the Continental fault as shown in Figure 3-6) is likely Quaternary active with an estimated length of 8.2 km. This fault was only included as part of a sensitivity analysis in Al Atik and Gregor (2016). There is a possibility of linked rupture between the Continental and the East Ridge faults due to the close proximity of these faults (< 1.5 km).
- The Klepper-Elk Park fault (referred to hereafter as the Elk Park fault) is a previously uncharacterized Quaternary fault and was not included in the Al Atik and Gregor (2016) study. This fault should be included in this study update.
- The Rocker fault is potentially Quaternary active with a lower slip rate than that of the continental fault. The estimated length of this fault is 59.8 km longer than the 43.5 km length used in the Al Atik and Gregor (2016).
- The southern part of the Elk Park fault and the northern parts of the Continental and East Ridge faults appear to form an accommodation zone in the vicinity of the site. Due to the dip reversal between the Elk Park fault and the Continental and East Ridge Faults, this accommodation zone is likely to represent a boundary to fault rupture (Wesnousky, 2008). However, given the complex multi-segment and triggered ruptures of historical earthquakes in Montana, linked rupture scenarios between the Elk Park, Continental and East Ridge faults should be considered as part of the source characterization of these faults.
- A layered fault source model that balances the slip rate along the Continental, East Ridge, and Elk Park faults is recommended for use in the source characterization of these faults.

Given the findings in LCI (2021a) and the potential complexity of the ruptures on the Continental, East Ridge and Elk Park faults, LCI was further contracted to develop an SSC hazard input document (HID) for these faults. This HID is documented in LCI (2021b) and provides best estimates and epistemic uncertainty in the parametrization of the characterization of the faults evaluated in LCI (2021a). A justification of this parametrization is also provided. The resulting logic tree for the Continental-Elk Park fault and the Rocker fault is shown in Figure 3-7 and incorporates the key findings from the Phase 1 fault study summarized in this section. As shown in Figure 3-7, the logic tree for the Continental-Elk Park and the Rocker faults includes nine nodes with one or more branches under each node. Branches connected with inclined lines at a dot represent alternative parameters reflecting the uncertainty in the characterized parameter. Branches connected by vertical lines, such as rupture scenarios for the Continental-Elk Park fault represent all elements of the model and not alternative representations.

For the Continental-Elk Park fault, two alternative rupture models, Rupture Model A and B, are characterized defining the possible rupture combinations of the Continental-Elk Park-East Ridge fault sections. Rupture model A considers the accommodation zone between the Continental-East Ridge and

the Elk Park faults as a rupture barrier. As a result, the Continental-East Ridge and Elk Park faults rupture independently as shown in the possible rupture scenarios of Rupture Model A. The alternative Rupture Model B assumes that the Continental, East Ridge, and Elk-Park are structurally connected by the accommodation zone. As a result, two linked rupture scenarios are considered for Rupture Model B as shown in the logic tree of Figure 3-7. Based on Wesnousky (2008) reporting that normal fault ruptures end around structural discontinuities such as an accommodation zone approximately 70% of the time (LCI, 2021b), Rupture Models A and B were assigned weights of 0.8 and 0.2, respectively. This weighting reflects a significantly higher degree of confidence in ruptures on the Continental-East Ridge and Elk Park faults happening independently as opposed to much longer linked ruptures of the Continental-East Ridge-Elk Park faults.

The best estimate slip rate on the Continental-Elk Park faults is set at 0.1 mm/year (LCI, 2021b) assuming a single event in 10,000 years compared to a best estimate slip rate of 0.02 mm/year used in Al Atik and Gregor (2016). LCI (2021b) notes that the slip rates on the Continental and Rocker faults remain poorly constrained. Based on the assumption that fault slip is transferred from the Continental fault in the south where the fault is a single strand to multiple overlapping faults in the center to the Elk Park fault in the north as shown in the zones in Figure 3-6, LCI (2021b) assigned for each rupture on the Continental-Elk Park fault slip rates of 0.05, 0.1, and 0.02 mm/year with weights of 0.6, 0.2, 0.2, respectively.

A summary of the parameters presented in the logic tree in Figure 3-7 is given in Table 3-2. Best estimate dip angle for the Continental-Elk Park fault is 70 degrees similar to the dip angle used for the Continental fault in the Al Atik and Gregor (2016). The dip direction of Rupture Model A scenarios is listed in Table 3-2. The Continental and East-Ridge ruptures dip towards the site (i.e., site located on the hanging wall of these ruptures) while the Elk Park fault ruptures dip away from the site in the East direction placing the site on the footwall of these ruptures. For Rupture Model B, a change in dip direction from west to east occurs between the continental and the Elk Park sections. The implementation of this change in dip direction within a single rupture in the PSHA program is discussed in Section 6.1.

The fault lengths and fault rupture lengths of the scenarios considered are based on the LCI (2021a) fault mapping. The characteristic magnitude for each rupture source is estimated in LCI (2021b) based on empirical relations between rupture dimensions and magnitude. Epistemic uncertainty around the best estimate of the characteristic magnitude is incorporated as shown in Table 3-2 and Figure 3-7. For Rupture Model A scenarios, the best estimate characteristic magnitude ranges from 6.6 to 6.8 while the characteristic magnitude for Rupture Model B scenarios is 7.0. We note that the characteristic magnitude used in the Al Atik and Gregor (2016) study for the Continental fault had a best estimate of 6.5. Two magnitude recurrence models, the maximum magnitude and the Youngs and Coppersmith (1985) characteristic magnitude models, are used in LCI (2021b) with weights of 0.3 and 0.7, respectively.

For the Rocker fault, the seismic source characterization is relatively simple with a single segment fault rupture. The best estimate dip angle is 55 degrees similar to the dip angle used in Al Atik and Gregor (2016). The dip direction is towards the west dipping away from the site, putting the site on the footwall of the Rocker fault. The slip rate is 0.02 mm/year (best estimate) similar to the slip rate used in Al Atik

and Gregor (2016). The characteristic magnitude is 7.1 (best estimate) compared to **M** 7 used in Al Atik and Gregor (2016).

The SSC of the Continental-Elk Park and Rocker faults based on LCI (2021b) and presented in Figure 3-7 and Table 3-2 is implemented in this PSHA update for the YDTI site. The closest rupture distance from the source shown in Table 3-2 are listed in Table 3-3. As shown in Table 3-3, the closest Rrup distance from the Continental-Elk Park fault to the site is 1.43 km from the west dipping segments (dipping towards the site) CF-S + CF-C + CF-N. For Rupture Model B, two closest distances are listed for the west-dipping and east-dipping segments. The closest distance to the Rocker fault is 7.14 km.

Table 3-2. Source parameters for the Continental-Elk Park and the Rocker faults (source: LCI, 2021b). The style-of-faulting is normal. Weights are given in brackets.

Fault Name	Rupture Models	Rupture Source	Fault Length (km)	Surface Rupture Length (km)*	Fault Dip (°)	Dip Dir.	Depth to Top of Rupture (km)	Seismogenic thickness (km)	M_{char}	Slip Rates (mm/yr)
Continental-Elk Park Fault	Rupture Model A	CF-S + CF-C + CF-N	25.7	24.5	40 [0.3] 70 [0.6] 80 [0.1]	W	0.0	12[0.2] 15[06] 18[0.2]	6.5[0.2] 6.8[0.6] 7.1[0.2]	0.10[0.2] 0.05[0.6] 0.01[0.2]
		CF-S + ERF	19.0	18.2	40 [0.3] 70 [0.6] 80 [0.1]	W	0.0	12[0.2] 15[06] 18[0.2]	6.4[0.2] 6.7[0.6] 7.0[0.2]	0.10[0.2] 0.05[0.6] 0.01[0.2]
		Elk-C + Elk-N	21.4	20.6	40 [0.3] 70 [0.6] 85 [0.1]	E	0.0	12[0.2] 15[06] 18[0.2]	6.4[0.2] 6.7[0.6] 7.0[0.2]	0.10[0.2] 0.05[0.6] 0.01[0.2]
		Elk-N	15.6	13.9	40 [0.3] 70 [0.6] 85 [0.1]	E	0.0	12[0.2] 15[06] 18[0.2]	6.3[0.2] 6.6[0.6] 6.9[0.2]	0.10[0.2] 0.05[0.6] 0.01[0.2]
	Rupture Model B	LS-1 (CF-S+CF-C+CF-N+Elk-N)	41.4	38.1	40 [0.3] 70 [0.6] 80 [0.1]	W and E	0.0	12[0.2] 15[06] 18[0.2]	6.7[0.2] 7.0[0.6] 7.3[0.2]	0.10[0.2] 0.05[0.6] 0.01[0.2]
		LS-2 (CF-S to ERF to Elk-C to Elk-N)	41.0	38.1	40 [0.3] 70 [0.6] 85 [0.1]	W and E	0.0	12[0.2] 15[06] 18[0.2]	6.7[0.2] 7.0[0.6] 7.3[0.2]	0.10[0.2] 0.05[0.6] 0.01[0.2]
Rocker Fault	Single Segment Rupture model	Rocker Fault	59.8	53.4	30[0.2] 55 [0.6] 70[0.2]	W	0.0	12[0.2] 15[06] 18[0.2]	6.8[0.2] 7.1[0.6] 7.4[0.2]	0.12[0.2] 0.02 [0.6] 0.005[0.2]

*Surface Rupture Length (SRL) is measure end to end and used to estimate Mchar and not the cumulative fault length measured along the fault trace.
**Rupture Model B sources change dips along strike. LS-1 changes dip from west to east from sections CF-N to Elk-N and LS-2 changes dip from west to east between sections ERF and Elk-C.

Table 3-3. Closest Rrup distance from the rupture scenarios on the Continental-Elk Park and the Rocker faults to the YDTI site.

Fault Name	**Continental-Elk Park Fault**						**Rocker Fault**
Rupture Model	Rupture Model A				Rupture Model B		
Rupture Scenario	CF-S + CF-C + CF-N	CF-S + ERF	Elk-C + Elk-N	Elk-N	LS-1 (CF-S+CF-C+CF-N+Elk-N)	LS-2 (CF-S to ERF to Elk-C to Elk-N)	
Closest Rrup to the Site (km)	1.43	3.26	3.15	8.62	8.62 (E) – 1.43 (W)	3.14 (E) – 3.26 (W)	7.14

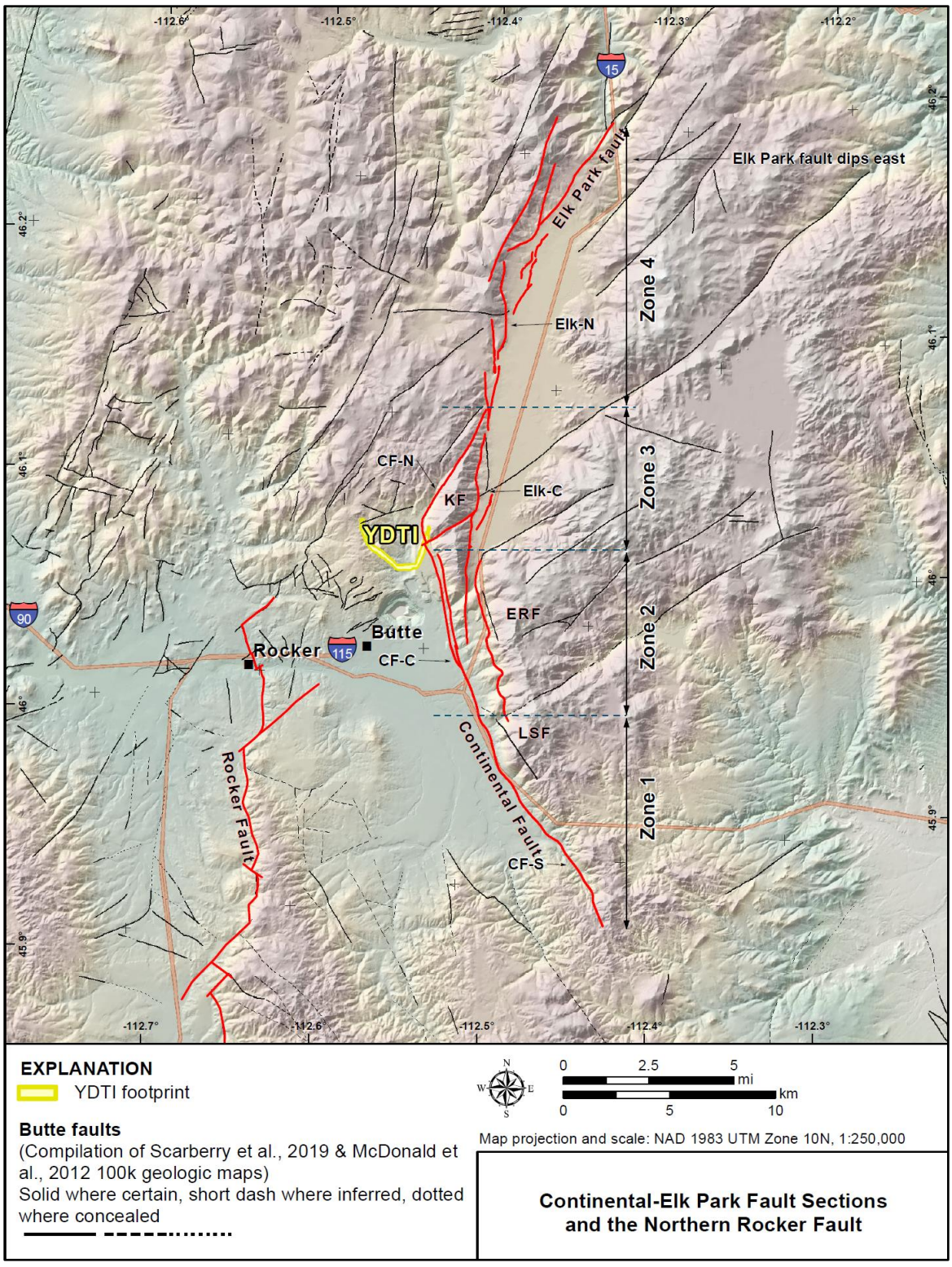

Figure 3-6. Fault sections part of the LCI (2021) study. Abbreviations: ERF = East Ridge fault, KP = Klepper fault, LSF = Lucky Strike fault, and CF = Continental fault) (source: LCI 2021b).

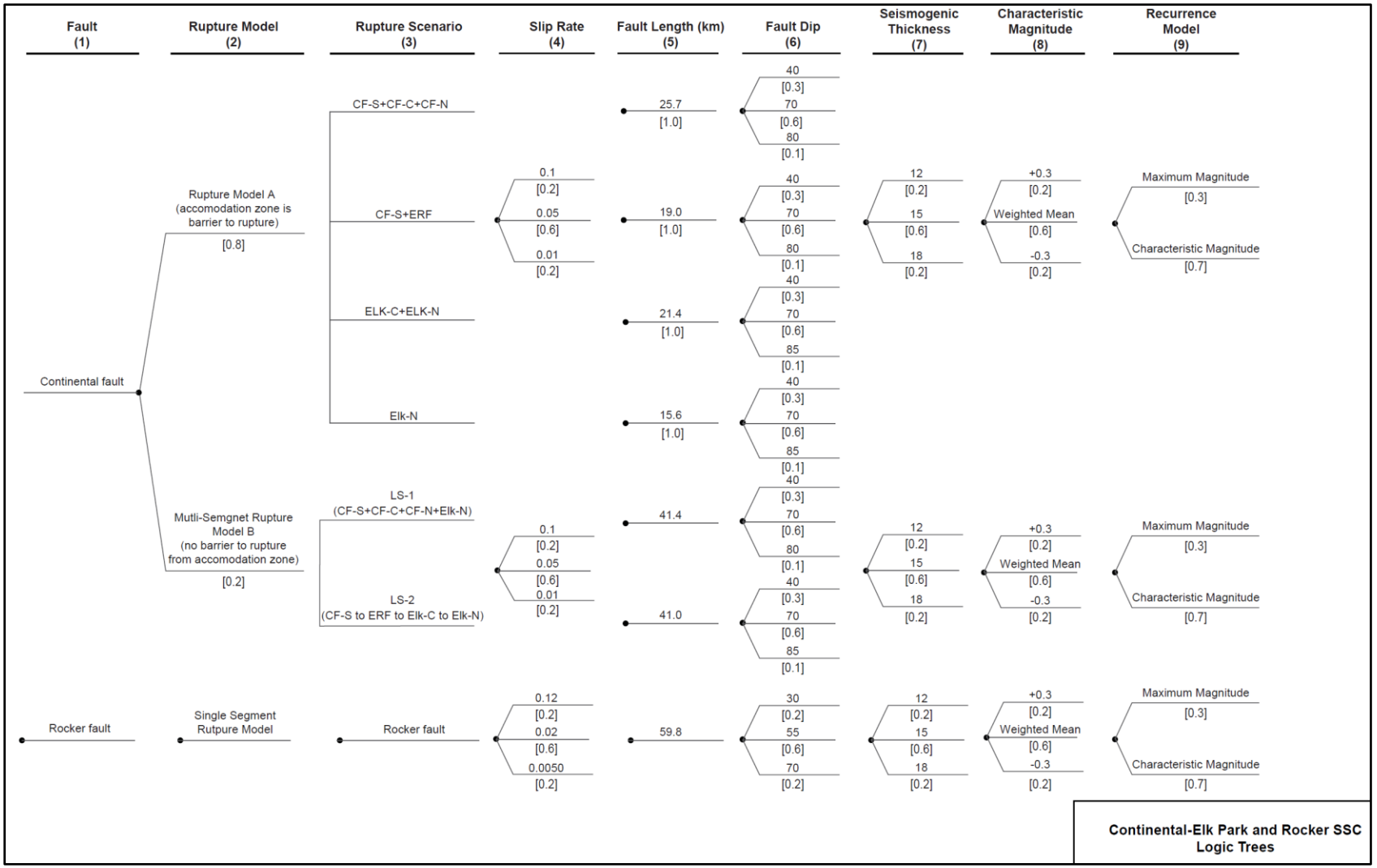

Figure 3-7. Continental-Elk Park and Rocker faults seismic source characterization logic trees (source: LCI 2021b).

3.3 Other Faults

In addition to the Continental-Elk Park and the Rocker faults, other fault sources that were used in Al Atik and Gregor (2016) are included in this study update. These faults are primarily based on Petersen et al. (2014) and are within 200 km of the YDTI site. These faults are shown in Figure 3-8 and their parameter characterization is listed in Tables 3-4 to 3-6. The Georgia Gulch fault is the closest from this set of fault sources to the YDTI site located at a closest rupture distance of 49 km. We note that the 2018 update to the NSHMs (Petersen et al., 2020) used the same fault sources as in Petersen et al. (2014). As a result, the characterization of these fault sources remains unchanged in this study update. We also note that hazard results by source type in the Al Atik and Gregor (2016) study indicated that these fault sources have a small contribution to the total hazard at the YDTI site.

Petersen et al. (2014) modeled fault rupture as full-source rupture and floating partial-source ruptures that generate earthquakes with **M** 6.5 to the magnitude of the full-source rupture. These two models of rupture are given weights of 0.667 and 0.333, respectively. The magnitude recurrence for the full-source ruptures is modeled with the maximum magnitude model as a truncated normal distribution with a standard deviation (σ) of 0.12 and truncated on the lower end at 2σ. The truncated exponential model with a minimum **M** of 6.5 is used to model the magnitude recurrence on the partial-source ruptures. A b-value of 0.8 was used for all sources. The Well and Coppersmith (1994) relations were used to assign maximum magnitudes for the full-source ruptures of the faults. All the faults included in this analysis have normal sense of slip. Each fault source extends from the ground surface to a depth of 15 km and is assigned a dip angle of 50 $\pm$ 15 degrees. Slip rates on these fault sources were estimated using a geologic-based model with weight of 0.8 and two equally weighted geodetic-based models (Bird 2013 and Zeng and Shen 2013) with a total weight of 0.2.

Table 3-4. Source parameters of other faults sources used in the Al Atik and Gregor (2016) study based on Petersen et al. (2014). Weights are given in parentheses. All faults have a normal style-of-faulting, top of rupture is at 0 km, seismogenic thickness is 15 km, and b value is 0.8.

Fault Number	Fault Name	Closest Distance to Site (km)	Mmin	Recurrence Model	Slip Rate (mm/yr)	Recurrence Interval (yr) [1]	Activity Rate - N(M>Mmin) [2]	Slip Rate / Recurrence Interval / Activity Rate Weight	Mmax	Dip (degrees)	Fault Length (km)
667	Georgia Gulch fault	49.2	5.00	Max Mag (1)	0.040	14006	n/a	(0.8)	6.42 (0.6)	50 W (0.6)	14
					0.360	1575	n/a	(0.1)	6.22 (0.2)	35 W (0.2)	
					0.050	11338	n/a	(0.1)	6.62 (0.2)	65 W (0.2)	
678	Helena Valley fault	82.1	6.50	Max Mag (0.667) Trunc Exp (0.333)	0.013	57143	0.000023	(0.8)	6.60 (0.6)	50 S (0.6)	20
					0.050	14925	0.000087	(0.1)	6.40 (0.2)	35 S (0.2)	
					0.010	74627	0.000017	(0.1)	6.80 (0.2)	65 S (0.2)	
655	Madison fault	94.1	6.50	Max Mag (0.667) Trunc Exp (0.333)	0.522	4951	0.000285	(0.8)	7.45 (0.6)	50 W (0.6)	111
					0.510	5051	0.000278	(0.1)	7.25 (0.2)	35 W (0.2)	
					0.480	5376	0.000262	(0.1)	7.65 (0.2)	65 W (0.2)	
671	Canyon Ferry fault	87.7	6.50	Max Mag (0.667) Trunc Exp (0.333)	0.170	6993	0.000107	(0.8)	6.92 (0.6)	50 SW (0.6)	39
					0.070	16920	0.000044	(0.1)	6.72 (0.2)	35 SW (0.2)	
					0.220	5376	0.000139	(0.1)	7.12 (0.2)	65 SW (0.2)	
644	Blacktail fault	97.1	6.50	Max Mag (0.667) Trunc Exp (0.333)	0.039	31546	0.000025	(0.8)	6.94 (0.6)	50 NE (0.6)	40
					0.030	41153	0.000019	(0.1)	6.74 (0.2)	35 NE (0.2)	
					0.050	24691	0.000032	(0.1)	7.14 (0.2)	65 NE (0.2)	
645	Sweetwater fault	99.3	5.00	Max Mag (1)	0.052	10373	n/a	(0.8)	6.38 (0.6)	50 NE (0.6)	13
					0.100	5405	n/a	(0.1)	6.18 (0.2)	35 NE (0.2)	
					0.060	9009	n/a	(0.1)	6.58 (0.2)	65 NE (0.2)	
648	Red Rock Hills fault	123.3	5.00	Max Mag (1)	0.222	2041	n/a	(0.8)	6.27 (0.6)	50 W (0.6)	11
					0.180	2519	n/a	(0.1)	6.07 (0.2)	35 W (0.2)	
					0.220	2058	n/a	(0.1)	6.47 (0.2)	65 W (0.2)	

(1) Recurrence interval was used for the maximum magnitude model

(2) Activity rate was used for the truncated exponential model

Table 3-5. Source parameters of other faults sources used in the Al Atik and Gregor (2016) study based on Petersen et al. (2014). Weights are given in parentheses. All faults have a normal style-of-faulting, top of rupture is at 0 km, seismogenic thickness is 15 km, and b value is 0.8 (cont'd).

Fault Number	Fault Name	Closest Distance to Site (km)	Mmin	Recurrence Model	Slip Rate (mm/yr)	Recurrence Interval (yr) [1]	Activity Rate - N(M>Mmin) [2]	Slip Rate / Recurrence Interval / Activity Rate Weight	Mmax	Dip (degrees)	Fault Length (km)
641	Red Rock fault	137	6.50	Max Mag (0.667) Trunc Exp (0.333)	0.653	1372	0.000667	(0.8)	6.73 (0.6)	50 E (0.6)	27
					0.100	8929	0.000102	(0.1)	6.53 (0.2)	35 E (0.2)	
					0.820	1092	0.000839	(0.1)	6.93 (0.2)	65 E (0.2)	
603	Beaverhead fault	150.2	6.50	Trunc Exp (1)	0.157	n/a	0.000319	(0.8)	7.00 (0.6)	50 SW (0.6)	134
					0.310	n/a	0.000631	(0.1)	6.80 (0.2)	35 SW (0.2)	
					0.210	n/a	0.000428	(0.1)	7.20 (0.2)	65 SW (0.2)	
642	Emigrant fault	151.2	6.50	Max Mag (0.667) Trunc Exp (0.333)	0.326	4926	0.000168	(0.8)	7.12 (0.6)	50 NW (0.6)	57
					0.170	9259	0.000087	(0.1)	6.92 (0.2)	35 NW (0.2)	
					0.420	3759	0.000215	(0.1)	7.32 (0.2)	65 NW (0.2)	
656	Hebgen-Red Canyon fault	157.6	6.50	Max Mag (0.667) Trunc Exp (0.333)	0.653	10299	0.000094	(0.8)	7.30 (0.6)	50 SW (0.6)	25
					1.250	5376	0.000181	(0.1)	7.10 (0.2)	35 SW (0.2)	
					0.730	9174	0.000106	(0.1)	7.50 (0.2)	65 SW (0.2)	
643	Centennial fault	155.5	6.50	Max Mag (0.667) Trunc Exp (0.333)	0.914	1862	0.000504	(0.8)	7.17 (0.6)	50 N (0.6)	64
					0.910	1869	0.000501	(0.1)	6.97 (0.2)	35 N (0.2)	
					1.390	1224	0.000766	(0.1)	7.37 (0.2)	65 N (0.2)	
698	Jocko fault	160.8	5.00	Max Mag (1)	0.104	5814	n/a	(0.8)	6.47 (0.6)	50 NW (0.6)	16
					0.220	2770	n/a	(0.1)	6.27 (0.2)	35 NW (0.2)	
					0.100	6098	n/a	(0.1)	6.67 (0.2)	65 NW (0.2)	

(1) Recurrence interval was used for the maximum magnitude model

(2) Activity rate was used for the truncated exponential model

Table 3-6. Source parameters of other faults sources used in the Al Atik and Gregor (2016) study based on Petersen et al. (2014). Weights are given in parentheses. All faults have a normal style-of-faulting, top of rupture is at 0 km, seismogenic thickness is 15 km, and b value is 0.8 (cont'd).

Fault Number	Fault Name	Closest Distance to Site (km)	Mmin	Recurrence Model	Slip Rate (mm/yr)	Recurrence Interval (yr) [1]	Activity Rate - N(M>Mmin) [2]	Slip Rate / Recurrence Interval / Activity Rate Weight	Mmax	Dip (degrees)	Fault Length (km)
699	Mission fault	173.4	6.50	Max Mag (0.667) Trunc Exp (0.333)	0.418	5435	0.000208	(0.8)	7.36 (0.6)	50 W (0.6)	92
					0.280	8065	0.000139	(0.1)	7.16 (0.2)	35 W (0.2)	
					0.430	5263	0.000214	(0.1)	7.56 (0.2)	65 W (0.2)	
602	Lemhi fault	189.9	6.50	Trunc Exp (1)	0.287	n/a	0.000642	(0.8)	7.00 (0.6)	50 SW (0.6)	147
					0.310	n/a	0.000693	(0.1)	6.80 (0.2)	35 SW (0.2)	
					0.380	n/a	0.000849	(0.1)	7.20 (0.2)	65 SW (0.2)	

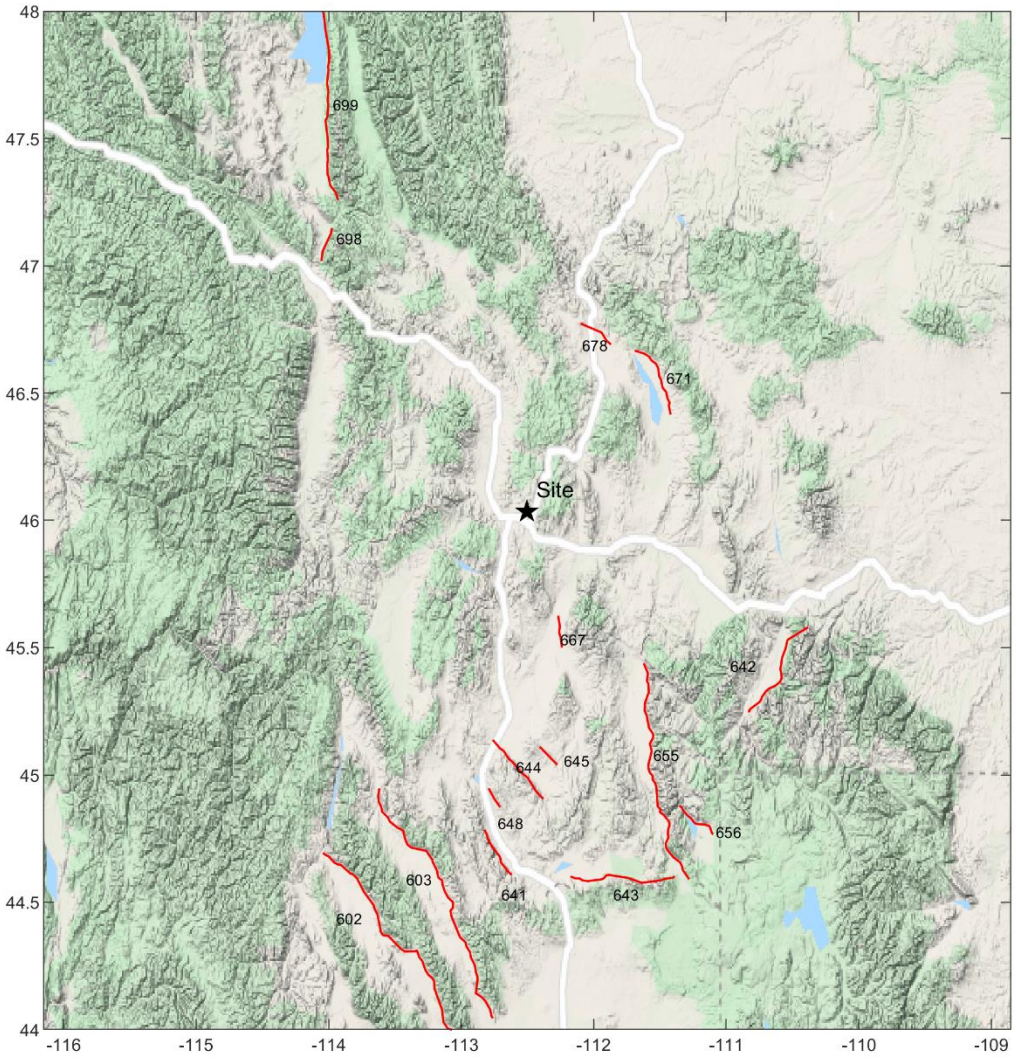

Figure 3-8. Fault sources in the vicinity of the YDTI site used in Al Atik and Gregor (2016) and based on Petersen et al. (2014). The Continental-Elk Park and Rocker faults are shown in Figure 3-6.

4. GROUND MOTION CHARACTERIZATION

As discussed in Section 2.0, Al Atik and Gregor (2016) used the 5 NGA-West2 GMPEs (ASK14, BSSA14, CB14, CY14, and Id14) and Wong et al. (2005) for the median prediction of ground motions given earthquakes in the YDTI site region. The NGA-West2 GMPEs were used along with their respective standard deviation models while Wong et al. (2005) was used with the ASK14 standard deviation model. The epistemic uncertainty model of Al Atik and Youngs (2014) was used to incorporate the epistemic uncertainty in the median prediction of the 5 NGA-West2 GMPEs. In this study update, an evaluation of the 5 NGA-West2 GMPEs, Wong et al. (2005), Akkar et al. (2014), and Boore et al. (2021) models is performed for applicability to the YDTI site region. This evaluation consists of a review of the datasets used in the development of these GMPEs, applicability limitations, comparisons of GMPE ground-motion predictions to empirical recordings in the study region, as well as comparison of predicted response spectra for hazard relevant scenarios for the YDTI site.

Similar to the GMPEs evaluation in Al Atik and Gregor (2016), the NGA-West2 GMPEs were favored because of the large uniformly processed datasets used to develop these models as well as their applicability to a wide magnitude and distance range. These GMPEs are considered the standard state of practice for ground-motion prediction from earthquakes in active tectonic regions. In general, these GMPEs are considered well suited for the tectonic environment in the YDTI site region. One potential drawback for the application of the NGA-West2 GMPEs to the YDTI site region is the relatively small subset of ground-motion data from normal earthquakes relative to strike-slip and reverse earthquakes in the NGA-West2 database. As a result, additional GMPEs (Akkar et al. 2014, and Boore et al. 2021) that have a larger subset of empirical data from normal earthquakes are evaluated for applicability to the YDTI site. For the NGA-West2 GMPEs, we note that Id14 is limited in its applicability to distances within 150 km and $V_{S30} \geq 450$ m/sec. Given that the hazard at the YDTI site is required for a reference V_{S30} of 760 m/sec as well as a site-specific V_{S30} of 420 m/sec, the Id14 GMPE is less suited for use in this study update.

Wong et al. (2005) is a stochastic-based GMPE developed specifically for eastern and western Montana to compensate for the lack of region-specific models. A point-source stochastic model was used to model earthquakes with **M** 5.5, 6.5, and 7.5 in the distance range of 1 to 400 km to generate a simulation database of ground motions. A single-corner source model with variable stress drop was used for western Montana. The final regression model given this database, which is a function of magnitude and rupture distance, is applicable to soft-rock site condition with V_{S30} of 760 m/sec. This GMPE is less suited for this study update given the need to develop ground motions for the site-specific V_{S30} of 420 m/sec. Moreover, the lead developer of this model recently recommended that Wong et al. (2005) not be used for the YDTI study update given that this model is derived based on stochastic simulations while other models such as the NGA-West2 GMPEs are better constrained by a large set of empirical data (Wong 2021, personal communication).

Akkar et al. (2014) is a pan-European GMPE developed based on ground-motion recordings from crustal earthquakes in Europe and the Middle East. This GMPE is applicable to earthquakes with **M** ≥ 4, distance up to 200 km, spectral periods of 0.01 to 4 sec, and a range of site conditions. This GMPE is evaluated for inclusion in this study update based on the relatively large dataset of ground-motion recordings from normal earthquakes used in its model development. Similarly, the Boore et al. (2021) GMPE is a recent

ground-motion model developed for application to Greece. It is based on a relatively large number of ground-motion recordings from normal earthquakes compared to strike-slip and reverse earthquakes and is, therefore, evaluated for inclusion in this study update. While both Akkar et al. (2014) and Boore et al. (2021) GMPEs include a relatively well-constrained style-of-faulting term for normal earthquakes, these two GMPEs are developed for a different tectonic environment than that of the YDTI region. Including these models in this study update would require a more careful evaluation of their applicability to Montana and the development of potential host-to-target region adjustments to these models to render them more applicable to the YDTI region.

Similar to the 2016 study, we compare ground-motion recordings from earthquakes in the YDTI region to median ground-motion predictions from the 8 GMPEs discussed in this section. In addition to the recordings from the **M** 6 Helena (mainshock and aftershock) and the **M** 5.6 Dillon earthquakes used in Al Atik and Gregor (2016), we add recordings from the 2005 **M** 5.8 Lincoln earthquake. The Helena and the Lincoln earthquakes have a strike slip faulting mechanism while the Dillon earthquake has a normal style of faulting. Some of the recording stations of these earthquakes do not have measured V_{S30} values and are assigned nominal V_{S30} of 550 m/sec. The empirical recordings ranged in distance from around 3 km (Helena mainshock and aftershock) to 266 km. Comparisons of GMPEs median predictions to these recorded ground motions did not indicate specific and consistent trends related to the applicability of these GMPEs to the empirical recordings from the YDTI region. In general, response spectra from the NGA-West2 GMPEs tended to be comparable to the recordings from the Dillon earthquake particularly at short distance but did not fit very well some of the other recordings. Similar observations are made regarding the Wong et al. (2005), Akkar et al. (2014), and Boore et al. (2021). Predicted median response spectra from these GMPEs did not consistently agree well with the empirical recordings.

The 8 candidate GMPEs discussed in this section are also evaluated for hazard relevant scenarios for the YDTI site. Comparisons of median predictions and standard deviations of these GMPEs are evaluated for the MCE scenarios on the Continental fault (**M** 6.8 earthquake scenario from Rupture Model A and **M** 7 scenario LS-1 from Rupture Model B) and a gridded seismicity-based earthquake scenario with **M** 6 and distance of 30 km.

Figure 4-1 (top) presents a comparison of the median ground-motion predictions of the 8 candidate GMPEs for the **M** 6.8 MCE Rupture Model A01 (CF-S+CF-C+CF-N) scenario on the Continental fault for a V_{S30} of 760 m/sec. This MCE scenario is at an Rrup distance of 1.43 km from the YDTI site with the site located on the hanging wall. Figure 4-1 (bottom) shows a comparison of the total standard deviation of the candidate GMPEs for this earthquake scenario. For median predictions, Figure 4-1 (top) shows a wide range of predictions from the 5 NGA-West2 GMPEs, particularly at short periods. This larger epistemic uncertainty from the NGA-West2 GMPEs is expected for this scenario earthquake given the lack of empirical data in the NGA-West2 GMPEs from normal earthquakes and at very short distances. We also note that the Id14 GMPE shows a somewhat unusual spectral shape at periods less than 0.05 sec with median predictions outside of the prediction range from the other NGA-West2 GMPEs for periods less than 0.03 sec. At long periods greater than 0.75 sec, the median prediction from Id14 falls below the range of predictions from the rest of the NGA-West2 GMPEs. Figure 4-1 (top) shows a different spectral shape for the median prediction of Wong et al. (2005) (wea05) compared to the NGA-West2 GMPEs with the peak of the spectrum shifted to shorter periods and predictions exceeding those of the NGA-West2 GMPEs for periods 0.04 and 0.1 sec and periods of 1 sec and larger. The median

prediction from Akkar et al. (2014) GMPE (Aea13) generally follows that of ASK14 with the values falling below the median prediction of the rest of the models at long periods greater than 0.5 sec. The median prediction from Boore et al. (2021) (Bea21) follows that of BSSA14 with values exceeding those of the rest of the GMPEs at periods greater than 1 sec. Comparing the standard deviation of the candidate models for this scenario, we note that Wea05 has a larger standard deviation compared to the rest of the models. The standard deviation of this model is not considered reliable due to the use of stochastic simulations in the development of this model. The Aea13 standard deviation is also larger than that of the NGA-West2 GMPEs. This is due to the predominance of small magnitude data used to develop this model and the homoscedastic nature of its standard deviation.

Figure 4-2 shows a comparison of the median predictions (top) and standard deviation (bottom) of the 8 candidate GMPEs for Rupture Model B LS-1 scenario earthquake on the Continental fault for V_{S30} of 760 m/sec. Using the generalized coordinates 2 system (GS2), the closest point from the site to the rupture surface is on the west dipping part of this rupture (CF-S+CF-C+CF-N) with an Rrup of 1.43 km. Similar observations can be made on the comparisons in Figure 4-2 as those made on Figure 4-1 given the similarity of the 2 earthquake scenarios. Figures 4-3 and 4-4 show similar comparisons of the 8 candidate GMPEs for a scenario with **M** 6 and distance of 30 km with the site located on the hanging wall and footwall, respectively, for V_{S30} of 760 m/sec. For this scenario, Wea05 shows similar median predictions for the site location on the hanging wall and the footwall. This is due to the absence of a hanging wall term in this GMPE. For the site location on the hanging wall, Figure 4-3 shows that the R_{JB}-based BSSA14 GMPE has the largest median prediction compared to the rest of the GMPEs. For both hanging wall and footwall cases, Wea05 has low median predictions compared to the rest of the GMPEs over the entire period range. For the footwall case, Figure 4-4 shows that the median predictions from Wea05, Aea13, and Bea21 are the low range of predictions from the candidate GMPEs for the footwall case.

Based on the need to develop ground motions for a V_{S30} of 420 m/sec along with the evaluation of the candidate GMPEs presented in this section, we select 4 NGA-West2 GMPEs for use for this study. These are: ASK14, BSS14, CB14, and CY14. We do not select Id14 because it is not applicable for V_{S30} of 420 m/sec and because of its unusual spectral shape for very short distances as shown in Figures 4-1 and 4-2. Similarly, Wea05 is only applicable for V_{S30} of 760 m/sec and is based on stochastic simulations and not empirical ground motion data. Based on that and the recommendation from Wong (2021, personal communication) not to use Wea05, we do not include Wea05 for this study update. The Aea13 and Bea21 GMPEs are not selected despite the abundance of normal faulting events in the datasets used to develop these models. We do not select these GMPEs because they are region-specific and would require a more careful evaluation and the potential development of host-to-target adjustments for applicability to southwest Montana. Similar to the 2016 update, we use the Al Atik and Youngs (2014) epistemic uncertainty model for the GMPE median prediction. The GMC logic tree for the YDTI study update is shown in Figure 4-5.

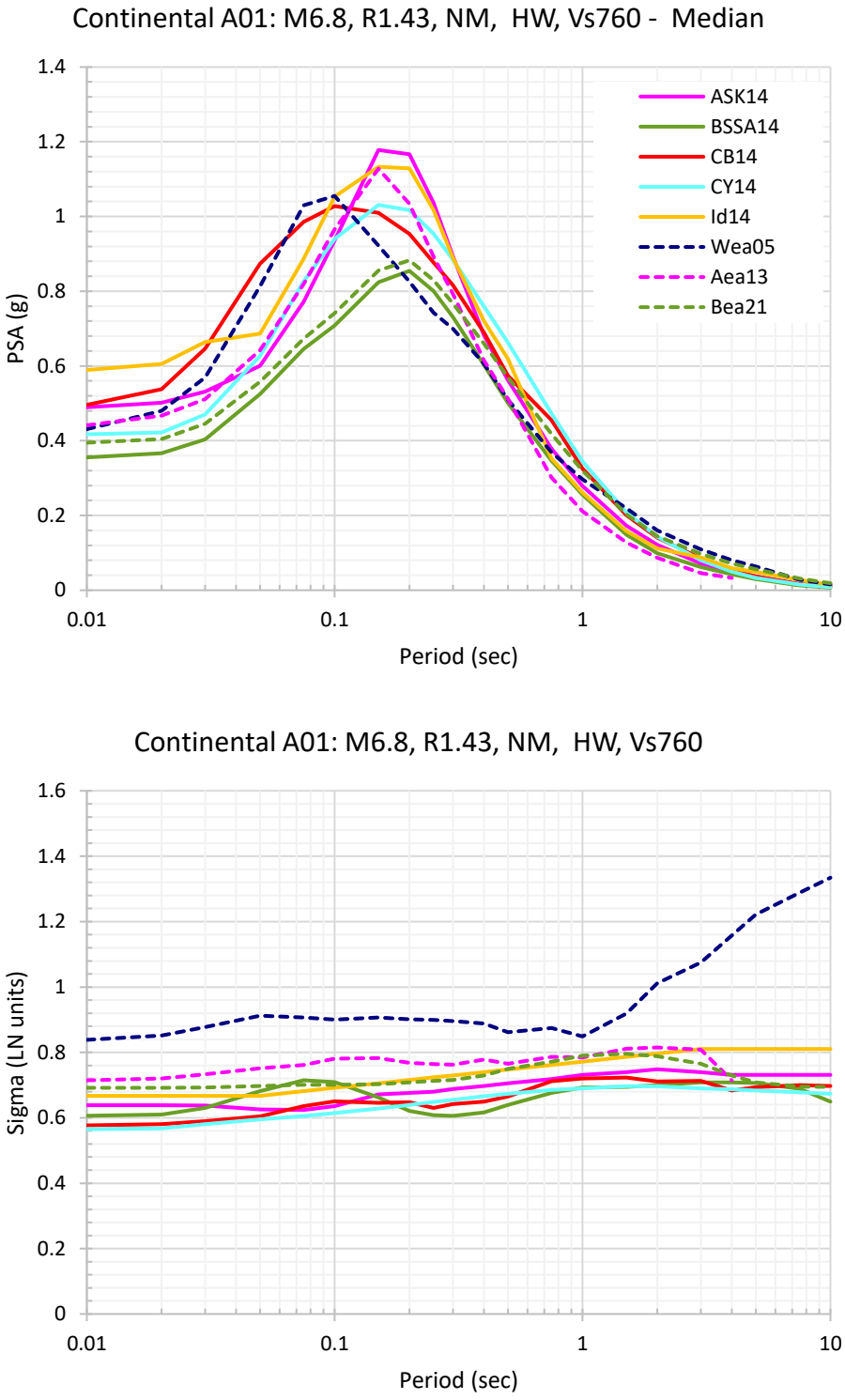

Figure 4-1. Comparison of the median prediction (top) and standard deviation (bottom) of the 8 candidate GMPEs for the Continental-Elk Park fault Rupture Model A01 (CF-S+CF-C+CF-N) scenario with M 6.8, Rrup of 1.43 km, and V_{S30} of 760 m/sec.

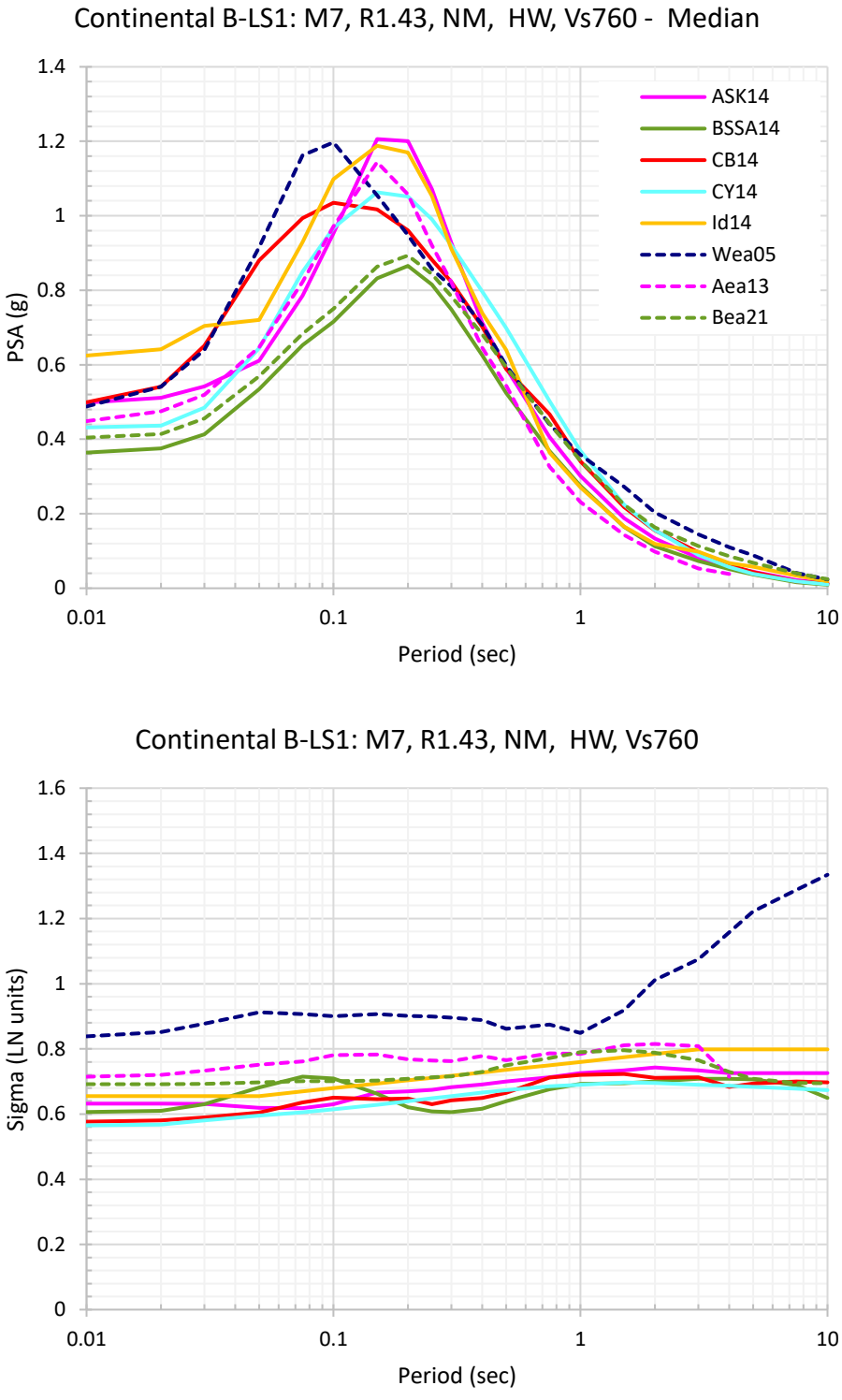

Figure 4-2. Comparison of the median prediction (top) and standard deviation (bottom) of the 8 candidate GMPEs for the Continental-Elk Park fault Rupture Model B-LS1 (CF-S+CF-C+CF-N+ELK-N) linked scenario with M 7, Rrup of 1.43 km, and V_{S30} of 760 m/sec.

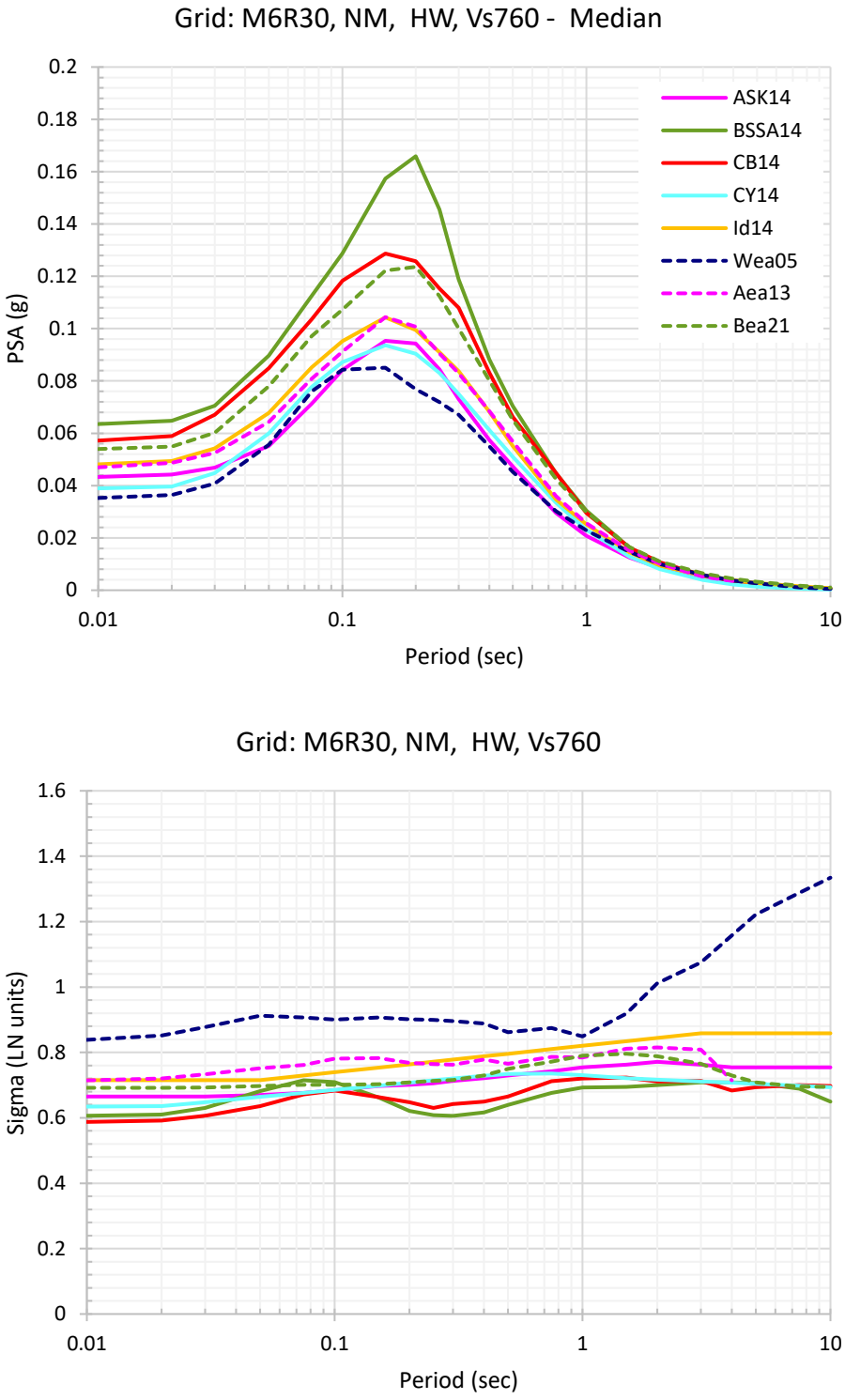

Figure 4-3. Comparison of the median prediction (top) and standard deviation (bottom) of the 8 candidate GMPEs for a gridded seismicity normal earthquake scenario with M 6, Rrup of 30 km, and V_{S30} of 760 m/sec and with the site located on the hanging wall.

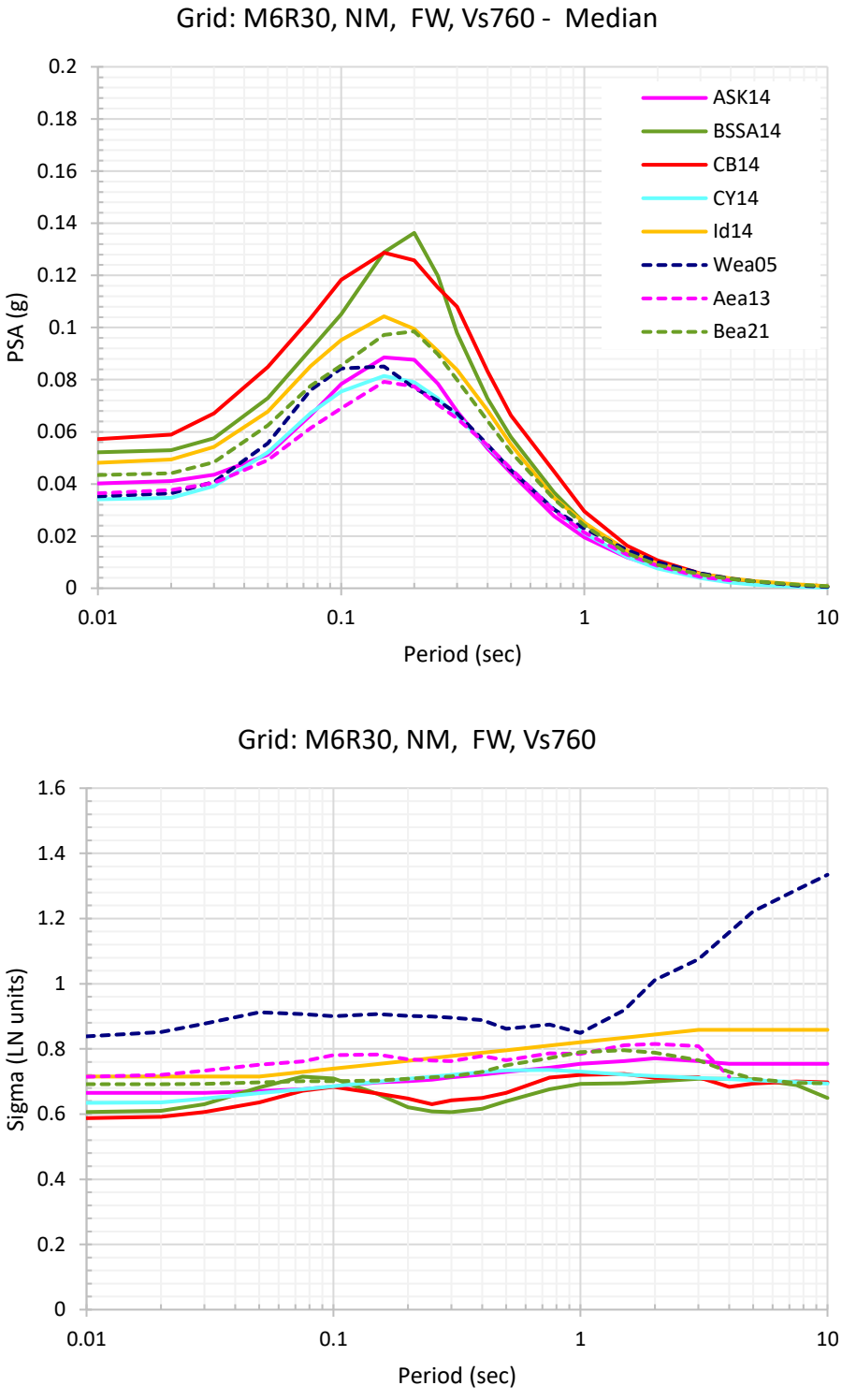

Figure 4-4. Comparison of the median prediction (top) and standard deviation (bottom) of the 8 candidate GMPEs for a gridded seismicity normal earthquake scenario with M 6, Rrup of 30 km, and V_{S30} of 760 m/sec and with the site located on the footwall.

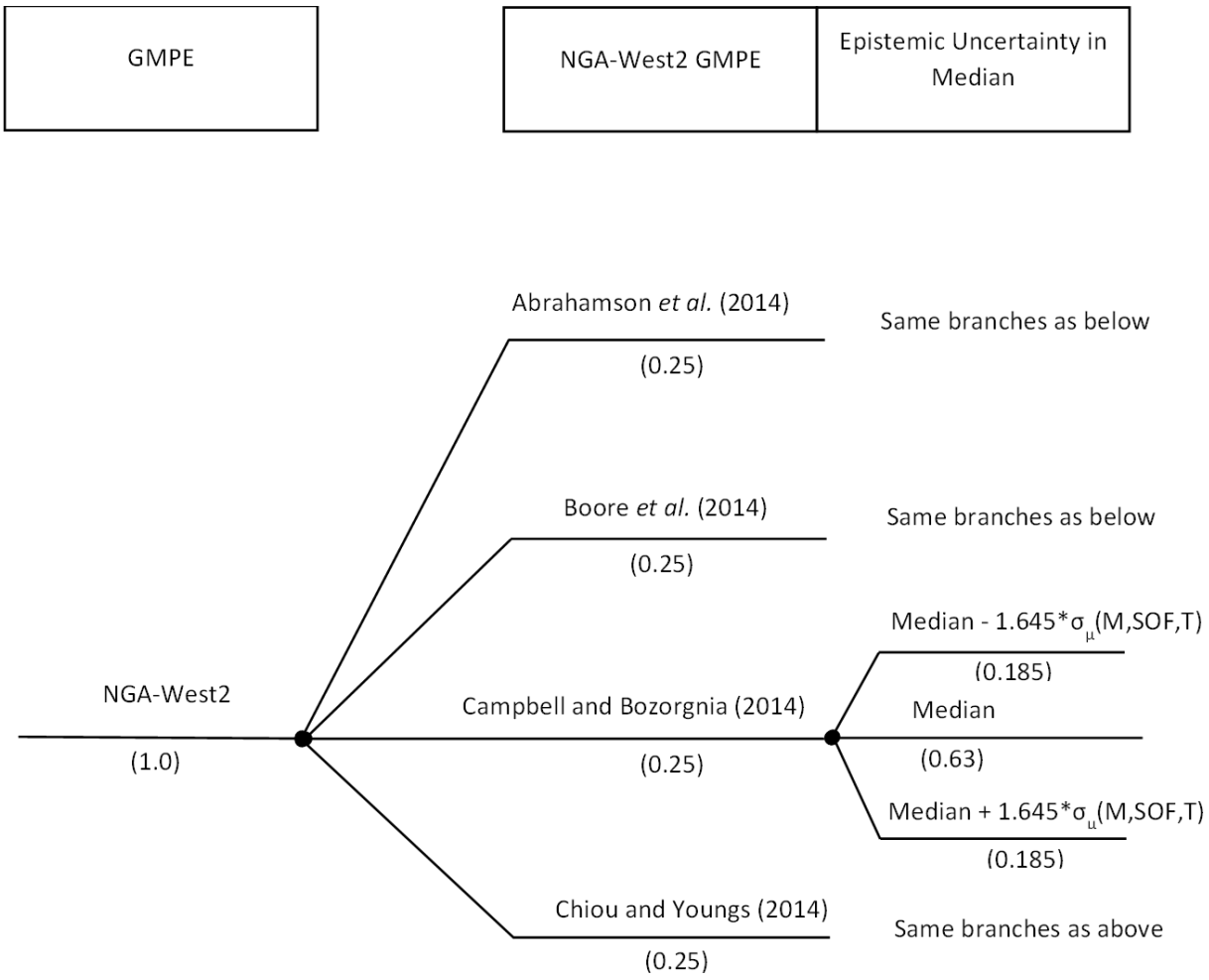

Figure 4-5. Logic tree for the median ground-motion model used in this study. σ refers to the additional epistemic uncertainty in LN units based on Al Atik and Youngs (2014). M refers to magnitude, SOF to style-of-faulting, and T to spectral period.

5. SITE CONDITIONS

The update of the PSHA and DSHA for the YDTI site is performed for the reference site class B/C with V_{S30} of 760 m/sec consistent with the 2016 study. For this reference site condition, basin depths to shear wave velocity horizons of 1 and 2.5 km/sec (Z1 and Z25), needed as input to the NGA-West2 GMPEs, are assigned based on the average empirical relationships between these depths and the V_{S30} value of 760 m/sec. Default Z1 and Z25 depths for V_{S30} of 760 m/sec are 0.045 and 0.607 km, respectively.

In addition to the reference site condition, the PSHA and DSHA are also performed for the site-specific condition at the YDTI site. Based on the recent site investigations at the Horseshoe Bend (HsB) area situated at the downstream embankment toe of the YDTI and documented in KP (2019 and 2020), a V_{S30} value of 420 m/sec is selected as representative of site-specific conditions at the YDTI site for this study update (KP 2021, personal communication). To estimate the corresponding Z1 and Z25 values, the V_S profiles obtained from the recent downhole seismic testing at boreholes DH18-03 and DH18-04 shown in Figure 5-1 are evaluated. These V_S profiles extended to a total depth of about 77 m and are shown in Figure 5-2. Both DH18-03 and DH18-04 V_S profiles encountered V_S greater than 1000 m/sec allowing for a site-specific estimate of Z1. The average site-specific estimate of Z1 from the two V_S profiles is 0.058 km and is listed in Table 5-1 along with the default Z1 value of 0.337 km for V_{S30} of 420 m/sec. A site-specific estimate of Z25 is not possible given that the measured V_S profiles did not encounter a V_S horizon of 2,500 m/sec. As a result, the site-specific Z1 of 0.058 km and the default Z25 estimate of 1.196 km are used in this study for V_{S30} of 420 m/sec. We note that the use of a site-specific Z1 that is shallower than the default value is expected to lead to a reduction of the median ground motion for periods greater than about 0.5 sec compared to the ground-motion prediction obtained using the default value Z1 for the ASK14, BSSA14, and CY14 GMPEs. The Z25 estimate is only used in the CB14 GMPE.

Table 5-1. Estimates of Z1 and Z25 values for V_{S30} of 420 and 760 m/sec for the YDTI site.

V_{S30} (m/sec)	Site-Specific Z1 (km)	Site-Specific Z25 (km)	Default Z1 (km)	Default Z25 (km)
420	0.058	-	0.337	1.196
760	-	-	0.045	0.607

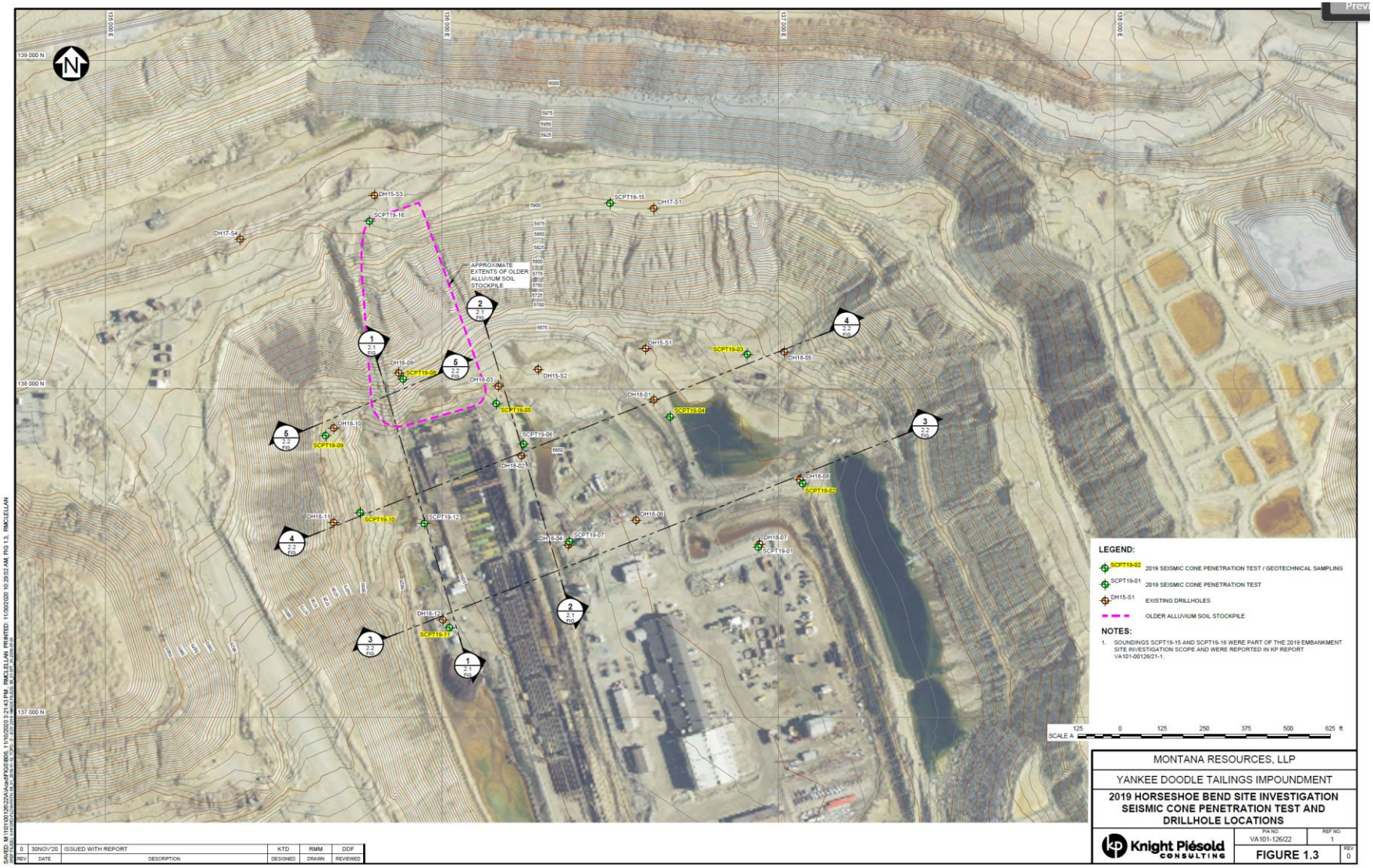

Figure 5-1. 2019 Horseshoe Bend site investigation seismic cone penetration test and drillhole locations (source: KP 2020)

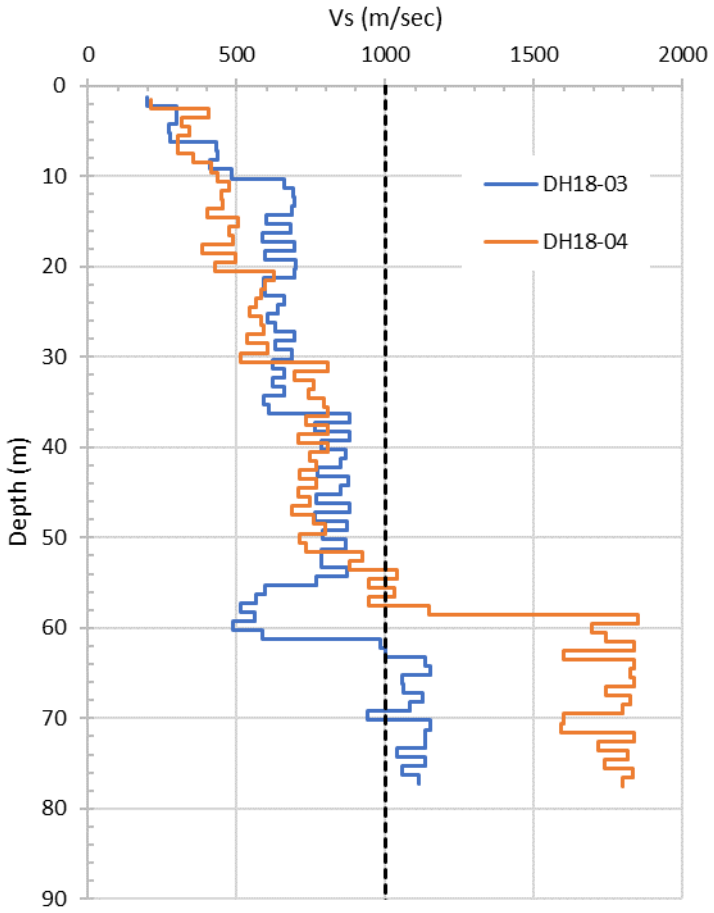

Figure 5-2. Measured V_S profiles from downhole seismic testing at DH18-03 and DH18-04 boreholes.

6. HAZARD RESULTS

Probabilistic and deterministic seismic hazard calculations are carried out using the computer program HAZ45.2 (Abrahamson and Gregor, 2015). This PSHA program follows a standard state of practice approach for probabilistic seismic hazard analysis given a seismic source model and a ground-motion model. A sigma truncation value of 8.0 is used for the PSHA and sources within a maximum distance of 300 km are included. The minimum magnitude used in the analysis is 5.0. Mean Hazard curves are computed for the following suite of spectral periods: PGA (0.01 sec), 0.02, 0.03, 0.04, 0.05, 0.075, 0.1, 0.15, 0.2, 0.25, 0.3, 0.4, 0.5, 0.75, 1.0, 1.5, 2.0, 3.0, 4.0, 5.0, 7.5 and 10.0 sec. Based on this suite of hazard curves, uniform hazard spectra (UHS) are computed for the suite of return periods of 475, 1,000, 2,475, and 10,000 years. Estimates of the mean magnitude, distance and epsilon values associated with the suite of return periods are also computed and presented for the site. Binned magnitude and distance contributions to the hazard for the suite of return periods are computed and presented below. Given the logic trees for the seismic sources and the ground-motion models, fractile hazard curves and fractile UHS are computed and presented below. These fractile curves allow for an evaluation of the uncertainty in the mean hazard results based on the epistemic uncertainty characterization of the seismic source and ground-motion models.

Given the changes in the source characterization of the seismicity-based background model, the Continental, and the Rocker faults as well as the changes in the GMC model compared to the 2016 study, we first present a sensitivity analysis showing the incremental impact of these changes on the PSHA results. This is followed by a presentation of the PSHA and DSHA results and comparisons for this study update.

6.1 Probabilistic Seismic Hazard Sensitivity Analyses

Using the GMC model of Al Atik and Gregor (2016) shown in Figure 2-1, probabilistic seismic hazard calculations are performed for the updated source model presented in Section 3 of this report. This sensitivity analysis allows for an evaluation of the isolated impact of the updates to the SSC model on the PSHA results. These updates involve the characterization of the seismicity-based background model, the Continental, and the Rocker faults. Figure 6-1 presents the hazard results from this run compared to the Al Atik and Gregor (2016) PSHA results for the gridded seismicity, Continental, and Rocker faults as well as for the total hazard at PGA and periods of 0.2, 1, and 3 sec for V_{S30} of 760 m/sec.

Using the 2016 GMC model, Figure 6-1 indicates a reduction in the hazard results for the updated seismicity-based background source compared to the 2016 background source at PGA and periods of 0.2, 1, and 3 sec. This is supported by the observed reduction in the 2018 NSHMs results at the YDTI site compared to the 2014 NSHMs results. The update of the Rocker fault characterization leads to a reduction in the hazard results at PGA and periods of 0.2, 1, and 3 sec compared to the 2016 results for this fault. This reduction in the hazard for the Rocker fault does not lead to a noticeable change in the total hazard at the YDTI site due to the low contribution from the Rocker fault to the hazard at the site. The updated characterization of the Continental-Elk Park fault leads to an expected increase in the hazard from this fault at the site compared to the 2016 results for this fault as shown in Figure 6-1.

The change in the total hazard due to the update of the SSC model compared to the 2016 model is also shown in Figure 6-1 and is represented by a decrease in the hazard at short return periods (large annual probability of exceedance) and an increase at long return periods (low annual probability of exceedance). The decrease in the hazard at short return periods is driven by the update to the seismicity-based background source while the increase at long return periods is driven by the update to the Continental fault characterization. Figure 6-2 shows the ratio of the UHS obtained using the updated SSC model with the 2016 GMC model to the UHS from Al Atik and Gregor (2016) for periods of 0.01 (PGA), 0.2, 1, and 3 sec for return periods of 475, 1,000, 2,475, 5,000, and 10,000 years. For the short return periods of 475 and 1,000 years, Figure 6-2 shows a reduction in the UHS on the order of 2 to 10% at periods of 0.01 to 3 sec due to the update of the SSC model. For return periods of 1,000 to 10,000 years, Figure 6-2 shows an increase in the UHS on the order of 2 to 16% as a result of the updated SSC model.

Next, we evaluate the impact of updating the GMC model from the 2016 model shown in Figure 2-1 to the one used for this study update shown in Figure 4-5. For this sensitivity analysis, we use the updated SSC model and we run the analysis for V_{S30} of 760 m/sec. Figure 6-3 shows the comparison of total hazard results as well as results by source type for PGA and spectral periods of 0.2, 1, and 3 sec based on the change in the GMC model. This figure indicates an increase in the hazard results at PGA and periods of 0.2 and 1 sec due to the use of the 4 NGA-West2 GMPEs compared to the 5 NGA-West2 models and Wea05. At period of 3 sec, a reduction in the hazard is observed with the updated GMC model. Figure 6-4 shows the ratio of the UHS obtained using the updated GMC model relative to the 2006 GMC model at spectral periods of 0.01 (PGA), 0.2, 1, and 3 sec and for return periods of 475, 1,000, 2,475, 5,000, and 10,000 years. As observed in the comparison of the hazard curves, Figure 6-4 indicates that, for V_{S30} of 760 m/sec, the UHS values are larger using the updated GMC model compared to the 2006 GMC models at short spectral periods. This increase is on the order of 6 to 18% for the 475-year return period and 5 to 11% for the 10,000-year return period. At the spectral period of 3 sec, a reduction in the UHS of about 16% is observed.

Finally, a comparison of the hazard results at the YDTI site obtained using the updated SSC and GMC models for V_{S30} of 760 m/sec to the results in the Al Atik and Gregor (2016) study are shown in Figure 6-5 for PGA and spectral periods of 0.2, 1, and 3 sec. This figure reflects the combined impact of updating the SSC and GMC models compared to the 2016 study results. This update leads to a general increase in the total hazard at PGA and spectral periods of 0.2 and 1 sec. At period of 3 sec, the study update leads to a reduction in the total hazard compared to the results from the 2016 study. Figure 6-6 shows the ratio of the UHS obtained using the updated SSC and GMC models to the UHS of the 2016 study for V_{S30} of 760 m/sec. For short spectral periods ≤ 1 sec, Figure 6-6 shows an increase in the UHS for this study update. This increase is ≤ 6% for the 475-year return period and on the order of 20 to 24% for the 10,000-year return period. At the long return period of 10,000 years, this increase is due to the increase in the hazard due to the update of both SSC and GMC models. At the spectral period of 3 sec, the study update shows a decrease in the UHS on the order of 4% for 10,000-year return period to 19% for the 475-year return period.

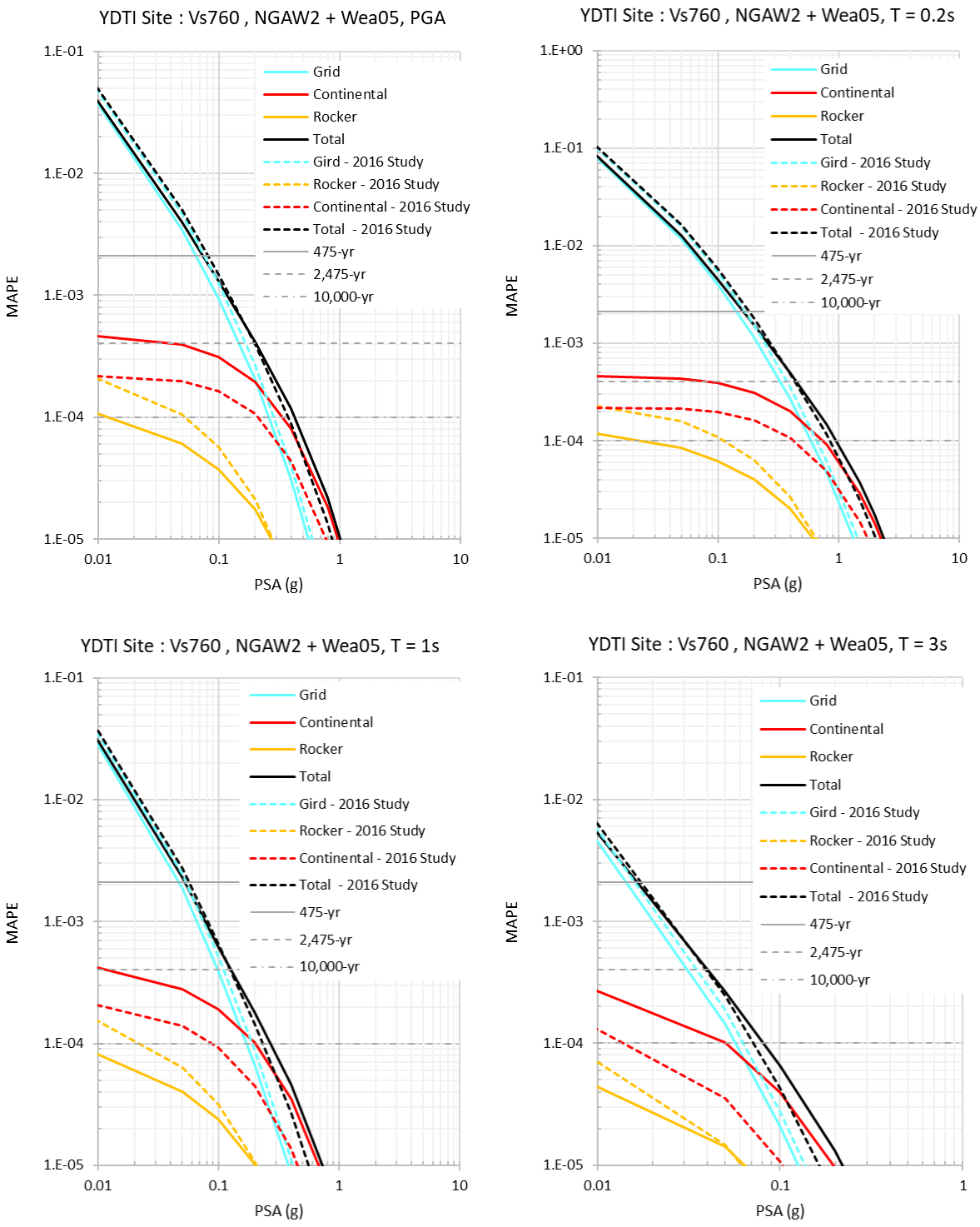

Figure 6-1. Comparison of mean annual probability of exceedance by source type at PGA (top left) and periods of 0.2 sec (top right), 1 sec (bottom left), and 3 sec (bottom right) using the updated SSC model and the GMC model of Al Atik and Gregor (2016) compared to results from the 2016 study for V_{S30} of 760 m/sec. Solid lines are for the updated SSC model and dashed lines are for the PSHA results of Al Atik and Gregor (2016).

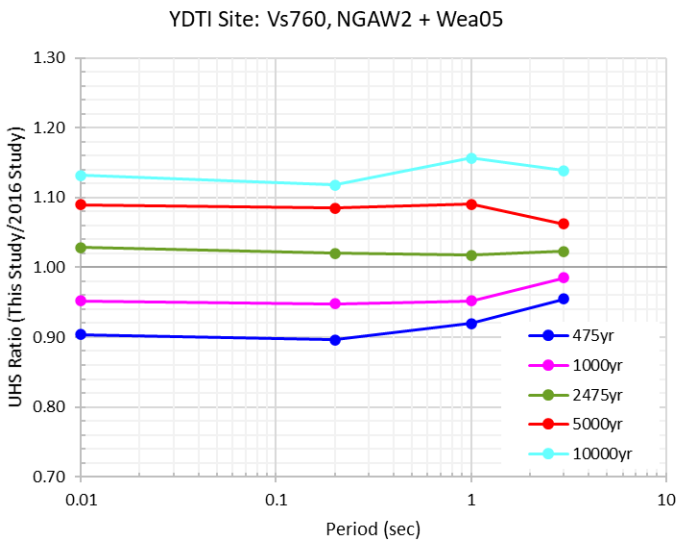

Figure 6-2. Ratio of UHS at periods of 0.01 (PGA), 0.2, 1, and 3 sec obtained using the updated SSC model and the GMC model of Al Atik and Gregor (2016) to the UHS from the 2016 study for V_{S30} of 760 m/sec.

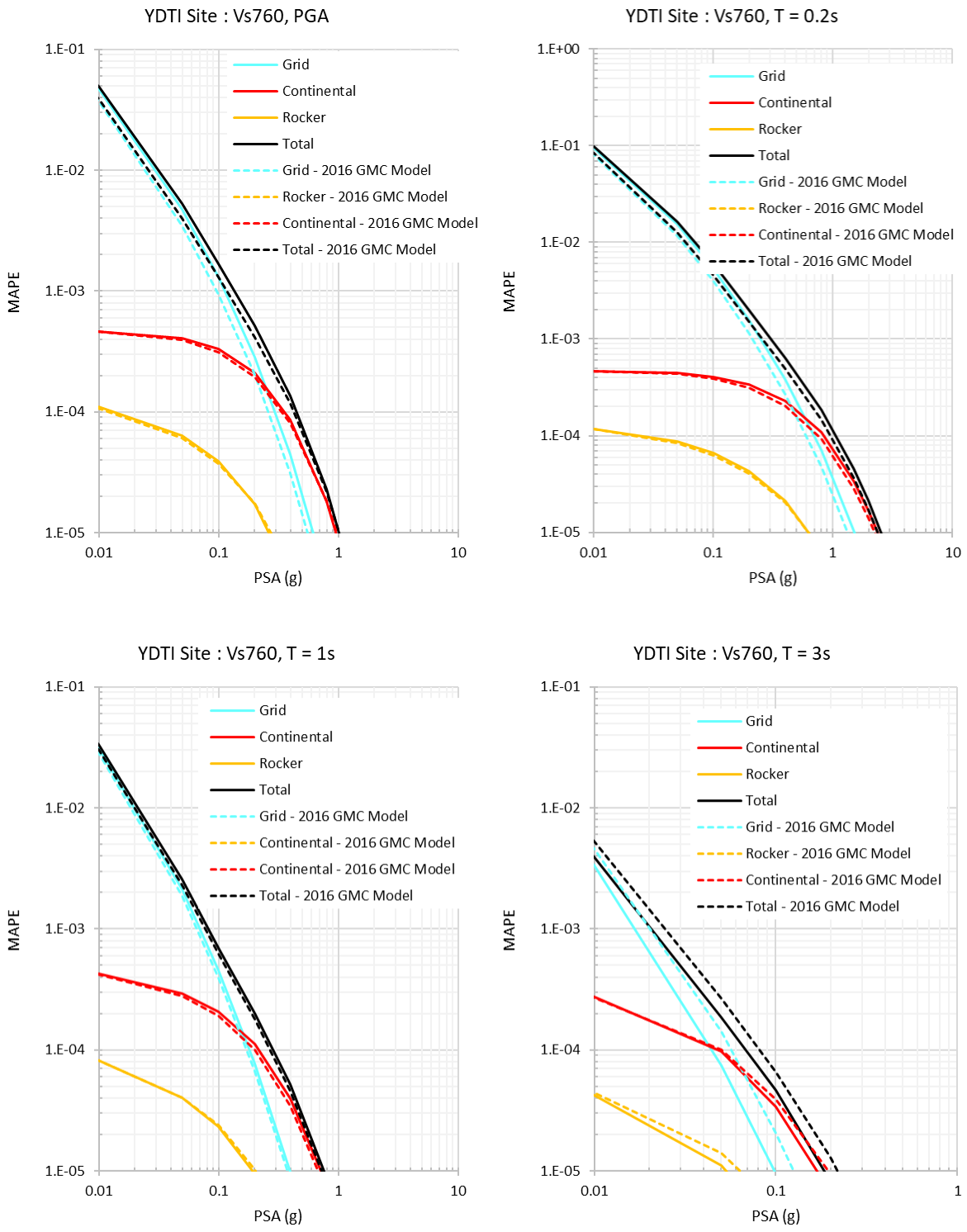

Figure 6-3. Comparison of mean annual probability of exceedance by source type at PGA (top left) and periods of 0.2 sec (top right), 1 sec (bottom left), and 3 sec (bottom right) using the updated GMC model compared to the GMC model of Al Atik and Gregor (2016) for the updated SSC model and for V_{S30} of 760 m/sec. Solid lines are for the updated GMC model and dashed lines are for the Al Atik and Gregor (2016) GMC model.

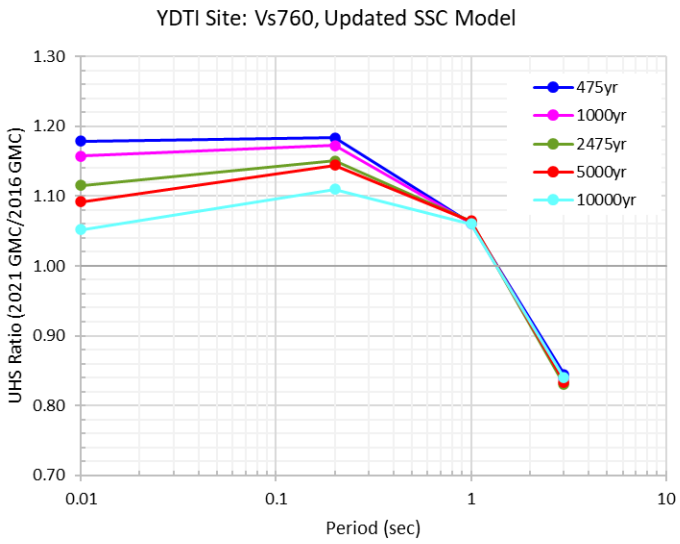

Figure 6-4. Ratio of UHS at periods of 0.01 (PGA), 0.2, 1, and 3 sec obtained using the updated GMC model and to the UHS obtained using the Al Atik and Gregor (2016) GMC model for the updated SSC model and for V_{S30} of 760 m/sec.

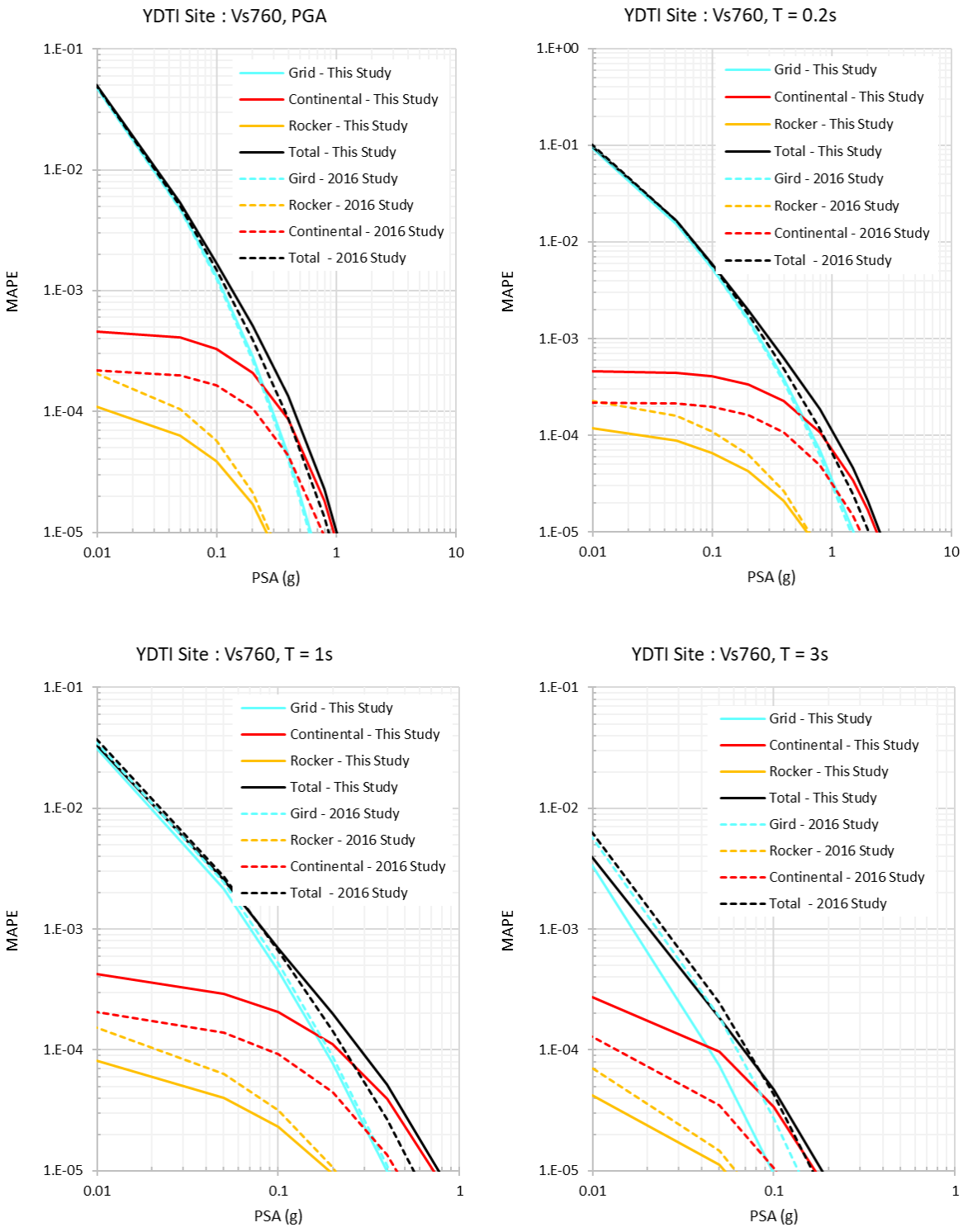

Figure 6-5. Comparison of mean annual probability of exceedance by source type at PGA (top left) and periods of 0.2 sec (top right), 1 sec (bottom left), and 3 sec (bottom right) for this study update (solid lines) compared to the Atik and Gregor (2016) results (dashed lines) for V_{S30} of 760 m/sec.

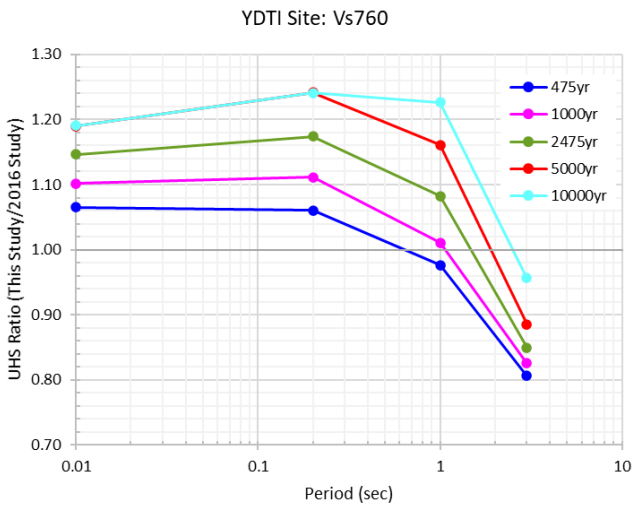

Figure 6-6. Ratio of UHS at periods of 0.01 (PGA), 0.2, 1, and 3 sec from this study to the UHS from Al Atik and Gregor (2016) for V_{S30} of 760 m/sec.

6.2 PSHA Results

Probabilistic mean hazard curves from this study update are shown in Figure 6-7 for PGA and spectral periods of 0.2, 1, and 3 sec for the YDTI site for V_{S30} of 760 m/sec. The hazard curves are shown by source type for the important sources controlling the hazard at the site. Figure 6-7 indicates that the seismicity-based background source controls the hazard for return periods less than 2,475 years at all spectral periods shown. For return periods greater than 2,475 years, the Continental-Elk Park fault (also referred to as Continental fault) become the dominant contributor to the hazard at the 4 spectral periods shown. For the seismicity-based background source, Figure 6-7 shows the total hazard from the gridded seismicity as well as the hazard from the extensional and compressional regime sources that make up the total hazard from the gridded seismicity. Figure 6-7 indicates that the extensional regime source is the largest contributor to the hazard from the gridded seismicity with a negligible contribution from the compressional regime source type. Similarly, the total hazard from the Continental-Elk Park fault is shown in Figure 6-7 along with the hazard from Rupture Models A and B that make up the total hazard from this fault. Figure 6-7 indicates that the Rupture Model A is a biggest contributor to the total hazard from the Continental fault with a negligible contribution from the linked Rupture Model B sources. This is expected given the 80% and 20% weights assigned to Rupture Models A and B, respectively. Finally, Figure 6-7 show a minor contribution to the hazard from the Rocker fault.

Given the hazard curves for the full suite of spectral periods, the computed uniform hazard spectra (UHS) for the YDTI site at return periods of 475, 1,000, 2,475, and 10,000-year return periods are listed in Table 6-1 and shown in Figure 6-8 in log-linear and log-log scales for V_{S30} of 760 m/sec. The dominant scenarios characterized in terms of the mean magnitude, distance, and number of standard deviations of ground motion (epsilon) are shown in Figure 6-9 and listed in Tables 6-2 to 6-4 for return periods of 475, 1,000, 2,475, and 10,000 years and for V_{S30} of 760 m/sec. As expected, Figure 6-9 indicates that the mean magnitude increases and the mean distance decreases with the increasing return period hazard level. For the ground motion at periods greater than 1 sec, Figure 6-9 shows that the mean magnitude

(**M** 6.6 to 7.0) is larger than that at shorter periods and the mean distance also increases compared to the shorter spectral periods. Mean epsilon increases with the increasing return period level but is generally below 1.

The binned magnitude and distance contributions to the 475-year hazard level are shown in Figure 6-10 for the YDTI site for PGA and spectral periods of 0.2, 1.0, and 3.0 sec. Similar plots are shown in Figure 6-11 to 6-13 for the 1,000, 2,475, and 10,000-year return periods, respectively. At PGA and spectral period of 0.2 sec, the 475 and 1,000-year deaggregation plots show that the background sources in the distance range of 10 – 50 km and magnitude range of 5.0 – 6.5 are the controlling sources of the hazard at the site. At spectral periods of 1 and 3 sec, the 475 and 1,000-year deaggregation plots show a more diffuse distribution of significant contribution from the background sources over the distance range of 10 – 150 km and magnitudes 6.0 to 7.5. For the 2,475-year return period and at PGA and period of 0.2 sec, the controlling distance is less than 30 km and controlling magnitude is in the range 5 to 7.5 reflecting contributions from both the background source and the Continental-Elk Park fault. The controlling magnitude range shifts to 6.0 to 7.5 for the longer spectral periods at the 2,475-year return period. For the 10,000-year return period, the controlling magnitude range is **M** 6.0 – 7.0 and distance less than 10 km at all spectral periods shown, reflecting the strong contribution from the Continental-Elk Park fault at this return period.

Table 6-1. Horizontal mean UHS for 5% damping for the YDTI site for V_{S30} of 760 m/sec.

Period (sec)	475-yr PSA (g)	1000-yr PSA (g)	2,475yr PSA (g)	10,000-yr PSA (g)
0.01/PGA	0.0876	0.1359	0.2276	0.4514
0.02	0.0898	0.1397	0.2345	0.4690
0.03	0.0995	0.1552	0.2616	0.5315
0.04	0.1132	0.1775	0.3006	0.6072
0.05	0.1270	0.1998	0.3399	0.6856
0.075	0.1612	0.2555	0.4349	0.8905
0.1	0.1831	0.2906	0.4961	1.0029
0.15	0.1986	0.3155	0.5414	1.1012
0.2	0.1923	0.3035	0.5211	1.0632
0.25	0.1765	0.2756	0.4688	0.9636
0.3	0.1598	0.2469	0.4160	0.8666
0.4	0.1312	0.1995	0.3324	0.6864
0.5	0.1116	0.1679	0.2775	0.5748
0.75	0.0776	0.1155	0.1894	0.3986
1	0.0553	0.0822	0.1346	0.2872
1.5	0.0346	0.0509	0.0820	0.1721
2	0.0242	0.0357	0.0573	0.1192
3	0.0139	0.0205	0.0328	0.0684
4	0.0092	0.0136	0.0217	0.0449
5	0.0066	0.0098	0.0158	0.0322
7.5	0.0037	0.0055	0.0087	0.0166
10	0.0024	0.0036	0.0058	0.0109

Table 6-2. Mean magnitude for the YDTI site for V_{S30} of 760 m/sec for return periods of 475, 1,000, 2,475, and 10,000-year return period.

	Mean Magnitude			
Period (sec)	**475-yr**	**1000-yr**	**2,475yr**	**10,000-yr**
0.01/PGA	6.16	6.19	6.26	6.38
0.02	6.15	6.18	6.26	6.38
0.03	6.14	6.17	6.24	6.38
0.04	6.11	6.15	6.23	6.36
0.05	6.10	6.14	6.22	6.35
0.075	6.08	6.12	6.20	6.34
0.1	6.08	6.12	6.20	6.34
0.15	6.12	6.16	6.25	6.36
0.2	6.16	6.21	6.29	6.40
0.25	6.22	6.26	6.33	6.44
0.3	6.26	6.30	6.36	6.47
0.4	6.36	6.39	6.43	6.51
0.5	6.44	6.46	6.48	6.55
0.75	6.55	6.56	6.57	6.59
1	6.60	6.62	6.62	6.62
1.5	6.71	6.72	6.70	6.68
2	6.77	6.78	6.76	6.72
3	6.84	6.85	6.82	6.77
4	6.89	6.89	6.87	6.81
5	6.92	6.92	6.90	6.85
7.5	6.99	7.02	7.02	6.99
10	7.03	7.06	7.07	7.07

Table 6-3. Mean distance (km) for the YDTI site for V_{S30} of 760 m/sec for return periods of 475, 1,000, 2,475, and 10,000-year return period.

	Mean Distance (km)			
Period (sec)	**475-yr**	**1000-yr**	**2,475yr**	**10,000-yr**
0.01/PGA	38.65	26.93	16.96	9.41
0.02	38.46	26.86	16.97	9.21
0.03	38.00	26.72	16.85	8.59
0.04	37.12	26.21	16.37	8.71
0.05	35.92	25.33	15.70	8.86
0.075	36.24	25.79	16.59	8.73
0.1	35.96	25.75	16.47	9.26
0.15	36.55	25.62	16.45	9.60
0.2	38.50	27.17	17.09	9.81
0.25	41.49	30.10	19.02	10.00
0.3	45.15	32.64	20.49	9.76
0.4	52.77	37.73	23.07	11.32
0.5	58.70	43.42	26.92	11.92
0.75	68.50	51.48	31.47	13.09
1	74.63	55.25	33.57	13.85
1.5	85.30	64.88	40.31	16.55
2	91.08	71.34	46.22	17.99
3	97.85	76.95	49.82	19.83
4	101.19	80.63	53.99	21.72
5	102.86	83.33	57.32	24.73
7.5	114.51	97.38	75.47	45.39
10	121.87	107.80	88.79	62.21

Table 6-4. Mean number of standard deviations of ground motion (Epsilon) for the YDTI site for V_{S30} of 760 m/sec for return periods of 475, 1,000, 2,475, and 10,000-year return period.

	Mean Epsilon			
Period (sec)	**475-yr**	**1000-yr**	**2,475yr**	**10,000-yr**
0.01/PGA	0.18	0.24	0.39	0.82
0.02	0.17	0.23	0.38	0.81
0.03	0.18	0.25	0.39	0.82
0.04	0.20	0.26	0.41	0.82
0.05	0.22	0.29	0.43	0.84
0.075	0.25	0.33	0.49	0.93
0.1	0.26	0.34	0.51	0.93
0.15	0.24	0.31	0.46	0.89
0.2	0.24	0.29	0.43	0.86
0.25	0.27	0.31	0.43	0.84
0.3	0.32	0.35	0.45	0.84
0.4	0.40	0.42	0.47	0.81
0.5	0.48	0.48	0.52	0.82
0.75	0.58	0.57	0.56	0.79
1	0.60	0.60	0.56	0.78
1.5	0.65	0.67	0.63	0.80
2	0.65	0.68	0.67	0.81
3	0.63	0.68	0.66	0.78
4	0.58	0.65	0.65	0.78
5	0.56	0.63	0.66	0.81
7.5	0.51	0.66	0.80	1.04
10	0.41	0.61	0.81	1.10

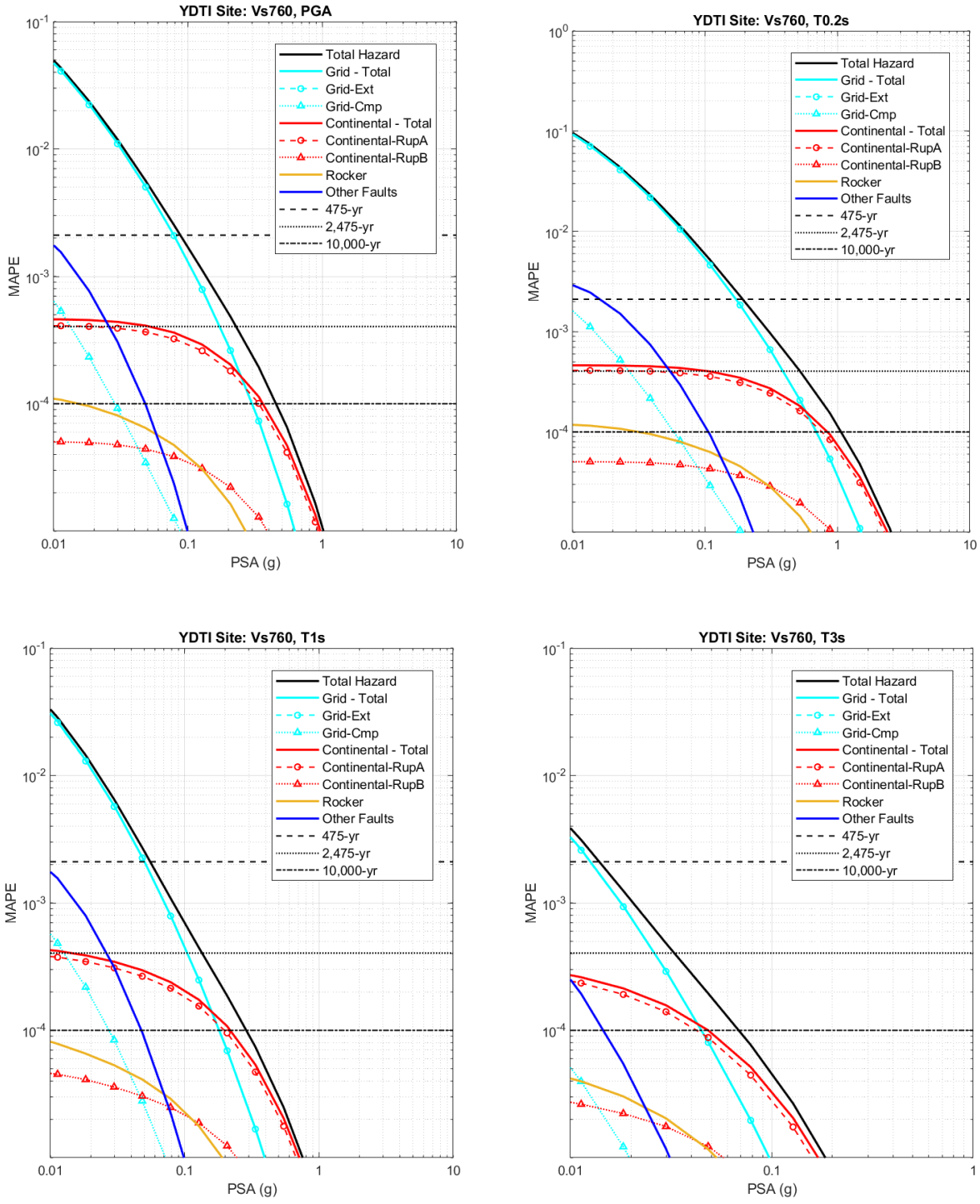

Figure 6-7. Mean annual probability of exceedance by source type at PGA (top left) and periods of 0.2 sec (top right), 1 sec (bottom left), and 3 sec (bottom right) for this study update for V_{S30} of 760 m/sec.

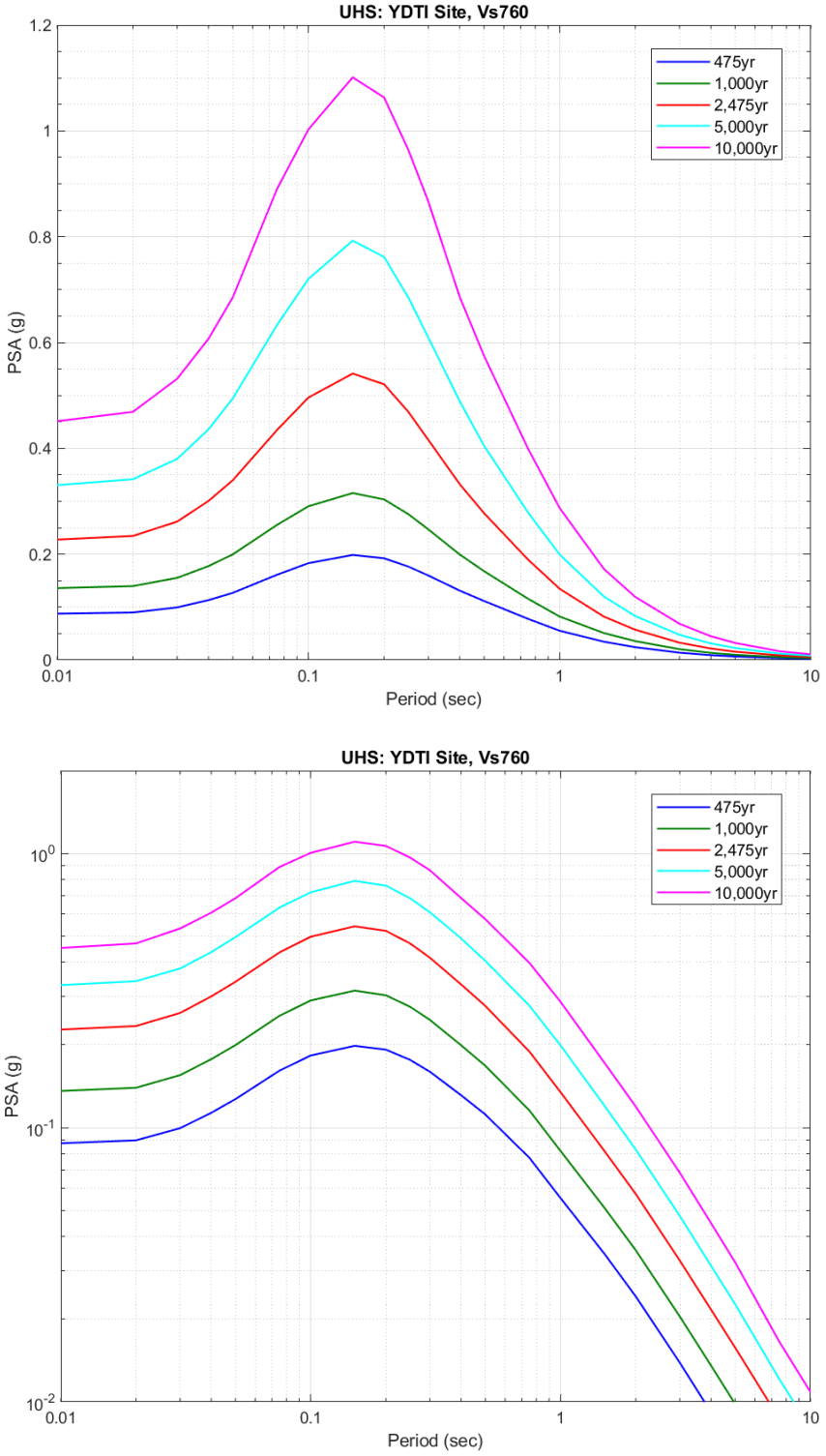

Figure 6-8. Uniform mean hazard spectra for the YDTI site in log-linear scale (top) and log-log scale (bottom) for V_{S30} of 760 m/sec.

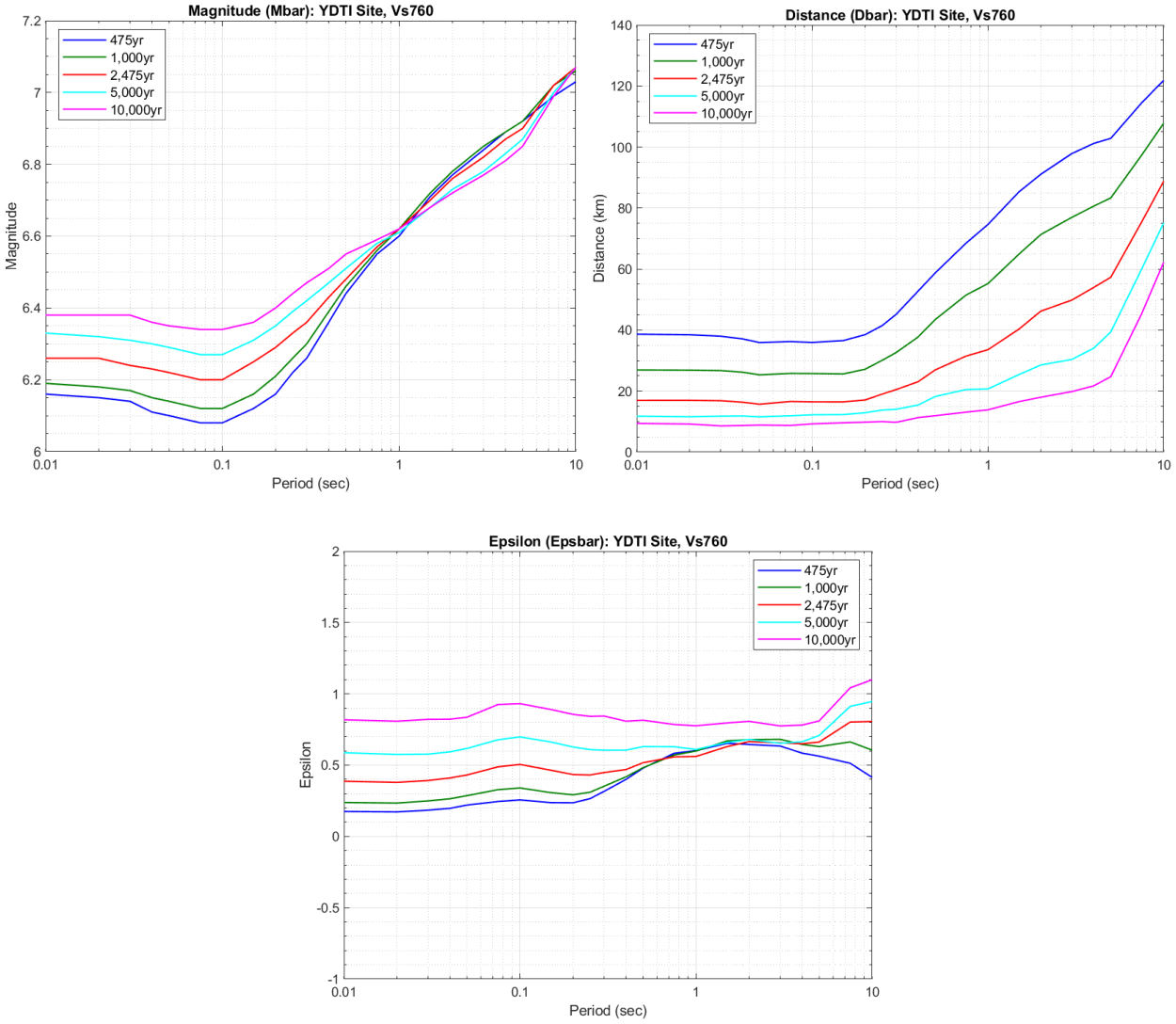

Figure 6-9. Mean magnitude (top left), distance (km) (top right), and epsilon (bottom) for the YDTI site for V_{S30} of 760 m/sec.

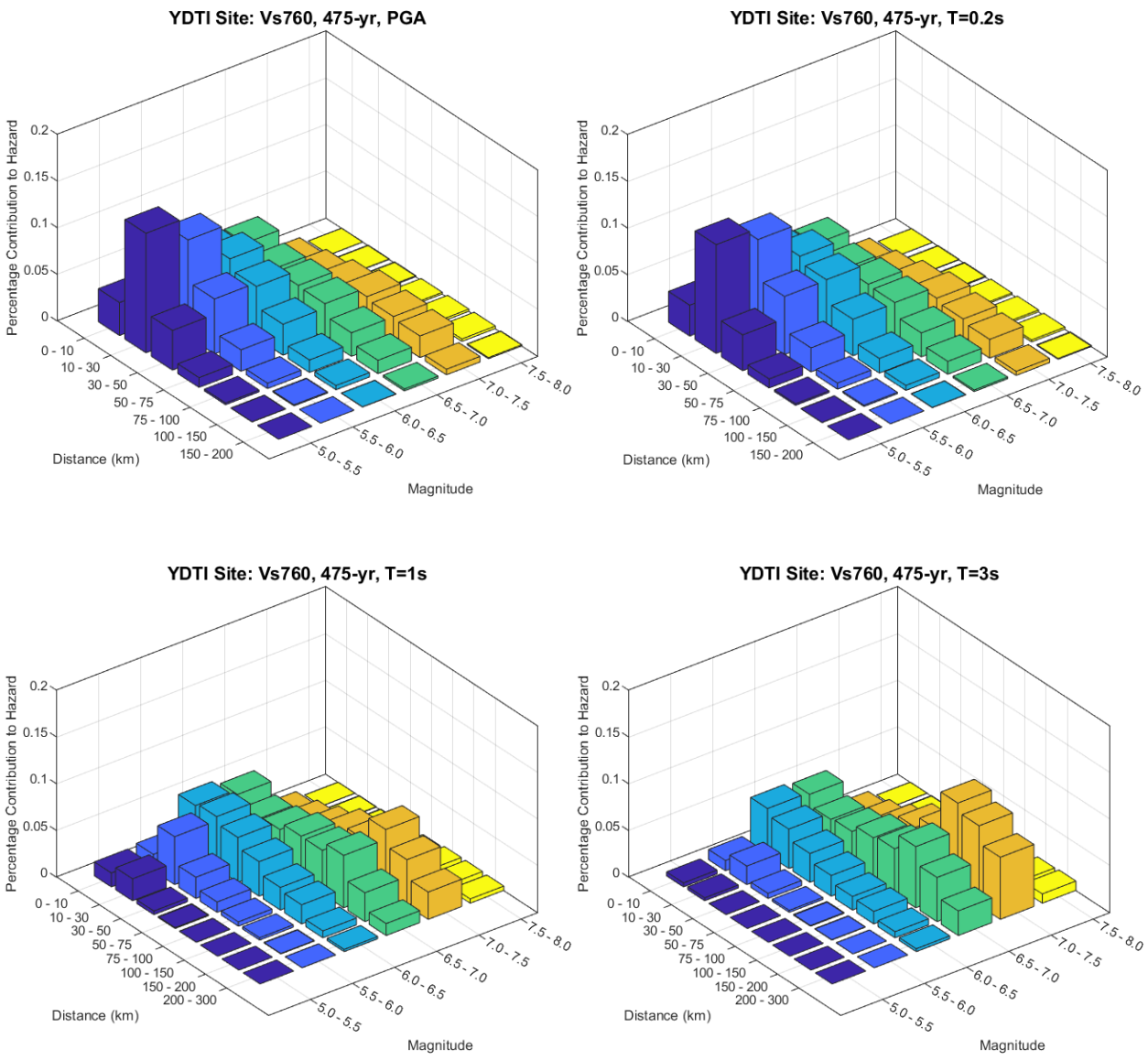

Figure 6-10. Magnitude-distance contribution to the 475-year return period hazard at PGA (top left) and periods of 0.2 sec (top right), 1 sec (bottom left), 3 sec (bottom right) for the YDTI for V_{S30} of 760 m/sec.

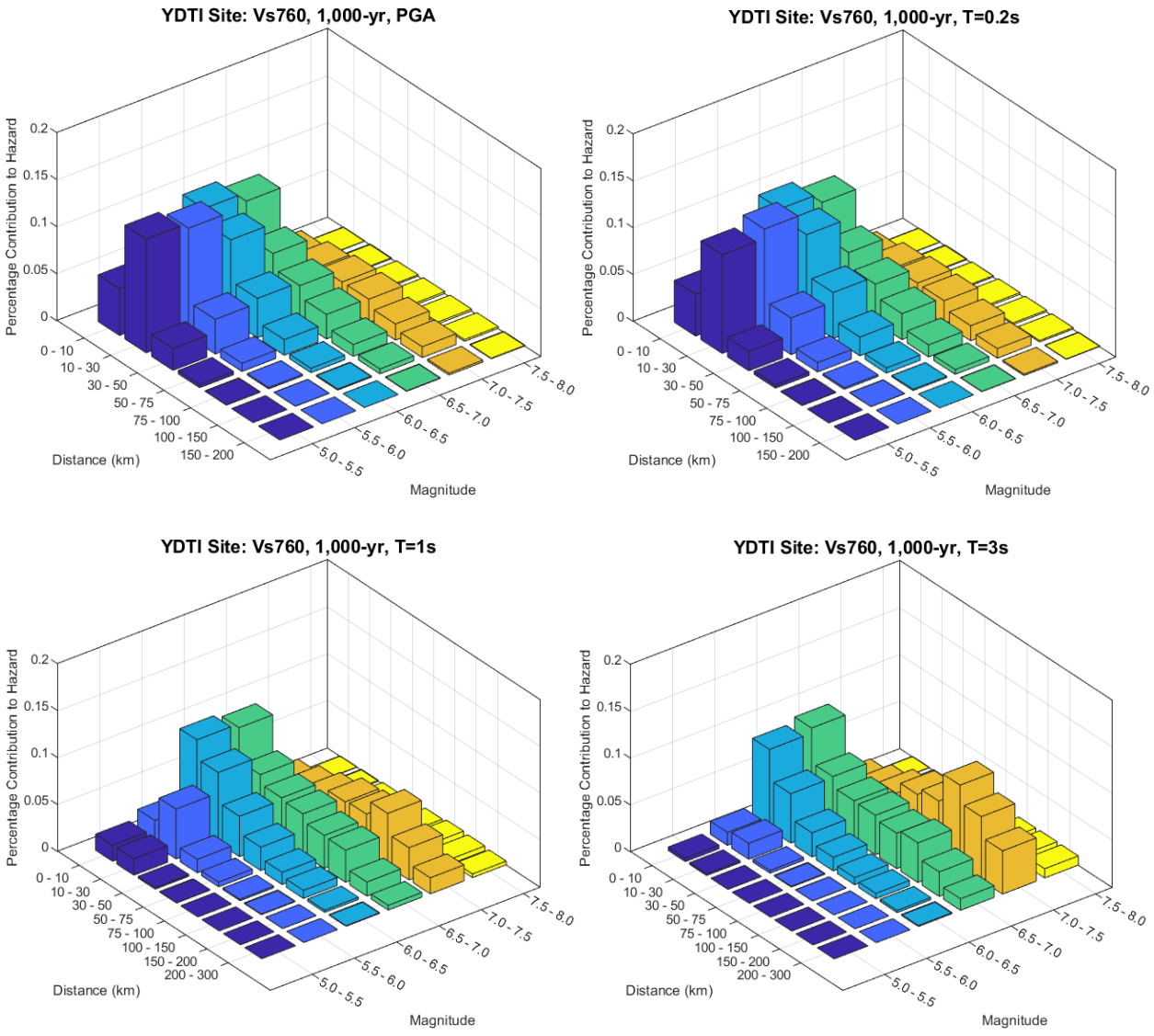

Figure 6-11. Magnitude-distance contribution to the 1,000-year return period hazard at PGA (top left) and periods of 0.2 sec (top right), 1 sec (bottom left), 3 sec (bottom right) for the YDTI for V_{S30} of 760 m/sec.

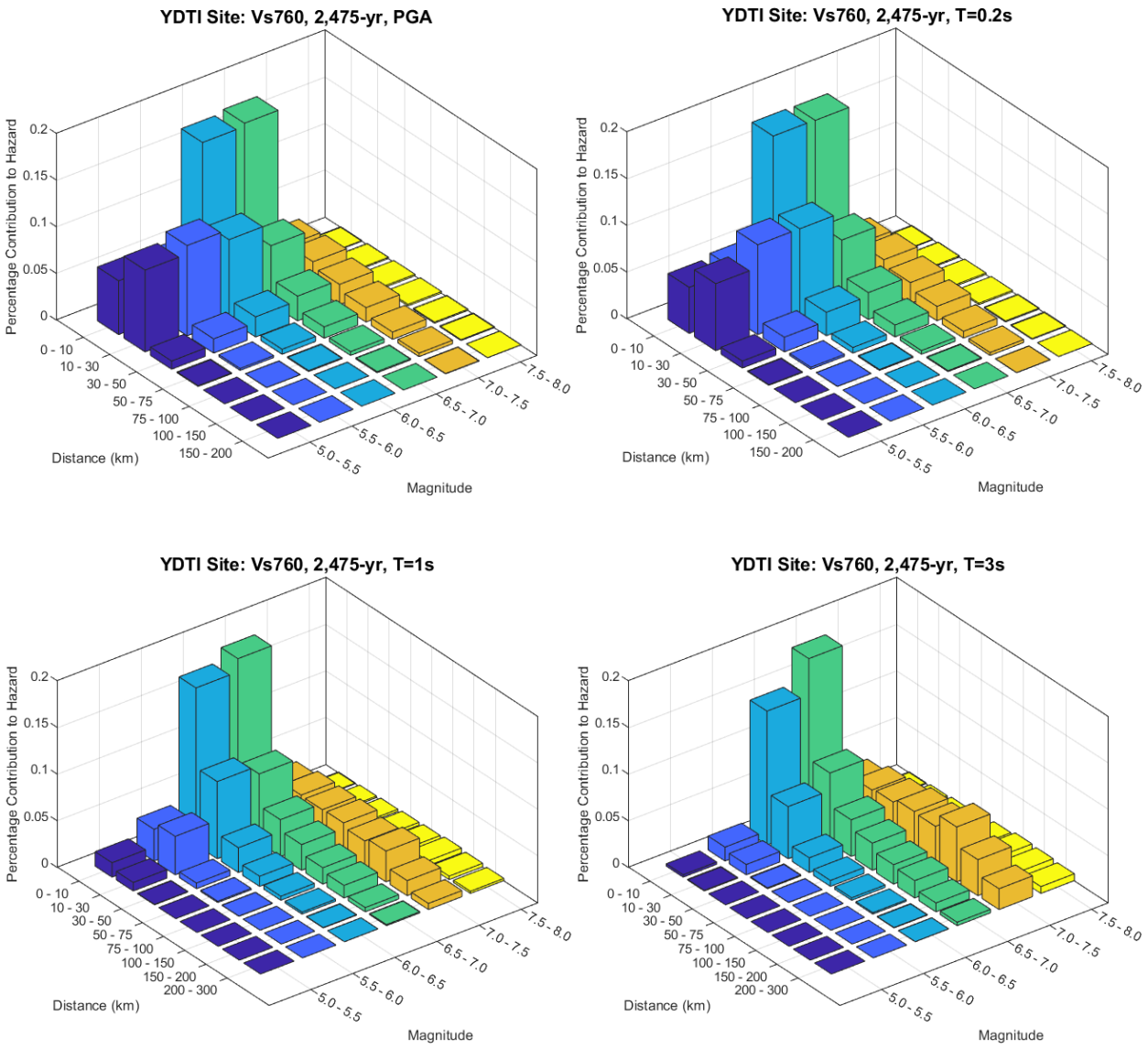

Figure 6-12. Magnitude-distance contribution to the 2,475-year return period hazard at PGA (top left) and periods of 0.2 sec (top right), 1 sec (bottom left), 3 sec (bottom right) for the YDTI for V_{S30} of 760 m/sec.

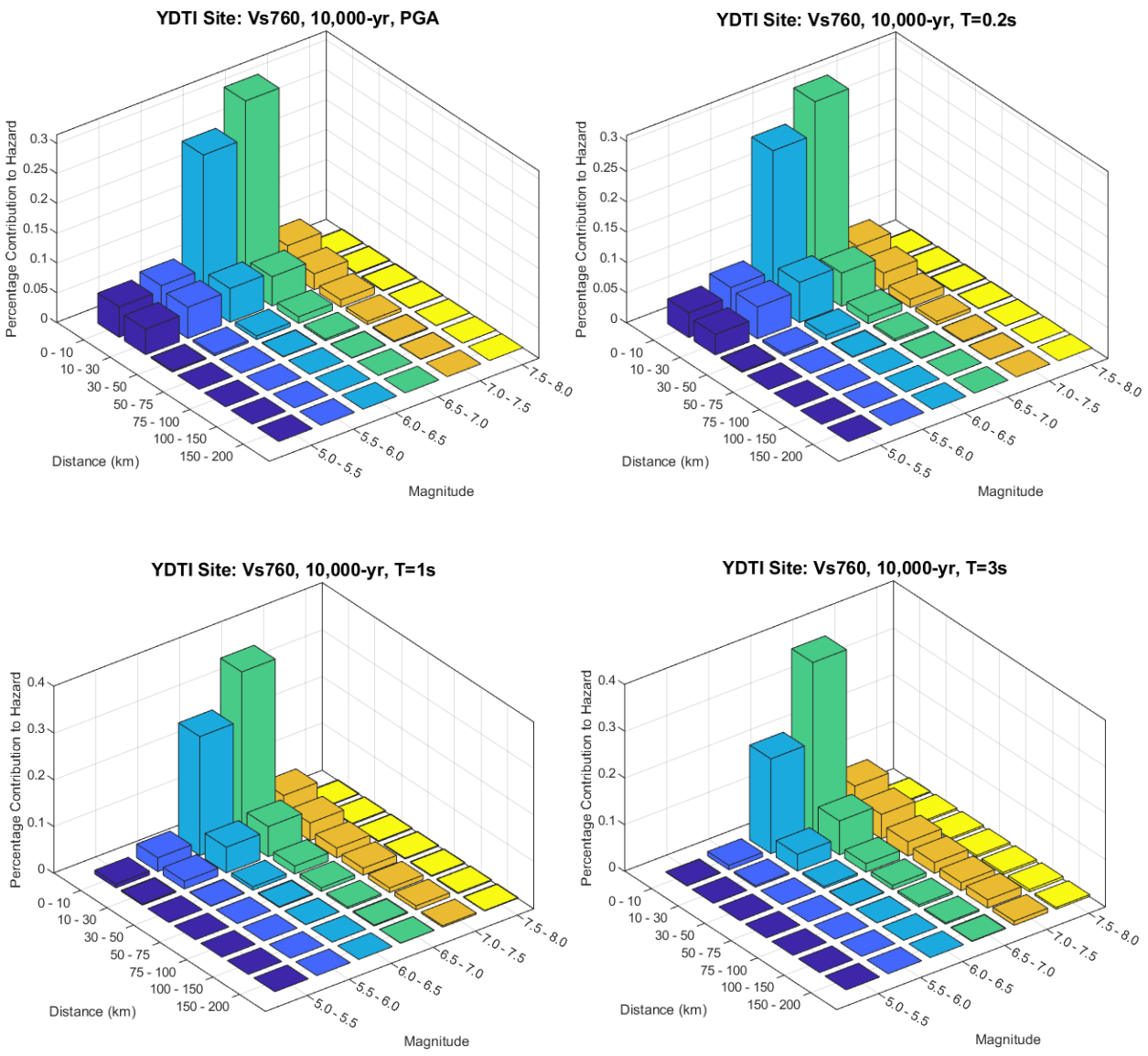

Figure 6-13. Magnitude-distance contribution to the 10,000-year return period hazard at PGA (top left) and periods of 0.2 sec (top right), 1 sec (bottom left), 3 sec (bottom right) for the YDTI for V_{S30} of 760 m/sec.

Similar sets of plots are shown for the site-specific condition (i.e., V_{S30} of 420 m/sec) to those for the reference site condition with V_{S30} of 760 m/sec. Figure 6-14 shows the hazard by source type for the YDTI site for V_{S30} of 420 m/sec for PGA and spectral periods of 0.2, 1, and 3 sec. Similar to the reference site condition with V_{S30} of 760 m/sec, Figure 6-14 indicates that the seismicity-based background source controls the hazard for return periods less than 2,475 years at all spectral periods shown. For return periods greater than 2,475 years, the Continental fault become the dominant contributor to the hazard at the 4 spectral periods shown. UHS curves are computed for V_{S30} of 420 m/sec and shown in Figure 6-15 in log-linear and log-log scales and their values are listed in Table 6-5 for return periods of 475, 1,000, 2,475, and 10,000-year return periods.

The mean magnitude, distance, and number of standard deviations of ground motion (epsilon) are shown in Figure 6-16 and listed in Tables 6-6 to 6.8 for return periods of 475, 1,000, 2,475, and 10,000 years and for V_{S30} of 420 m/sec. As expected, Figure 6-16 indicates that the mean magnitude increases and the mean distance decreases with the increasing return period hazard level. Mean epsilon increases with the increasing return period level but is generally below 1 similar to the trend observed for the reference V_{S30} of 760 m/sec.

The binned magnitude and distance contributions to the 475, 1,000, 2,475, and 10,000-year return periods are shown in Figures 6-17 to 6-20, respectively, for the YDTI site for V_{S30} of 420 m/sec and for PGA and spectral periods of 0.2, 1.0, and 3.0 sec. Similar trends and observations on the controlling magnitude and distance ranges for the different return periods and spectral periods can be made on these deaggregation plots as those observed for V_{S30} of 760 m/sec.

Table 6-5. Horizontal mean UHS for 5% damping for the YDTI site for V_{S30} of 420 m/sec.

Period (sec)	475-yr PSA (g)	1000-yr PSA (g)	2,475yr PSA (g)	10,000-yr PSA (g)
0.01/PGA	0.1120	0.1709	0.2783	0.5311
0.02	0.1137	0.1739	0.2839	0.5447
0.03	0.1216	0.1863	0.3043	0.5772
0.04	0.1344	0.2066	0.3376	0.6319
0.05	0.1473	0.2263	0.3682	0.6914
0.075	0.1869	0.2868	0.4638	0.8722
0.1	0.2213	0.3401	0.5494	1.0076
0.15	0.2616	0.4009	0.6463	1.1949
0.2	0.2743	0.4211	0.6853	1.2992
0.25	0.2690	0.4122	0.6754	1.3094
0.3	0.2509	0.3825	0.6288	1.2412
0.4	0.2122	0.3196	0.5251	1.0489
0.5	0.1822	0.2720	0.4445	0.9091
0.75	0.1274	0.1883	0.3068	0.6436
1	0.0899	0.1326	0.2160	0.4612
1.5	0.0547	0.0800	0.1282	0.2686
2	0.0362	0.0532	0.0849	0.1778
3	0.0201	0.0296	0.0474	0.0997
4	0.0128	0.0190	0.0304	0.0632
5	0.0089	0.0132	0.0213	0.0441
7.5	0.0047	0.0071	0.0112	0.0217
10	0.0030	0.0046	0.0073	0.0140

Table 6-6. Mean magnitude for the YDTI site for V_{S30} of 420 m/sec for return periods of 475, 1,000, 2,475, and 10,000-year return period.

	Mean Magnitude			
Period (sec)	**475-yr**	**1000-yr**	**2,475yr**	**10,000-yr**
0.01/PGA	6.15	6.19	6.25	6.36
0.02	6.15	6.18	6.25	6.36
0.03	6.14	6.17	6.23	6.35
0.04	6.12	6.15	6.22	6.32
0.05	6.11	6.14	6.20	6.30
0.075	6.08	6.11	6.18	6.29
0.1	6.07	6.11	6.18	6.28
0.15	6.11	6.16	6.22	6.32
0.2	6.17	6.21	6.28	6.38
0.25	6.22	6.26	6.32	6.42
0.3	6.27	6.30	6.36	6.45
0.4	6.36	6.38	6.43	6.50
0.5	6.43	6.44	6.48	6.53
0.75	6.53	6.54	6.55	6.57
1	6.59	6.60	6.59	6.60
1.5	6.70	6.71	6.69	6.67
2	6.76	6.77	6.74	6.70
3	6.83	6.83	6.80	6.75
4	6.87	6.88	6.85	6.80
5	6.90	6.90	6.88	6.83
7.5	6.98	7.00	7.00	6.97
10	7.01	7.05	7.06	7.04

Table 6-7. Mean distance (km) for the YDTI site for V_{S30} of 420 m/sec for return periods of 475, 1,000, 2,475, and 10,000-year return period.

	Mean Distance (km)			
Period (sec)	**475-yr**	**1000-yr**	**2,475yr**	**10,000-yr**
0.01/PGA	39.30	28.18	18.21	9.83
0.02	38.96	27.94	17.99	9.52
0.03	38.00	27.27	17.46	9.59
0.04	37.49	26.15	16.76	9.92
0.05	37.64	26.71	17.30	10.16
0.075	36.92	26.95	17.98	10.18
0.1	36.72	26.33	17.53	10.84
0.15	38.39	28.34	19.21	11.58
0.2	40.44	29.94	20.17	11.77
0.25	43.54	32.16	21.35	12.06
0.3	46.24	33.71	21.78	11.79
0.4	52.82	37.64	23.07	11.91
0.5	57.47	42.80	26.68	11.45
0.75	66.89	49.74	30.02	12.30
1	73.54	53.73	31.82	12.89
1.5	85.23	64.29	39.22	16.07
2	90.43	69.71	43.96	17.44
3	96.88	75.02	48.00	19.73
4	99.52	78.15	50.80	21.88
5	102.00	81.57	55.65	24.02
7.5	114.27	97.62	75.34	43.73
10	122.02	108.25	89.93	60.40

Table 6-8. Mean number of standard deviations of ground motion (Epsilon) for the YDTI site for V_{S30} of 420 m/sec for return periods of 475, 1,000, 2,475, and 10,000-year return period.

	Mean Epsilon			
Period (sec)	**475-yr**	**1000-yr**	**2,475yr**	**10,000-yr**
0.01/PGA	0.21	0.29	0.46	0.92
0.02	0.21	0.29	0.45	0.92
0.03	0.23	0.31	0.48	0.94
0.04	0.25	0.33	0.51	0.95
0.05	0.27	0.37	0.55	0.98
0.075	0.31	0.43	0.62	1.08
0.1	0.33	0.45	0.65	1.09
0.15	0.30	0.42	0.61	1.06
0.2	0.29	0.38	0.56	1.00
0.25	0.31	0.38	0.53	0.94
0.3	0.35	0.41	0.52	0.90
0.4	0.43	0.46	0.52	0.86
0.5	0.50	0.51	0.54	0.84
0.75	0.61	0.59	0.56	0.77
1	0.63	0.61	0.56	0.75
1.5	0.67	0.69	0.63	0.77
2	0.65	0.68	0.64	0.75
3	0.63	0.67	0.63	0.72
4	0.56	0.63	0.61	0.72
5	0.53	0.61	0.63	0.75
7.5	0.49	0.64	0.78	0.99
10	0.41	0.59	0.78	1.06

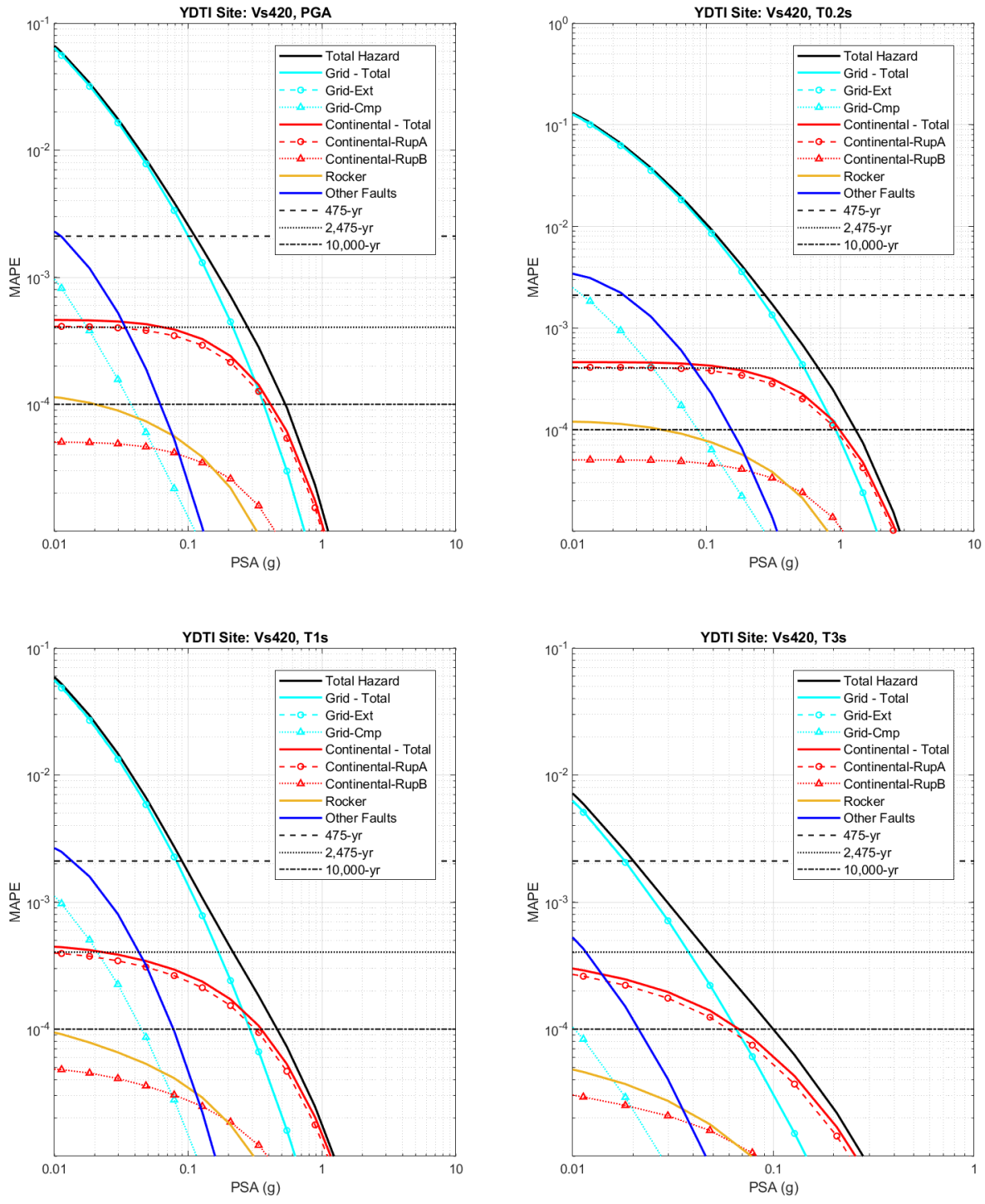

Figure 6-14. Mean annual probability of exceedance by source type at PGA (top left) and periods of 0.2 sec (top right), 1 sec (bottom left), and 3 sec (bottom right) for this study update for V_{S30} of 420 m/sec.

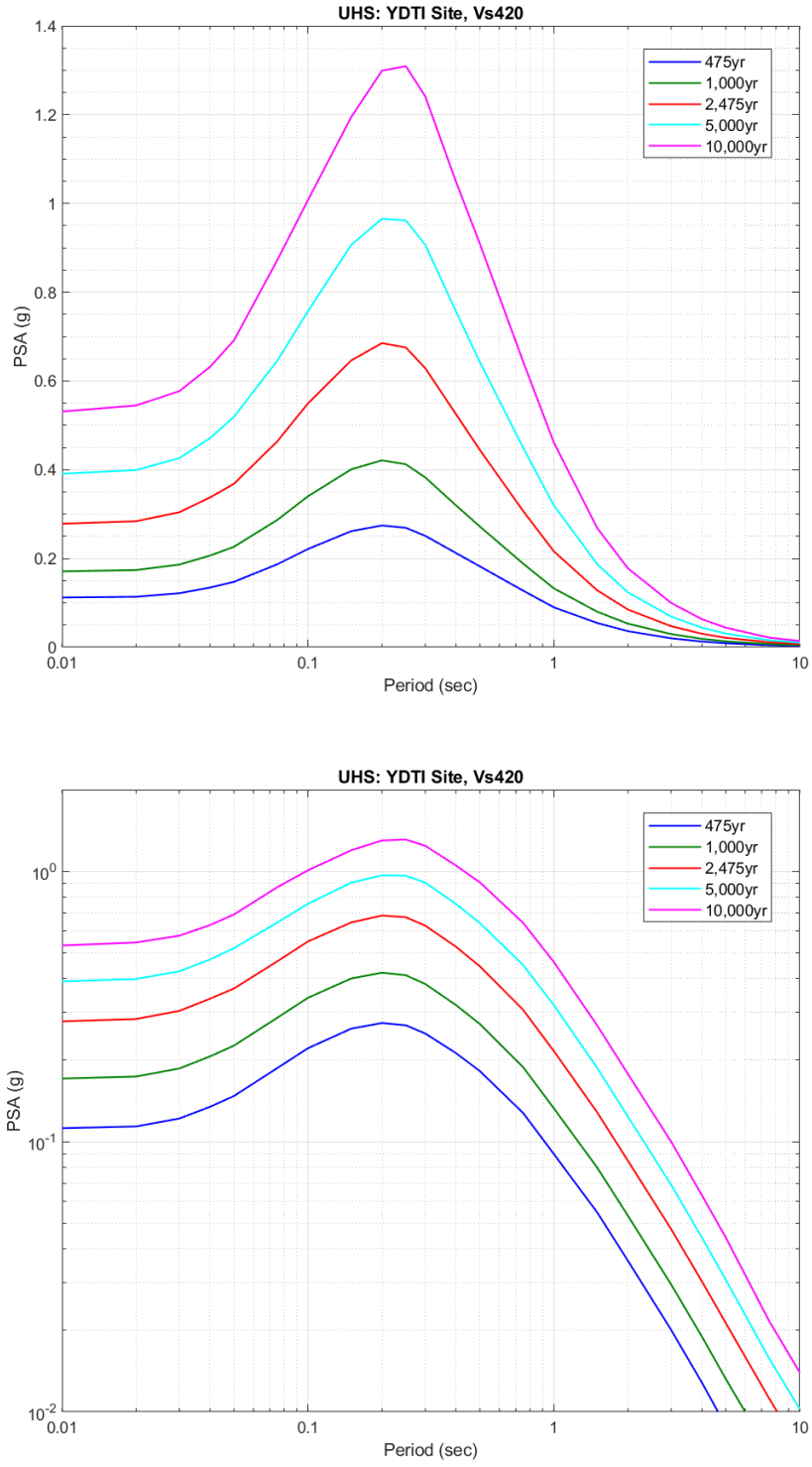

Figure 6-15. Uniform mean hazard spectra for the YDTI site in log-linear scale (top) and log-log scale (bottom) for V_{S30} of 420 m/sec.

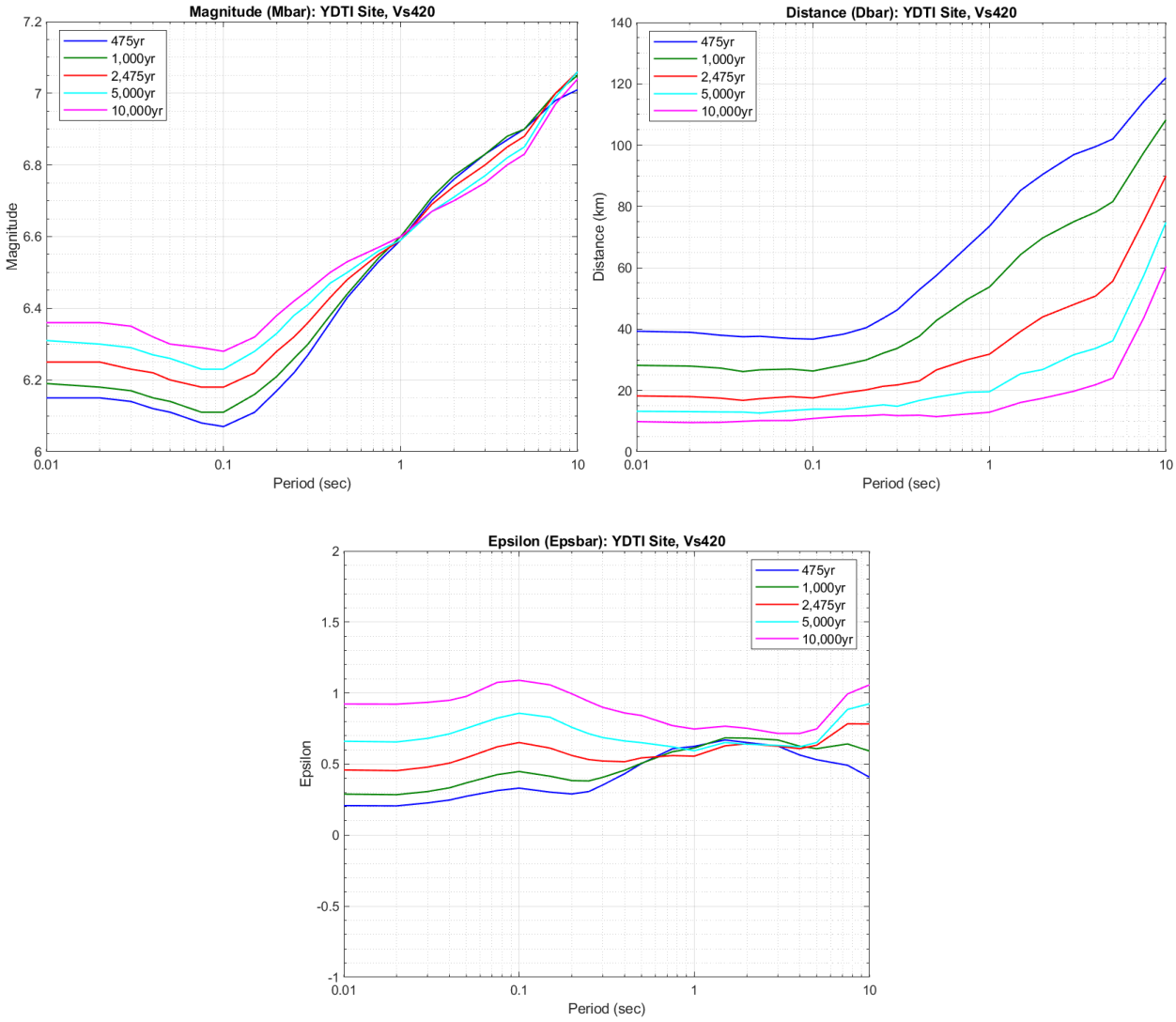

Figure 6-16. Mean magnitude (top left), distance (km) (top right), and epsilon (bottom) for the YDTI site for V_{S30} of 420 m/sec.

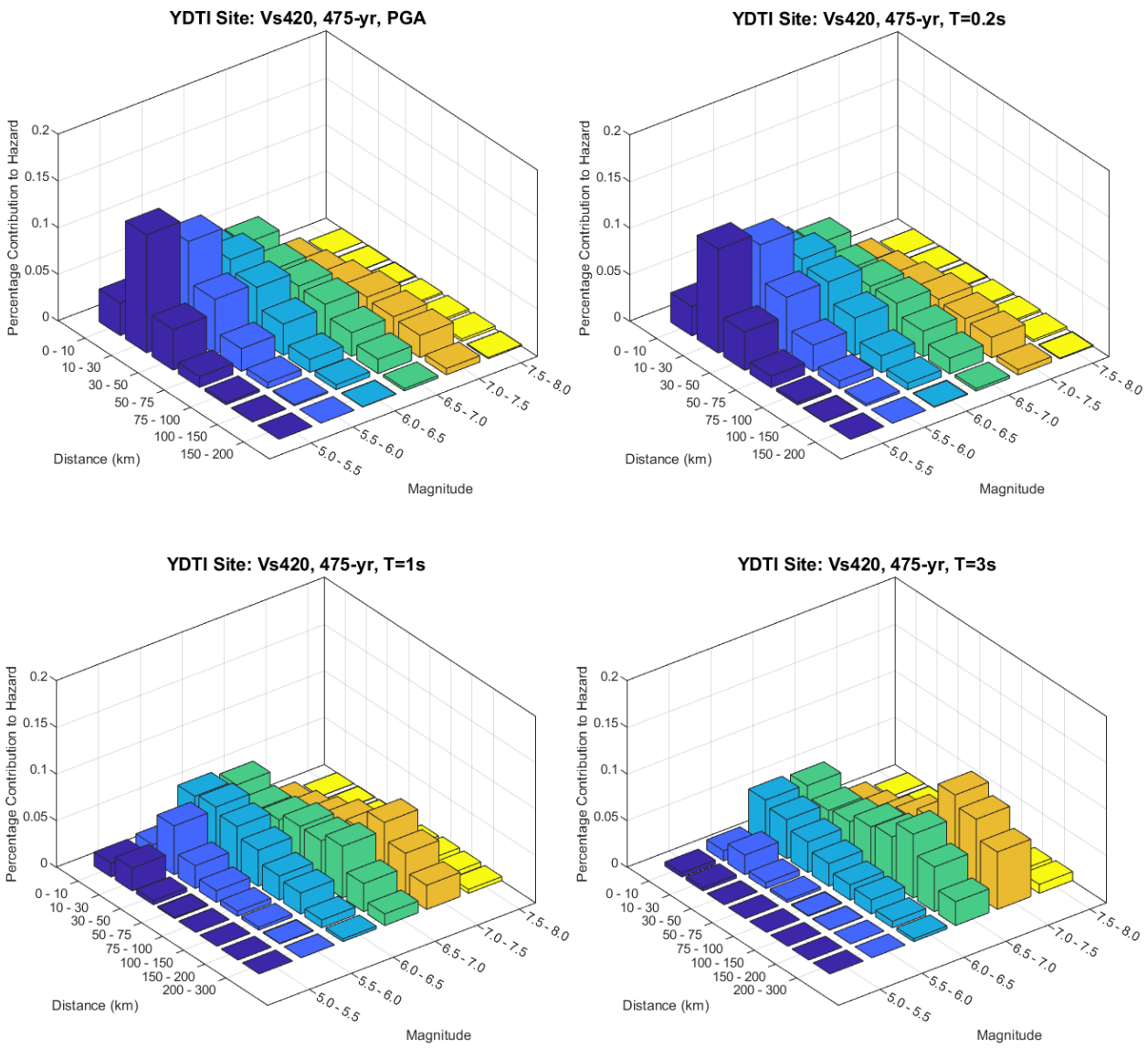

Figure 6-17. Magnitude-distance contribution to the 475-year return period hazard at PGA (top left) and periods of 0.2 sec (top right), 1 sec (bottom left), 3 sec (bottom right) for the YDTI for V_{S30} of 420 m/sec.

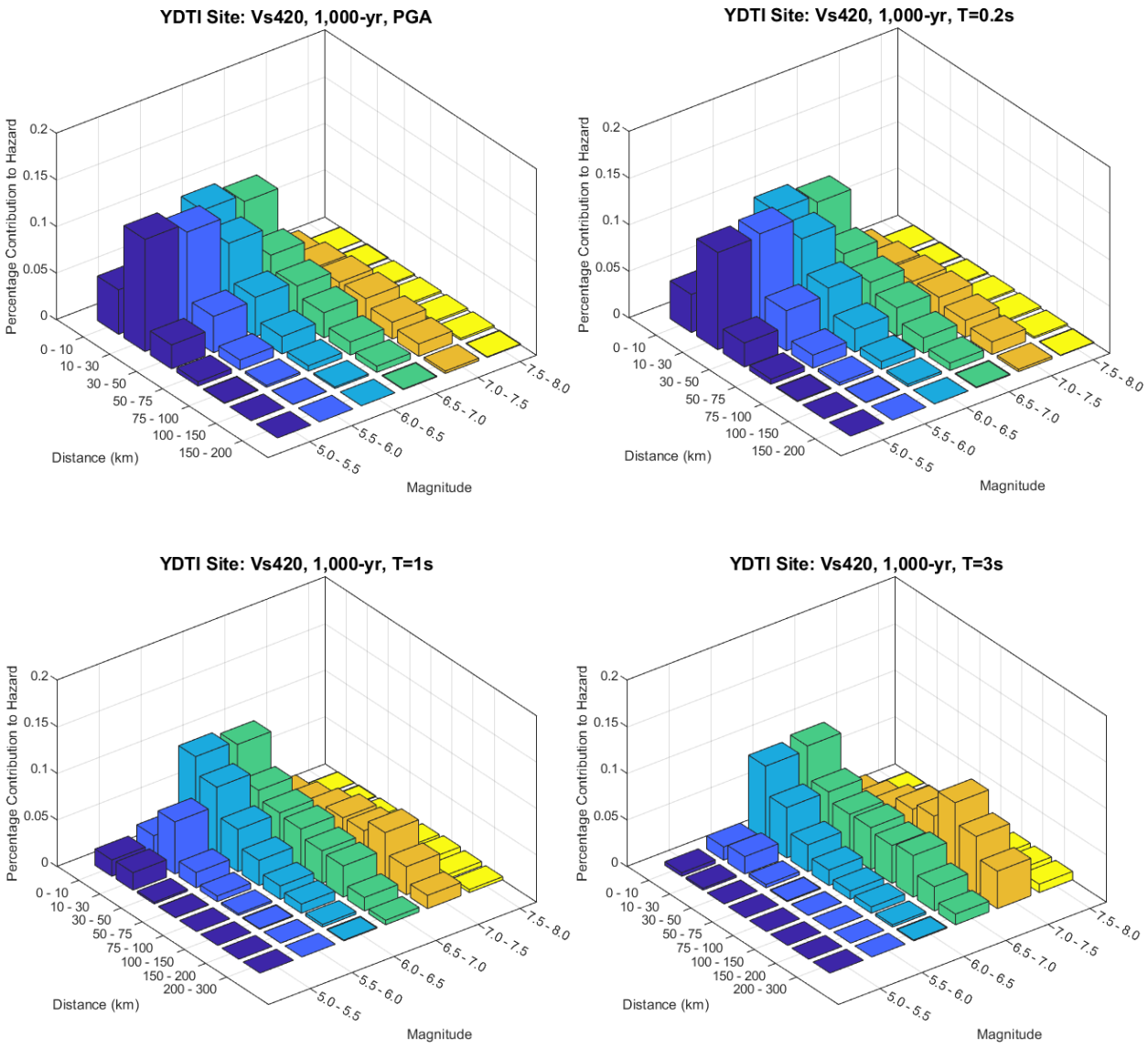

Figure 6-18. Magnitude-distance contribution to the 1,000-year return period hazard at PGA (top left) and periods of 0.2 sec (top right), 1 sec (bottom left), 3 sec (bottom right) for the YDTI for V_{S30} of 420 m/sec.

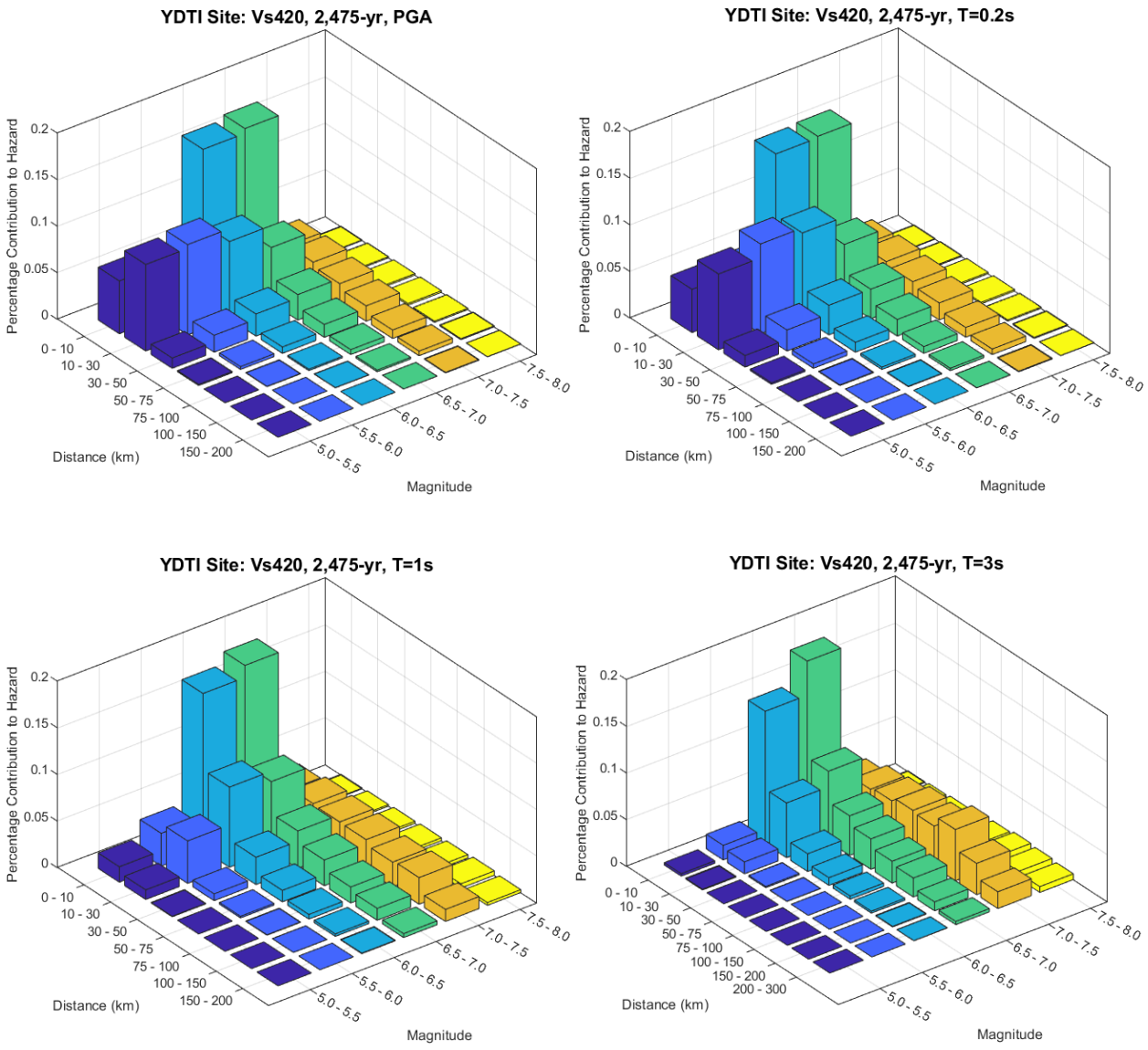

Figure 6-19. Magnitude-distance contribution to the 2,475-year return period hazard at PGA (top left) and periods of 0.2 sec (top right), 1 sec (bottom left), 3 sec (bottom right) for the YDTI for V_{S30} of 420 m/sec.

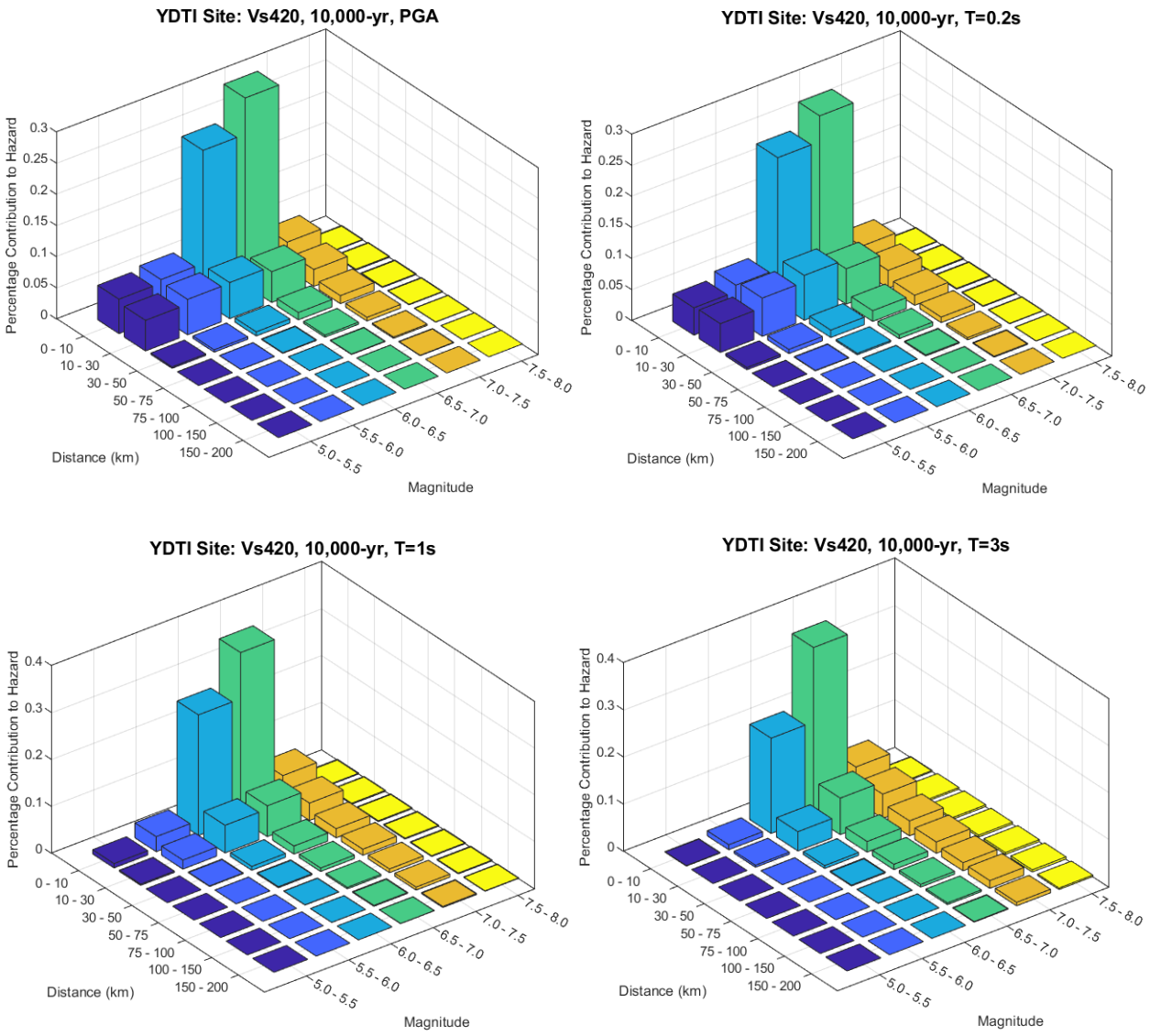

Figure 6-20. Magnitude-distance contribution to the 10,000-year return period hazard at PGA (top left) and periods of 0.2 sec (top right), 1 sec (bottom left), 3 sec (bottom right) for the YDTI for V_{S30} of 420 m/sec.

Given the SSC and the GMC models logic trees, fractile hazard curves and corresponding UHS are computed for the YDTI site for the reference site condition with V_{S30} of 760 m/sec. These fractile hazard curves are plotted in Figure 6-21 for PGA and spectral periods of 0.2, 1, and 3 sec. Figure 6-21 shows the 5th, 16th, 50th, 84th and 94th percentile hazard curves as well as the mean hazard in terms annual frequency of exceedance versus ground motion for these spectral periods. These fractile curves show the uncertainty in the mean hazard given the epistemic uncertainty in the source and the ground motion models. Figure 6-22 shows the UHS for the different hazard fractiles for return periods of 475, 1,000, 2,475, and 10,000 years for V_{S30} of 760m/sec. Fractile hazard and UHS curves are not shown for V_{S30} of 420 m/sec because of the expected similarity in the hazard range to the V_{S30} of 760 m/sec case.

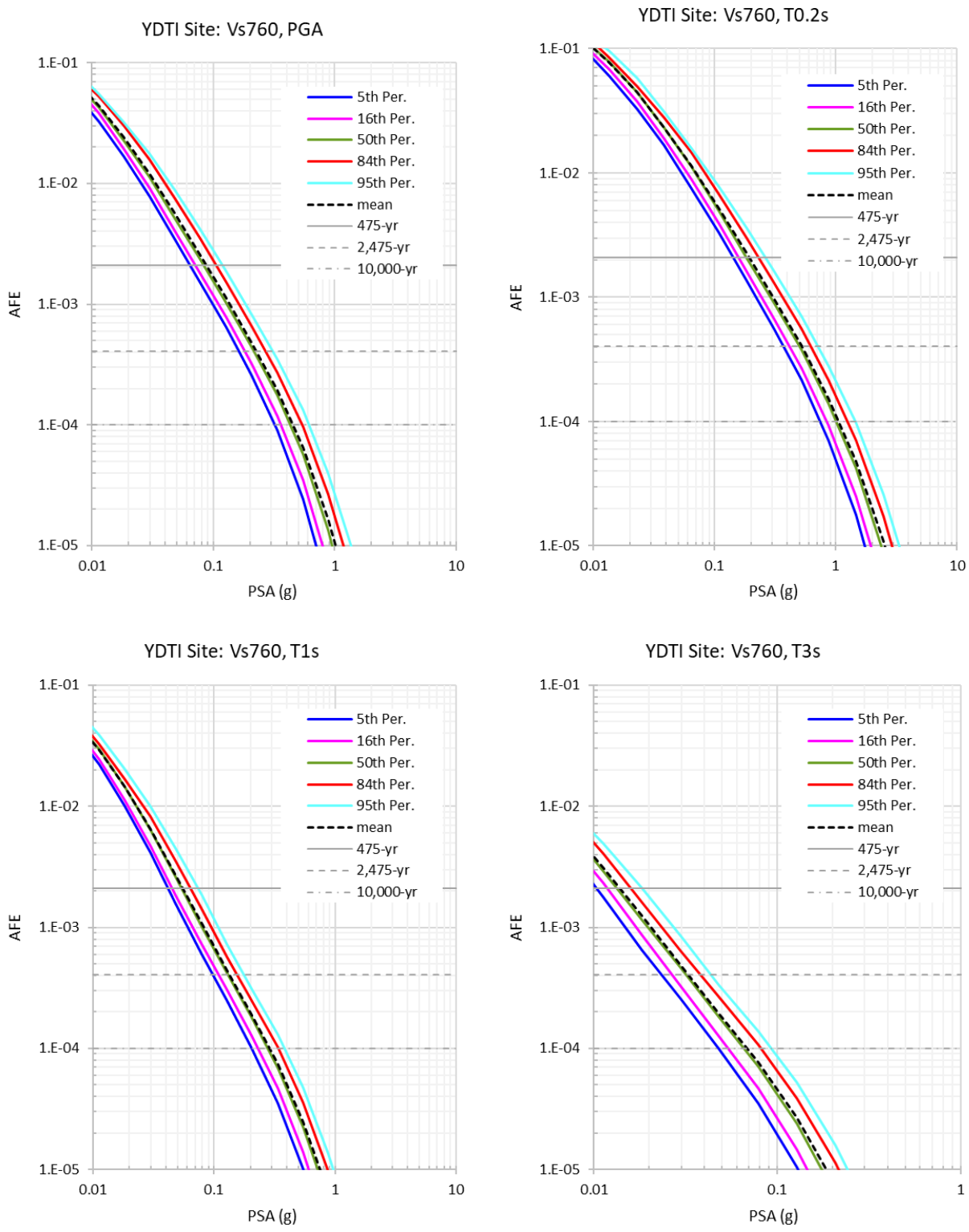

Figure 6-21. Annual frequency of exceedance (AFE) fractile hazard curves for PGA (top left) and periods of 0.2 sec (top right), 1 sec (bottom left), and 3 sec (bottom right) for the YDTI site for V_{S30} of 760 m/sec.

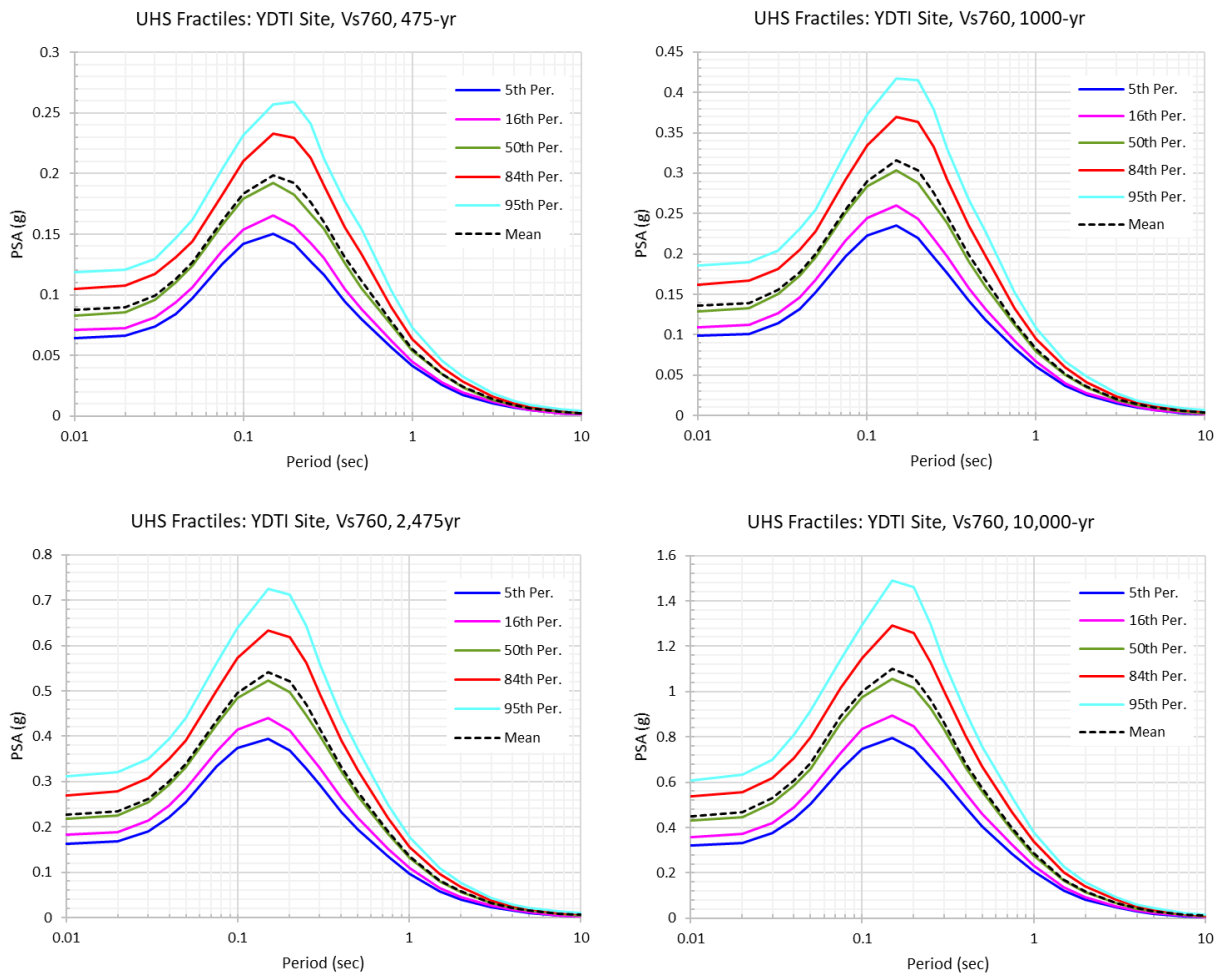

Figure 6-22. Fractile UHS for the YDTI site for VS30 of 760 m/sec for return periods of 475 (top left), 1,000 (top right), 2,475 (bottom left), and 10,000 years (bottom right).

6.3 DSHA Results

Median and 84th percentile deterministic response spectra are calculated for the MCE on the Continental-Elk Park and the Rocker faults using the ground-motion characterization model discussed in Section 4. The four equally weighted NGA-West2 GMPEs are used along with the epistemic uncertainty in median prediction model of Al Atik and Youngs (2014) for the calculation of the deterministic spectra. For the Continental-Elk Park fault, MCE scenarios are evaluated for the four scenarios of Rupture Model A and two scenarios of Rupture Model B. The parameters used in the deterministic calculations for the MCE scenarios on the Continental-Elk Park and Rocker faults are listed in Table 6-9.

As listed in Table 6-9, the best estimate of the characteristic magnitude is used for the different MCE scenarios. Similarly, the best estimates of the dip angle and seismogenic thickness are used in the calculations. For the four MCE scenarios of Rupture Model A (RupA-01 to RupA-04) on the Continental-Elk Park fault, the magnitude is similar ranging from 6.6 to 6.8 and the rupture distance ranges from 1.43

km for the west dipping sections (dipping towards the site) to 8.62 km for the east dipping sections (dipping away from the site). For each of the two rupture scenarios of Rupture Model B (RupB-LS1 and RupB-LS2) on the Continental-Elk Park fault, we calculate the deterministic spectra with the rupture distance calculated based on the east dipping and west dipping sections of the rupture. As an example, for the RupB-LS1 scenario, we calculate the spectra for two cases: **M** 7 and Rrup of 8.62 km based on the Elk-N section dipping east with the site located on the footwall and **M** 7 and Rrup of 1.43 km based on the CF-S+CF-C+CF-N sections dipping west with the site located on the hanging wall. We note that for the Rupture Model B scenarios, the west dipping part of these linked ruptures leads to the smallest distance to the site with the site located on the hanging wall, resulting in larger calculated response spectra. For the Rocker fault, a single MCE scenario is considered with **M** 7.1 and Rrup of 7.14 km. This fault dips towards the west with the site located on its footwall.

Median and 84th percentile response spectra are calculated and presented for the four NGA-West2 GMPEs and the weighted mean of the GMC logic tree for select MCE scenarios on the Continental-Elk Park fault from Table 6-9. Figure 6-23 shows the median and 84th percentile deterministic response spectra for scenarios RupA-01, RupA-02, and RupA-04 on the Continental-Elk Park fault for V_{S30} of 760 m/sec. These plots show the range of predictions from the NGA-West2 GMPEs and indicate that CB14 predicts larger response spectra at short spectral periods while the rest of the GMPEs are in general agreement in their predictions. Similarly, Figures 6-24 and 6-25 show the median and 84th percentile deterministic response spectra for scenario RupB-LS1 (E and W) on the Continental-Elk Park fault and the MCE scenario on the Rocker fault, respectively, for V_{S30} of 760 m/sec. Similar observations can be made on these plots as those made on the plots of Figure 6-23.

Figure 6-26 presents a comparison of the weighted median and 84th percentile response spectra for the MCE scenarios listed in Table 6-9 for V_{S30} of 760 m/sec. For Rupture Model B scenarios on the Continental-Elk Park fault, the parameters associated with the west dipping sections generate larger response spectra. For both median and 84th percentile response spectra, Figure 6-26 indicates that the largest response spectrum is that of RupB-LS1-W with **M** 7.0 and Rrup of 1.43 km followed closely with the spectrum of RupA-01 with **M** 6.8 and Rrup of 1.43 km. The lowest response spectrum is that of RupA-04 with **M** 6.6 and Rrup of 8.62 km and with the site located on the footwall. Similarly, the response spectrum of the MCE scenario on the Rocker fault is in the lower range of the response spectra from the evaluated MCE scenarios. Given these comparisons, we choose the MCE scenario RupB-LS1-W on the Continental-Elk Park fault to generate deterministic median and 84th percentile response spectra for the YDTI site V_{S30} of 760 m/sec. We note that this scenario is assigned a smaller weight of 0.2 in the SSC logic tree compared to the more likely scenario RupA-01 with an assigned weight of 0.8. However, given the similarity of the response spectra for scenarios RupB-LS1-W and RupA-01, we choose the slightly larger deterministic spectra of MCE scenario RupB-LS1-W instead of those of RupA-01. The deterministic median and 84th percentile response spectra of the MCE scenario on the Continental-Elk Park fault (scenario RupB-LS1-W) are listed in Table 6-10 for V_{S30} of 760 m/sec.

Similar deterministic plots and comparisons are presented for the deterministic spectra for the site-specific V_{S30} of 420 m/sec. Figures 6-27 to 6-29 show the median and 84th percentile deterministic response spectra for select scenarios from Table 6-9 on the Continental-Elk Park fault and for the MCE scenario on the Rocker fault. These figures indicate a reasonably good agreement among the four NGA-West2 GMPEs with CB14 resulting in larger response spectra at long periods and ASK14 having larger

peaks compared to the rest of the GMPEs. Figure 6-30 presents comparisons of the weighted median and 84th percentile response spectra for all the scenarios listed in Table 6-9 for V_{S30} of 420 m/sec. Similar observations can be made on these comparisons to those made for the reference V_{S30} of 760 m/sec. The largest median and 84th percentile response spectra are those of scenarios RupB-LS1-W and RupA-01 on the Continental-Elk Park fault. Again, given the similarity in the response spectra for these two scenarios, we choose the slightly larger deterministic spectra of RupB-LS1-W. The values for these spectra are listed in Table 6-10 for V_{S30} of 420 m/sec.

Finally, we compare in Figure 6-31 the deterministic median and 84th percentile response spectra for the YDTI site for the MCE scenario on the Continental-Elk Park fault obtained from this study update to the corresponding deterministic spectra from the 2016 study for the MCE scenario on the Continental fault. Al Atik and Gregor (2016) used an MCE scenario on the Continental fault with **M** 6.5 and Rrup of 1.2 km with the site located on the hanging wall while this study update using a scenario with **M** 7 and Rrup of 1.43 km. Given the increase in the magnitude of the MCE scenario in this study update and the differences in the GMC models, Figure 6-31 indicates that the median and 84th response spectra for the MCE scenario for this study update are larger than those of the 2016 study. The ratios of the deterministic spectra from this study relative to those from the 2016 study are shown in Figure 6-32. At short spectral periods, Figure 6-32 indicates that the difference in the median and 84th percentile spectra from this study update compared to the 2016 study is small (generally less than 10%). This difference increases for periods between 0.1 sec 3 sec and becomes on the order of 10 to 35%.

Table 6-9. MCE scenario parameters considered for the Continental-Elk Park and the Rocker faults. All scenarios have normal style of faulting and rupture to the ground surface.

Fault	Scenario	Sections	Magnitude	Rrup (km)	Dip angle (deg.)	Dip Direction	HW/FW
Continental-Elk Park	RupA-01	CF-S+CF-C+CF-N	6.8	1.43	70	West	HW
	RupA-02	CF-S+ERF	6.7	3.26	70	West	HW
	RupA-03	Elk-C+Elk-N	6.7	3.14	70	East	FW
	RupA-04	Elk-N	6.6	8.62	70	East	FW
	RupB-LS1-E	Elk-N	7	8.62	70	East	FW
	RupB-LS1-W	CF-S+CF-C+CF-N	7	1.43	70	West	HW
	RupB-LS2-E	Elk-C+Elk-N	7	3.14	70	East	FW
	RupB-LS2-W	CF-S+CF-C+ERF	7	3.26	70	West	HW
Rocker			7.1	7.14	55	West	FW

Table 6-10. Median and 84th percentile deterministic response spectra for the MCE scenario on the Continental-Elk Park fault (scenario RupB-LS1-W) for V_{S30} of 760 and 420 m/sec.

	V_{S30} = 760 m/sec		V_{S30} = 420 m/sec	
Period (sec)	**Median PSA (g)**	**84th Percentile PSA (g)**	**Median PSA (g)**	**84th Percentile PSA (g)**
0.01/PGA	0.4520	0.8203	0.5008	0.8751
0.02	0.4696	0.8539	0.5119	0.8945
0.03	0.5270	0.9665	0.5405	0.9481
0.04	0.6048	1.1187	0.5896	1.0420
0.05	0.6730	1.2531	0.6307	1.1213
0.075	0.8270	1.5687	0.7468	1.3453
0.1	0.9248	1.7669	0.8526	1.5362
0.15	1.0378	1.9891	1.0257	1.8311
0.2	1.0275	1.9615	1.1505	2.0622
0.25	0.9469	1.8011	1.2063	2.1961
0.3	0.8607	1.6474	1.1938	2.2270
0.4	0.7140	1.3780	1.0583	2.0081
0.5	0.6043	1.1819	0.9324	1.8002
0.75	0.4386	0.8806	0.7018	1.4005
1	0.3235	0.6560	0.5170	1.0440
1.5	0.2002	0.4083	0.3121	0.6349
2	0.1403	0.2860	0.2100	0.4270
3	0.0857	0.1745	0.1240	0.2523
4	0.0573	0.1154	0.0797	0.1602
5	0.0412	0.0833	0.0554	0.1117
7.5	0.0189	0.0381	0.0243	0.0490
10	0.0116	0.0231	0.0145	0.0290

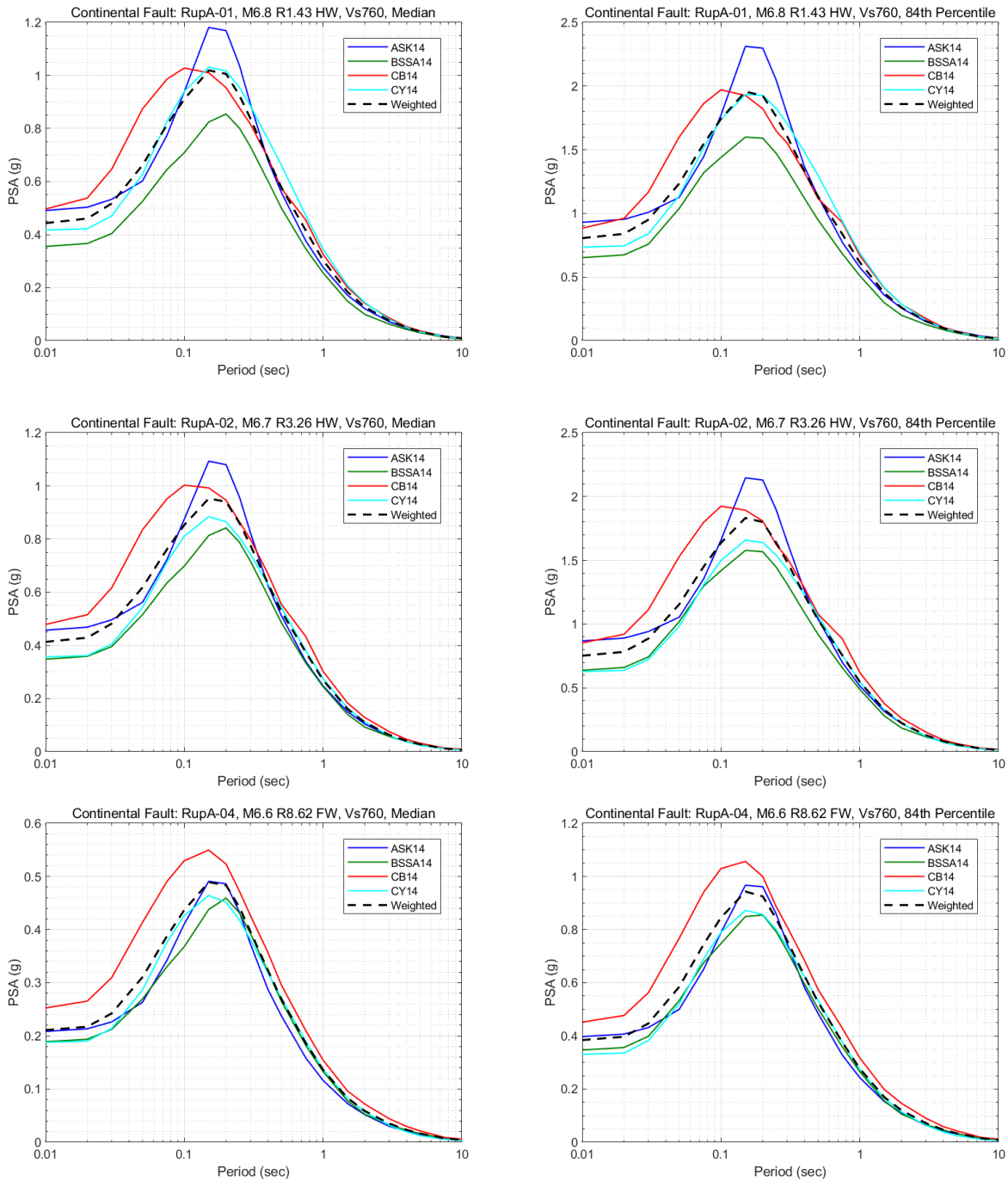

Figure 6-23. Median (left) and 84th percentile (right) deterministic response spectra for scenarios RupA-01 (top), RupA-02 (middle), and RupA-04 (bottom) of Rupture Model A on the Continental-Elk Park fault for V_{S30} of 760 m/sec.

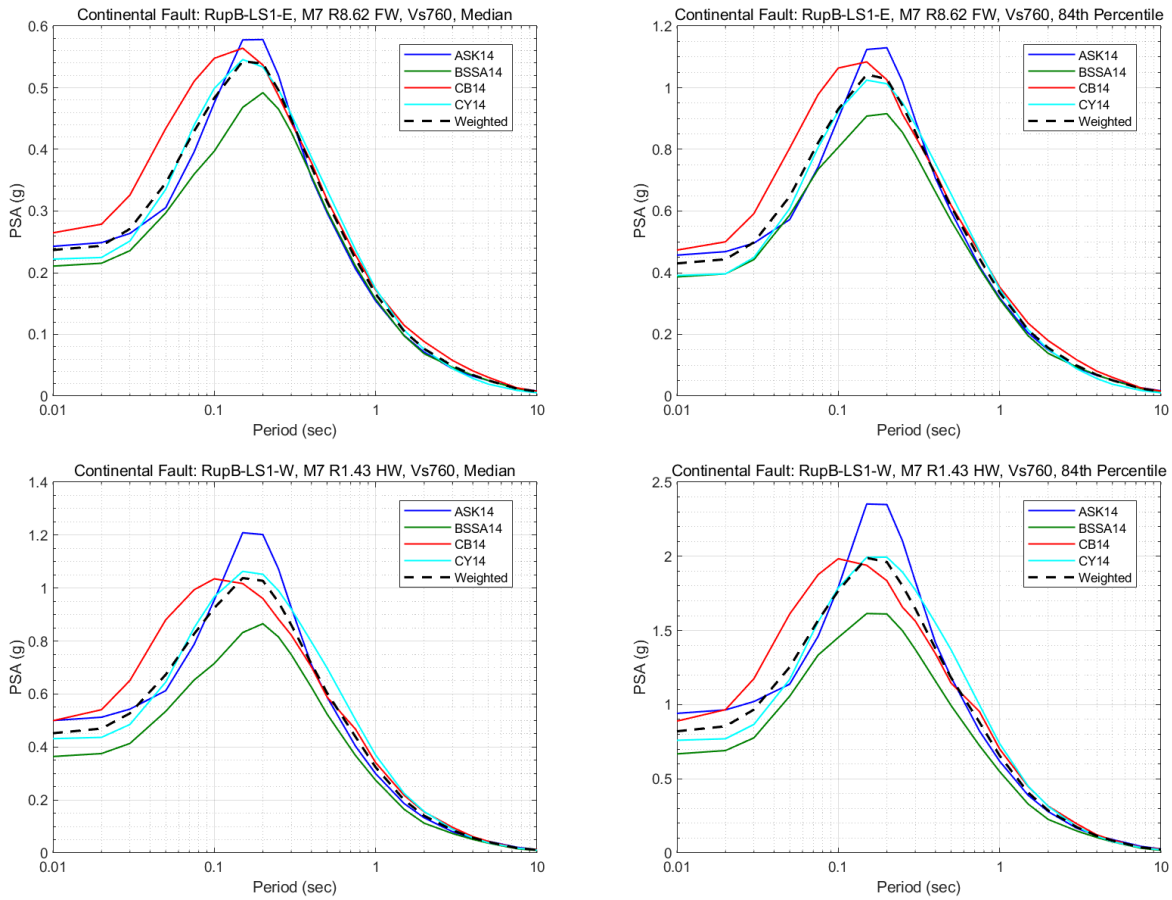

Figure 6-24. Median (left) and 84th percentile (right) deterministic response spectra for scenario RupB-LS1 east (top) and west dipping (bottom) of Rupture Model B on the Continental-Elk Park fault for V_{S30} of 760 m/sec.

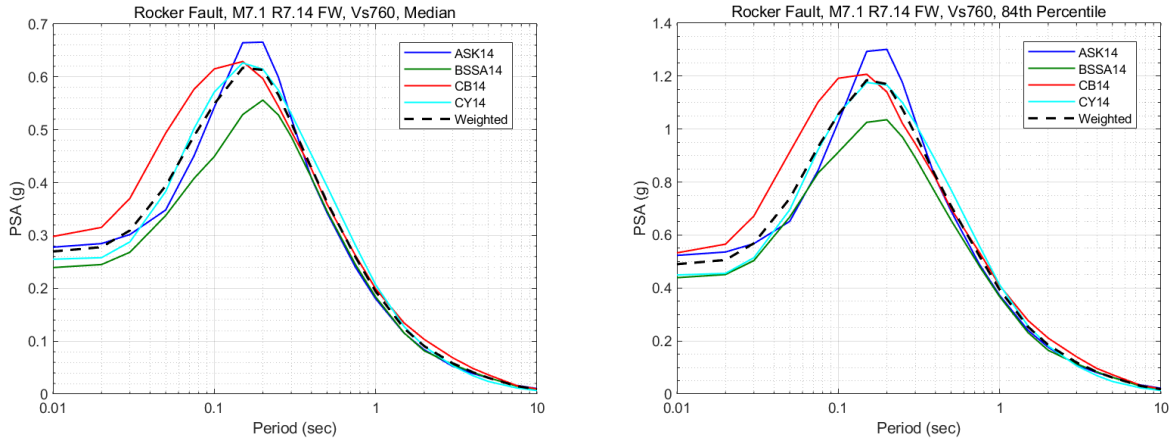

Figure 6-25. Median (left) and 84th percentile (right) deterministic response spectra for the MCE scenario on the Rocker fault for V_{S30} of 760 m/sec.

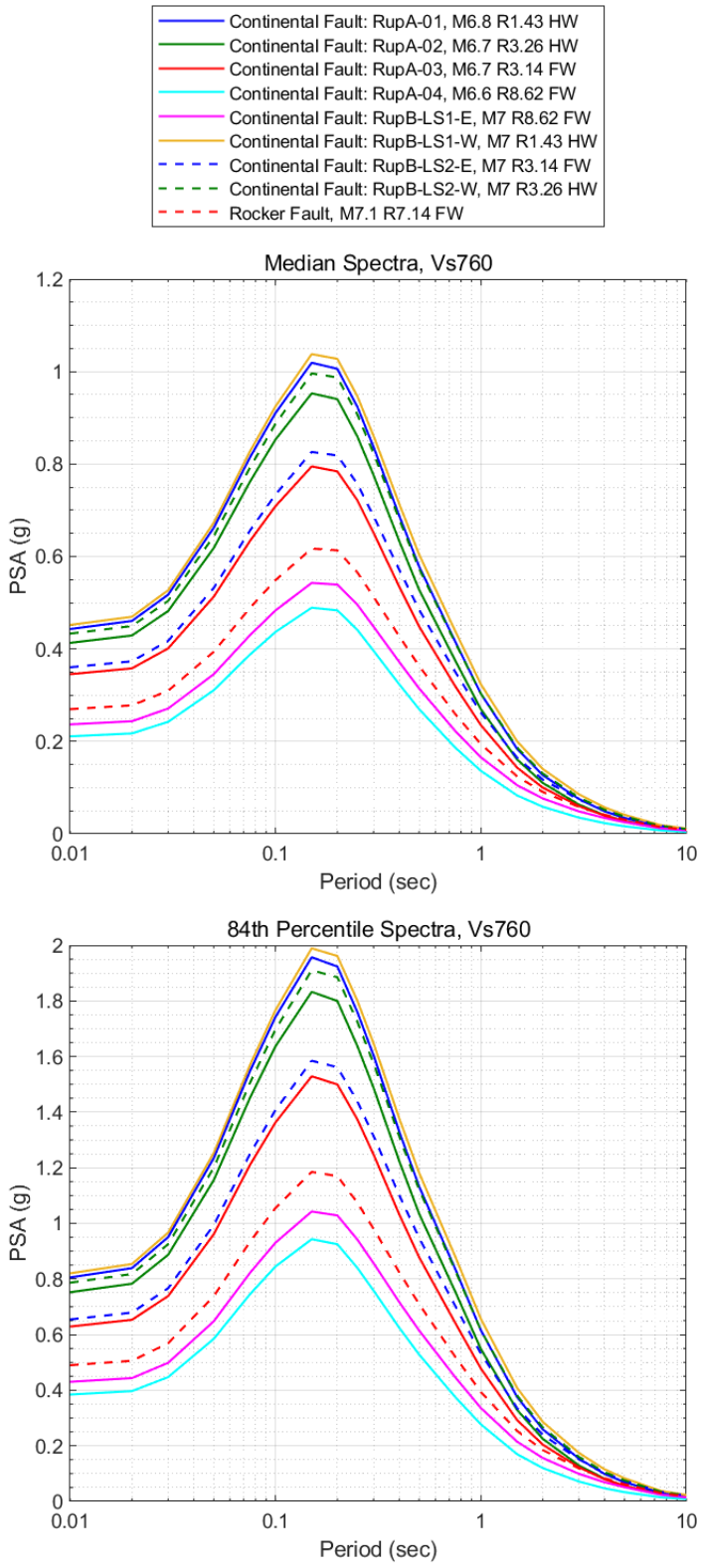

Figure 6-26. Comparison of the median (top) and 84th percentile deterministic response spectra for the MCE scenarios on the Continental-Elk Park and the Rocker faults at the YDTI site for V_{S30} of 760 m/sec.

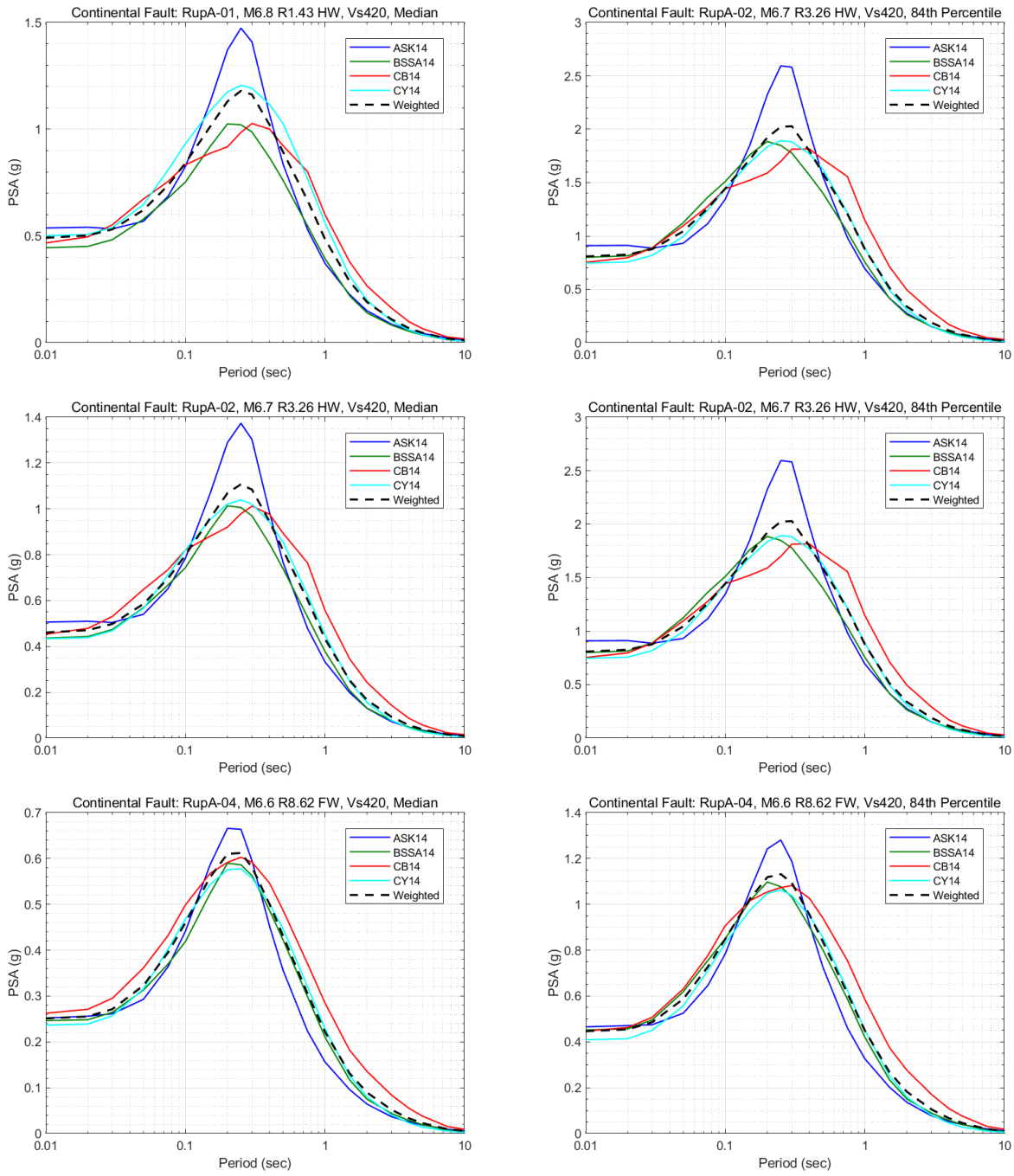

Figure 6-27. Median (left) and 84th percentile (right) deterministic response spectra for scenarios RupA-01 (top), RupA-02 (middle), and RupA-04 (bottom) of Rupture Model A on the Continental-Elk Park fault for V_{S30} of 420 m/sec.

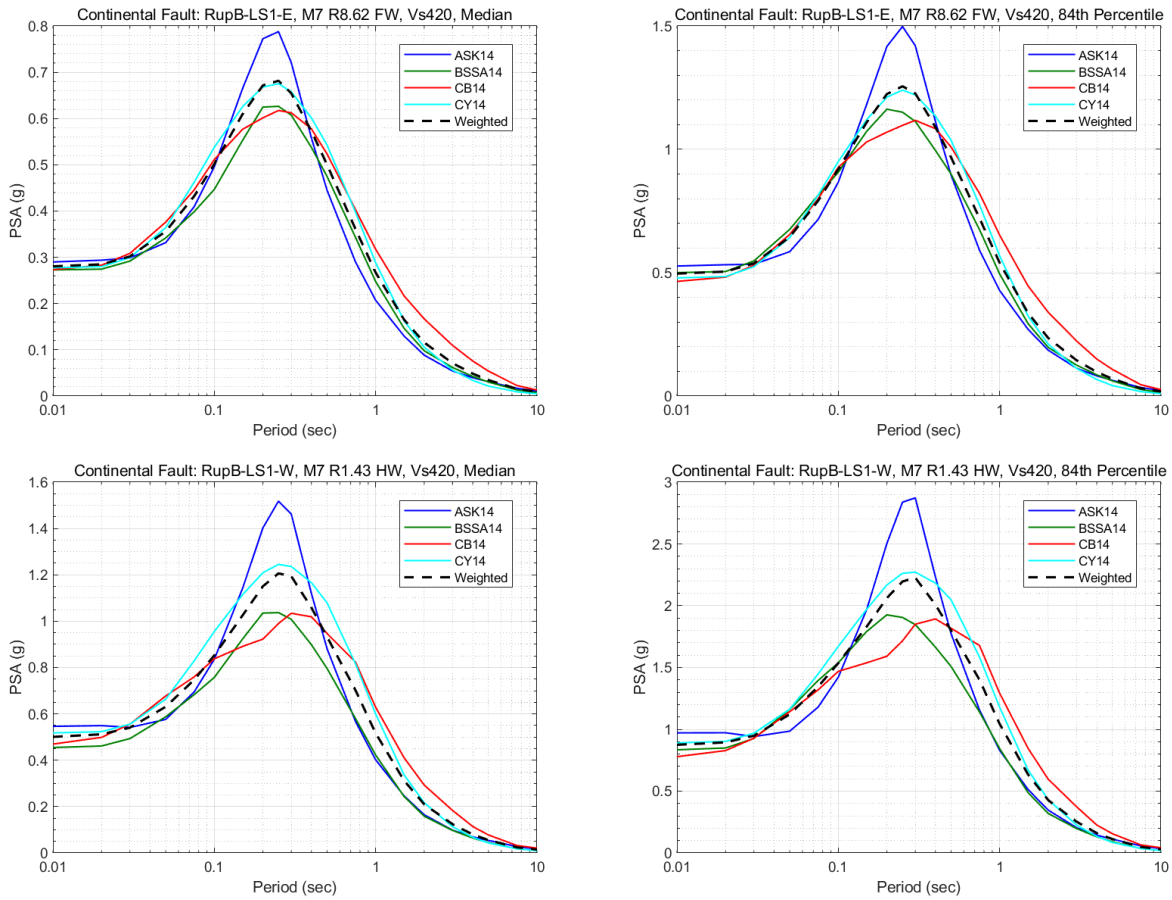

Figure 6-28. Median (left) and 84th percentile (right) deterministic response spectra for scenario RupB-LS1 east (top) and west dipping (bottom) of Rupture Model B on the Continental-Elk Park fault for V_{S30} of 420 m/sec.

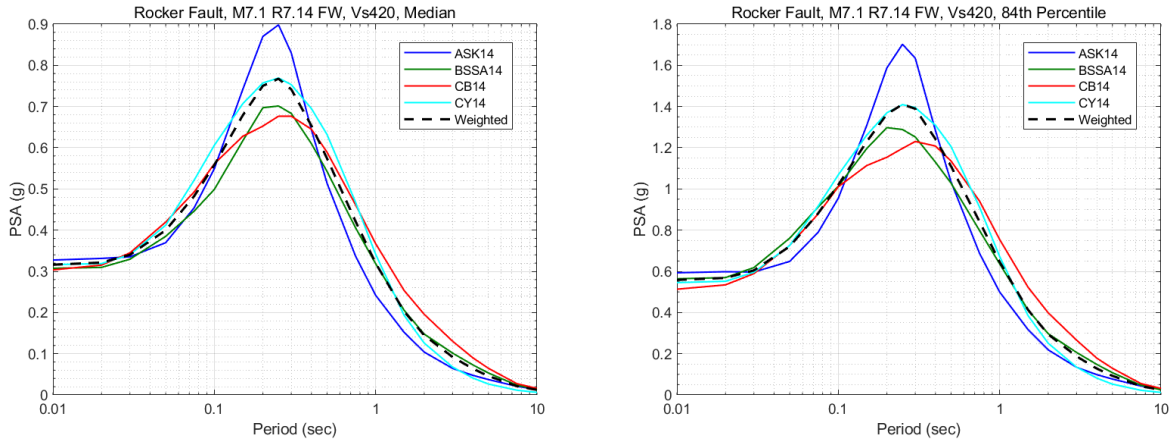

Figure 6-29. Median (left) and 84th percentile (right) deterministic response spectra for the MCE scenario on the Rocker fault for V_{S30} of 420 m/sec.

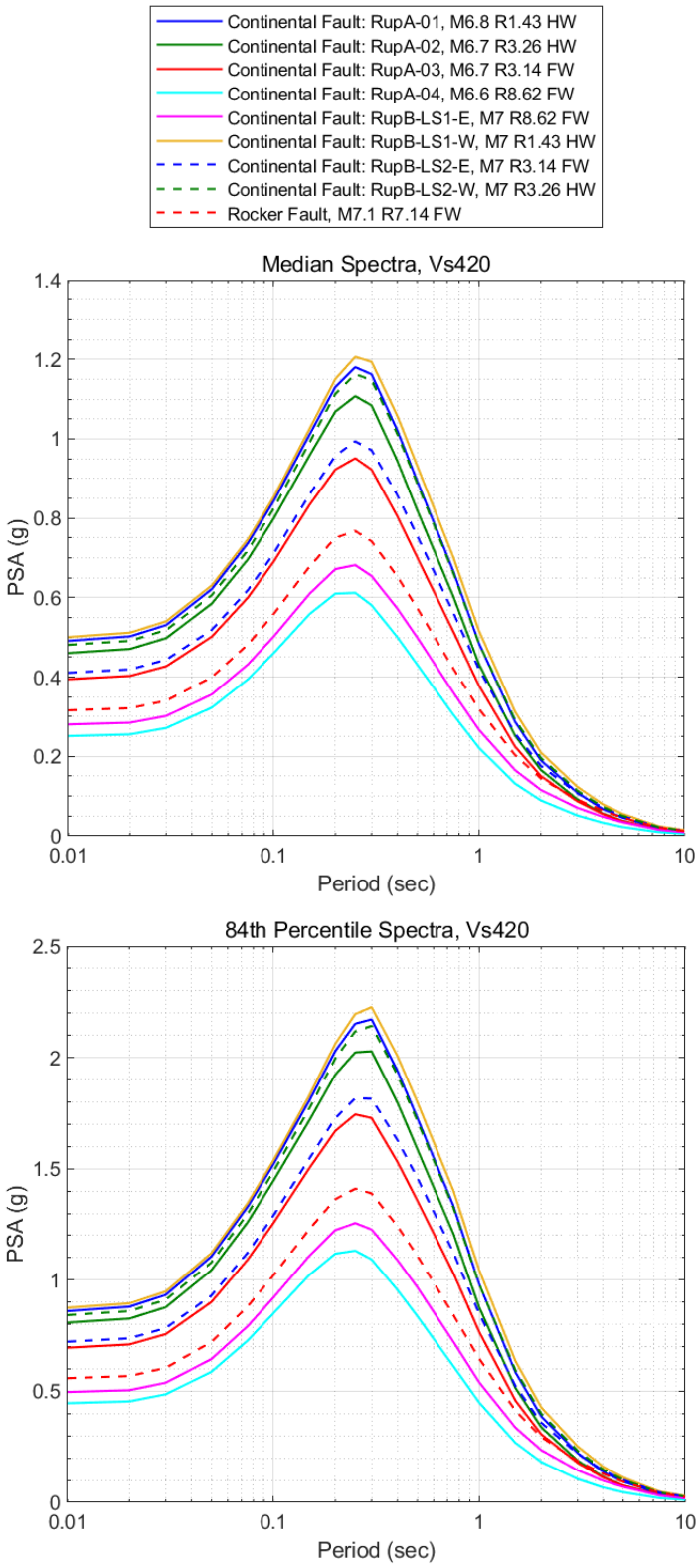

Figure 6-30. Comparison of the median (top) and 84th percentile deterministic response spectra for the MCE scenarios on the Continental-Elk Park and the Rocker faults at the YDTI site for V_{S30} of 420 m/sec.

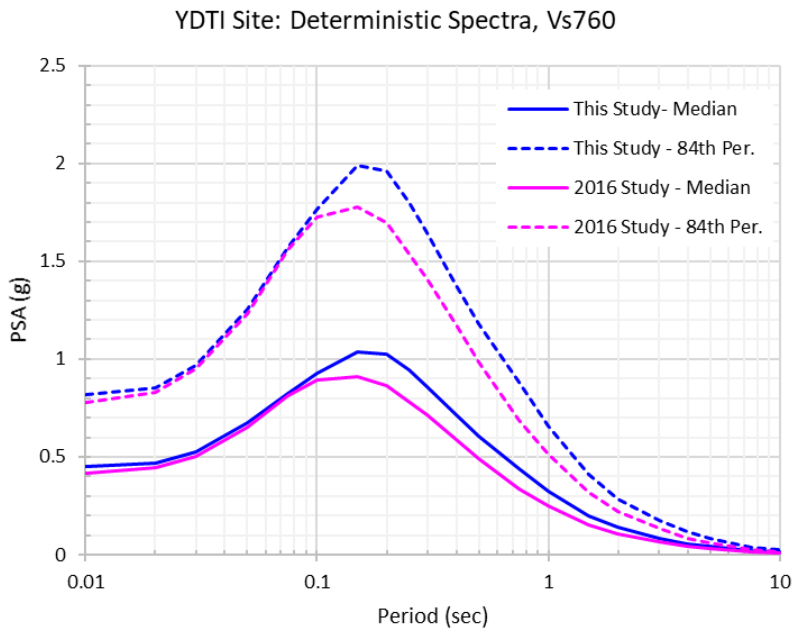

Figure 6-31. Comparison of the median and 84th percentile deterministic response spectra for the MCE scenario on the Continental fault at the YDTI site from this study to the corresponding deterministic spectra from Al Atik and Gregor (2016) for V_{S30} of 760 m/sec.

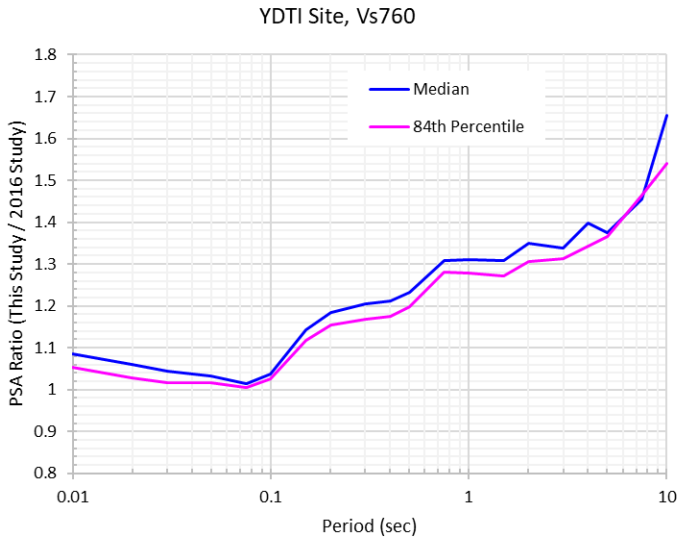

Figure 6-32. Ratio of the median and 84th percentile deterministic response spectra for the MCE scenario on the Continental fault at the YDTI site from this study to the corresponding deterministic spectra from Al Atik and Gregor (2016) for V_{S30} of 760 m/sec.

7. DESIGN SPECTRA

7.1 Horizontal Design Spectra

Figure 7-1 presents a comparison of the UHS at the YDTI site for return periods of 475, 1,000, 2,475, 5,000, and 10,000 years to the deterministic median and 84th percentile spectra for the MCE scenario on the Continental-Elk Park fault for V_{S30} of 760 m/sec. The comparison is shown both in log-linear and log-log scales. For comparison purposes, the UHS for a return period of 100,000 years is also included in the plots. Similar comparisons of the UHS and the median and 84th percentile deterministic response spectra are shown in Figure 7-2 for the site-specific V_{S30} of 420 m/sec. Figures 7-1 and 7-2 indicate that the median deterministic spectra for the Continental-Elk Park fault correspond to a PSHA return period close to 10,000 years for both V_{S30} of 760 and 420 m/sec. The 84th percentile deterministic spectra are closer to a return period of 100,000 years.

For the deterministic case, the choice of using the median versus the 84th percentile response spectra needs a careful evaluation. As noted above, the 84th percentile response spectra for the MCE scenarios on the Continental fault correspond to a very rare probabilistic case with a return period close to 100,000 years. Moreover, we note a precedence for using median deterministic spectra for dam design. Specifically, the California Division of Safety of Dams (DSOD) published guidelines for selecting the deterministic PGA level based on the fault's slip rate and the damage potential at the site Dams (DSOD, 2000). The DSOD consequence-hazard matrix is shown in Table 7-1. Despite the increase in the slip rate of the Continental fault in this study compared to the 2016 study, the current best estimate slip rate of 0.1 mm/year is still considered low to moderate. For faults with low slip rates, the hazard matrix in Table 7-1 requires the use of 50th to 84th percentile ground motion parameters for dams with high and extreme consequences of failure. For moderate and low consequence of failure, the hazard matrix requires the use of the median ground-motion parameters for faults with low slip rates. Ultimately, the decision to use the median versus the 84th percentile deterministic design spectrum depends on the regulatory body governing the YDTI site and needs to be made based on feedback reviews from the client or the independent reviewers.

Figure 7-3 presents the horizontal design spectra in terms of UHS at return periods of 475, 1,000, 2,475, and 10,000 years and deterministic median and 84th percentile spectra at the YDTI site for V_{S30} of 760 m/sec with the values listed in Table 7-2. Similarly, horizontal design spectra are shown in Figure 7-4 and listed in Table 7-3 for V_{S30} of 420 m/sec.

Table 7-1. DSOD Hazard matrix (DSOD 2000).

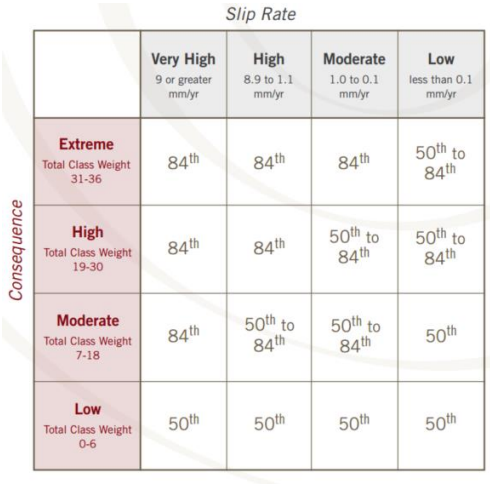

Table 7-2. Horizontal design spectra for 5% damping for the YDTI site for V_{S30} of 760 m/sec.

	UHS PSA (g)				Deterministic PSA (g)	
Period (sec)	**475 yr**	**1,000 yr**	**2,475 yr**	**10,000 yr**	**Median**	**84th Percentile**
0.01/PGA	0.0876	0.1359	0.2276	0.4514	0.4520	0.8203
0.02	0.0898	0.1397	0.2345	0.4690	0.4696	0.8539
0.03	0.0995	0.1552	0.2616	0.5315	0.5270	0.9665
0.04	0.1132	0.1775	0.3006	0.6072	0.6048	1.1187
0.05	0.1270	0.1998	0.3399	0.6856	0.6730	1.2531
0.075	0.1612	0.2555	0.4349	0.8905	0.8270	1.5687
0.1	0.1831	0.2906	0.4961	1.0029	0.9248	1.7669
0.15	0.1986	0.3155	0.5414	1.1012	1.0378	1.9891
0.2	0.1923	0.3035	0.5211	1.0632	1.0275	1.9615
0.25	0.1765	0.2756	0.4688	0.9636	0.9469	1.8011
0.3	0.1598	0.2469	0.4160	0.8666	0.8607	1.6474
0.4	0.1312	0.1995	0.3324	0.6864	0.7140	1.3780
0.5	0.1116	0.1679	0.2775	0.5748	0.6043	1.1819
0.75	0.0776	0.1155	0.1894	0.3986	0.4386	0.8806
1	0.0553	0.0822	0.1346	0.2872	0.3235	0.6560
1.5	0.0346	0.0509	0.0820	0.1721	0.2002	0.4083
2	0.0242	0.0357	0.0573	0.1192	0.1403	0.2860
3	0.0139	0.0205	0.0328	0.0684	0.0857	0.1745
4	0.0092	0.0136	0.0217	0.0449	0.0573	0.1154
5	0.0066	0.0098	0.0158	0.0322	0.0412	0.0833
7.5	0.0037	0.0055	0.0087	0.0166	0.0189	0.0381
10	0.0024	0.0036	0.0058	0.0109	0.0116	0.0231

Table 7-3. Horizontal design spectra for 5% damping for the YDTI site for V_{S30} of 420 m/sec.

	UHS PSA (g)				Deterministic PSA (g)	
Period (sec)	**475 yr**	**1,000 yr**	**2,475 yr**	**10,000 yr**	**Median**	**84th Percentile**
0.01/PGA	0.1120	0.1709	0.2783	0.5311	0.5008	0.8751
0.02	0.1137	0.1739	0.2839	0.5447	0.5119	0.8945
0.03	0.1216	0.1863	0.3043	0.5772	0.5405	0.9481
0.04	0.1344	0.2066	0.3376	0.6319	0.5896	1.0420
0.05	0.1473	0.2263	0.3682	0.6914	0.6307	1.1213
0.075	0.1869	0.2868	0.4638	0.8722	0.7468	1.3453
0.1	0.2213	0.3401	0.5494	1.0076	0.8526	1.5362
0.15	0.2616	0.4009	0.6463	1.1949	1.0257	1.8311
0.2	0.2743	0.4211	0.6853	1.2992	1.1505	2.0622
0.25	0.2690	0.4122	0.6754	1.3094	1.2063	2.1961
0.3	0.2509	0.3825	0.6288	1.2412	1.1938	2.2270
0.4	0.2122	0.3196	0.5251	1.0489	1.0583	2.0081
0.5	0.1822	0.2720	0.4445	0.9091	0.9324	1.8002
0.75	0.1274	0.1883	0.3068	0.6436	0.7018	1.4005
1	0.0899	0.1326	0.2160	0.4612	0.5170	1.0440
1.5	0.0547	0.0800	0.1282	0.2686	0.3121	0.6349
2	0.0362	0.0532	0.0849	0.1778	0.2100	0.4270
3	0.0201	0.0296	0.0474	0.0997	0.1240	0.2523
4	0.0128	0.0190	0.0304	0.0632	0.0797	0.1602
5	0.0089	0.0132	0.0213	0.0441	0.0554	0.1117
7.5	0.0047	0.0071	0.0112	0.0217	0.0243	0.0490
10	0.0030	0.0046	0.0073	0.0140	0.0145	0.0290

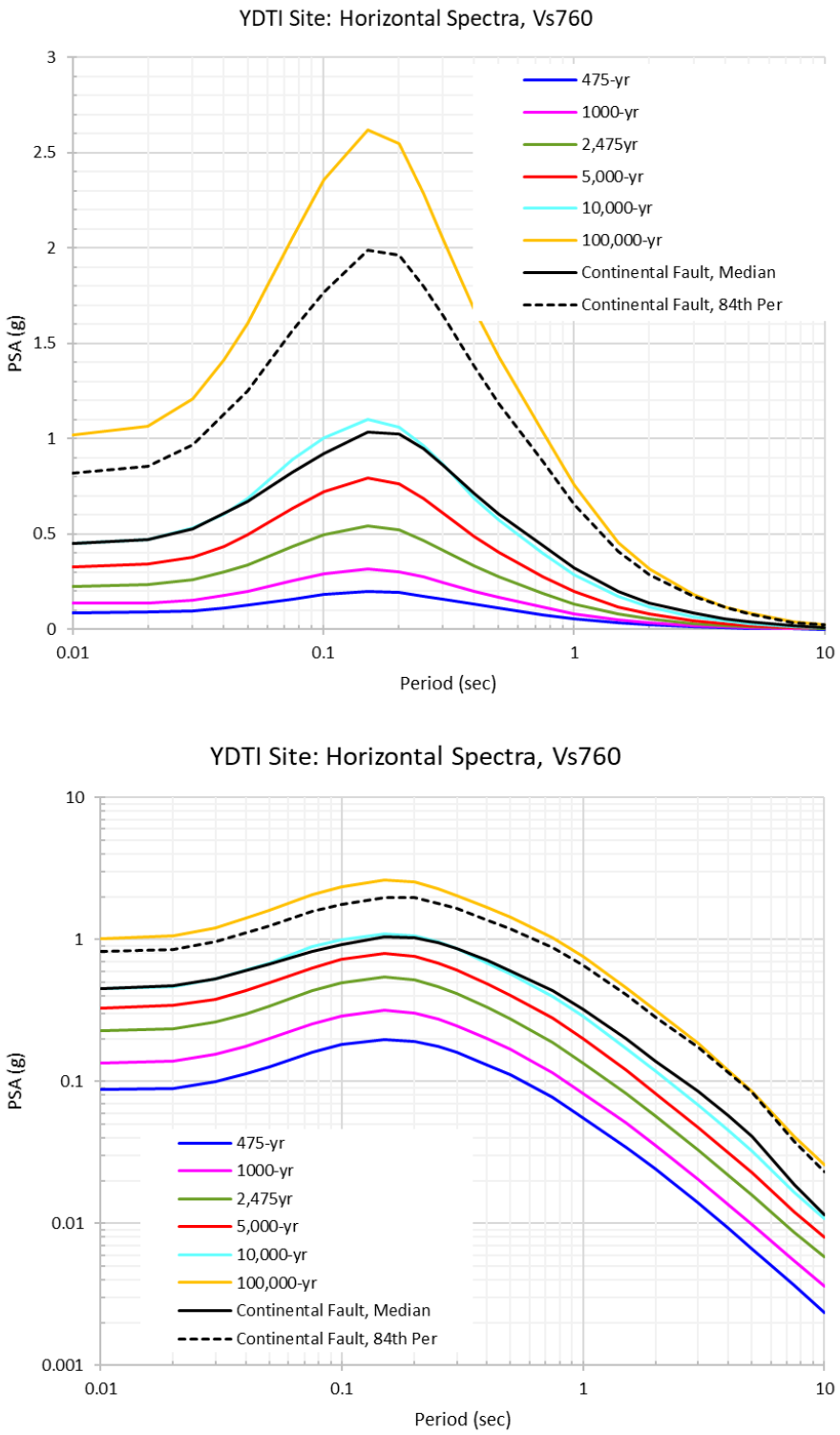

Figure 7-1. Comparison of the UHS (475, 1,000, 2,475, 5,000, 10,000, and 100,000-year return period) to the median and 84th percentile deterministic response spectra for the MCE scenario on the Continental-Elk Park fault at the YDTI site for V_{S30} of 760 m/sec in log-linear (top) and log-log (bottom) scales.

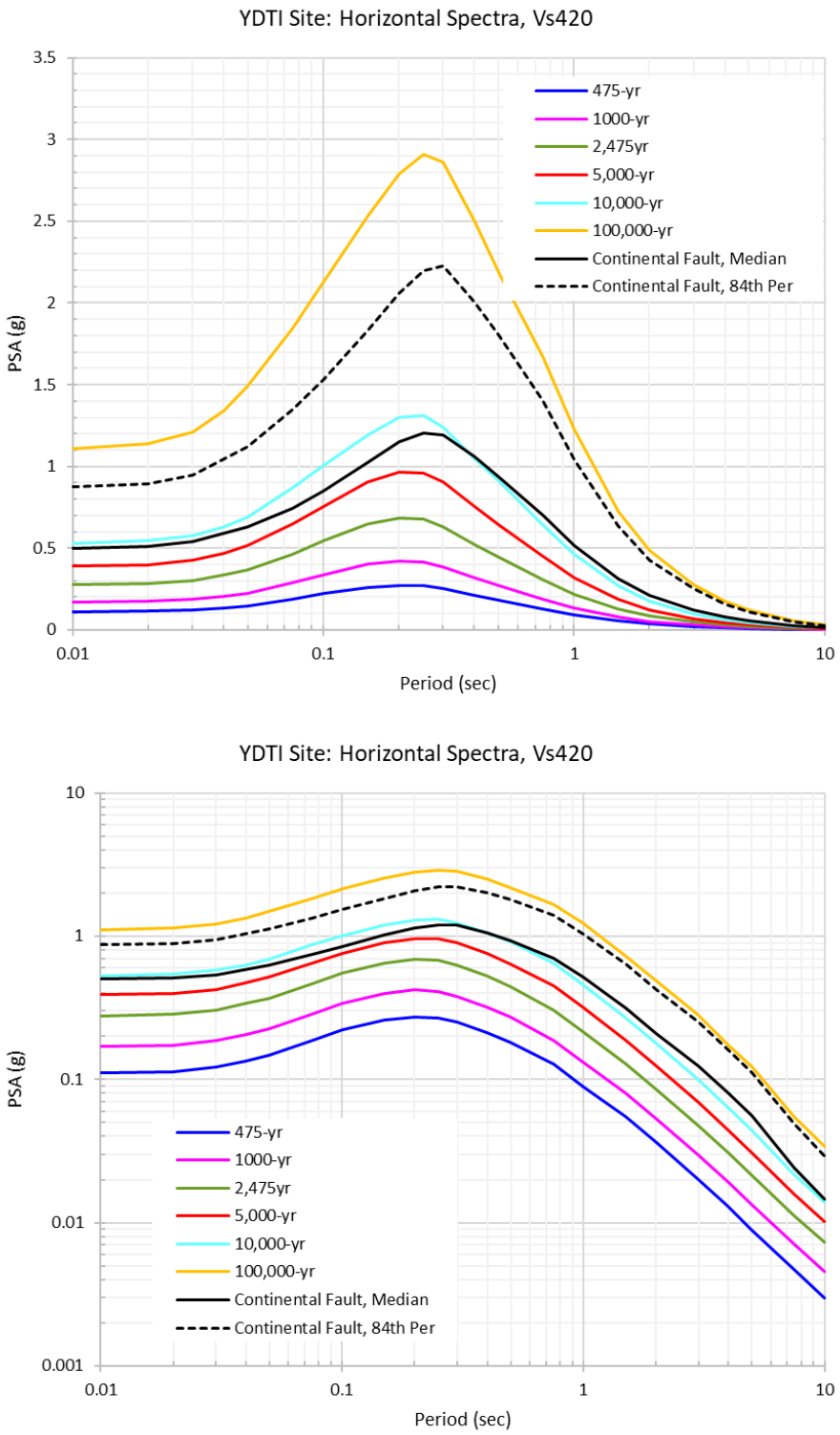

Figure 7-2. Comparison of the UHS (475, 1,000, 2,475, 5,000, 10,000, and 100,000-year return period) to the median and 84th percentile deterministic response spectra for the MCE scenario on the Continental-Elk Park fault at the YDTI site for V_{S30} of 420 m/sec in log-linear (top) and log-log (bottom) scales.

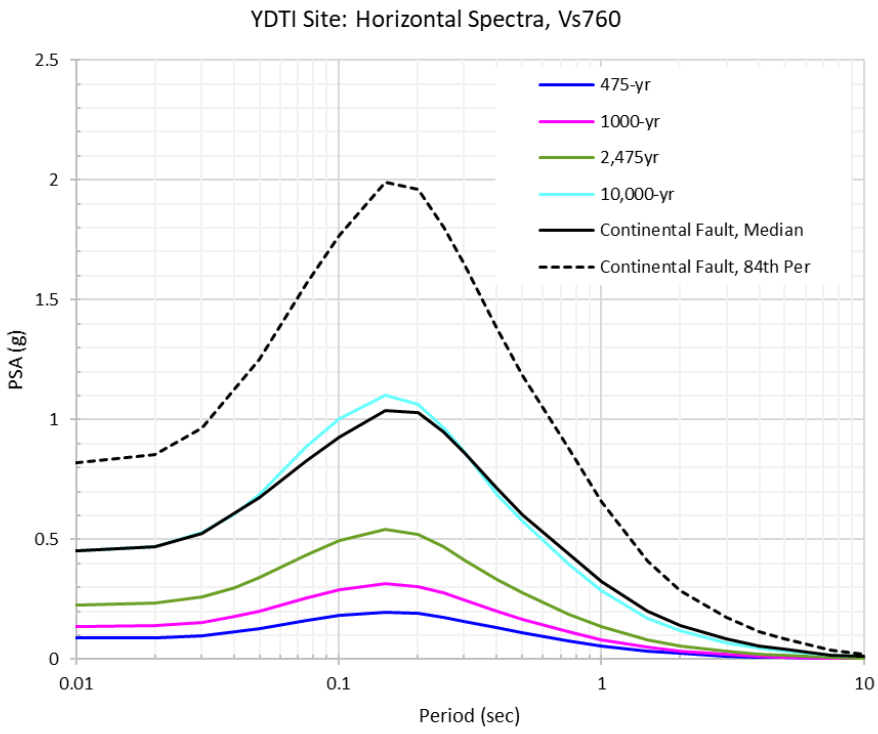

Figure 7-3. Horizontal design spectra at the YDTI site for V_{S30} of 760 m/sec.

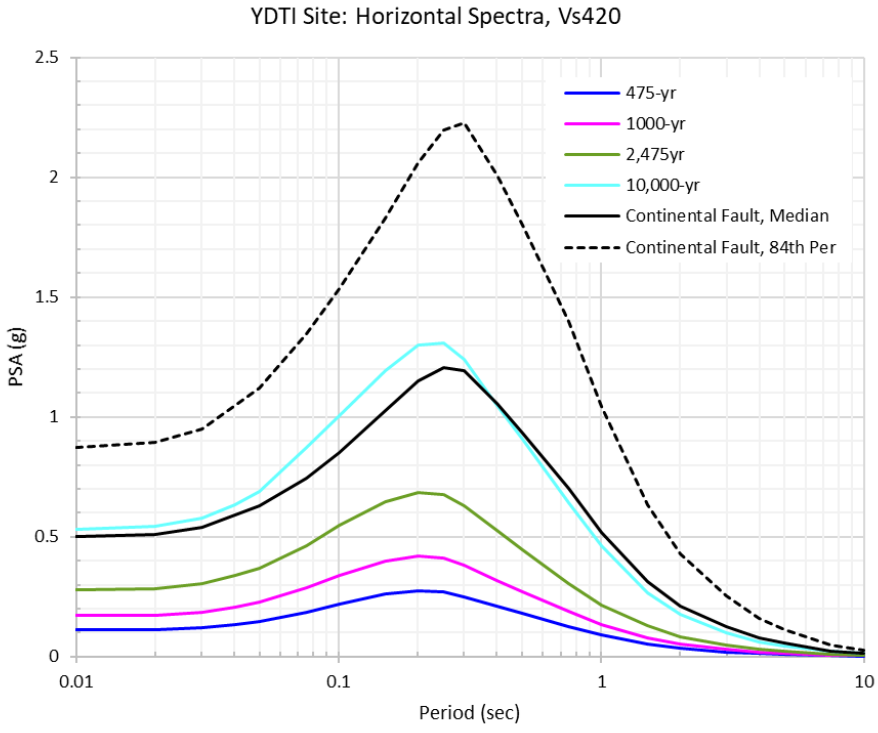

Figure 7-4. Horizontal design spectra at the YDTI site for V_{S30} of 420 m/sec.

7.2 Vertical Design Spectra

Vertical design spectra are developed for the YDTI study update based on the use of vertical-to-horizontal (V/H) ratios that are applied to the design horizontal spectra. This approach, also used in Al Atik and Gregor (2016), is the standard state of practice for the development of design vertical response spectra that are consistent with the horizontal ground motions and use consistent controlling scenario earthquakes for the horizontal and vertical ground motions. This approach involves the selection of controlling earthquake scenarios for the suite of hazard return periods based on the hazard deaggregation results. The MCE scenarios are used for the deterministic design spectra. One or multiple V/H models as then selected and used to develop V/H ratios for the selected scenario earthquakes. When multiple controlling scenario earthquakes are selected for a return period, the resulting V/H ratios are typically enveloped to reduce the number of separate vertical spectra and potentially vertical time histories needed for analyses. These V/H ratios are multiplied by their respective horizontal design spectra for the suite of PSHA return periods and for the deterministic MCE case to obtain the corresponding design vertical response spectra.

For the calculation of V/H ratios, Al Atik and Gregor (2016) used the Gulerce and Abrahamson (2011) model that is based on empirical ground-motion data from active tectonic regions in the NGA-West1 region. In this study update, the Gulerce and Abrahamson (2011) and Bozorgnia and Campbell (2016) models are used and assigned equal weights. The Bozorgnia and Campbell (2016) model is based on the expanded empirical ground-motion data from active tectonic regions in the NGA-West2 database. The use of both Gulerce and Abrahamson (2011) and Bozorgnia and Campbell (2016) is the current state of practice for the development of V/H ratios for active tectonic regions.

The hazard deaggregation results presented in Section 6.2 for V_{S30} of 760 and 420 m/sec are used to selected controlling scenario earthquakes for the suite of return periods of 475, 1,000, 2,475, and 10,000 years. Based on the similarity of the deaggregation results in terms of binned magnitude-distance contribution to the hazard for the two site conditions evaluated, the same scenarios earthquakes are used for V_{S30} of 760 and 420 m/sec. These controlling events are dependent on the spectral period of interest and on the hazard level. For the 475, 1,000, and 2,475-year return periods, two short distance scenarios with **M** 5.75 and 6.6 are selected based on the short spectral periods deaggregeation. An additional **M** 7.0 and Rrup of 100 km scenario is selected based on the deaggregation at the longer spectral periods (≥ 1 sec). For the return period of 10,000 years, one controlling scenario with **M** 6.6 and Rrup of 10 km is selected. For the deterministic analysis, the same earthquake parameters of scenario RupB-LS1-W on the Continental-Elk Park fault used for the horizontal motions are applied for the V/H model calculation. Table 7-4 summarizes the scenario events used for the V/H estimates. These controlling scenario earthquakes are different from those used in Al Atik and Gregor (2016) based on the changes to the SSC and GMC models in this study update. Al Atik and Gregor (2016) selected two scenarios with **M** 6.15 at Rrup of 30 km and **M** 6.6 at Rrup of 60 km for the 475 and 1,000-year return periods. For the 2,475 and 10,000-year return periods, two scenarios with **M** 6.15 at Rrup of 15 km and **M** 6.6 at Rrup of 30 km were used in the 2016 study. MCE scenarios on the Continental fault with **M** 6.5 at Rrup of 1.2 km and 0.1 km were used in AL Atik and Gregor (2016) for the deterministic analysis.

Table 7-4. Scenario events used for the estimation of the V/H ratios.

Hazard Level	Controlling Scenario Earthquakes
475, 1,000, and 2,475 yr	**M** 5.75 - Rrup 20 km (background) **M** 6.6 - Rrup 10 km (Continental) **M** 7.0 - Rrup 100 km (background)
10,000 yr	**M** 6.6 - Rrup 10 km (Continental)
MCE on Continental-Elk Park Fault (RupB-LS1-W)	**M** 7.0 - Rrup 1.43 km

For each of the probabilistic scenario events, the faulting mechanism is assigned to normal. The dip angle for the scenarios with **M** 5.75 - Rrup 20 km and **M** 7.0 - Rrup 100 km is assigned to 45 degrees and the top of rupture at 2 km depth, consistent with the background seismicity source with the site located on the footwall. For the **M** 6.6 - Rrup 10 km controlling scenario assumed to be on the Continental fault, the dip angle is assigned to 70 degrees rupturing to the ground surface with the site located on the hanging wall. The calculated V/H ratios for each of the three probabilistic controlling scenarios are shown in Figure 7-5 for the two V/H models used as well as their weighted average for V_{S30} of 760 m/sec. Figure 7-5 indicates that V/H ratios obtained using the Gulerce and Abrahamson (2011) model (GA2010) are generally larger than those obtained using the Bozorgnia and Campbell (2016) model (BC2016).

For the Continental-Elk Park fault scenario event, the faulting mechanism is normal with a dip angle of 70 degrees and a top of rupture at the ground surface with the site located on the hanging wall of the rupture. Figure 7-5 (bottom left) shows the V/H ratios calculated for the MCE scenario on the Continental-Elk fault using the two V/H models as well as their weighted average for V_{S30} of 760 m/sec. In this study update, nonlinear site effects in the Gulerce and Abrahamson (2011) and the Bozorgnia and Campbell (2016) model are calculated based on their dependence on the median PGA value for a reference rock condition with V_{S30} of 1,100 m/sec. In Al Atik and Gregor (2016), the nonlinear site response was calculated based on its dependence on the PGA value, as opposed to the median PGA value, on reference rock. As a result, the 2016 study used different V/H ratios for the median and 84th percentile deterministic event while this study update uses one set of V/H ratios for both median and 84th percentile ground motion. The change to use median PGA on rock for the nonlinear site response as opposed to PGA value on rock is based on Abrahamson (2019, personal communication).

Figure 7-6 shows the recommended V/H ratios for the probabilistic and deterministic controlling events for V_{S30} of 760 m/sec. These ratios are listed in Table 7-5. For the 475, 1,000, and 2,475-year return period, three controlling scenarios are selected and the recommended V/H ratio for these return periods is based on enveloping the weighted average V/H obtained for each scenario as shown in Figure 7-6 (upper left). This envelope is based on the V/H ratios of the scenario with **M** 6.6 – Rrup 10 km at spectral periods ≤ 0.15 sec and on those of scenario **M** 7.0 – Rrup 100 km for the longer spectral periods. For the 10,000-year return period and for the DSHA, one scenario is selected for each case and the corresponding recommended V/H ratios are shown in Figure 7-6 and listed in Table 7-5. A comparison of the V/H ratios from this study update to those of the 2016 study is shown in Figure 7-7 for the deterministic and probabilistic design levels for V_{S30} of 760 m/sec. This figure indicates that the V/H

ratios for this study update are generally lower than those of Al Atik and Gregor (2016), primarily as a result of including the Bozorgnia and Campbell (2016) model, which predicts lower V/H ratios than the Gulerce and Abrahamson (2011) model.

The recommended V/H ratios listed in Table 7-5 are used to multiply the horizontal design spectra of Table 7-2 to obtain the corresponding vertical design spectra for V_{S30} of 760 m/sec. The vertical design spectra are listed in Table 7-6. The horizontal and vertical design spectra are shown in Figures 7-8 to 7-10 for the deterministic median and 84th percentile and for the probabilistic ground motions with return periods of 475, 1,000, 2,475, and 10,000 years for V_{S30} of 760 m/sec.

Table 7-5. Recommended V/H ratios for the YDTI site for V_{S30} of 760 m/sec.

Period (sec)	475, 1,000, and 2,475 yr	10,000 yr	Deterministic (Median and 84th)
0.01/PGA	0.6646	0.6646	0.7038
0.02	0.6683	0.6683	0.7099
0.03	0.7225	0.7225	0.7699
0.04	0.7644	0.7644	0.8216
0.05	0.7998	0.7998	0.8679
0.075	0.7677	0.7677	0.8257
0.1	0.7040	0.7040	0.7401
0.15	0.5865	0.5865	0.6022
0.2	0.5462	0.5133	0.5044
0.25	0.5350	0.4989	0.4798
0.3	0.5366	0.4865	0.4689
0.4	0.5619	0.4928	0.4760
0.5	0.5810	0.4932	0.4780
0.75	0.6154	0.5191	0.4962
1	0.7070	0.5894	0.5531
1.5	0.7268	0.6356	0.6013
2	0.7387	0.6640	0.6108
3	0.7614	0.6823	0.6182
4	0.7775	0.6946	0.6366
5	0.8119	0.6955	0.6664
7.5	0.8967	0.7346	0.7539
10	0.8344	0.6802	0.7149

Table 7-6. Vertical design spectra for 5% damping for the YDTI site for V_{S30} of 760 m/sec.

	Probabilistic				Deterministic	
Period (sec)	**475 yr**	**1,000 yr**	**2,475 yr**	**10,000 yr**	**Median**	**84th Percentile**
0.01/PGA	0.0582	0.0904	0.1512	0.3000	0.3181	0.5773
0.02	0.0600	0.0933	0.1567	0.3134	0.3334	0.6062
0.03	0.0719	0.1122	0.1890	0.3840	0.4058	0.7442
0.04	0.0865	0.1357	0.2298	0.4642	0.4969	0.9192
0.05	0.1016	0.1598	0.2719	0.5483	0.5841	1.0876
0.075	0.1237	0.1961	0.3338	0.6836	0.6828	1.2953
0.1	0.1289	0.2046	0.3492	0.7060	0.6844	1.3077
0.15	0.1165	0.1851	0.3175	0.6458	0.6249	1.1978
0.2	0.1050	0.1658	0.2846	0.5457	0.5183	0.9894
0.25	0.0944	0.1474	0.2508	0.4807	0.4543	0.8642
0.3	0.0857	0.1325	0.2233	0.4216	0.4036	0.7724
0.4	0.0737	0.1121	0.1868	0.3383	0.3398	0.6559
0.5	0.0648	0.0976	0.1612	0.2835	0.2889	0.5650
0.75	0.0478	0.0711	0.1165	0.2069	0.2176	0.4370
1	0.0391	0.0581	0.0952	0.1693	0.1789	0.3628
1.5	0.0252	0.0370	0.0596	0.1094	0.1204	0.2455
2	0.0179	0.0264	0.0423	0.0792	0.0857	0.1747
3	0.0106	0.0156	0.0249	0.0467	0.0530	0.1079
4	0.0071	0.0106	0.0169	0.0312	0.0365	0.0735
5	0.0054	0.0080	0.0128	0.0224	0.0275	0.0555
7.5	0.0033	0.0049	0.0078	0.0122	0.0143	0.0287
10	0.0020	0.0030	0.0048	0.0074	0.0083	0.0165

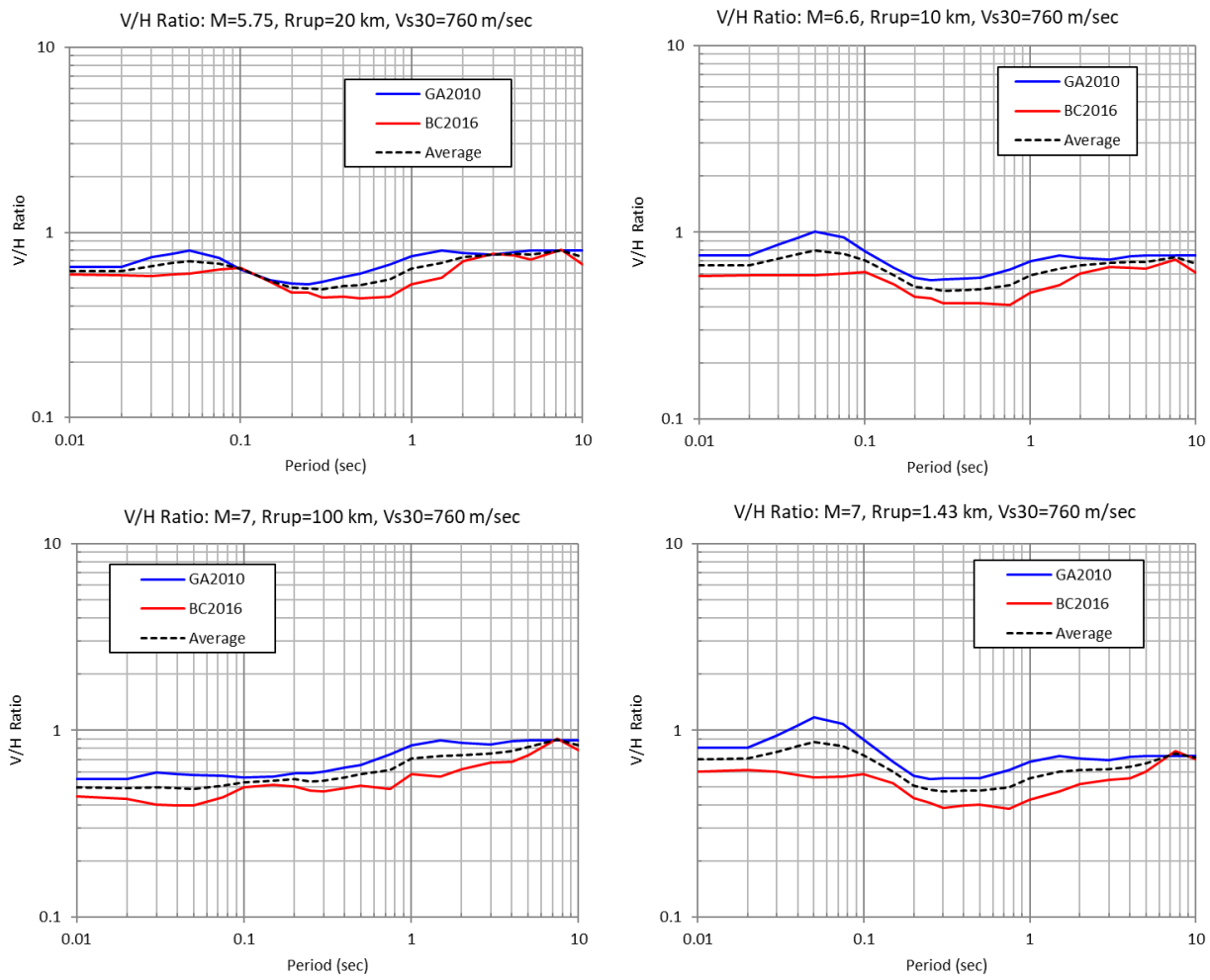

Figure 7-5. V/H ratios for the probabilistic and deterministic controlling scenarios for V_{S30} of 760 m/sec.

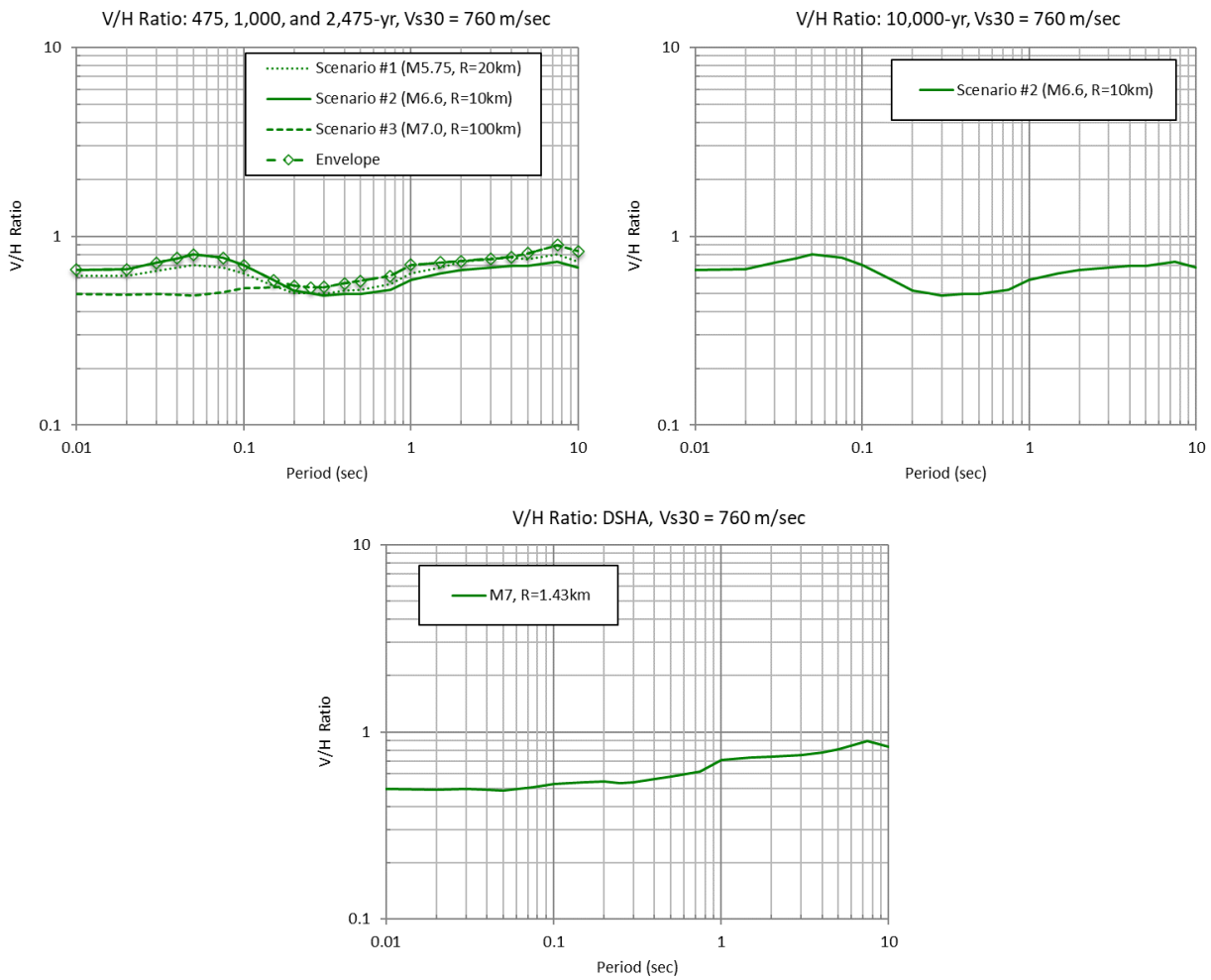

Figure 7-6. Recommended V/H ratios for the 475, 1,000, and 2,475-yr return period (top right, envelope), 10,000-yr return period (top left) and for the deterministic scenario for V_{S30} of 760 m/sec.

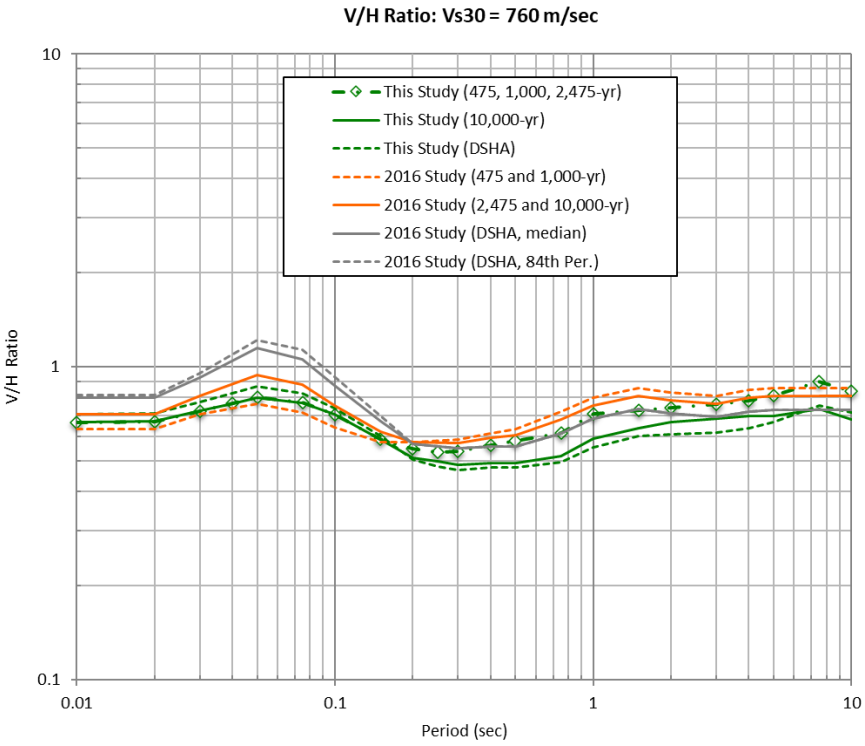

Figure 7-7. Comparison of recommended V/H ratios for this study (green curves) to those from the Al Atik and Gregor (2016) study for V_{S30} of 760 m/sec.

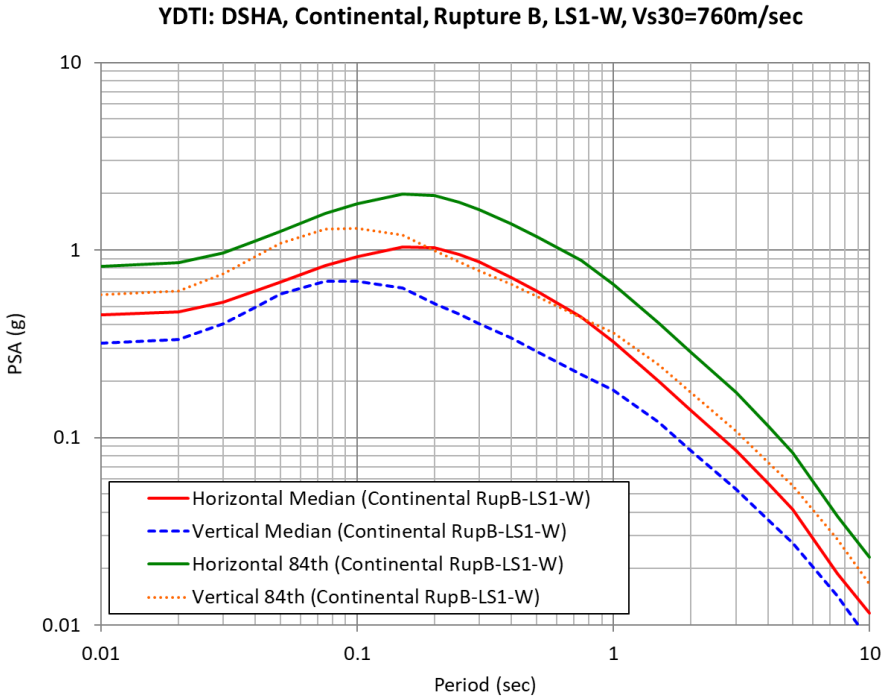

Figure 7-8. Horizontal and vertical design spectra for the deterministic MCE on the Continental-Elk Park fault for V_{S30} of 760 m/sec.

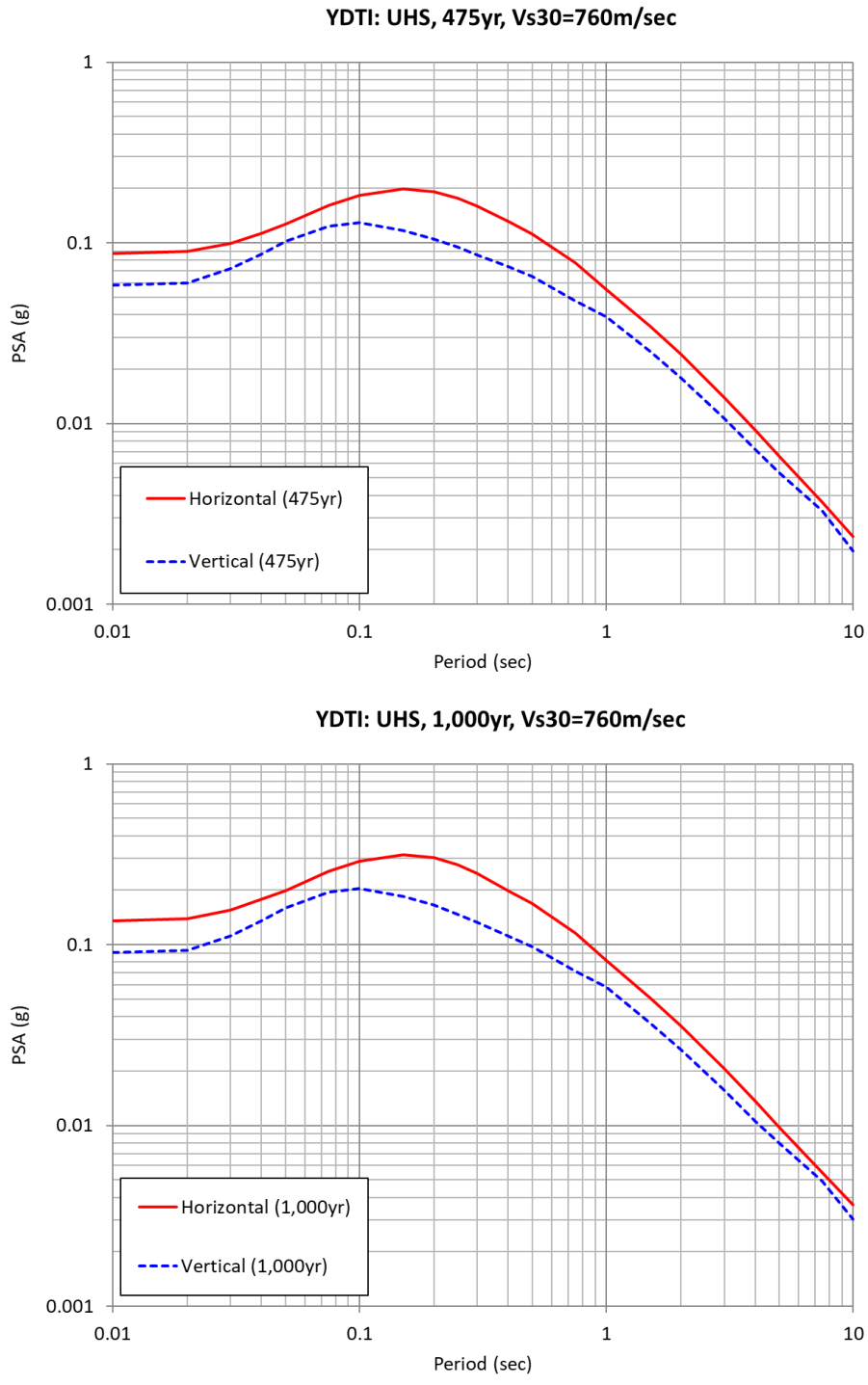

Figure 7-9. Horizontal and vertical design spectra for the 475-yr (top) and 1,000-yr (bottom) return periods for V_{S30} of 760 m/sec.

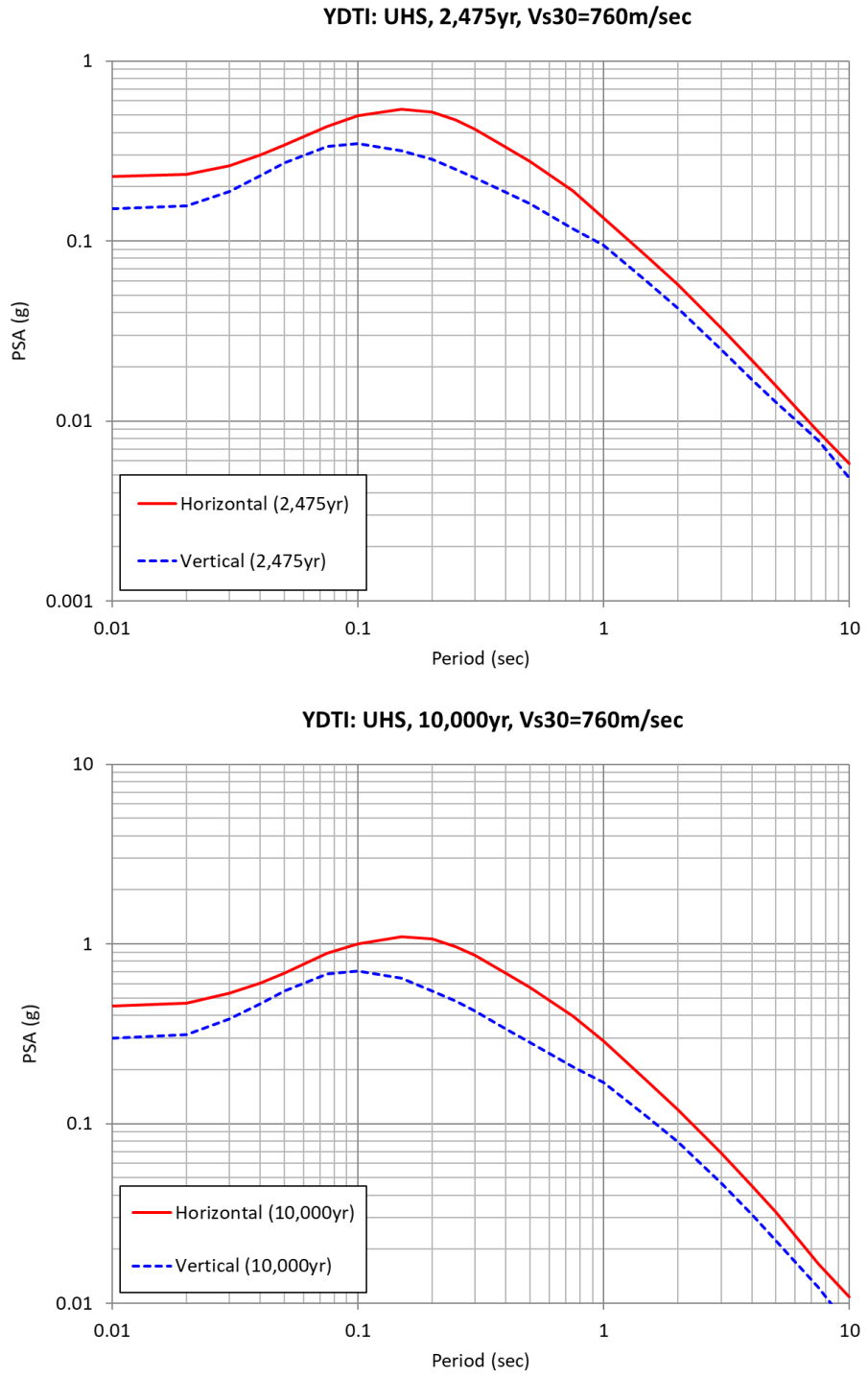

Figure 7-10. Horizontal and vertical design spectra for the 2,475-yr (top) and 10,000-yr (bottom) return periods for V_{S30} of 760 m/sec.

A similar analysis is performed to develop vertical design spectra for the site-specific V_{S30} of 420 m/sec. Figure 7-11 shows the computed V/H ratios for the different controlling scenarios listed in Table 7-4 for the Gulerce and Abrahamson (2011) and the Bozorgnia and Campbell (2016) models as well as their

weighted average. Similar to the V_{S30} of 760 m/sec case, the Bozorgnia and Campbell (2016) model generally predicts lower V/H ratios than the Gulerce and Abrahamson (2011) model but the difference between V/H ratios from the two models is generally smaller for V_{S30} of 420 m/sec. Figure 7-12 shows the recommended V/H ratios for V_{S30} of 420 m/sec for the different probabilistic and deterministic design levels. These recommended V/H values are listed in Table 7-7. Figures 7-13 to 7-15 show the design horizontal and vertical response spectral for the different probabilistic and deterministic design levels for V_{S30} of 420 m/sec. The vertical design spectra are listed in Table 7-8 for the site-specific condition at the YDTI site.

Table 7-7. Recommended V/H ratios for the YDTI site for V_{S30} of 420 m/sec.

Period (sec)	475, 1,000, and 2,475 yr	10,000 yr	Deterministic (Median and 84th)
0.01/PGA	0.7093	0.7093	0.8485
0.02	0.7148	0.7148	0.8606
0.03	0.7917	0.7917	0.9671
0.04	0.8832	0.8832	1.1056
0.05	0.9620	0.9620	1.2310
0.075	0.9733	0.9733	1.2589
0.1	0.8609	0.8609	1.1028
0.15	0.6834	0.6834	0.8620
0.2	0.5646	0.5646	0.6764
0.25	0.4915	0.4915	0.5496
0.3	0.4423	0.4423	0.4797
0.4	0.4410	0.4071	0.4160
0.5	0.4444	0.3858	0.3802
0.75	0.4636	0.3909	0.3689
1	0.5265	0.4382	0.4051
1.5	0.5438	0.4776	0.4454
2	0.5866	0.5275	0.4777
3	0.6225	0.5569	0.4979
4	0.6354	0.5689	0.5146
5	0.6538	0.5602	0.5309
7.5	0.6959	0.5705	0.5791
10	0.6416	0.5237	0.5434

Table 7-8. Vertical design spectra for 5% damping for the YDTI site for V_{S30} of 420 m/sec.

	Probabilistic				Deterministic	
Period (sec)	**475 yr**	**1,000 yr**	**2,475 yr**	**10,000 yr**	**Median**	**84th Percentile**
0.01/PGA	0.0794	0.1212	0.1974	0.3767	0.4249	0.7425
0.02	0.0813	0.1243	0.2029	0.3894	0.4406	0.7699
0.03	0.0963	0.1475	0.2409	0.4570	0.5227	0.9169
0.04	0.1187	0.1824	0.2982	0.5581	0.6519	1.1521
0.05	0.1417	0.2177	0.3542	0.6651	0.7764	1.3803
0.075	0.1819	0.2792	0.4514	0.8490	0.9401	1.6936
0.1	0.1905	0.2928	0.4730	0.8675	0.9402	1.6941
0.15	0.1788	0.2740	0.4417	0.8166	0.8841	1.5783
0.2	0.1549	0.2378	0.3869	0.7335	0.7782	1.3949
0.25	0.1322	0.2026	0.3320	0.6435	0.6629	1.2069
0.3	0.1110	0.1692	0.2781	0.5489	0.5727	1.0683
0.4	0.0936	0.1409	0.2315	0.4270	0.4403	0.8354
0.5	0.0810	0.1209	0.1975	0.3507	0.3545	0.6845
0.75	0.0591	0.0873	0.1423	0.2516	0.2589	0.5167
1	0.0473	0.0698	0.1137	0.2021	0.2094	0.4229
1.5	0.0297	0.0435	0.0697	0.1283	0.1390	0.2828
2	0.0212	0.0312	0.0498	0.0938	0.1003	0.2040
3	0.0125	0.0184	0.0295	0.0555	0.0617	0.1256
4	0.0081	0.0121	0.0193	0.0360	0.0410	0.0824
5	0.0058	0.0087	0.0139	0.0247	0.0294	0.0593
7.5	0.0033	0.0049	0.0078	0.0124	0.0141	0.0284
10	0.0019	0.0029	0.0047	0.0073	0.0079	0.0158

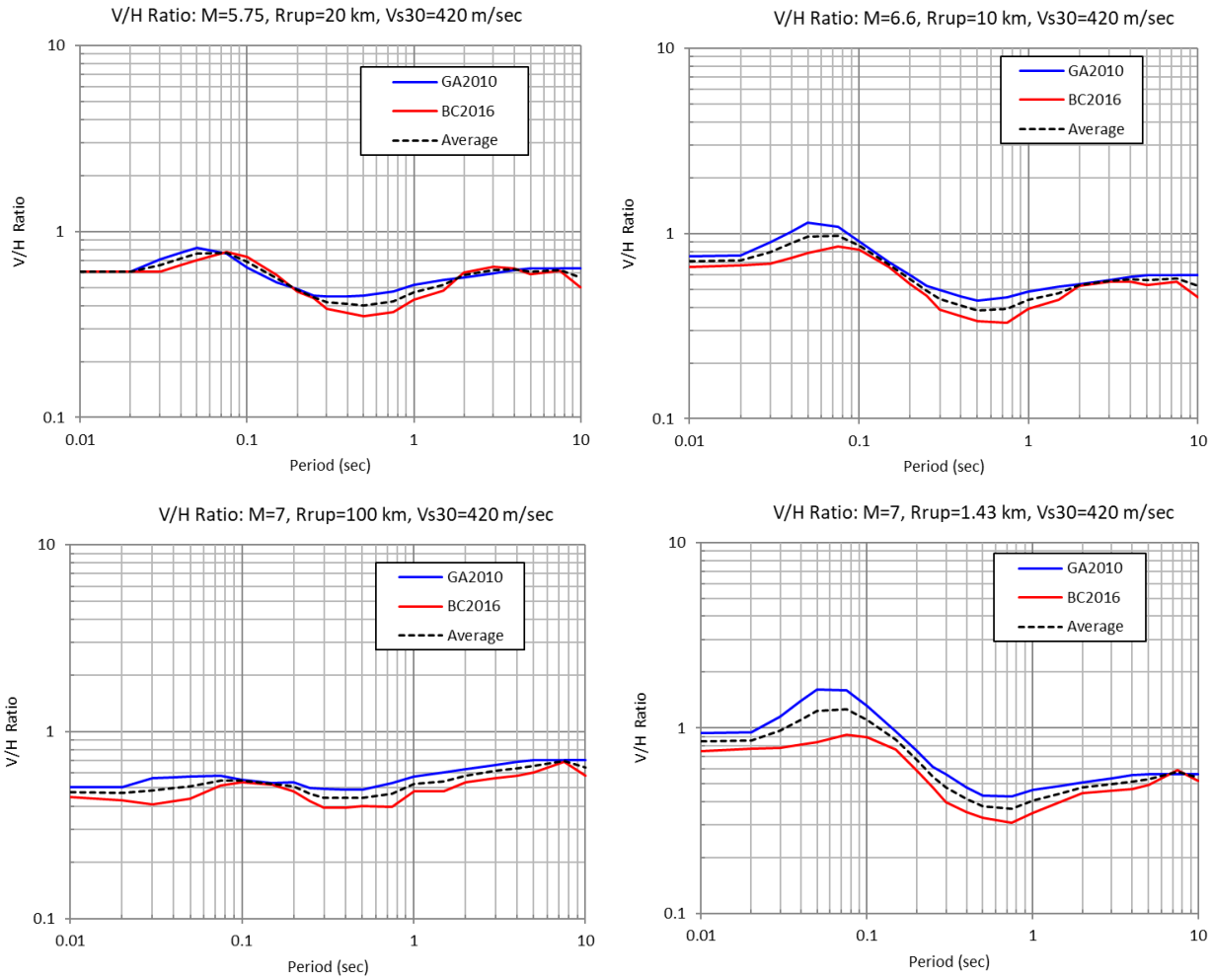

Figure 7-11. V/H ratios for the probabilistic and deterministic controlling scenarios for V_{S30} of 420 m/sec.

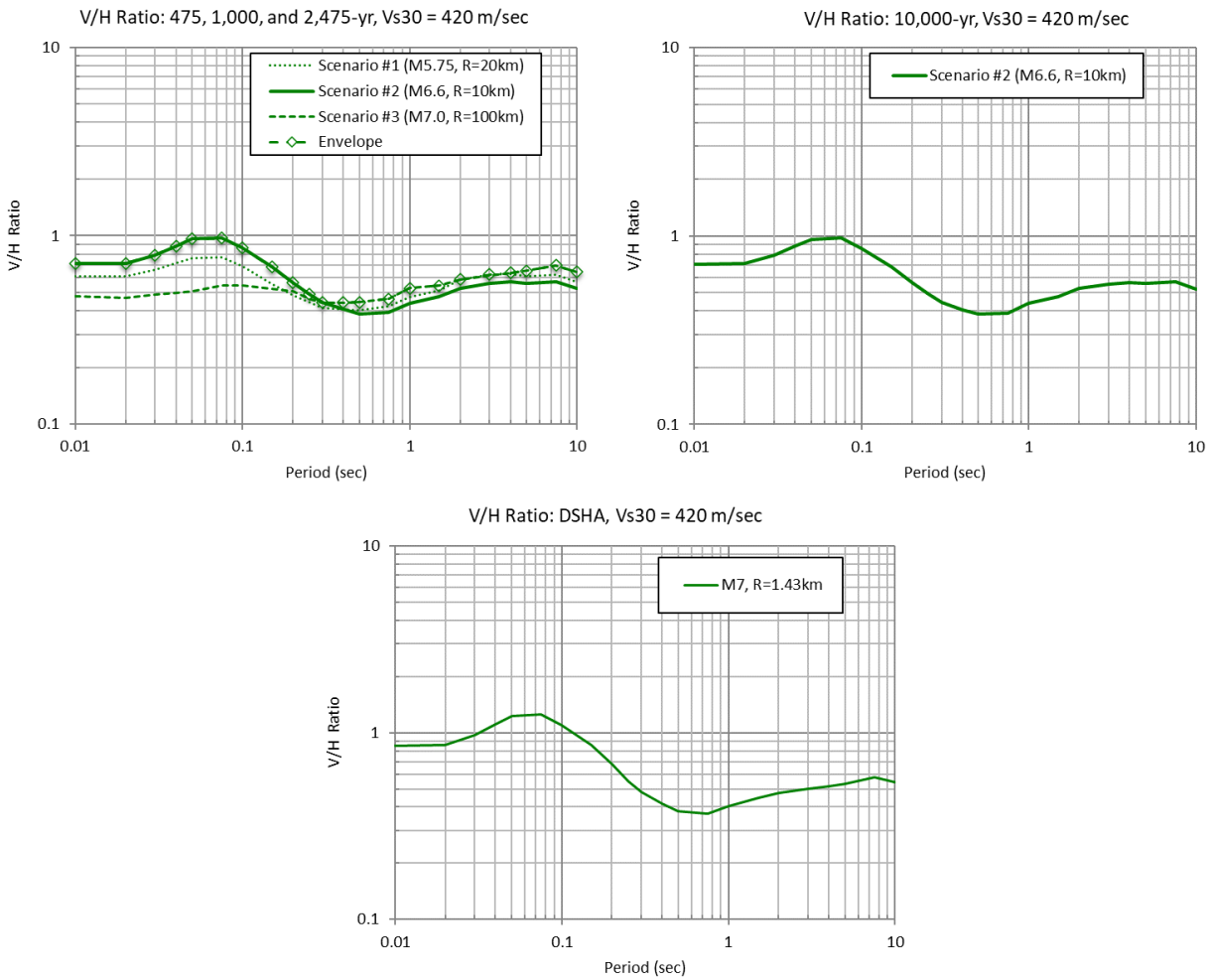

Figure 7-12. Recommended V/H ratios for the 475, 1,000, and 2,475-yr return period (top right, envelope), 10,000-yr return period (top left) and for the deterministic scenario for V_{S30} of 420 m/sec.

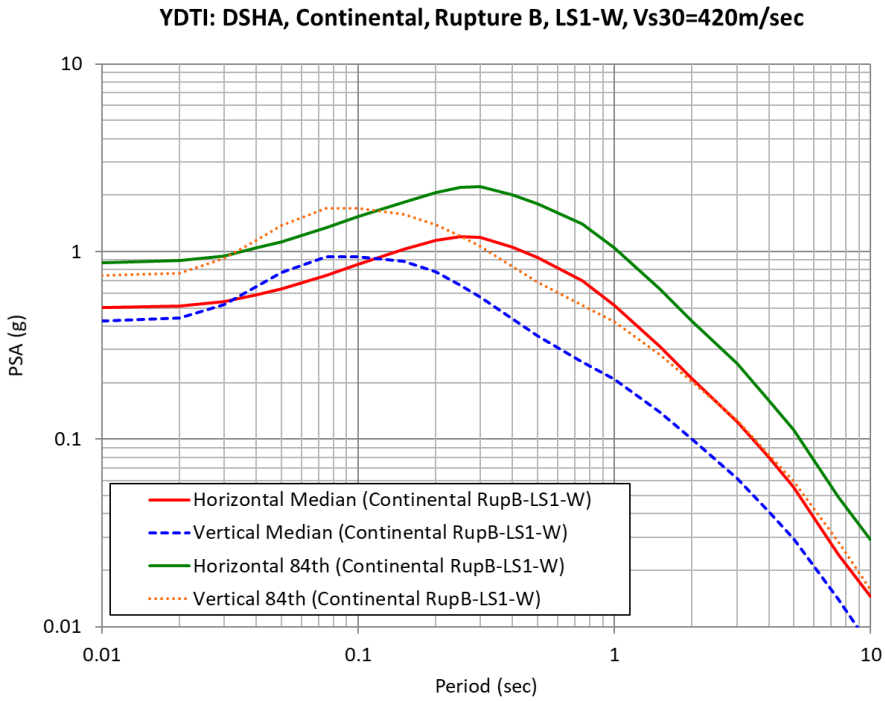

Figure 7-13. Horizontal and vertical design spectra for the deterministic MCE on the Continental-Elk Park fault for V_{S30} of 420 m/sec.

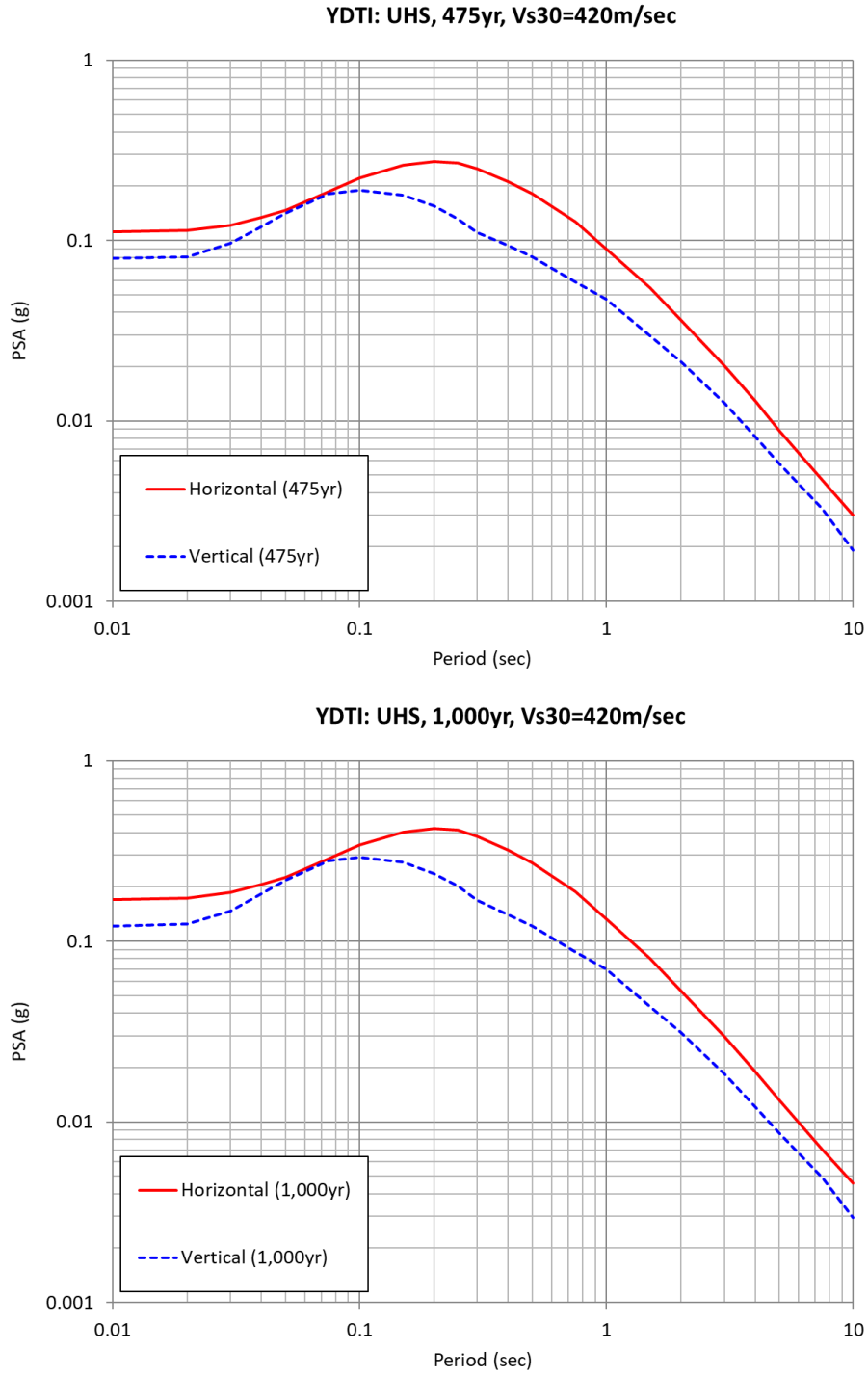

Figure 7-14. Horizontal and vertical design spectra for the 475-yr (top) and 1,000-yr (bottom) return periods for V_{S30} of 420 m/sec.

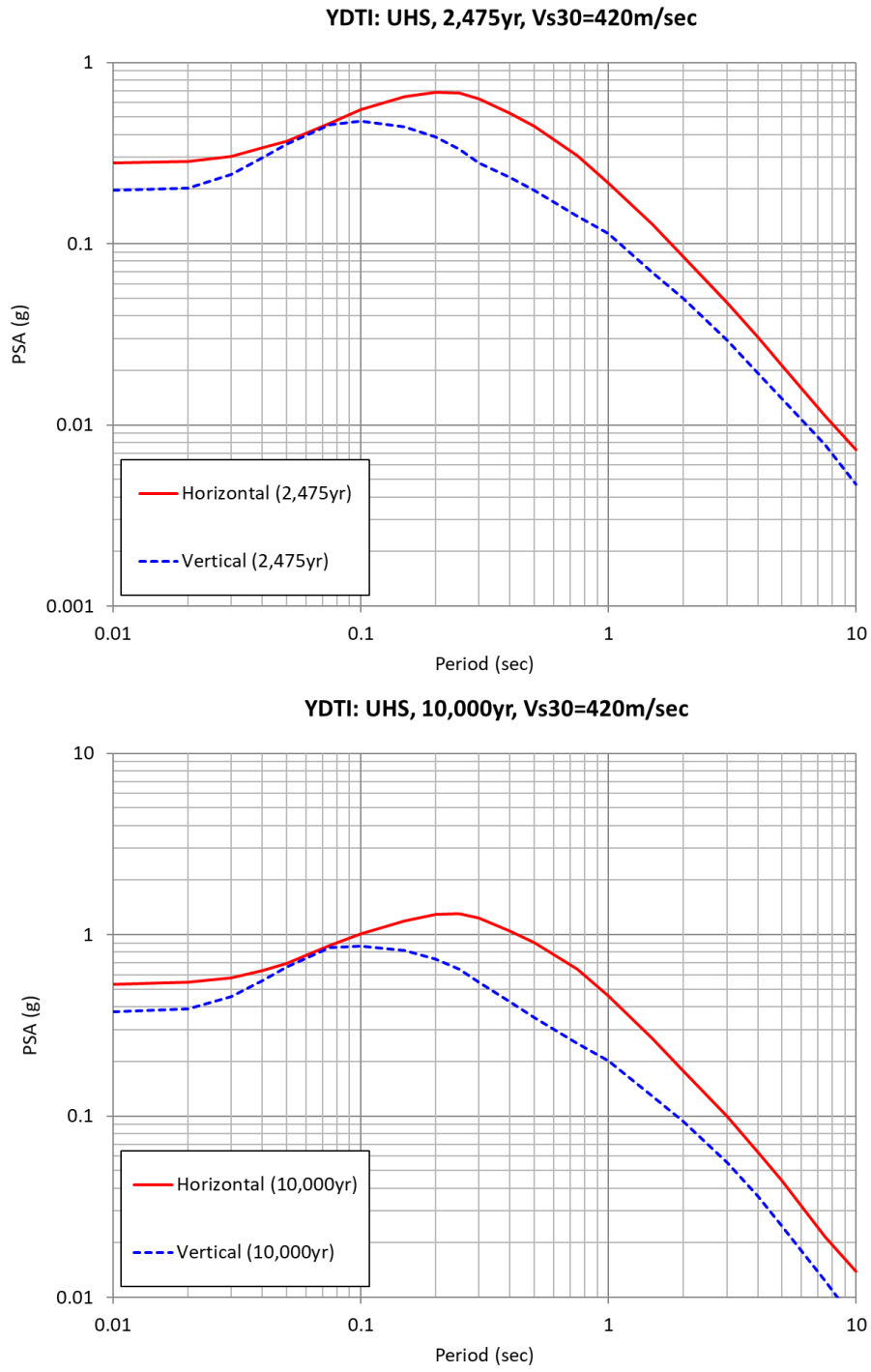

Figure 7-15. Horizontal and vertical design spectra for the 2,475-yr (top) and 10,000-yr (bottom) return periods for V_{S30} of 420 m/sec.

8. CONTINENTAL FAULT DISPLACEMENT HAZARD

Al Atik and Gregor (2016) evaluated the fault displacement hazard on the Continental fault using an "informed deterministic" approach as described in Thompson et al. (2016). This approach is deterministic in principle and does not consider earthquake rates as a parameter. Unlike the traditional deterministic approach where a single MCE scenario and a single fault displacement prediction equation (DPE) are used to calculate the average or maximum displacement on a fault, this approach considers the epistemic uncertainty in defining the MCE. Epistemic uncertainty and aleatory variability in the DPEs are also included in this approach. The informed deterministic approach results in hazard curves with exceedance probability ranging from 0 to 1 (as opposed to annual rate of exceedance in the probabilistic approach) plotted versus displacement. As a result of accounting for the uncertainties in the MCE and the DPE, the informed deterministic approach acknowledges the considerable uncertainty involved in estimating the net fault displacement at a project site.

Al Atik and Gregor (2016) used their seismic source characterization of the Continental fault along with three alternative DPEs (Wells and Coppersmith 1994 for all slip types, Wells and Coppersmith 1994 for normal faults, and Hecker et al. 2013 for all slip types) in their fault displacement analysis. Using the fault and displacement characterization models, Al Atik and Gregor (2016) estimated the median and 84th percentile displacement on the Continental fault for both the average and maximum displacement. These estimates are listed in Table 8-1. Their analysis provided estimates of primary displacement on the Continental fault and did not consider off-fault distributed deformation or secondary or triggered deformation that may occur on adjacent faults.

Table 8-1. Surface fault displacement hazard results on the Continental fault from Al Atik and Gregor (2016).

Exceedance	Percentile	Average Displacement (m)	Maximum Displacement (m)
0.50	50	0.51	0.74
0.16	84	1.44	2.07

In this study update, we use the same methodology as the 2016 study to estimate the maximum and average displacements on the Continental-Elk Park fault following the informed deterministic approach. We use the same DPEs logic tree as that used in Al Atik and Gregor (2016) along with the updated characterization of the Continental-Elk Park fault in this study update. In the following sections, we provide an overview of the approach used and a description of the fault and displacement models characterization followed with estimates of fault displacements from this study update. Similar to the 2016 study, we provide estimates of primary fault displacement for the Continental-Elk Park fault, and we do not consider off-fault distributed deformation or secondary displacement.

8.1 Approach

Fault displacement calculations require estimates of the MCE magnitude and selection of fault DPEs. The informed deterministic approach accounts for the epistemic uncertainty in the MCE and DPE through the use of logic trees whereby each path on the tree represents a viable set of parameters and equations for estimating fault displacement. The confidence in each path is reflected by the combined path weight. The aleatory variability in the displacement along each logic tree path is captured though

the use of a probability density function. This variability is typically represented by the standard deviation of the prediction equations.

Fault displacement is calculated for each path of the logic tree. Results can be expressed as a weighted mean displacement hazard curve in the form of a complementary cumulative distribution function (CCDF); whereby the probability from 0 to 1 of a displacement value being exceeded is plotted against displacement. In addition to the mean hazard curve, CCDFs can be plotted for the individual logic tree paths as well as hazard fractiles (i.e., 50th, 10th, and 90th fractiles). The mean and the median hazard curves represent the central tendency of the hazard results while the separation among the fractile curves represents the epistemic uncertainty in the models and parameters used on the results and provides a measure of confidence in the mean hazard estimate.

8.2 Source and Displacement Characterization

In this study update, we use the updated seismic source characterization of the Continental-Elk Park fault discussed in Section 3.2. The Continental-Elk Park fault logic tree is shown in Figure 3-7 with parameters listed in Table 3-2. A sensitivity analysis of the fault displacement is performed for the controlling MCE sources of Rupture Models A and B where we evaluate the displacement hazard from each of the MCE scenarios RupA-01 and RupB-LS1 from Rupture Models A and B, respectively. For each of these MCE sources, the weighted three-point characteristic magnitude estimates are used in the displacement hazard analysis. Given the higher likelihood of Rupture Model A compared to Rupture Model B, our final analysis uses two weighted MCE scenarios on the Continental-Elk Park fault with their respective magnitude distribution. The MCE scenarios RupA-01 from Rupture Model A and RupB-LS1 from Rupture Model B are used with weights of 0.8 and 0.2, respectively, as shown in the logic tree of Figure 8-1.

To characterize the displacement on the Continental-Elk Park fault from the scenarios shown in Figure 8-1, we use alternative DPEs that predict best estimates of displacement as a function of earthquake magnitude along with the variability in the displacement. The use of multiple DPEs captures the epistemic uncertainty in the displacement prediction. The aleatory variability for each DPE represents variability in the event-to-event displacement as well as measurement errors in the dataset used to derive a DPE. Three alternative DPEs are used to estimate the average displacement on the Continental-Elk Park fault as shown in Figure 8-1: Wells and Coppersmith (1994) for all slip types, Wells and Coppersmith (1994) for normal faults, and Hecker et al. (2013). These relationships have the following form:

$$\log_{10} AD = a\boldsymbol{M} + b \pm \sigma_{AD} \qquad (1)$$

where AD is the average surface displacement (i.e., mean displacement along the rupture length) and $\sigma_{AD}$is the regression standard deviation in log10 units. Average displacement (median estimate) versus magnitude predicted by these three empirical relationships is shown in Figure 8-2. Figure 8-2 indicates that the Wells and Coppersmith (1994) relationships for all slip types (WC94, all) and for normal faults (WC94, N) predict similar average fault displacement as a function of magnitude. Because the relationship for all fault types is based on a larger dataset and provides more reliable results, we give the Wells and Coppersmith relationships for all fault types and for normal faults weights of 0.5 and 0.3,

respectively. The Hecker et al. (2013) (HEA13, all) relationship is based on a least-squares fit to data from Wesnousky (2008). As shown in Figure 8-2, this relationship has a smaller slope (i.e., flatter line) than the Wells and Coppersmith relationships. We give the Hecker et al. (2013) relationship a weight of 0.2 since the dataset used to derive it is smaller than that of Wells and Coppersmith (1994) (a total of 37 versus 56 events). Table 8-2 lists the a- and b-coefficients of the three DPEs along with their published standard deviations (σ_{AD}). The σ_{AD} values represent the variability in predicting the average surface-fault displacement. Since our goal is to estimate the primary surface displacement at the intersection of the Continental-Elk Park fault with the YDTI site and not the average surface displacement over the entire surface rupture, the variability in displacement along the surface rupture about the average displacement must be included to estimate the total standard deviation of the net surface displacement at a site (rather than average displacement) given an earthquake of magnitude **M** (Abrahamson 2008). Equation (1) is modified as follows:

$$\log_{10} AD = a\boldsymbol{M} + b \pm \sigma_T \qquad (2)$$

where σ_T is the square root of the sum of squares of regression standard deviation (σ_{AD}) and the along-strike standard deviation (σ_{AS}). Estimates of σ_{AS} are obtained from the analysis of along-strike displacements in Hecker et al. (2013) that suggested a coefficient of variation of 0.6 for strike-slip fault ruptures with comparable estimate for other slip types. This coefficient of variation results in σ_{AS} of 0.24 applied to all three DPEs used in this analysis.

Total standard deviations for each DPE are listed in Table 8-2. The σ_T estimates represent a combination of epistemic uncertainty resulting from imperfect empirical datasets and true aleatory variability in displacement at a particular location along the rupture estimated based on magnitude. Hecker et al. (2013) analyzed available paleoseismic data and observed that the aleatory variability in displacement at a site is lower than the values presented in Table 8-2. They estimated the aleatory standard deviation to be about 0.22 compared to the σ_T values of about 0.4 listed in Table 8-2. The epistemic uncertainty standard deviation part of σ_T, denoted as $\sigma_{\mu e}$, can be estimated using the true aleatory variability of 0.22 and the σ_T estimates in Table 8-2. This additional epistemic uncertainty belongs in the logic tree and can be represented by a 5-point approximation based on Miller and Rice (1983) to discretely sample the values of $\sigma_{\mu e}$. Using the three alternative DPEs and the 5-point approximation to discretize the epistemic uncertainty component of σ_T results in 15 branches describing the median displacement at a site given the MCE magnitude. All 15 DPE branches have an aleatory variability of 0.22 (value based on Hecker et al. (2013) and assumed to apply to the other DPEs).

Table 8-2. Parameters of the DPEs used in the net fault displacement hazard analysis for the YDTI site crossing of the Continental-Elk Park fault.

DPE	Weight	a	b	σ_{AD}	σ_{AS}	σ_T
Wells and Coppersmith (1994) – All slip types	0.5	0.69	-4.80	0.36	0.24	0.43
Wells and Coppersmith (1994) – Normal Faults	0.3	0.63	-4.45	0.33	0.24	0.41
Hecker et al. (2013) – All slip types	0.2	0.41	-2.79	0.33	0.24	0.41

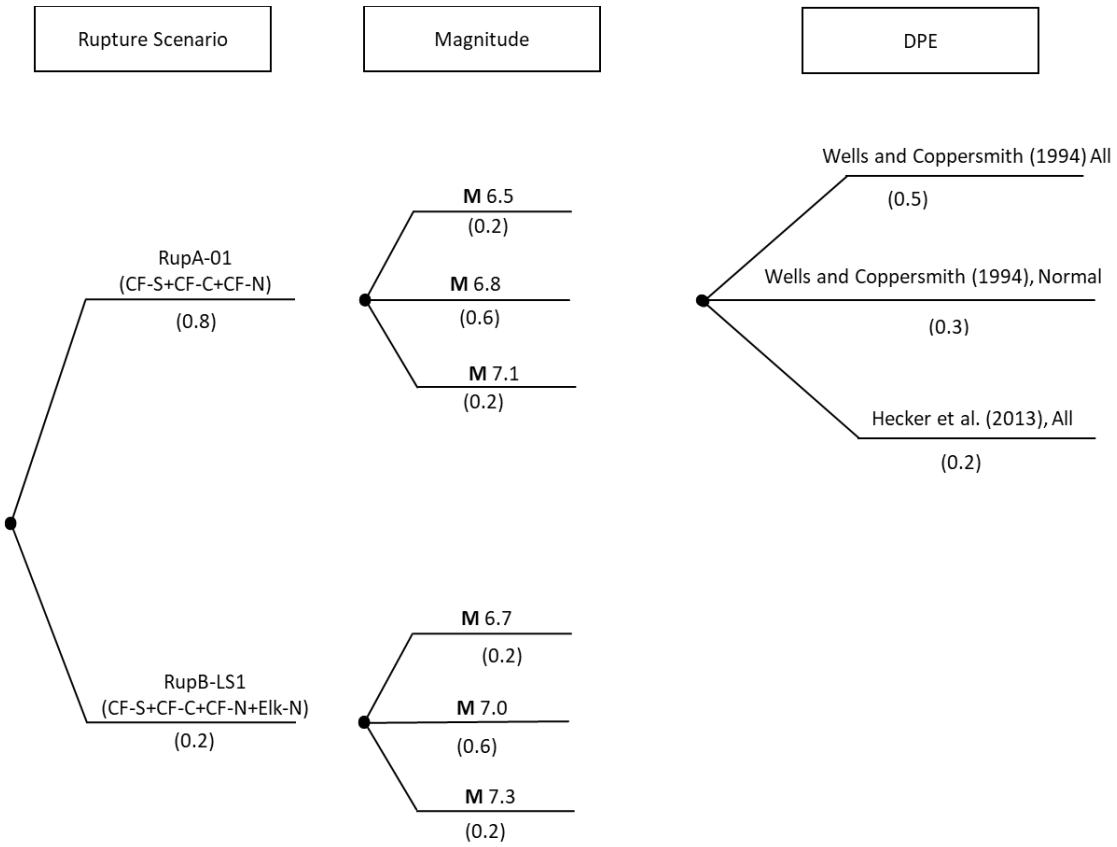

Figure 8-1. Logic tree for fault displacement hazard analysis. Weights are given between parentheses.

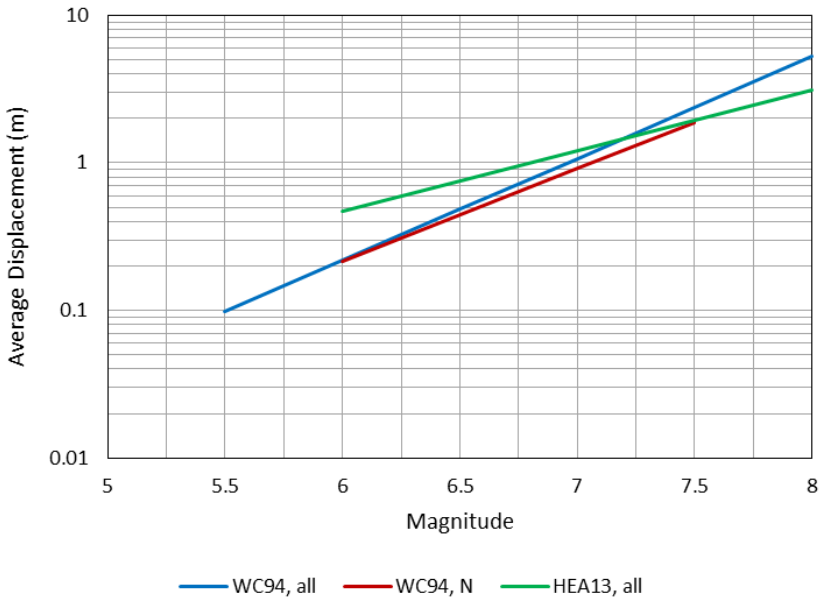

Figure 8-2. Empirical relationships of average displacement (median estimates) versus magnitude (source: Al Atik and Gregor 2016).

8.3 Results

As a sensitivity analysis, we first evaluate the displacement hazard independently from MCE scenarios RupA-01 and RupB-LS1 from Rupture Models A and B using the DPEs logic tree shown in Figure 8-1. For each rupture scenario, the three weighted estimates of the characteristic magnitudes listed in Table 3-2 are used. For each rupture scenario, three MCE magnitude branches and 15 DPE branches yield a total of 45 logic tree paths for the estimation of average displacement on the Continental-Elk Park fault. Displacement hazard is also evaluated for the logic tree shown in Figure 8-1 using both RupA-01 and RupB-LS1 MCE scenarios with weights of 0.8 and 0.2, respectively. For this case, a total of 90 logic tree paths are used for the estimation of average displacement on the Continental-Elk Park fault.

Table 8-3 summarizes the average displacement hazard results and lists the median and 84th percentile predictions of the net displacement on a point on the Continental-Elk fault for scenarios RupA-01 and RupB-LS1 independently as wells as for the logic tree of Figure 8-1 using both weighted MCE scenarios. Table 8-3 indicates that using RupB-LS1 results in the largest estimate of median and 84th percentile average displacement on the Continental-Elk Park fault due to the larger magnitudes associated with this scenario compared to the RupA-01. We recommend using both weighted MCE scenarios RupA-01 and RupB-LS1 to estimate the fault displacement hazard as opposed to the use of the relatively rare MCE scenario RupB-LS1 (i.e., assigned weight of 0.2) which results in the largest estimates of fault displacement hazard. Using both MCE weighted scenarios, the average displacement of the Continental-Elk Park fault is 0.83 and 2.33 m for the median and 84th percentile, respectively, compared to 0.51 and 1.44 m estimated for the median and 84th percentile in Al Atik and Gregor (2016) study. The increase of fault displacement estimates in this study compared to the 2016 study is a direct result of the updated characterization of the Continental-Elk Park fault resulting in larger estimates of characteristic magnitude compared to the 2016 study.

In addition to the average displacement hazard, the informed deterministic approach is also applied to compute the maximum surface displacement hazard on the Continental-Elk Park fault. The calculation of the maximum displacement hazard uses the Wells and Coppersmith (1994) relationships for all slip types and for normal faults with weights of 0.625 and 0.375, respectively. These weights are based on the re-normalized weights shown in Figure 8-1 reflecting a greater confidence in the all-slip type relationship due to the larger dataset used compared to the relationship for normal faults. The maximum displacement relationships are defined with the same functional form as Equation (1) and have slope, intercept and regression standard deviation (aleatory variability) of 0.82, -5.46, and 0.42, respectively, for the all-slip type and 0.89, -5.9, and 0.38 for the normal faults type. For a particular rupture scenario with three estimates of magnitude, this results in six logic tree paths for calculating maximum displacement. Table 8-3 summarizes the results of the maximum displacement hazard for the three cases analyzed for the Continental-Elk Park fault. Similar to the results for average displacement. RupB-LS1 leads to the largest estimates of maximum displacement given the larger magnitudes associated with this event. Again, we recommend the use of weighted MCE scenarios RupA01 and RupB-LS1 to calculate maximum displacement estimates. These estimates are 1.47 and 3.5 m for the median and 84th percentile, respectively, compared to maximum displacement estimates of 0.74 and 2.07 m in Al Atik and Gregor (2016).

Estimates of displacement listed in Table 8-3 are based on the weighted mean of the exceedance probabilities of each of the logic tree paths shown in Figure 8-1. Using the 90 logic tree paths of Figure 8-1 for weighted MCE scenarios RupA-01 and RupB-LS1, we can calculate displacement exceedance curves for the weighted mean as well as the 10th, 25th, 50th, 75th, 84th, and 90th fractiles as shown in Figure 8-3. These fractiles are selected logic tree combinations that may represent the correct model, with the steeper slope of the exceedance curve representing only the aleatory variability. For example, the 50th fractile represents the median logic tree combination (i.e., half of the branch combinations produce lower displacement values) while the 84th fractile represents a model for which approximately 84% of the weighted logic tree combinations yield lower displacement values. Similar to the ground motion fractiles, displaying the fractiles for the fault displacement allows one to visualize the uncertainty in the weighted mean displacement estimates given the epistemic uncertainty in the logic tree.

Table 8-3. Surface fault displacement hazard results on the Continental-Elk Park fault. Scenario and magnitude weights are given between brackets. Estimates for the weighted RupA-01 and RupB-LS1 case (third row of the table) are recommended.

		Average Displacement (m)		Maximum Displacement (m)	
MCE Scenario	**Magnitude**	**Median**	**84th Percentile**	**Median**	**84th Percentile**
RupA-01	6.5 [0.2] 6.8 [0.6] 7.1 [0.2]	0.79	2.19	1.36	3.19
RupB-LS1	6.7 [0.2] 7.0 [0.6] 7.3 [0.2]	1.04	2.89	2.02	4.71
RupA-01 [0.8] RupB-LS1 [0.2]	6.2 [0.16] 6.5 [0.48] 6.8 [0.16] 6.7 [0.04] 7.0 [0.12] 7.3 [0.04]	0.83	2.33	1.47	3.5

We note that the use of the net displacement at a point rather than the maximum displacement results is more appropriate for design considerations at the YDTI site. The maximum displacement values represent a conservative upper bound of the predicted displacement on the Continental-Elk Park fault. Moreover, the intersection of the YDTI site with the Continental fault occurs towards the northern end of the fault. Youngs et al. (2003) studied the variation in the amount of surface displacement along the principal rupture for historical Basin and Range normal faulting events compiled by Wheeler (1989). Figure 8-4 presents their distribution of D/MD (fault displacement normalized by maximum displacement) as a function of X/L, where X/L expresses the location of a point along the rupture (X is the distance from one end of the rupture to the point in question and L is the rupture length). As shown in Figure 8-4, fault surface displacement tends to die out towards the end of the fault rupture and displacement peaks at a limited interval along the rupture primarily towards the midpoint. As a result, we consider the use of the net average displacement values for the YDTI site to be more appropriate than the maximum displacement values. Similar to the discussion regarding the use of the median versus 84th percentile deterministic response spectra presented in Section 7.1, the decision to use the median versus 84th percentile values of the net displacement should be carefully evaluated. Given the low to moderate slip rate on the Continental-Elk Park fault, a hazard matrix similar to the one presented in Table 7-1 can be developed. For high or extreme consequences of failure, the 50th to 84th percentile average displacement can be used. For low to moderate consequences, the use of the 50th percentile net displacement can be used.

Finally, we note that there is an ongoing Fault Displacement Hazard Initiative (FDHI) Project at the University of California, Los Angeles. This is a multi-year community-based research project tasked with the collection of updated and standardized fault displacement measurements and surface rupture maps and the development of Next-Generation fault displacement models. As part of this project, the database collection task is complete, but the development of fault displacement models is still in progress and expected to be finalized in the next 12 months. Early evaluation of some of these preliminary displacement models indicates that estimates of fault displacement are expected to increase for these new models compared to the generation of models used in this study. We note that these new fault displacement models are still subject to change, and we recommend a revision of the fault displacement hazard study for the YDTI site when the Next-Generation fault displacement models are published.

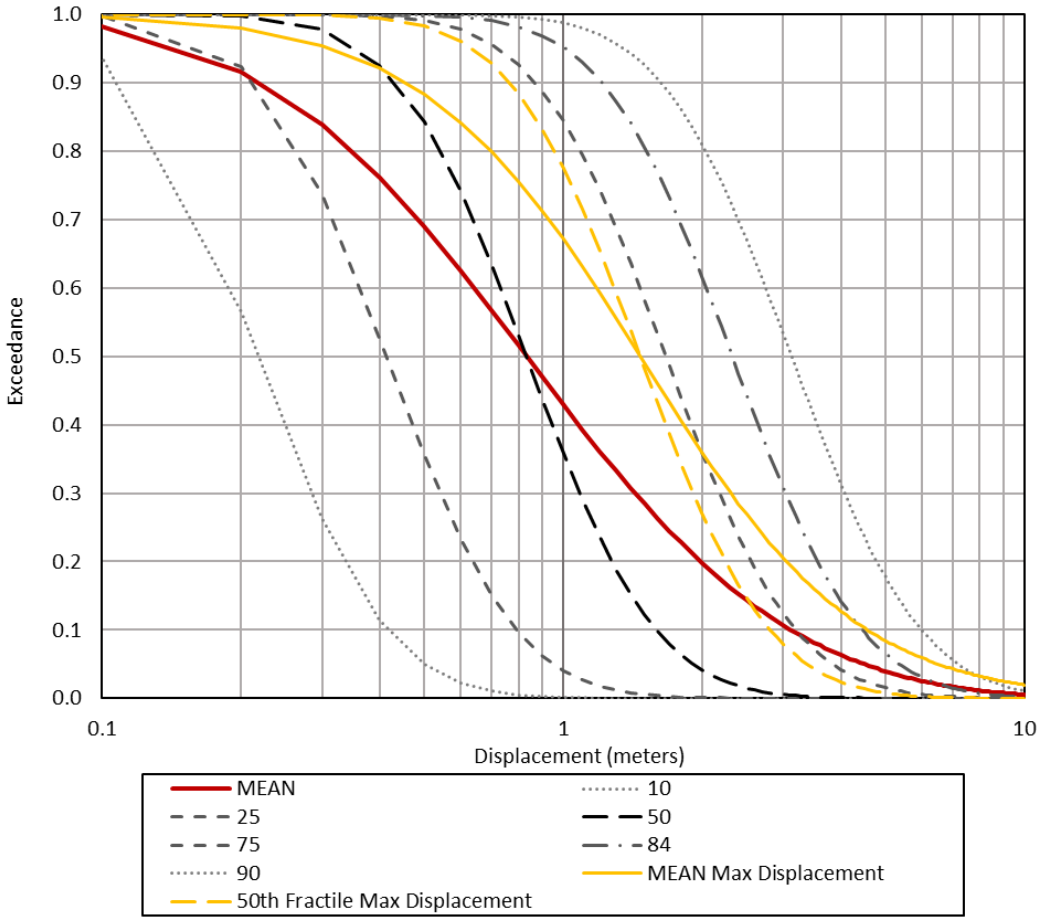

Figure 8-3. Displacement exceedance curves for the net displacement at a point on the Continental-Elk Park fault compared to the maximum displacement exceedance curves (in yellow).

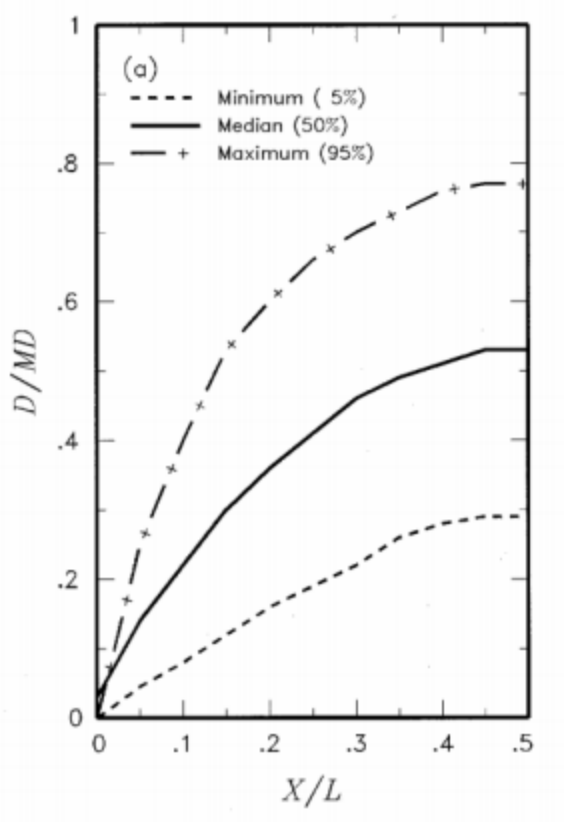

Figure 8-4. Distribution of the ratio of D/MD based on the data in Wheeler (1989) (source: Youngs et al. 2003).

9. DESIGN TIME HISTORIES

9.1 Selection of Time Histories

A total of 5 sets of two-component (i.e., one horizontal and one vertical) design time histories are developed for the each of following design levels:

- DSHA median and 84th percentile response spectra for the MCE scenario on the Continental-Elk Park Fault (RupB-LS1-W) with magnitude 7 and rupture distance of 1.43 km.
- Probabilistic spectra with return period of 1000 years.

The selection of seed input time histories is based on project-specific parameters such as magnitude and source-to-site distance for the MCE scenario and as determined from the deaggregation of the 1000-year return period hazard as well as the overall agreement in spectral shape between the time histories response spectra for the horizontal and vertical components and the target design spectra. Fault rupture mechanism and site conditions were not restricted in the selection process because these criteria are considered to be less important in the selection of representative time histories (Al Atik and Abrahamson, 2010). Moreover, the spectral matching process corrects for differences in the frequency content resulting from different site conditions. Based on the deaggregation results of the PSHA and the magnitude and distance of the deterministic MCE scenario, the selection of the 5 sets of time histories is distributed into the magnitude and distance bins listed in Table 9-1.

The period range of interest for the YDTI dam is estimated at 1.3 – 1.8 sec (KP 2022, personal communication). Based on the close proximity of the YDTI site to the Continental-Elk Park Fault and the period range of interest for the dam, a number of the seed time histories are selected to have a ground-motion pulse. The presence of this pulse in the velocity time histories is an important attribute of near-fault effects. Hayden et al. (2014) is used to provide guidance on the number of expected time histories with directivity pulse for the 3 target spectra cases. The criteria in Hayden et al. (2014) are defined in terms of the dominant epsilon values (number of standard deviations from the median ground motion) and distances identified from the deaggregation analysis. For the deterministic MCE scenario, the rupture distance is 1.43 km, and the epsilon values are 0 and 1 for the median and the 84th percentile target spectra, respectively. Based on these distance and epsilon parameters and using Hayden et al. (2014), 3 and 4 of the 5 sets of time histories are selected to contain a near-field pulse for the median and the 84th percentile target spectra, respectively.

For the 1000-year return period, the mean distance for the long period range of 0.75 to 3 sec is in the range of 51 to 77 km and the mean epsilon is on the order of 0.6 to 0.7. Given these parameters and based on Hayden et al. (2014), near-field pulse recordings are not included in the design time histories for the 1000-year return period target case. The horizontal components of all selected time histories with near-field pulse are then rotated to the fault normal (FN) and fault parallel (FP) directions. The FN component of the near-field pulse recordings is selected. The horizontal components of the recordings that do not contain near-field pulse are used not rotated to FN and FP and are used as-recorded.

Tables 9-2 to 9-4 summarize the parameters of the selected seed input time histories used for the development of spectrally compatible design time histories for the deterministic MCE median and 84th

percentile target spectra and for the 1000-year return period target case. Given the similar controlling event parameters and spectral shape between the median and the 84th percentile target spectra, several of the same time histories are used for both cases. All ground motions were obtained from the Pacific Earthquake Engineering Research Center (PEER) NGA-West2 ground motion database (http://ngawest2.berkeley.edu).

Table 9-1. Magnitude and distance range for the selection of seed input time histories.

Case	Magnitude Range	Distance Range	Number of Sets
1000-yr Return Period	5.5 – 6.0	10 – 30	1
	6.3 – 7.0	0 – 20	3
	6.75 – 7.25	75 – 125	1
MCE Median and 84th Percentile	6.75 – 7.25	0 – 10	5

Table 9-2. Characteristics of selected time histories for the MCE median target with M 7 and Rrup of 1.43 km. Pulse period is reported for the recordings that contain near-field pulse in the horizontal component.

Set #	Earthquake	Year	Station Name	NGA #	M	Rrup (km)	Mech	V_{S30} (m/sec)	5-75% Dur (sec)[1]	5-95% Dur (sec)[1]	Pulse Period (sec)	Scale Factor at PGA - H	Rec. Length (sec)
1	Loma Prieta	1989	Saratoga - Aloha Ave	802	6.93	8.5	Reverse Oblique	380.89	4.1	9.4	4.574	1.44	39.995
2	Cape Mendocino	1992	Petrolia	828	7.01	8.18	Reverse	422.17	6.5	17.7	2.996	0.64	35.985
3	Darfield, New Zealand	2010	LINC	6927	7.0	7.11	Strike Slip	263.2	8.3	12.7	7.385	0.99	74.35
4	Kobe, Japan	1995	Nishi-Akashi	1111	6.9	7.08	Strike Slip	609	4.5	11.2	-	0.96	40.96
5	Irpinia, Italy-01	1980	Auletta	284	6.9	9.55	Normal	476.62	13	19.3	-	7.90	34.29

(1) Based on PEER's reported durations

Table 9-3. Characteristics of selected time histories for the MCE 84th percentile target with M 7 and Rrup of 1.43 km. Pulse period is reported for the recordings that contain near-field pulse in the horizontal component.

Set #	Earthquake	Year	Station Name	NGA #	M	Rrup (km)	Mech	V_{S30} (m/sec)	5-75% Dur (sec)[1]	5-95% Dur (sec)[1]	Pulse Period (sec)	Scale Factor at PGA - H	Rec. Length (sec)
1	Loma Prieta	1989	Saratoga - Aloha Ave	802	6.93	8.5	Reverse Oblique	380.89	4.1	9.4	4.574	2.61	39.995
2	Cape Mendocino	1992	Petrolia	828	7.01	8.18	Reverse	422.17	6.5	17.7	2.996	1.16	35.985
3	Darfield, New Zealand	2010	LINC	6927	7.0	7.11	Strike Slip	263.2	8.3	12.7	7.385	1.80	74.35
4	Kobe, Japan	1995	Nishi-Akashi	1111	6.9	7.08	Strike Slip	609	4.5	11.2	-	1.77	40.96
5	Irpinia, Italy-01	1980	Bagnoli Irpinio	285	6.9	8.18	Normal	649.67	5.2	19.6	1.742	4.32	36.865

(1) Based on PEER's reported durations

Table 9-4. Characteristics of selected time histories for the 1000-yr return period target.

Set #	Earthquake	Year	Station Name	NGA #	M	Rrup (km)	Mech	V_{S30} (m/sec)	5-75% Dur (sec)[1]	5-95% Dur (sec)[1]	Scale Factor at PGA - H	Rec. Length (sec)
1	Livermore-01	1980	Del Valle Dam (Toe)	212	5.8	24.95	Strike Slip	403.37	4.8	12.1	1.05	31.005
2	Loma Prieta	1989	Gilroy Array #6	769	6.93	18.33	Reverse Oblique	663.31	4.5	13.0	0.80	39.995
3	Imperial Valley-06	1979	Compuer tas	167	6.53	15.3	Strike Slip	259.86	13.4	28.7	0.73	57.025
4	Northridge-01	1994	Burbank - Howard Rd.	957	6.69	16.88	Reverse	581.93	5.9	11.6	1.22	29.985
5	Hector Mine	1999	Wrightwood - Nielson Ranch	1841	7.13	113.45	Strike Slip	506	14.8	23.6	2.51	81.92

(1) Based on PEER's reported durations

9.2 Spectrum-Compatible Time Histories for the MCE Median Target

Each of the horizontal components of the selected seed acceleration time histories (see Table 9.2) is modified such that their response spectra match the target deterministic MCE median response spectrum. Similarly, the vertical components are spectrally modified to match the corresponding target vertical spectrum.

Time-domain spectral matching as implemented in the computer program RSPMatch (Abrahamson 2003) is used for the ground-motion modification. A more recent version of the program that implements more efficient algorithms is used in this analysis. The time-domain spectral matching procedure involves adding finite wavelets in the time domain to decrease the spectral differences between the seed motion and the target spectrum. The objective of spectral matching process is to reduce the individual spectral peaks and troughs of the seed input motion improving the spectral match with the given target spectrum while preserving the non-stationary characteristics of the seed motion (Al Atik and Abrahamson, 2010).

Seed time histories are matched to the component-specific target spectra for periods from PGA (0.01 sec) to 5 sec. The spectral matching process is an iterative procedure with each step involving the matching of a larger incremental range in spectral period from 0.01 to 5 sec. After each iteration, and after the final iteration, a baseline correction is applied to the modified time history to ensure the resulting modified spectrum-compatible time history is consistent with expected transient features of a time history (i.e., no long period drift and or permanent offset). Finally, the acceleration response spectra of the modified spectrum-compatible time histories are compared to the target response spectrum to ensure a close match between the two spectra. In addition, comparisons are performed to ensure that the non-stationary characteristics of the seed input time histories and modified time histories (i.e., acceleration, velocity, and displacement) and the associated peak ground motion parameters and durations are reasonable and acceptable.

Comparisons of the spectrally matched motion to the original seed motion for the horizontal and vertical components of the 5 sets of time histories are shown in Appendix I for the MCE median case. The initial time histories and acceleration response spectra shown in these comparison plots are scaled to the target PGA values. Comparisons between the matched and scaled seed motions are provided for the acceleration, velocity and displacements as well as the response spectra, Fourier amplitude spectra, and normalized Arias intensity. Comparisons of the normalized displacement for the matched and seed time histories are also provided to better evaluate the differences between the seed and matched time histories resulting from the spectral matching process.

Figures 9-1 and 9-2 show a comparison of the response spectra of the scaled initial seed time histories to the MCE median target spectra for the horizontal and vertical components, respectively. A plot showing the comparison of the matched response spectra to the target spectrum is also included in each figure. Figures 9-1 and 9-2 show the change in the response spectra of the seed time histories due to the matching process. Figures 9-3 and 9-4 compare the target MCE median response spectra to the average response spectra of the 5 matched time histories for the horizontal and vertical components, respectively. The acceptability of the spectral matches is based on a visual inspection of the individual matches and as well a requirement that the average of the full set of the 5 matched time histories

generally falls within +/-10% of the target horizontal and vertical spectra. This visual inspection and requirement are applied to spectral periods shorter than 5 sec.

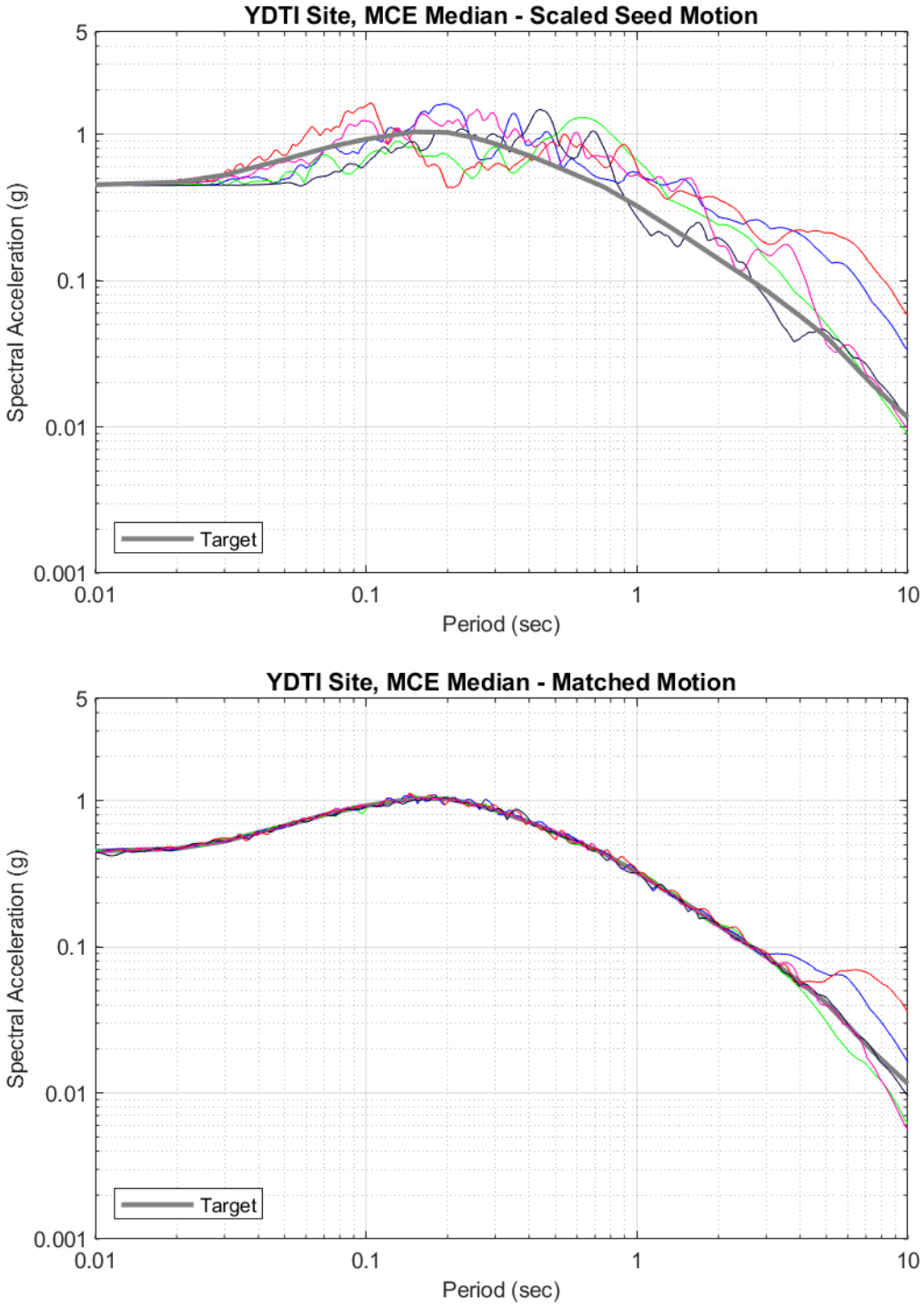

Figure 9-1. Comparison of the target horizontal response spectrum (median MCE) to the response spectra of the horizontal component of the scaled seed time histories (top) and matched time histories (bottom).

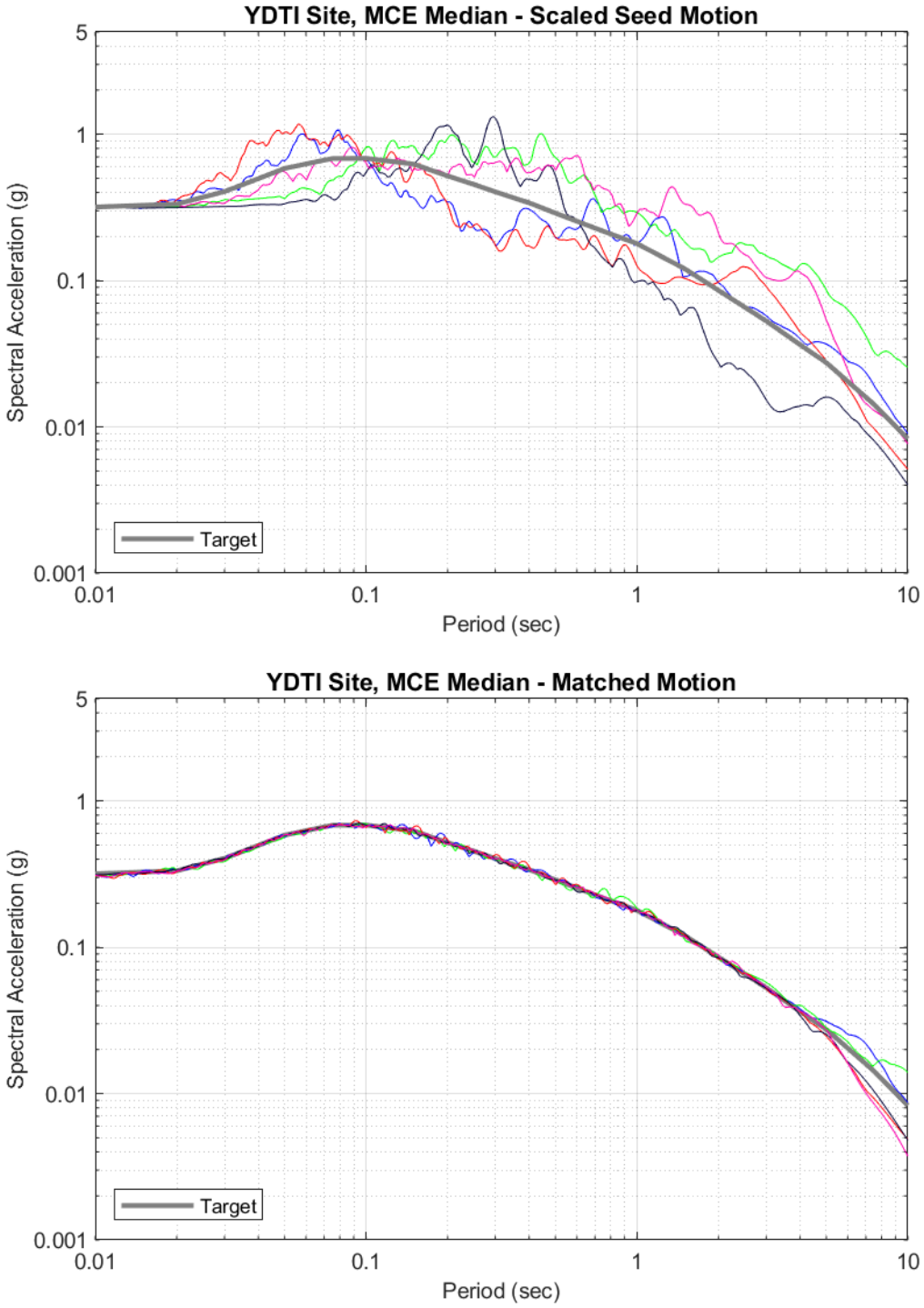

Figure 9-2. Comparison of the target vertical response spectrum (median MCE) to the response spectra of the vertical component of the scaled seed time histories (top) and matched time histories (bottom).

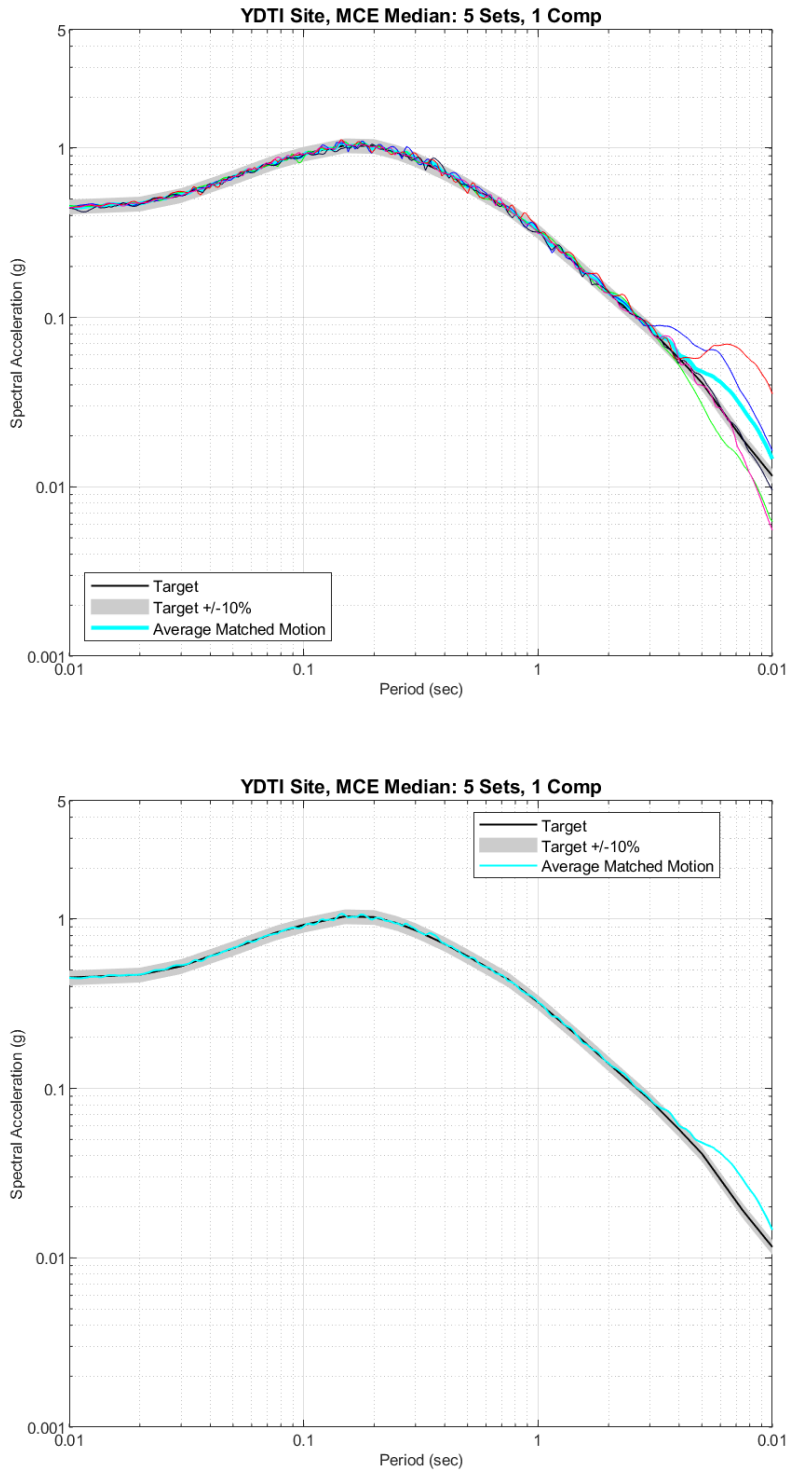

Figure 9-3. Comparison of the average (geometric mean) of the matched response spectra to the target horizontal response spectrum (median MCE). Top plot shows the matched response spectra for the 5 sets and bottom plot shows the average of the matched spectra.

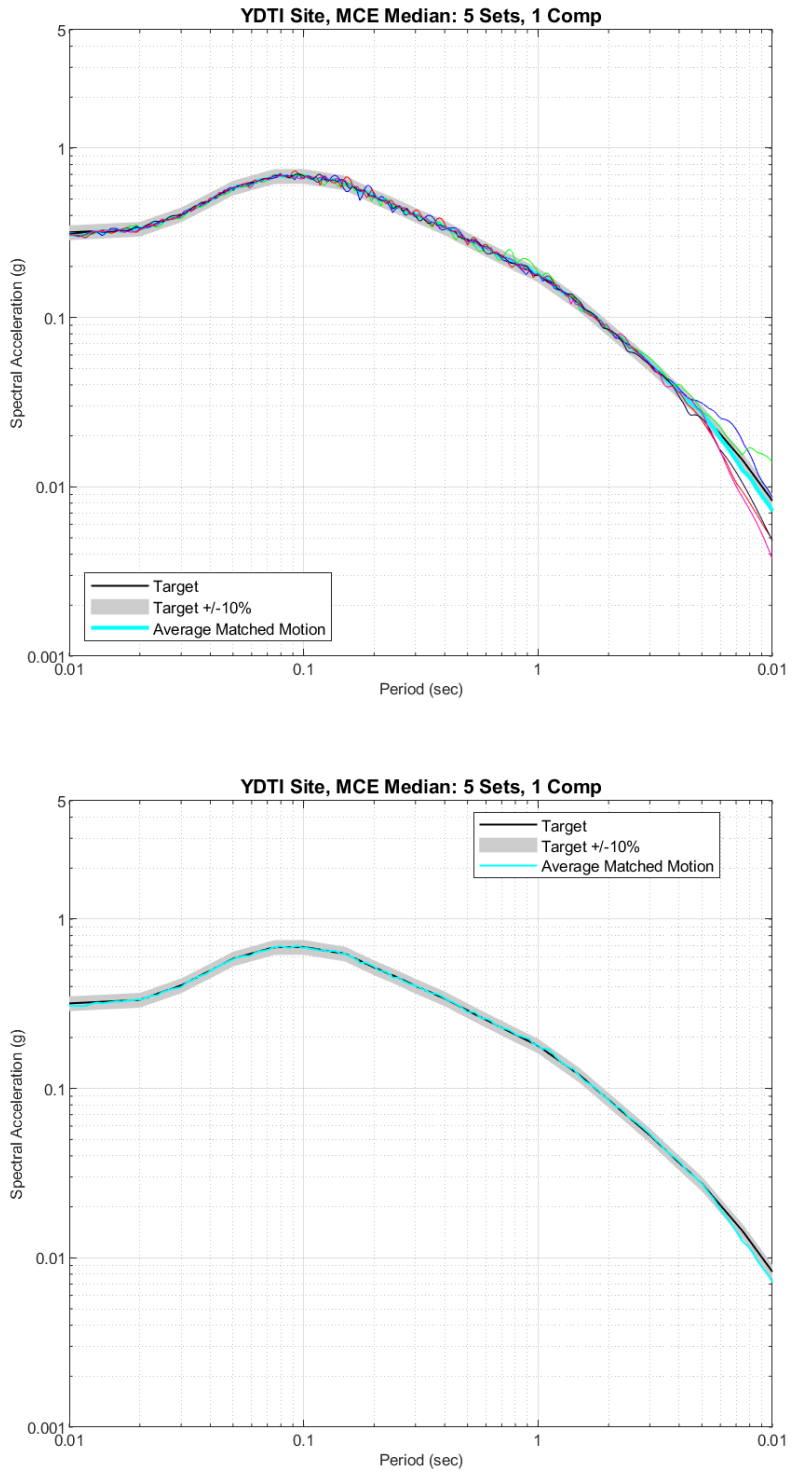

Figure 9-4. Comparison of the average (geometric mean) of the matched response spectra to the target vertical response spectrum (median MCE). Top plot shows the matched response spectra for the 5 sets and bottom plot shows the average of the matched spectra.

Tables 9-5 and 9-6 list the characteristics of the spectrum-compatible design time histories for the horizontal and the vertical components, respectively. These characteristics include the peak ground acceleration (PGA), velocity (PGV), displacement (PGD), duration, number of points (Npts), time step (dt), PGV/PGA (referred to as V/A), PGA*PGD/PGV2 (referred to as AD/V*V), 5-75% and 5-95% duration, cumulative absolute velocity (referred to as CAV), Arias Intensity, and pulse period of the near-field motions with a velocity pulse.

Table 9-5. Characteristics of the matched time histories for the MCE median target case for the horizontal component.

Set #	Npts	dt (sec)	PGA (g)	PGV (cm/sec)	PGD (cm)	V/A	AD/V *V	5 – 75% Dur (sec)	5 – 95% Dur (sec)	CAV (m/sec)	Arias Intensity (m/sec)	Pulse Period (sec)
1	7999	0.005	0.4559	36.913	25.437	80.963	8.347	2.81	6.02	7.63	1.19	7.07
2	7197	0.005	0.4491	40.620	16.003	90.447	4.271	1.70	3.90	5.55	0.87	2.49
3	14870	0.005	0.4451	55.700	31.728	125.149	4.464	8.22	13.16	13.72	1.90	7.95
4	8191	0.005	0.4251	31.089	11.257	73.134	4.855	5.19	12.24	10.16	1.49	-
5	11824	0.0029	0.4399	27.211	8.546	61.856	4.979	14.57	20.80	17.76	2.94	-

Table 9-6. Characteristics of the matched time histories for the MCE median target case for the vertical component.

Set #	Npts	dt (sec)	PGA (g)	PGV (cm/sec)	PGD (cm)	V/A	AD/V* V	5 – 75% Dur (sec)	5 – 95% Dur (sec)	CAV (m/sec)	Arias Intensity (m/sec)
1	7999	0.005	0.3034	21.737	12.210	71.656	7.687	3.79	9.71	5.71	0.55
2	7197	0.005	0.2958	18.956	16.532	64.083	13.347	5.18	16.97	6.28	0.53
3	14870	0.005	0.2883	25.407	8.403	88.125	3.680	5.61	7.38	7.56	0.80
4	8191	0.005	0.3033	19.128	6.660	63.070	5.414	6.91	11.96	6.25	0.52
5	11824	0.0029	0.2902	14.066	5.592	48.475	8.043	14.84	21.64	11.54	1.21

Figure 9-5 shows a comparison of the 5-75% and 5-95% duration values of the matched time histories to the estimated values from Afshari and Stewart (2016) which is based on the empirical database from the NGA-West2 program. For these model estimates (i.e., median and plus and minus one sigma values), a scenario event with a magnitude value of 7 at a distance of 1.43 km is used. In general, the durations for the horizontal component of the matched time histories are in agreement with the empirical estimates with the durations values for sets 1, 2, and 5 falling slightly outside of the range of +/- one standard deviation of the estimated values.

A similar comparison for the CAV parameter is presented in Figure 9-6 for the matched time histories and the empirical model of Campbell and Bozorgnia (2019). This empirical model is also based on the NGA-West2 database. A scenario earthquake with magnitude 7 at a distance of 1.43 km and with V_{S30} of 760 m/sec is used for the empirical estimates. Figure 9-6 indicates that the CAV values for the matched time histories are in general agreement with the empirical estimates obtained using Campbell and Bozorgnia (2019) for the scenario considered. A comparison of the Arias Intensity of the matched time

histories to empirical estimates computed using the Campbell and Bozorgnia (2019) is shown in Figure 9-7 for the MCE scenario with magnitude 7 and distance of 1.43 km. This figure indicates that the Arias Intensity for the horizontal component of the matched time histories generally falls within the range of the estimates from the model.

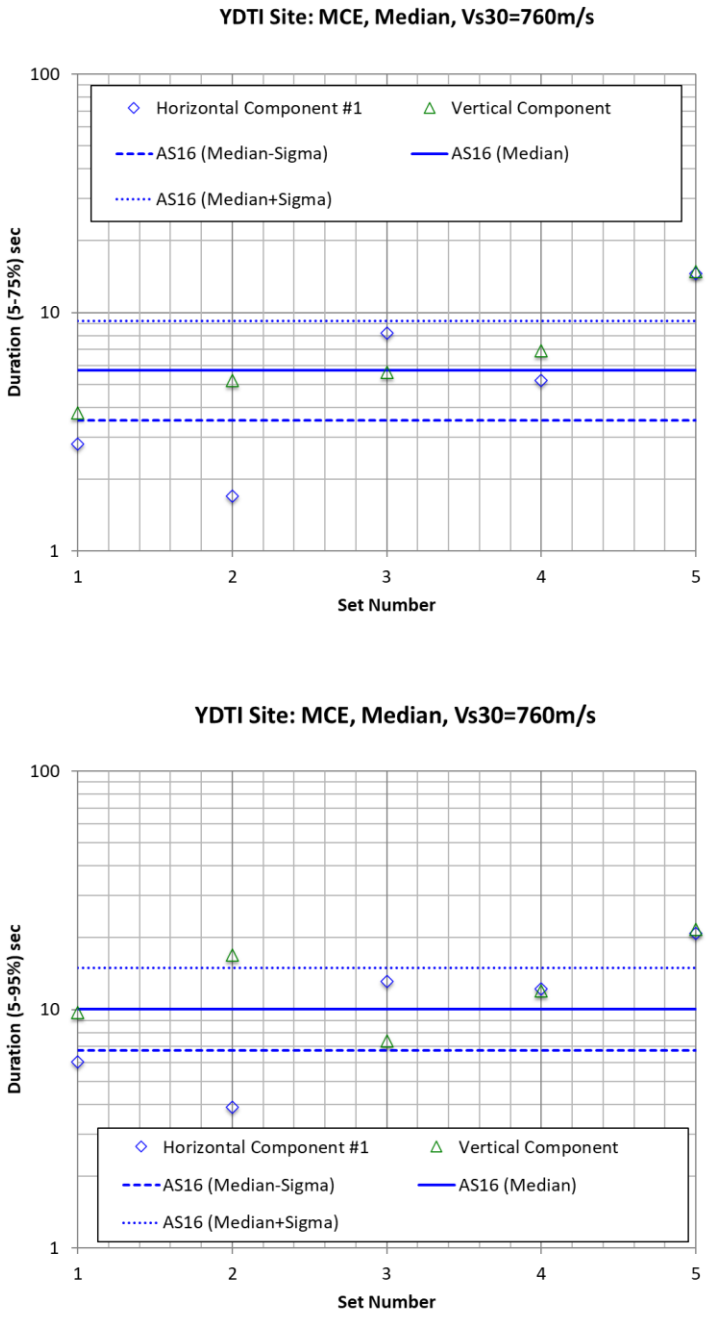

Figure 9-5. Comparison of the 5-75% durations (top) and 5-95% durations (bottom) of the matched time histories for the median MCE target and the model estimates from Afshari and Stewart (2016).

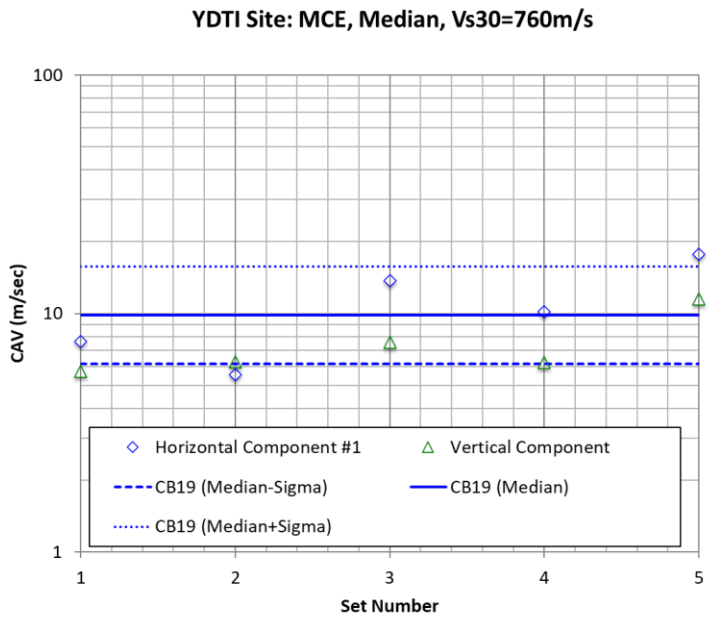

Figure 9-6. Comparison of the CAV of the matched time histories for the median MCE target and the model estimates from Campbell and Bozorgnia (2019).

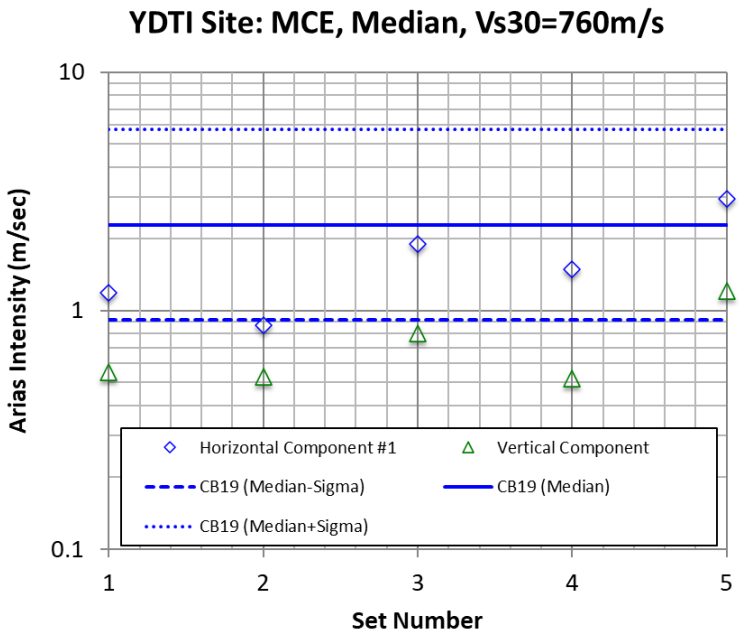

Figure 9-7. Comparison of the Arias Intensity of the matched time histories for the median MCE target and the model estimates from Campbell and Bozorgnia (2019).

9.3 Spectrum-Compatible Time Histories for the MCE 84th Percentile Target

Each of the horizontal and vertical components of the selected seed acceleration time histories (see Table 9.3) is modified such that their response spectra match the deterministic MCE 84th percentile target response spectrum and its corresponding vertical target spectrum. The same procedure implemented for the development of spectrally matched time histories for the MCE median target case is applied for the MCE deterministic 84th percentile target. Individual comparisons of the spectrally matched motion to the original seed motion for the 5 sets of time histories presented in this section are shown in Appendix II.

Figures 9-8 and 9-9 show a comparison of the response spectra of the scaled initial seed time histories to the MCE 84th percentile target spectra for the horizontal and vertical components, respectively. A plot showing the comparison of the matched response spectra to the target spectrum is also included in each figure. Figures 9-8 and 9-9 show the change in the response spectra of the seed time histories due to the matching process. Figures 9-10 and 9-11 compare the target MCE 84th percentile response spectra to the average response spectra of the 5 matched time histories for the horizontal and vertical components, respectively. The acceptability of the spectral matches is based on a visual inspection of the individual matches and as well a requirement that the average of the full set of the 5 matched time histories generally falls within +/-10% of the target horizontal and vertical spectra. This visual inspection and requirement are applied to spectral periods shorter than 5 sec as shown in Figures 9-10 and 9-11.

Tables 9-7 and 9-8 list the characteristics of the spectrum-compatible design time histories for the horizontal and the vertical components, respectively. These characteristics include the peak ground acceleration (PGA), velocity (PGV), displacement (PGD), duration, number of points (Npts), time step (dt), PGV/PGA (referred to as V/A), PGA*PGD/PGV2 (referred to as AD/V*V), 5-75% and 5-95% duration, cumulative absolute velocity (referred to as CAV), Arias Intensity, and pulse period of the near-field motions with a velocity pulse.

Table 9-7. Characteristics of the matched time histories for the MCE 84th percentile target for the horizontal component.

Set #	Npts	dt (sec)	PGA (g)	PGV (cm/sec)	PGD (cm)	V/A	AD/V* V	5 – 75% Dur (sec)	5 – 95% Dur (sec)	CAV (m/sec)	Arias Intensity (m/sec)	Pulse Period (sec)
1	7999	0.005	0.7982	70.557	50.066	88.393	7.872	2.93	6.08	15.38	4.66	7.49
2	7197	0.005	0.8437	81.081	28.640	96.098	3.605	1.70	4.95	10.99	3.36	2.49
3	14870	0.005	0.8295	98.940	42.536	119.278	3.535	5.27	7.87	17.73	4.49	7.73
4	8191	0.005	0.7585	62.000	22.979	81.743	4.446	4.99	12.00	18.91	5.36	-
5	12712	0.0029	0.7853	77.924	24.646	99.224	3.126	2.15	8.64	13.67	3.36	2.03

Table 9-8. Characteristics of the matched time histories for the MCE 84th percentile target for the vertical component.

Set #	Npts	dt (sec)	PGA (g)	PGV (cm/sec)	PGD (cm)	V/A	AD/V* V	5 – 75% Dur (sec)	5 – 95% Dur (sec)	CAV (m/sec)	Arias Intensity (m/sec)
1	7999	0.005	0.5384	44.760	23.379	83.137	6.161	4.02	8.20	11.33	2.16
2	7197	0.005	0.5462	37.063	29.169	67.858	11.374	5.63	17.19	12.63	2.10
3	14870	0.005	0.5284	52.701	16.713	99.732	3.118	5.38	7.48	14.34	2.87
4	8191	0.005	0.5537	37.833	13.581	68.333	5.152	6.84	11.51	11.92	1.97
5	12712	0.0029	0.5396	33.541	18.998	62.163	8.936	5.09	16.32	11.71	1.78

Figure 9-12 shows a comparison of the 5-75% and 5-95% duration values of the matched time histories to the estimated values from Afshari and Stewart (2016) which is based on the empirical database from the NGA-West2 program. For these model estimates (i.e., median and plus and minus one sigma values), a scenario event with a magnitude value of 7 at a distance of 1.43 km is used. In general, the durations for the horizontal component of the matched time histories are in agreement with the range of values from the empirical estimates.

A similar comparison for the CAV parameter is presented in Figure 9-13 for the matched time histories and the empirical model of Campbell and Bozorgnia (2019). A scenario earthquake with magnitude 7 at a distance of 1.43 km and with V_{S30} of 760 m/sec is used for the empirical estimates. Figure 9-13 indicates that the CAV values for the matched time histories are in general agreement with the empirical estimates obtained using Campbell and Bozorgnia (2019) for the scenario considered. The CAV values for the matched time histories for the MCE 84th percentile target are in better agreement with the 84th percentile of the empirical estimate. A comparison of the Arias Intensity of the matched time histories to empirical estimates computed using Campbell and Bozorgnia (2019) is shown in Figure 9-14 for the MCE scenario with magnitude 7 and distance of 1.43 km. This figure indicates that the Arias Intensity for the horizontal component of the matched time histories generally falls within the range of the empirical estimates from Campbell and Bozorgnia (2019).

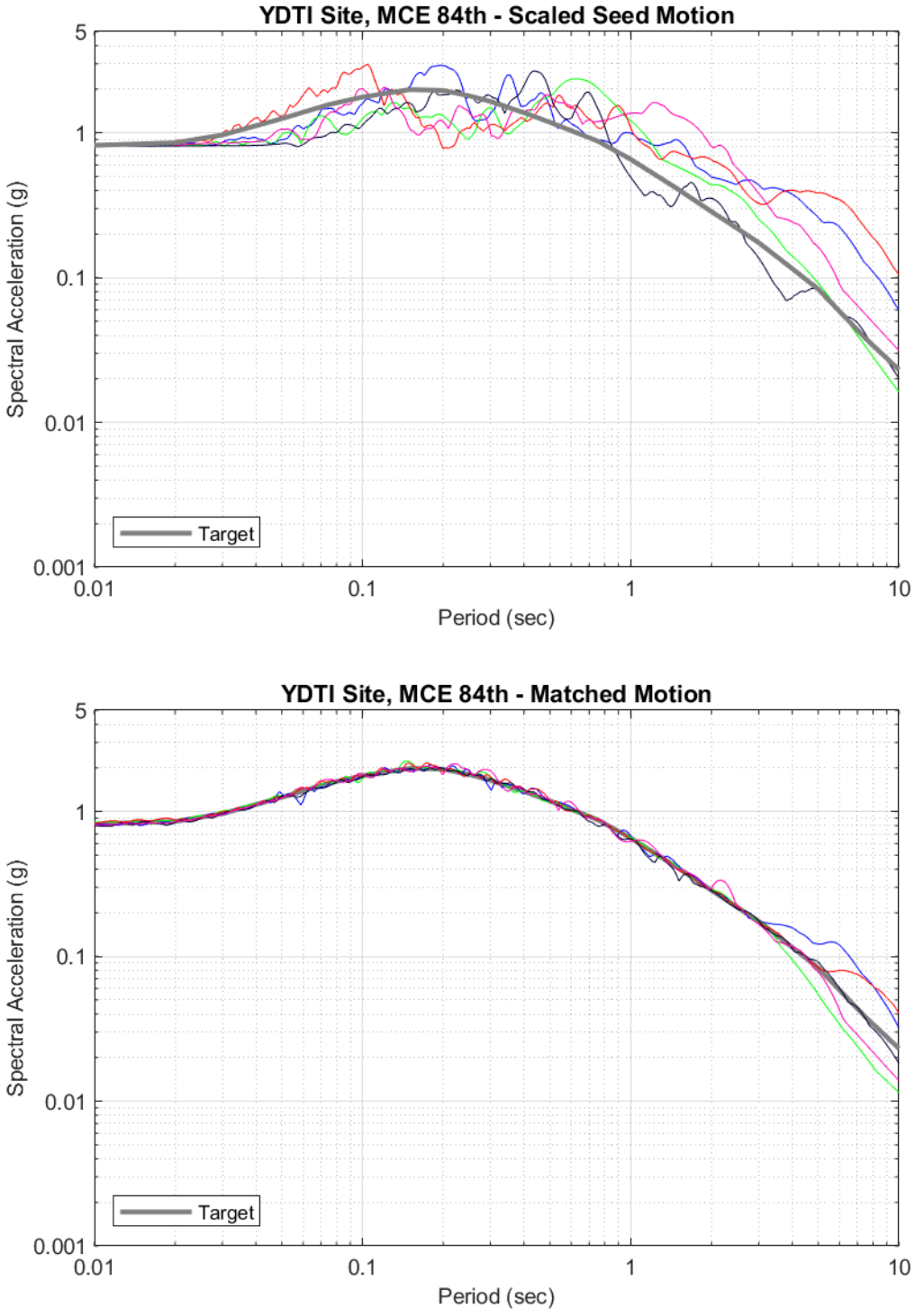

Figure 9-8. Comparison of the target horizontal response spectrum (MCE 84th percentile) to the response spectra of the horizontal component of the scaled seed time histories (top) and matched time histories (bottom).

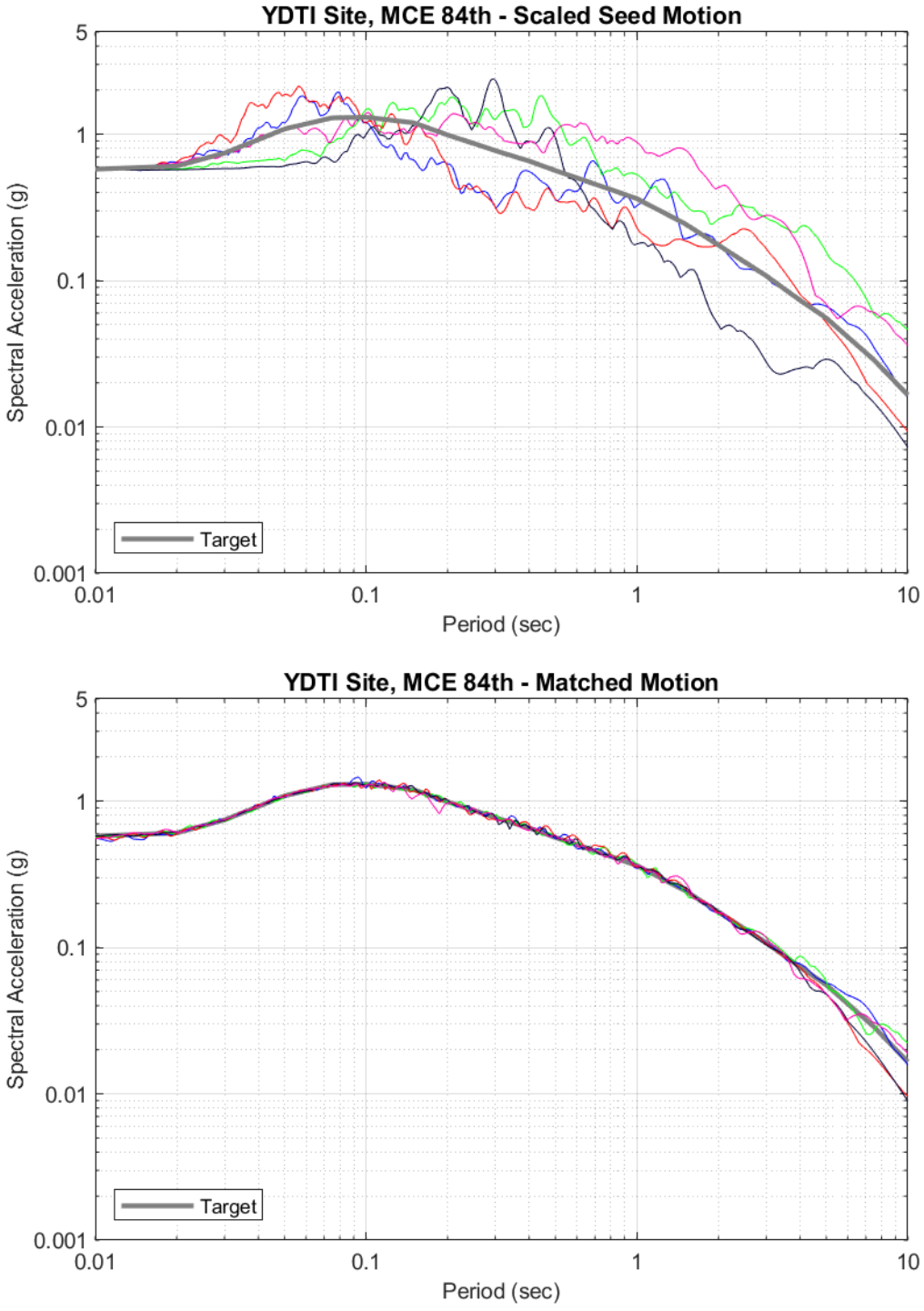

Figure 9-9. Comparison of the target vertical response spectrum (MCE 84th percentile) to the response spectra of the vertical component of the scaled seed time histories (top) and matched time histories (bottom).

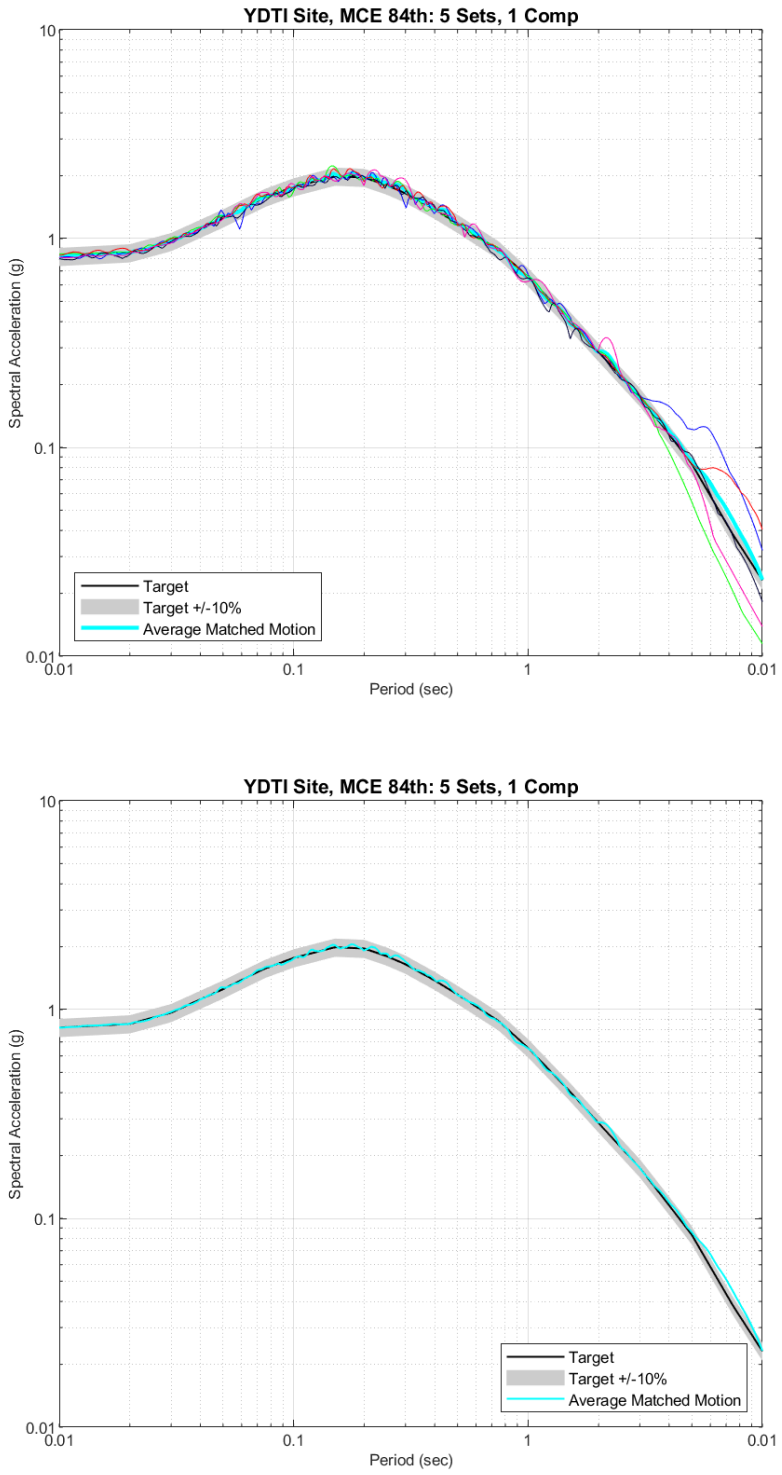

Figure 9-10. Comparison of the average (geometric mean) of the matched response spectra to the target horizontal response spectrum (MCE 84th percentile). Top plot shows the matched response spectra for the 5 sets and bottom plot shows the average of the matched spectra.

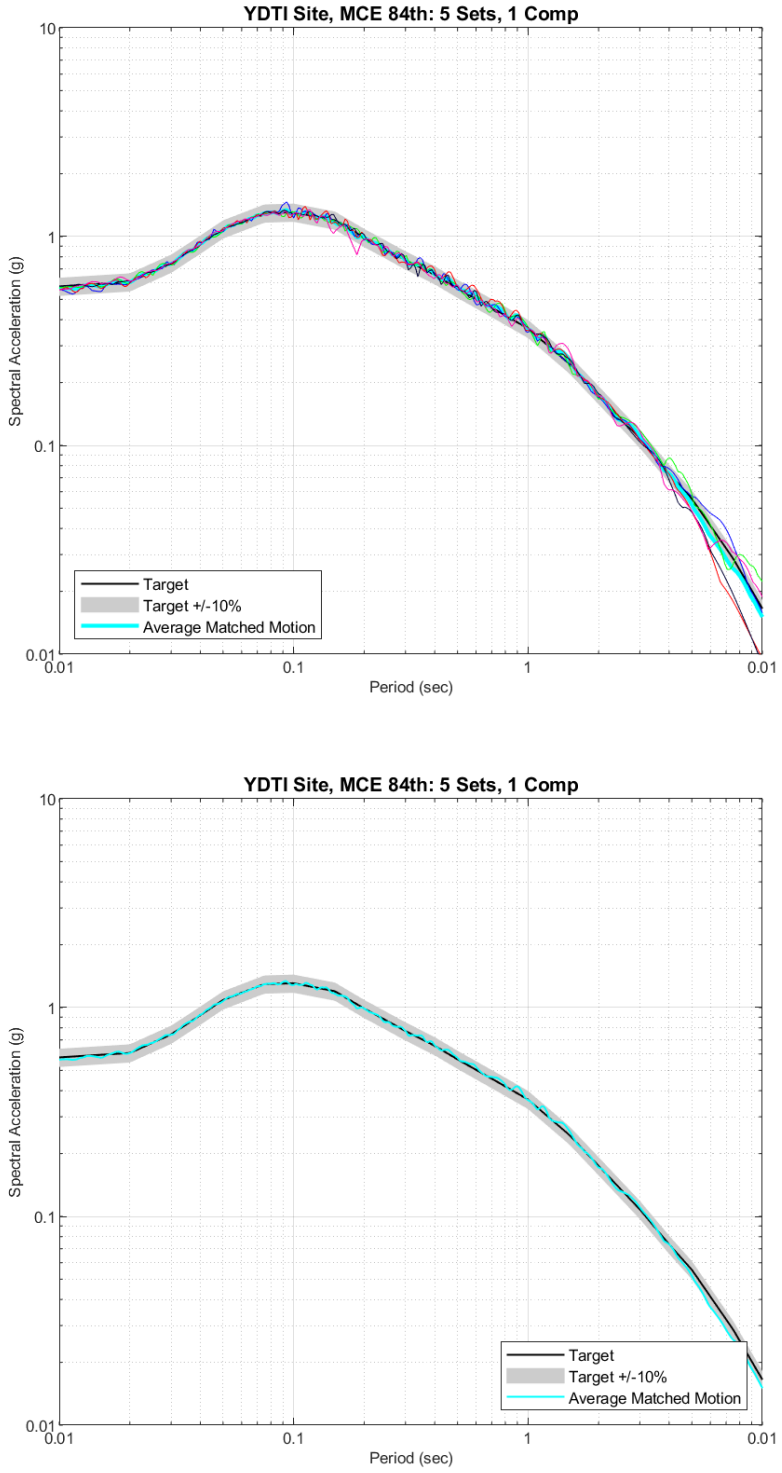

Figure 9-11. Comparison of the average (geometric mean) of the matched response spectra to the target vertical response spectrum (MCE 84th percentile). Top plot shows the matched response spectra for the 5 sets and bottom plot shows the average of the matched spectra.

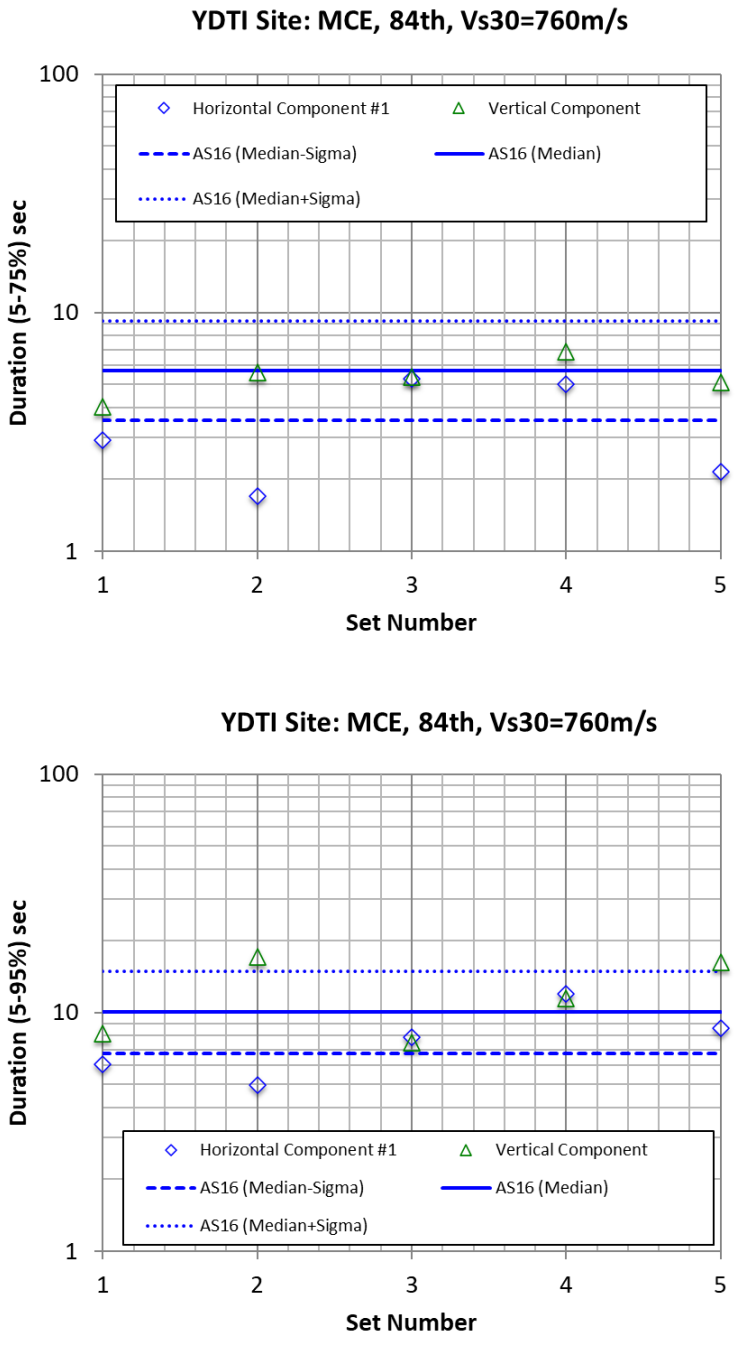

Figure 9-12. Comparison of the 5-75% durations (top) and 5-95% durations (bottom) of the matched time histories for the MCE 84th percentile target and the model estimates from Afshari and Stewart (2016).

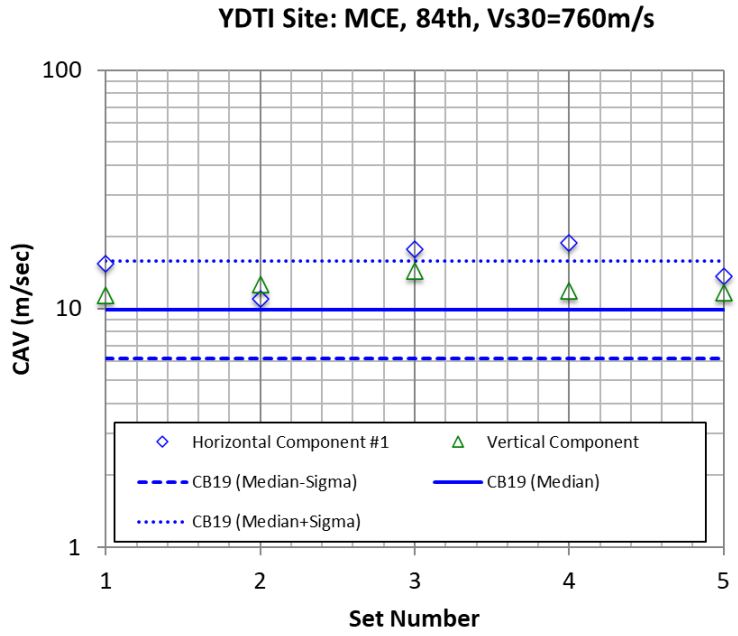

Figure 9-13. Comparison of the CAV of the matched time histories for the MCE 84th percentile target and the model estimates from Campbell and Bozorgnia (2019).

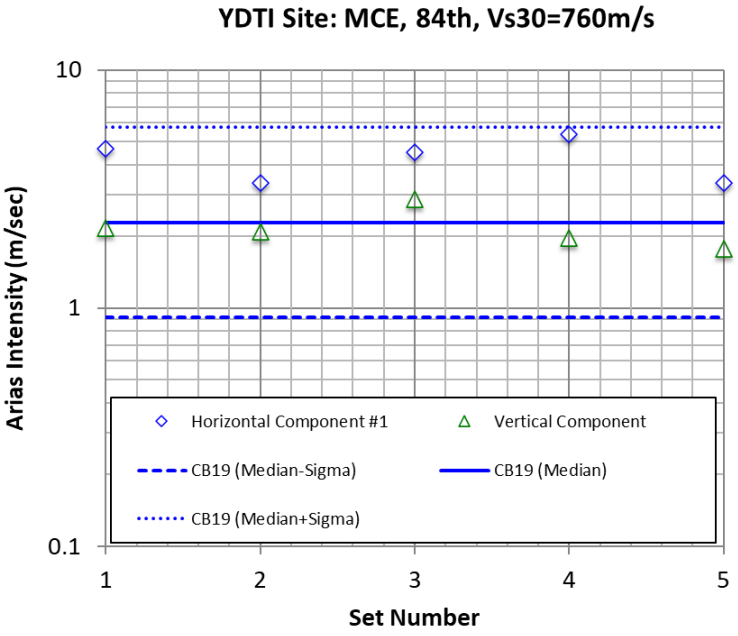

Figure 9-14. Comparison of the Arias Intensity of the matched time histories for the MCE 84th percentile target and the model estimates from Campbell and Bozorgnia (2019).

9.4 Spectrum-Compatible Time Histories for the 1000-yr Return Period

Each of the horizontal and vertical components of the selected seed acceleration time histories (see Table 9.4) is modified such that their response spectra match the 1000-year return period UHS target response spectrum and its corresponding vertical target spectrum. The same procedure implemented for the development of spectrally matched time histories for the MCE median and 84th percentile target cases is applied here. Individual comparisons of the spectrally matched motion to the original seed motion for the 5 sets of time histories presented in this section are shown in Appendix III for the 1000-year return period target.

Figures 9-15 and 9-16 show a comparison of the response spectra of the scaled initial seed time histories to the 1000-year return period target spectra for the horizontal and vertical components, respectively. A plot showing the comparison of the matched response spectra to the target spectrum is also included in each figure. Figures 9-15 and 9-16 show the change in the response spectra of the seed time histories due to the matching process. Figures 9-17 and 9-18 compare the target 1000-year return period response spectra to the average response spectra of the 5 matched time histories for the horizontal and vertical components, respectively. The acceptability of the spectral matches is based on a visual inspection of the individual matches and as well a requirement that the average of the full set of the 5 matched time histories generally falls within +/-10% of the target horizontal and vertical spectra. This visual inspection and requirement are applied to spectral periods shorter than 5 sec as shown in Figures 9-17 and 9-18.

Tables 9-9 and 9-10 list the characteristics of the spectrum-compatible design time histories for the horizontal and the vertical components, respectively. These characteristics include the peak ground acceleration (PGA), velocity (PGV), displacement (PGD), duration, number of points (Npts), time step (dt), PGV/PGA (referred to as V/A), PGA*PGD/PGV2 (referred to as AD/V*V), 5-75% and 5-95% duration, cumulative absolute velocity (referred to as CAV), Arias Intensity, and pulse period of the near-field motions with a velocity pulse.

Figure 9-19 shows a comparison of the 5-75% and 5-95% duration values of the matched time histories to the estimated values from Afshari and Stewart (2016) which is based on the empirical database from the NGA-West2 program. For these model estimates (i.e., median and plus and minus one sigma values), a scenario event with a magnitude value of 6.6 at a distance of 30 km is used based on the average of the magnitude and distance of the 5 sets of time histories. In general, the durations for the horizontal component of the matched time histories are in agreement with the range of values from the empirical estimates.

A similar comparison for the CAV parameter is presented in Figure 9-20 for the matched time histories and the empirical model of Campbell and Bozorgnia (2019). A scenario earthquake with magnitude 6.6 at a distance of 30 km and with V_{S30} of 760 m/sec is used for the empirical estimates. Figure 9-20 indicates that the CAV values for the matched time histories are in general agreement with the empirical estimates obtained using Campbell and Bozorgnia (2019) for the scenario considered. A comparison of the Arias Intensity of the matched time histories to empirical estimates computed using Campbell and Bozorgnia (2019) is shown in Figure 9-21 for the scenario with magnitude 6.6 and distance of 30 km. This figure indicates that the Arias Intensity for the horizontal component of the matched time histories generally falls within the range of the empirical estimates from Campbell and Bozorgnia (2019).

Table 9-9. Characteristics of the matched time histories for the 1000-year return period target for the horizontal component.

Set #	Npts	dt (sec)	PGA (g)	PGV (cm/sec)	PGD (cm)	V/A	AD/V* V	5 – 75% Dur (sec)	5 – 95% Dur (sec)	CAV (m/sec)	Arias Intensity (m/sec)
1	6201	0.005	0.1314	10.134	2.786	77.142	3.495	4.17	9.46	2.52	0.11
2	7999	0.005	0.1374	7.272	3.036	52.924	7.735	6.97	14.60	3.79	0.17
3	11405	0.005	0.1367	10.113	2.659	73.958	3.486	13.50	26.06	4.95	0.19
4	5997	0.005	0.1309	9.480	3.399	72.440	4.853	6.86	12.97	3.70	0.19
5	16384	0.005	0.1315	8.798	2.483	66.912	4.136	13.23	23.59	6.01	0.24

Table 9-10. Characteristics of the matched time histories for the 1000-year return period target for the vertical component.

Set	Npts	dt (sec)	PGA (g)	PGV (cm/sec)	PGD (cm)	V/A	AD/V* V	5 – 75% Dur (sec)	5 – 95% Dur (sec)	CAV (m/sec)	Arias Intensity (m/sec)
1	6201	0.005	0.0886	4.384	1.324	49.491	5.985	5.39	11.81	1.98	0.06
2	7999	0.005	0.0875	7.969	4.149	91.065	5.607	5.71	15.35	2.29	0.07
3	11405	0.005	0.0892	5.296	1.590	59.368	4.958	13.08	21.91	3.71	0.11
4	5997	0.005	0.0898	4.910	1.913	54.689	6.986	6.84	12.71	2.31	0.08
5	16384	0.005	0.0895	4.280	1.813	47.819	8.686	20.55	31.31	6.52	0.23

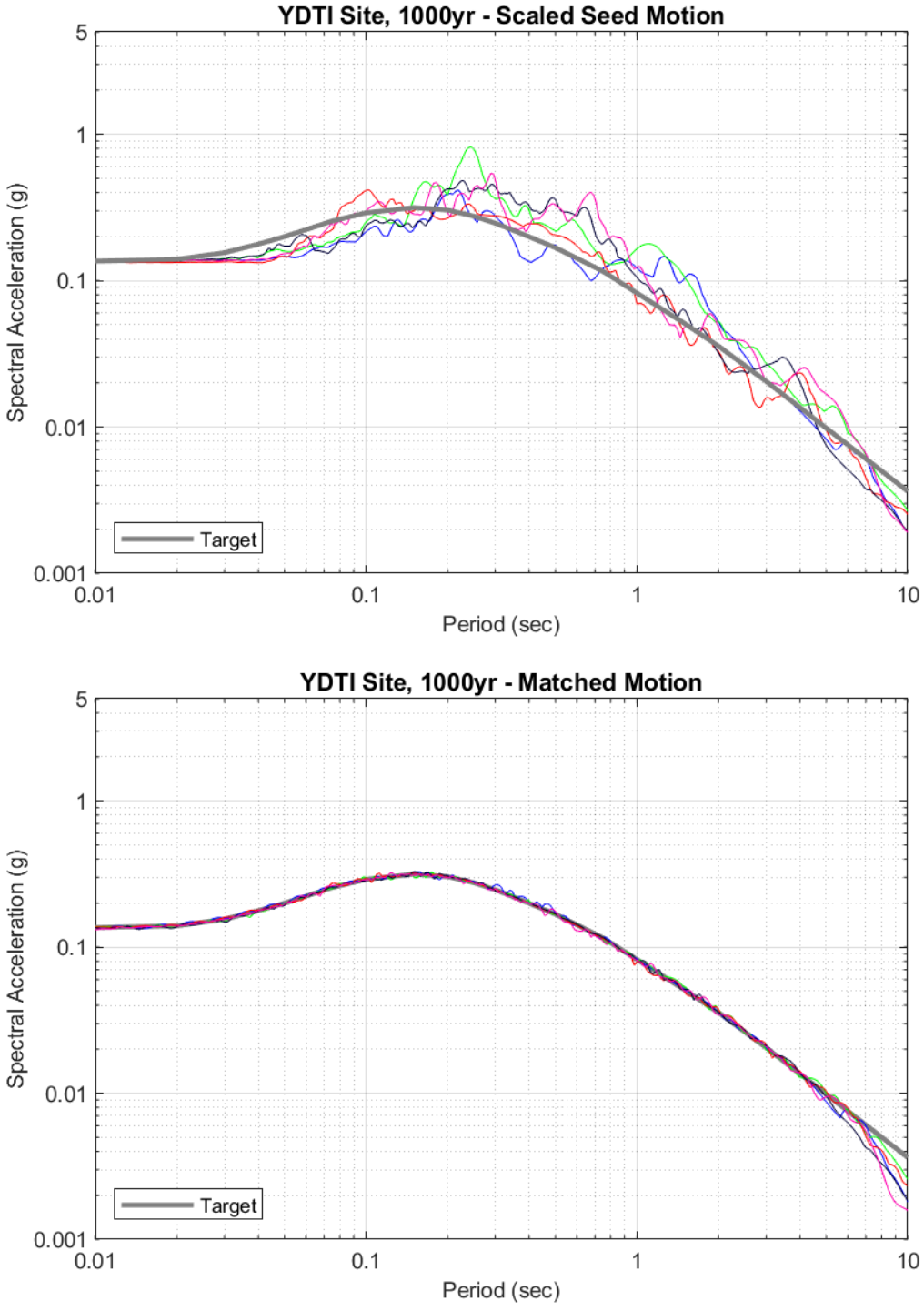

Figure 9-15. Comparison of the target horizontal response spectrum (1000-year return period) to the response spectra of the horizontal component of the scaled seed time histories (top) and matched time histories (bottom).

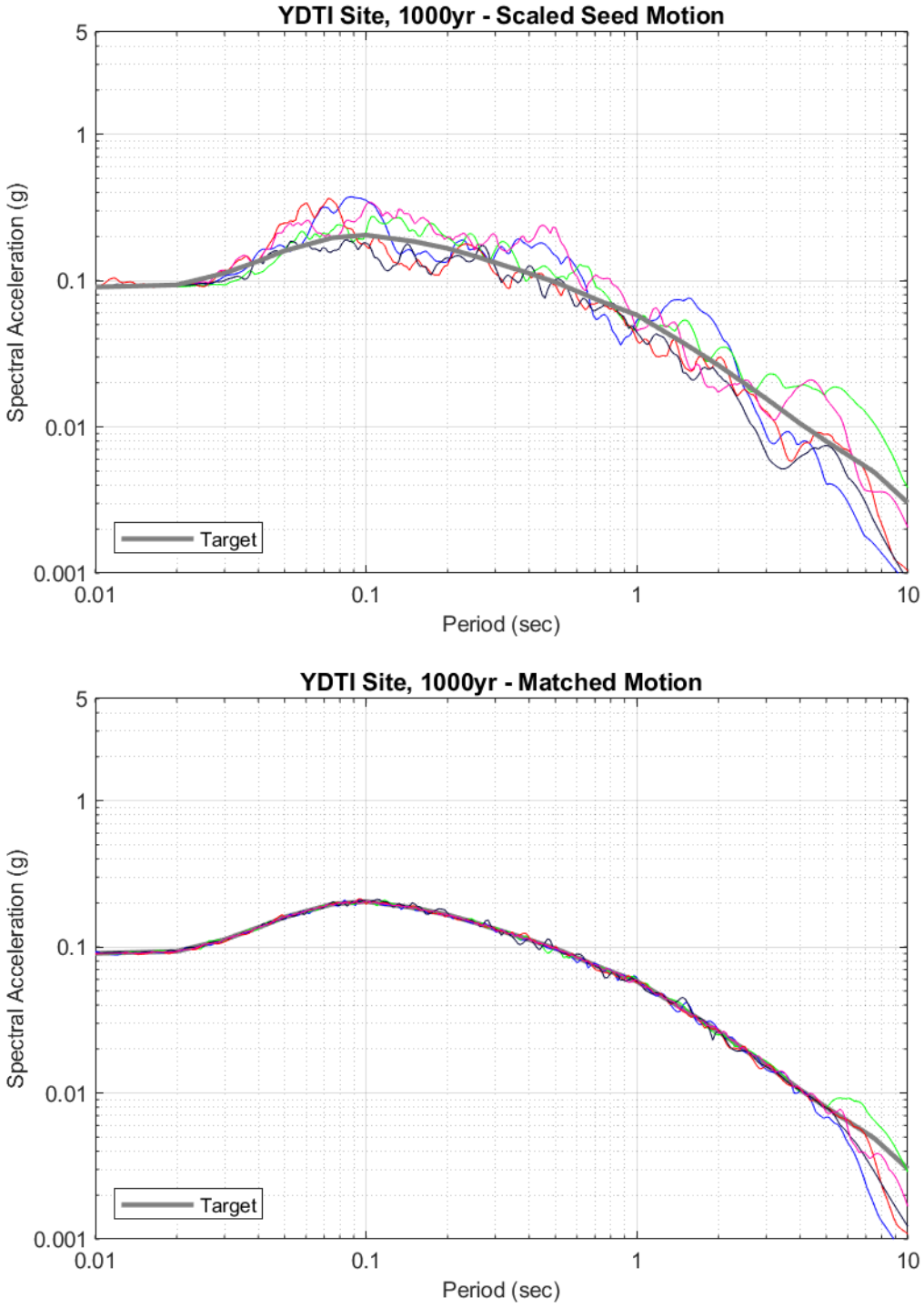

Figure 9-16. Comparison of the target vertical response spectrum (1000-year return period) to the response spectra of the vertical component of the scaled seed time histories (top) and matched time histories (bottom).

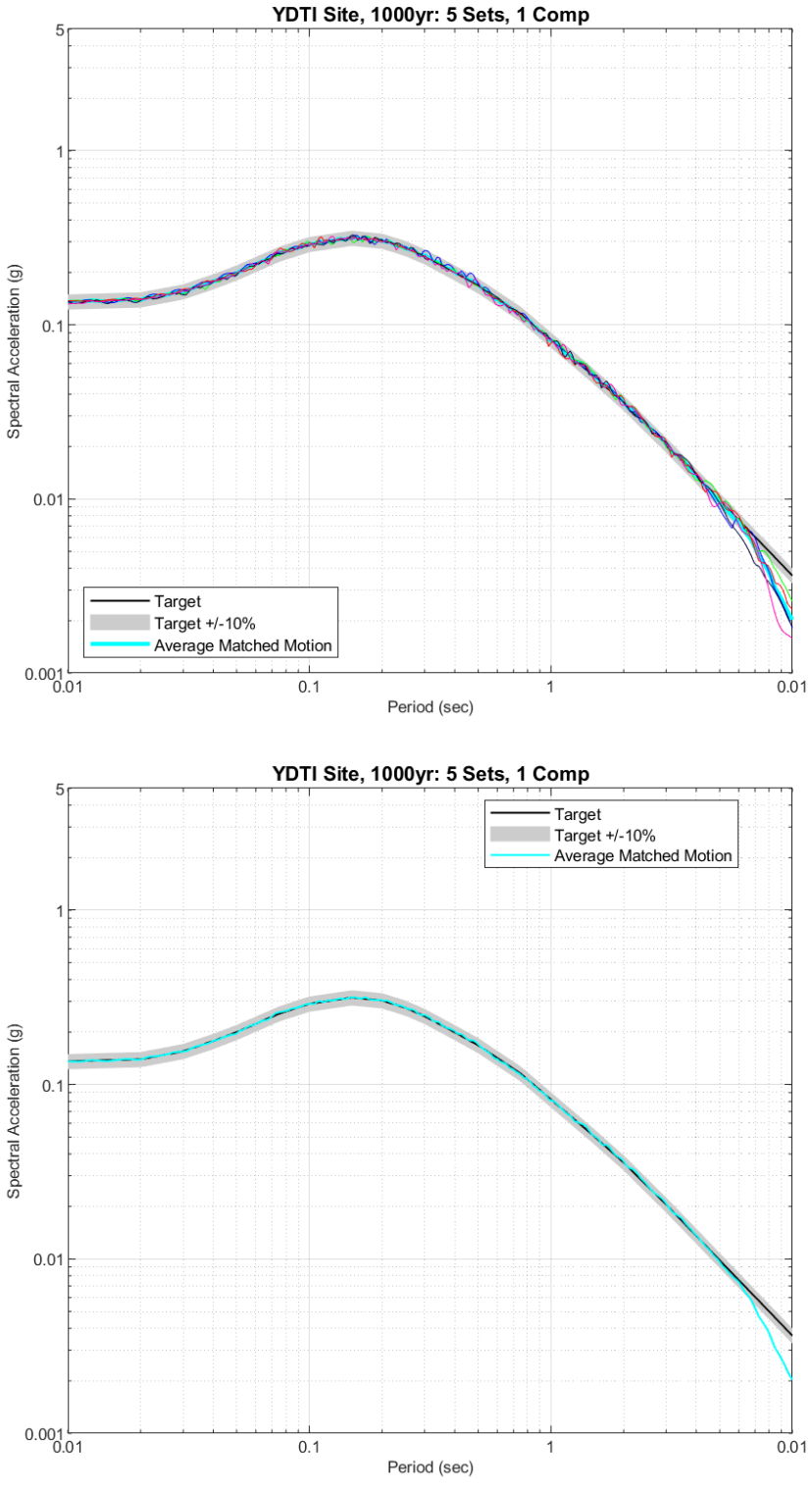

Figure 9-17. Comparison of the average (geometric mean) of the matched response spectra to the target horizontal response spectrum (1000-year return period). Top plot shows the matched response spectra for the 5 sets and bottom plot shows the average of the matched spectra.

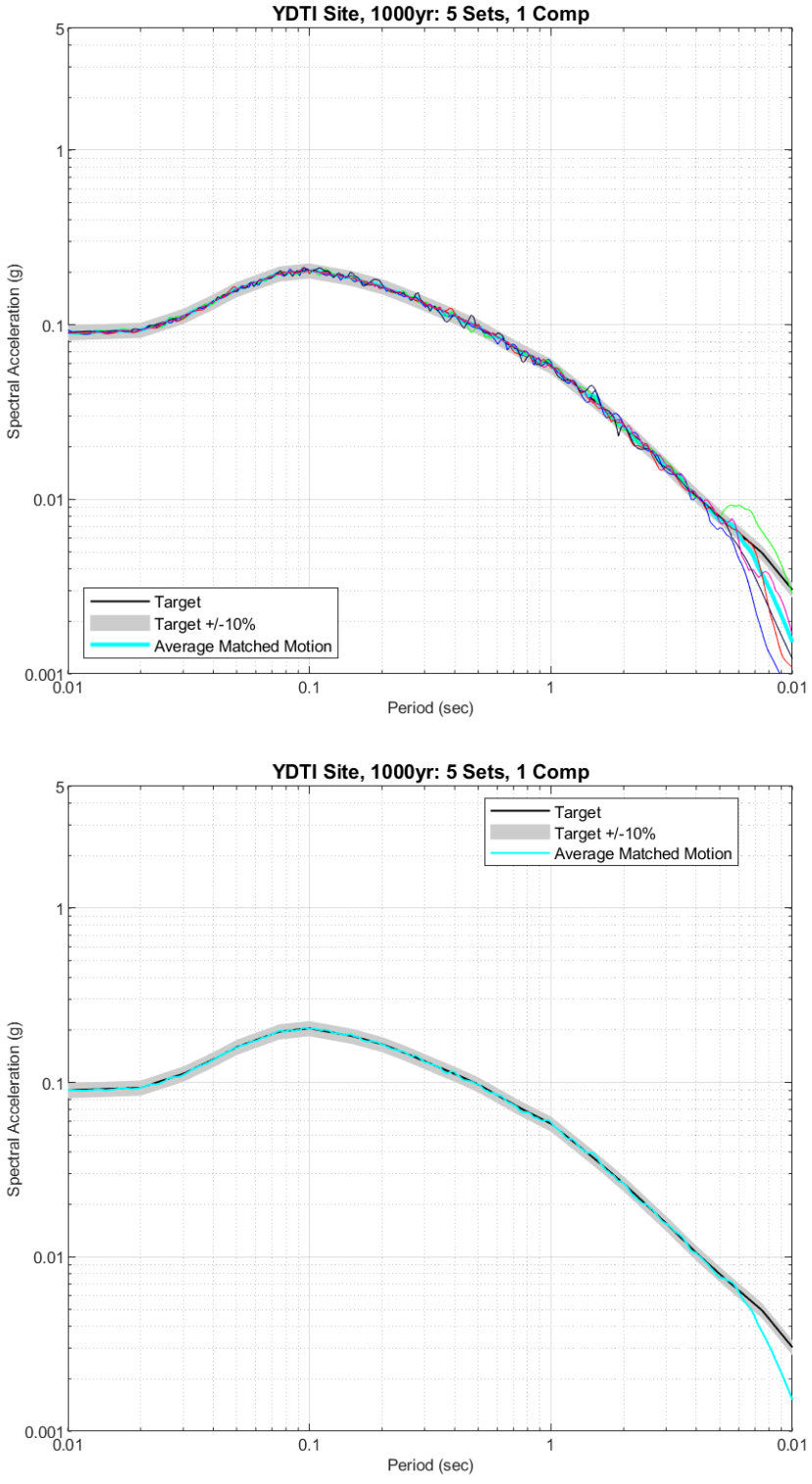

Figure 9-18. Comparison of the average (geometric mean) of the matched response spectra to the target vertical response spectrum (1000-year return period). Top plot shows the matched response spectra for the 5 sets and bottom plot shows the average of the matched spectra.

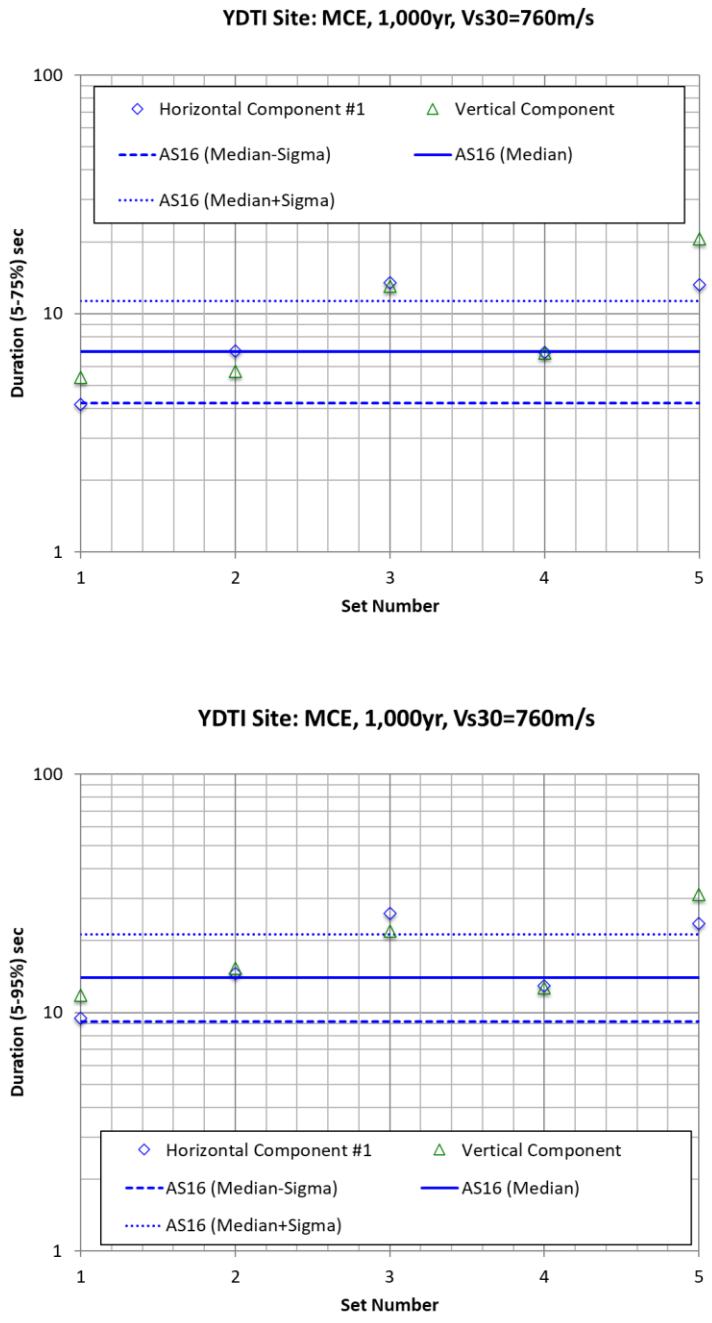

Figure 9-19. Comparison of the 5-75% durations (top) and 5-95% durations (bottom) of the matched time histories for the 1000-year return period target and the model estimates from Afshari and Stewart (2016).

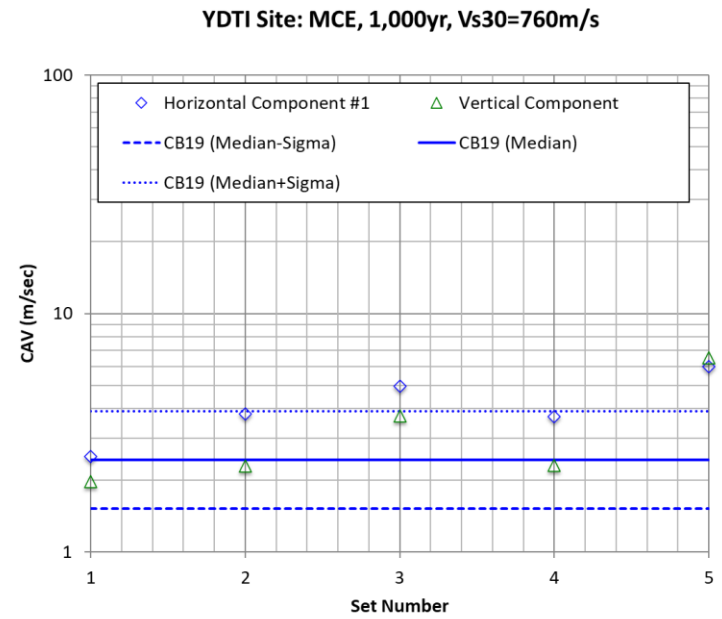

Figure 9-20. Comparison of the CAV of the matched time histories for the 1000-year return period target and the model estimates from Campbell and Bozorgnia (2019).

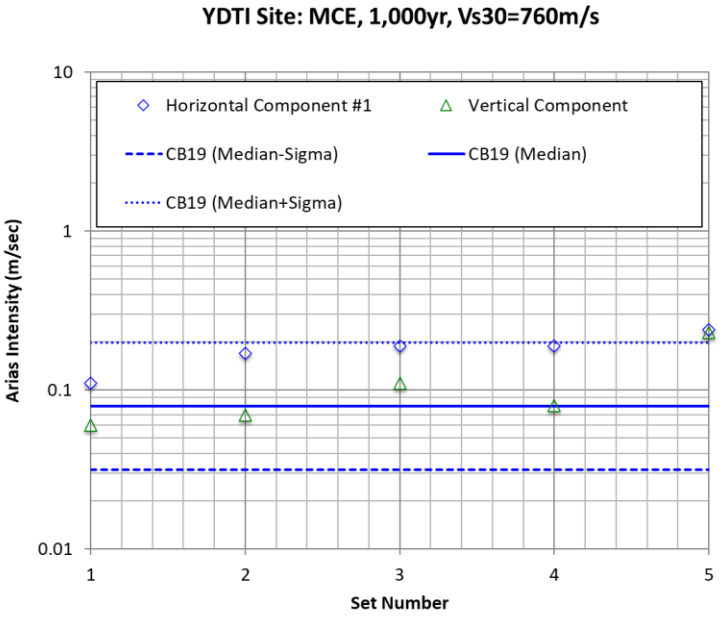

Figure 9-21. Comparison of the Arias Intensity of the matched time histories for the 1000-year return period target and the model estimates from Campbell and Bozorgnia (2019).

10. REFERENCES

Abrahamson, N.A., 2003. RSPMATCH, Personal Communication.

Abrahamson, N.A., Silva, W.J. and Kamai, R., 2014. Summary of the ASK14 ground motion relation for active crustal regions. *Earthquake Spectra*, *30*(3), pp. 1025-1055.

Abrahamson, N. A. and Gregor, N., 2015. Haz45, Seismic Hazard Analysis Software.

Abrahamson, N. 2008. Appendix C—Probabilistic fault rupture hazard analysis, in San Francisco Public Utilities Commission (SFPUC), Seismic Design Criteria, revised 2008, 7 pages.

Afshari, K. and Stewart, J.P., 2016. Physically parameterized prediction equations for significant duration in active crustal regions. *Earthquake Spectra*, *32*(4), pp. 2057-2081.

Akkar, S., Sandıkkaya, M.A. and Bommer, J.J., 2014. Empirical ground-motion models for point-and extended-source crustal earthquake scenarios in Europe and the Middle East. *Bulletin of earthquake engineering*, *12*(1), pp. 359-387.

Al Atik, L. and Abrahamson, N., 2010. An improved method for nonstationary spectral matching, *Earthquake Spectra*, *26*(3), pp. 601-617.

Al Atik, L. and Youngs, R.R., 2014. Epistemic uncertainty for NGA-West2 models. *Earthquake Spectra*, *30*(3), pp. 1301-1318.

Al Atik, L. and Gregor, N., 2016. Seismic Hazard Assessment for the Yankee Doodle Tailings Impoundment Site, Butte, Montana. Final report, February 19, 2016.

Bird, P. 2013. Estimation of fault slip rates in the conterminous Western United States with statistical and kinematic finite-element programs, Appendix C, in Petersen, M.D., Zeng, Yuehua, Haller, K.M., McCaffrey, Robert, Hammond, W.C., Bird, Peter, Moschetti, Morgan, and Thatcher, Wayne, Geodesy- and geology-based slip-rate models for the Western United States (excluding California) national seismic hazard maps: U.S. Geological Survey Open-File Report 2013-1293, p. 48–57.

Boore, D.M., Stewart, J.P., Seyhan, E. and Atkinson, G.M., 2014. NGA-West2 equations for predicting PGA, PGV, and 5% damped PSA for shallow crustal earthquakes. *Earthquake Spectra*, *30*(3), pp. 1057-1085.

Boore, D.M., Stewart, J.P., Skarlatoudis, A.A., Seyhan, E., Margaris, B., Theodoulidis, N., Scordilis, E., Kalogeras, I., Klimis, N. and Melis, N.S., 2021. A ground-motion prediction model for shallow crustal earthquakes in Greece. *Bulletin of the Seismological Society of America*, *111*(2), pp. 857-874.

Bozorgnia, Y. and Campbell, K.W., 2016. Ground motion model for the vertical-to-horizontal (V/H) ratios of PGA, PGV, and response spectra. *Earthquake Spectra*, *32*(2), pp. 951-978.

Campbell, K.W. and Bozorgnia, Y., 2014. NGA-West2 ground motion model for the average horizontal components of PGA, PGV, and 5% damped linear acceleration response spectra. *Earthquake Spectra*, *30*(3), pp. 1087-1115.

Campbell, K.W. and Bozorgnia, Y., 2019. Ground motion models for the horizontal components of Arias Intensity (AI) and Cumulative Absolute Velocity (CAV) using the NGA-West2 database. *Earthquake Spectra, 35*(3), pp. 1289-1310.

Chiou, B.S.J. and Youngs, R.R., 2014. Update of the Chiou and Youngs NGA model for the average horizontal component of peak ground motion and response spectra. *Earthquake Spectra*, *30*(3), pp. 1117-1153.

Division of Safety of Dams, 2000. Guidelines for use of the consequence-hazard matrix and selection of ground motion parameters. October 4, 2002.

Gardner, J.K. and Knopoff, L., 1974. Is the sequence of earthquakes in Southern California, with aftershocks removed, Poissonian? *Bulletin of the seismological society of America*, *64*(5), pp. 1363-1367.

Gülerce, Z. and Abrahamson, N.A., 2011. Site-specific design spectra for vertical ground motion. *Earthquake Spectra*, *27*(4), pp. 1023-1047.

Hayden, C.P., Bray, J.D., and Abrahamson, N.A., 2014. Selection of near-fault pulse motions. *Journal of Geotechnical and Geoenvironmental Engineering*, *140*(7).

Hecker, S., Abrahamson, N.A. and Wooddell, K.E., 2013. Variability of displacement at a point: Implications for earthquake-size distribution and rupture hazard on faults. *Bulletin of the seismological society of America*, *103*(2A), pp. 651-674.

Idriss, I.M., 2014. An NGA-West2 empirical model for estimating the horizontal spectral values generated by shallow crustal earthquakes. *Earthquake Spectra*, *30*(3), pp. 1155-1177.

Jack Benjamin and Associates (JBA), URS Corporation, Geomatrix Consultants, Inc. and Shannon and Wilson, 2012. Probabilistic seismic hazard analyses project for Mid- Columbia dams. Prepared for Public Utility Districts of Chelan, Douglas and Grant Counties, Final Report, October 2011.

Knight Piesold Ltd. (KP), 2015. Montana Resources – Yankee Doodle Tailings Impoundment request for proposal for seismic hazard assessment services, VA15-03097.

Knight Piesold Ltd. (KP), 2020. 2019 Horseshoe Bend geotechnical site investigation. Final report (KP Reference No. VA101-126/22-1 Rev. 0), Vancouver, British Columbia, December 1, 2020.

Lettis Consultants International, Inc. (LCI), 2021a. Continental and Rocker fault phase 1 assessment, Butte, Montana, November 3, 2021.

Lettis Consultants International, Inc. (LCI), 2021b. Continental-Elk Park and Rocker faults phase 1 seismic source characterization hazard input document, Butte, Montana, November 3, 2021.

Miller III, A.C. and Rice, T.R., 1983. Discrete approximations of probability distributions. *Management science*, *29*(3), pp. 352-362.

Mueller, C.S., 2019. Earthquake catalogs for the USGS national seismic hazard maps. *Seismological Research Letters*, *90*(1), pp. 251-261.

Petersen, M.D., Moschetti, M.P., Powers, P.M., Mueller, C.S., Haller, K.M., Frankel, A.D., Zeng, Y., Rezaeian, S., Harmsen, S.C., Boyd, O.S. and Field, N., 2015. The 2014 United States national seismic hazard model. *Earthquake Spectra*, *31*(1_suppl), pp. S1-S30.

Petersen, M.D., Shumway, A.M., Powers, P.M., Mueller, C.S., Moschetti, M.P., Frankel, A.D., Rezaeian, S., McNamara, D.E., Luco, N., Boyd, O.S. and Rukstales, K.S., 2020. The 2018 update of the US National Seismic Hazard Model: Overview of model and implications. *Earthquake Spectra*, *36*(1), pp. 5-41.

Thompson, S., Madugo, C., Lewandowski, N., Lee, C.-H., and Hull, A., 2016. Deterministic fault displacement hazard methodologies for gas Pipeline crossings. Fault Displacement Hazard Analysis Workshop Presentation, December 9, 2016.

Wells, D.L. and Coppersmith, K.J., 1994. New empirical relationships among magnitude, rupture length, rupture width, rupture area, and surface displacement. *Bulletin of the seismological Society of America*, *84*(4), pp. 974-1002.

Wesnousky, S.G., 2008. Displacement and geometrical characteristics of earthquake surface ruptures: Issues and implications for seismic-hazard analysis and the process of earthquake rupture. *Bulletin of the Seismological Society of America*, *98*(4), pp. 1609-1632.

Wheeler, R.L., 1989. Persistent segment boundaries on basin-range normal faults, in *Proceedings, Conference XLV-Fault Segmentation and Controls on Rupture Initiation and Termination*, eds. D.P. Schwartz and R.H. Sibson, U.S. Geological Survey Open File Report 89-315, pp. 432-444.

Wong, I., Olig, S., Dober, M., Wright, D., Nemser, E., Lageson, D., Silva, W., Stickney, M., Lemieux, M. and Anderson, L., 2005. Probabilistic earthquake hazard maps for the state of Montana. *Special Publication 117*, Montana Bureau of Mines and Geology.

Youngs, R.R., Arabasz, W.J., Anderson, R.E., Ramelli, A.R., Ake, J.P., Slemmons, D.B., McCalpin, J.P., Doser, D.I., Fridrich, C.J., Swan III, F.H. and Rogers, A.M., 2003. A methodology for probabilistic fault displacement hazard analysis (PFDHA). *Earthquake spectra*, *19*(1), pp. 191-219.

Youngs, R.R. and Coppersmith, K.J., 1985. Implications of fault slip rates and earthquake recurrence models to probabilistic seismic hazard estimates. *Bulletin of the Seismological society of America*, *75*(4), pp. 939-964.

Zeng, Y. and Shen, Z., 2013. A fault-based model for crustal deformation in the Western United States, Appendix D, in Petersen, M.D., Zeng, Yuehua, Haller, K.M., McCaffrey, Robert, Hammond, W.C., Bird, Peter, Moschetti, Morgan, and Thatcher, Wayne, Geodesy- and geology-based slip-rate models for the Western United States (excluding California) national seismic hazard maps: U.S. Geological Survey Open-File Report 2013-1293, p. 58–68.

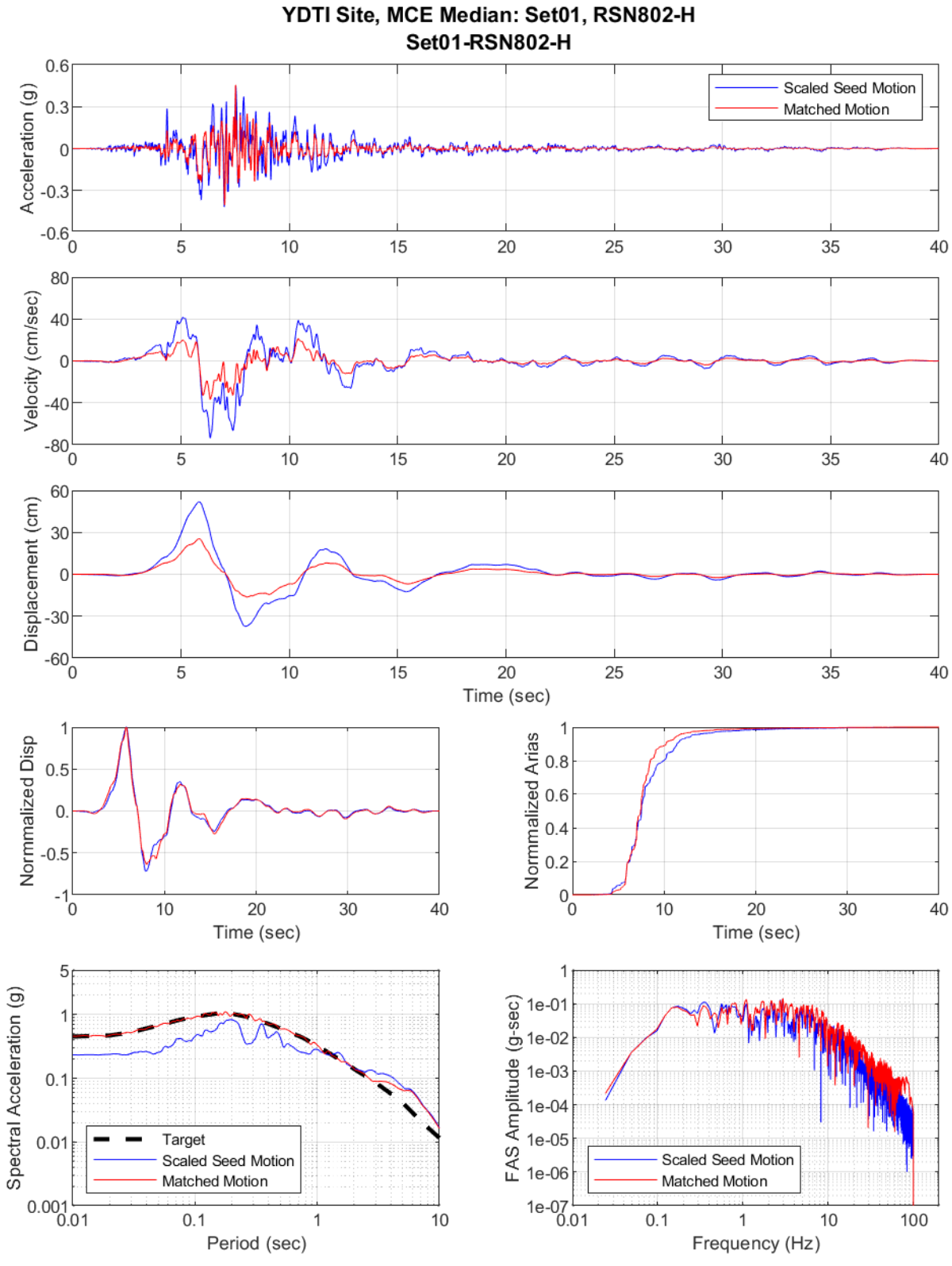
YDTI Site, MCE Median: Set01, RSN802-H
Set01-RSN802-H
Scaled Seed Motion
Matched Motion
Acceleration (g)
Velocity (cm/sec)
Displacement (cm)
Time (sec)
Normmalized Disp
Time (sec)
Normmalized Arias
Time (sec)
Spectral Acceleration (g)
Target
Scaled Seed Motion
Matched Motion
Period (sec)
FAS Amplitude (g-sec)
Scaled Seed Motion
Matched Motion
Frequency (Hz)

YDTI Site, MCE Median: Set01, RSN802-V
Set01-RSN802-V

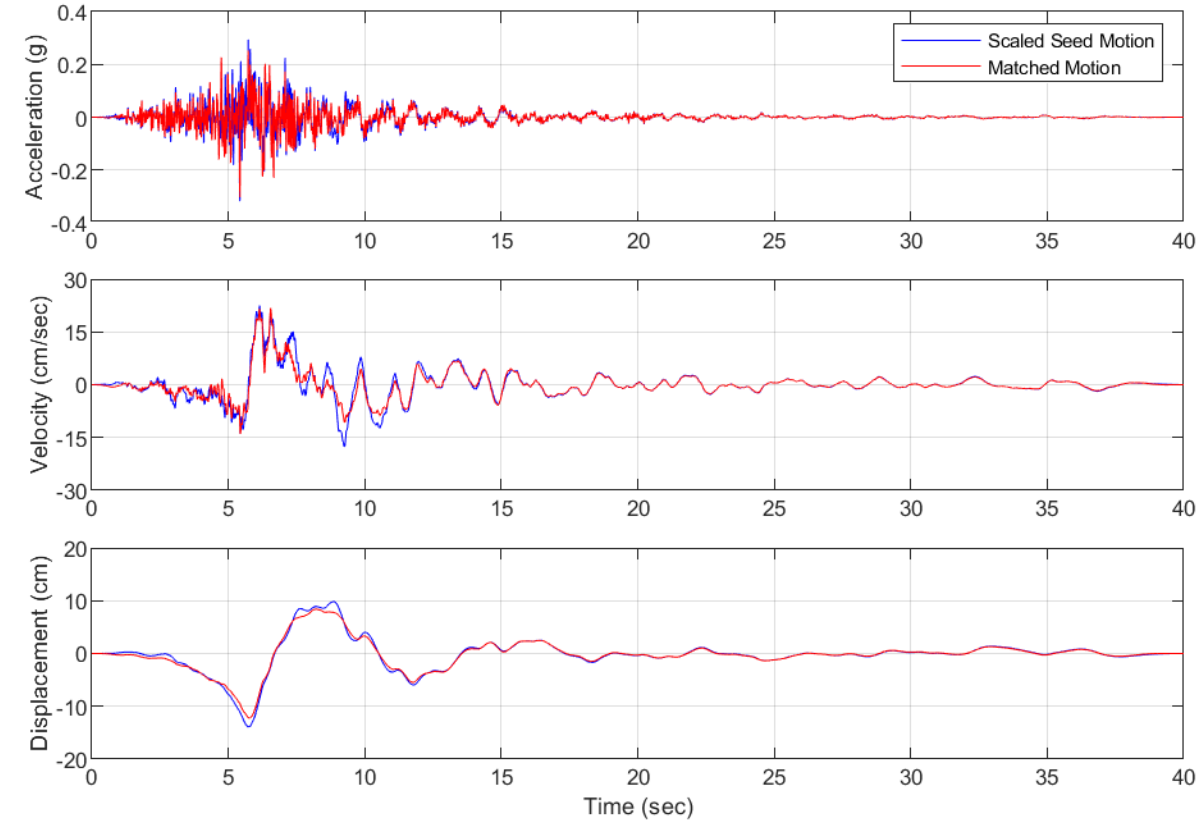

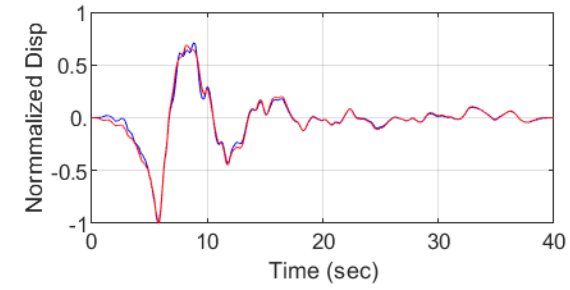

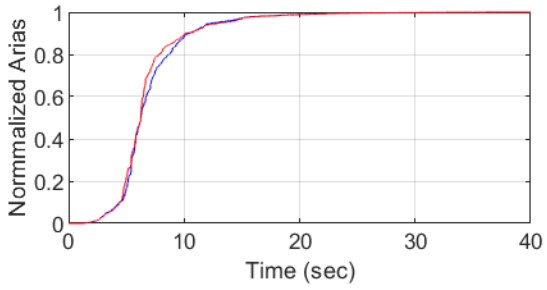

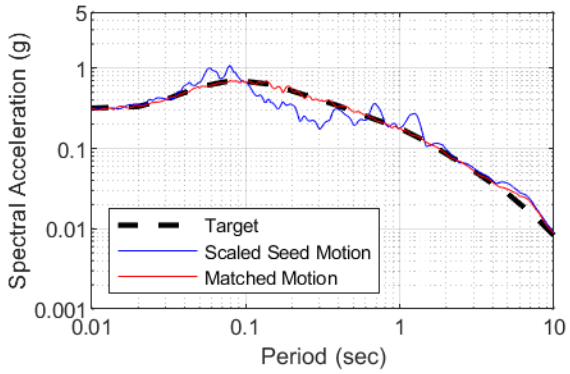

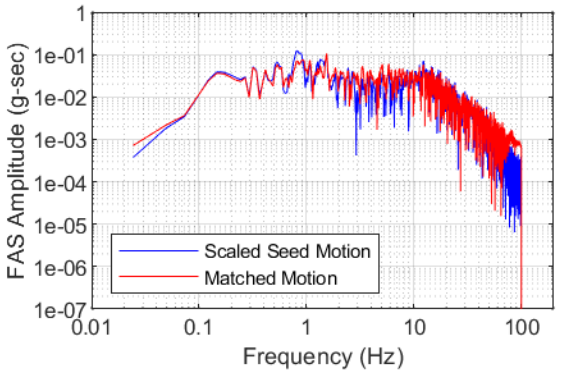

YDTI Site, MCE Median: Set02, RSN828-H
Set02-RSN828-H

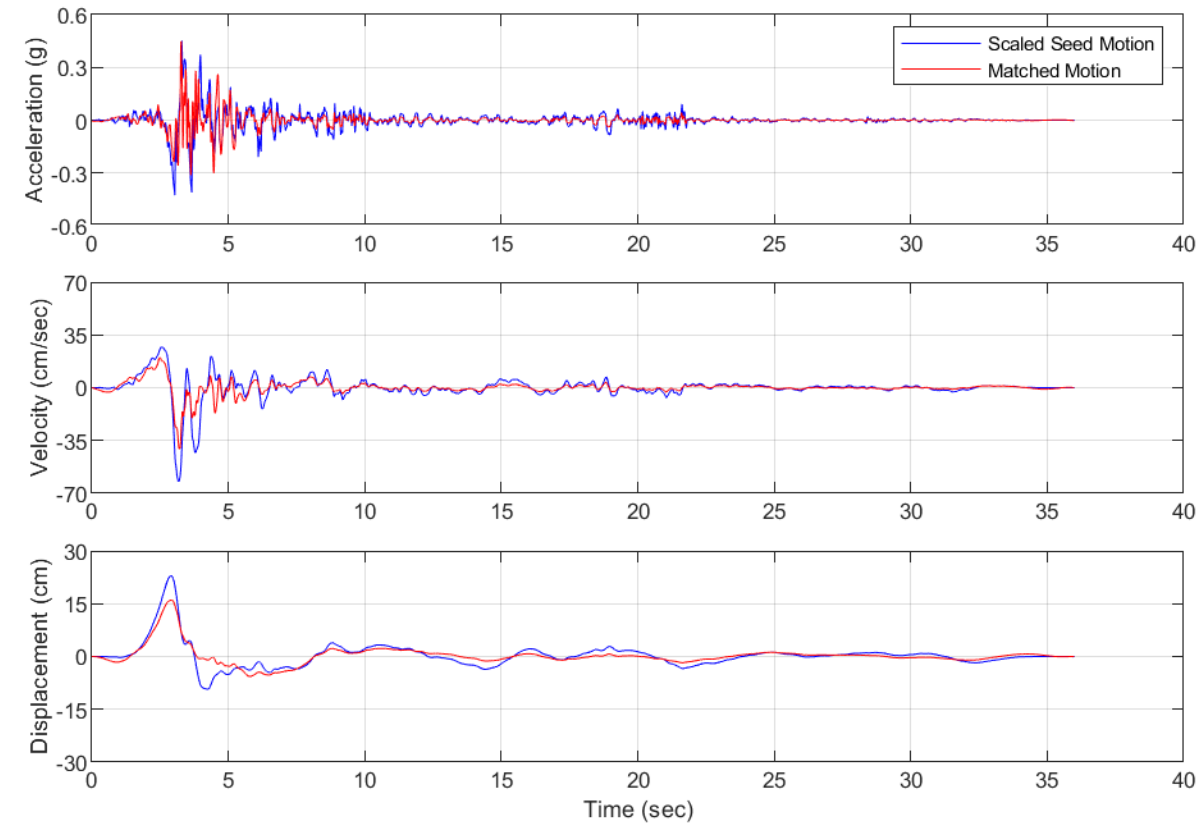

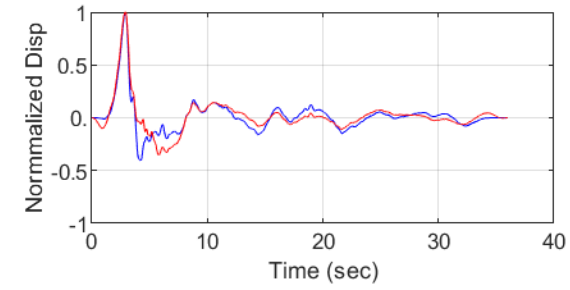

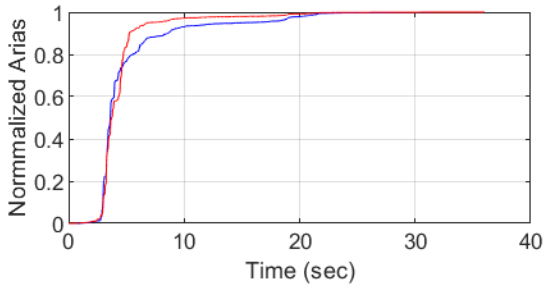

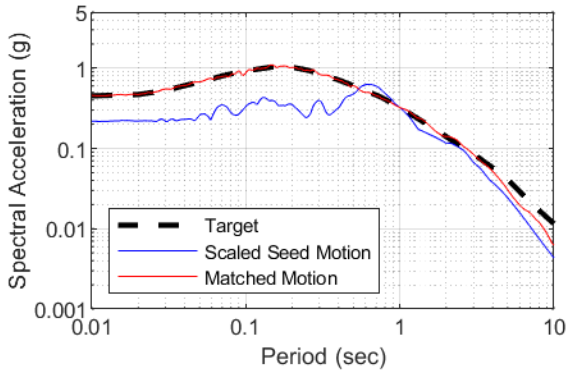

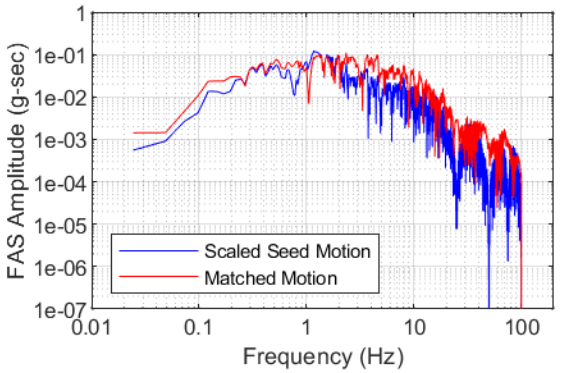

YDTI Site, MCE Median: Set02, RSN828-V
Set02-RSN828-V

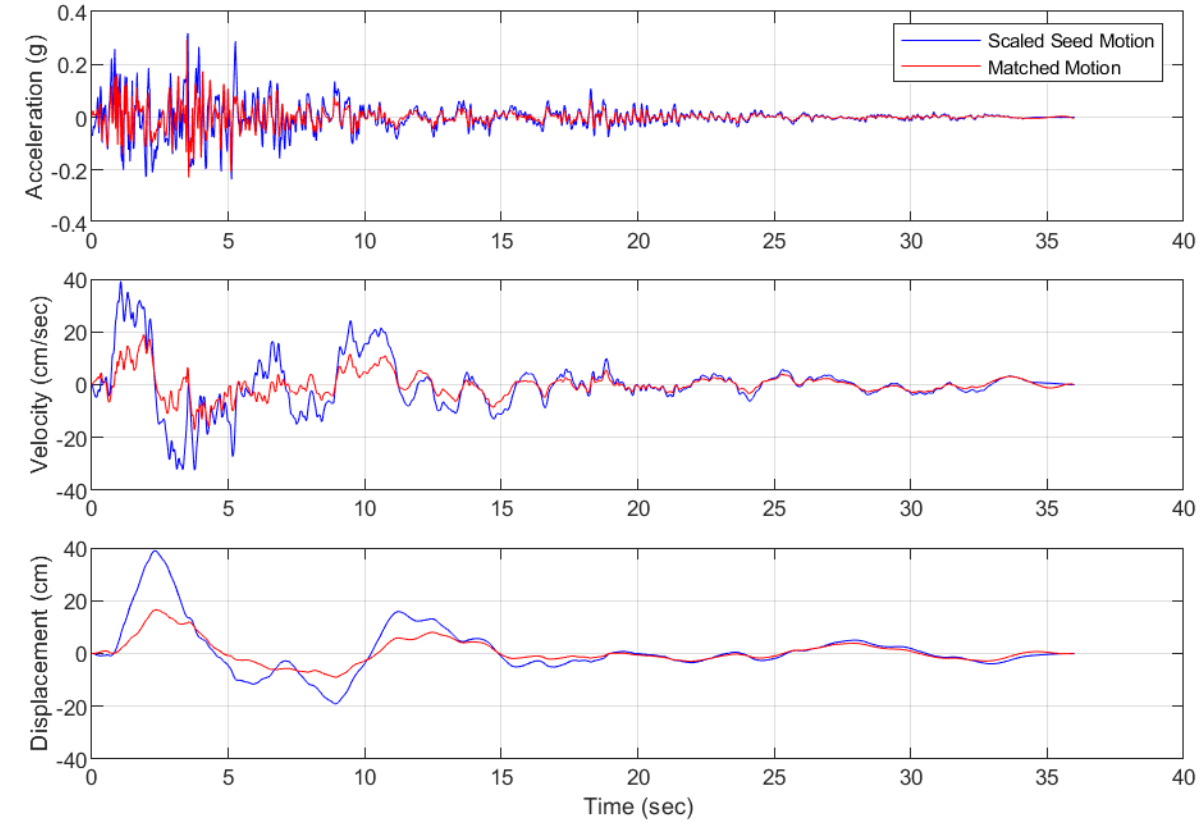

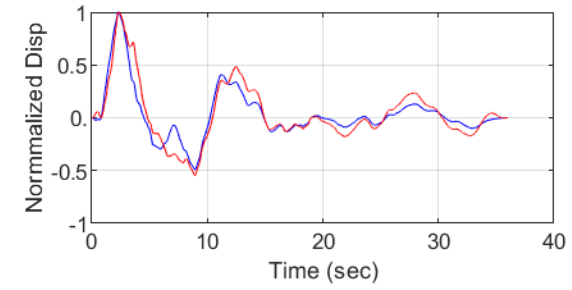

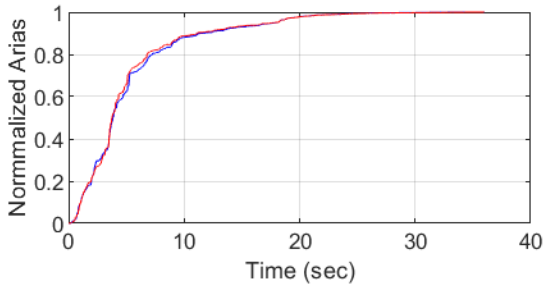

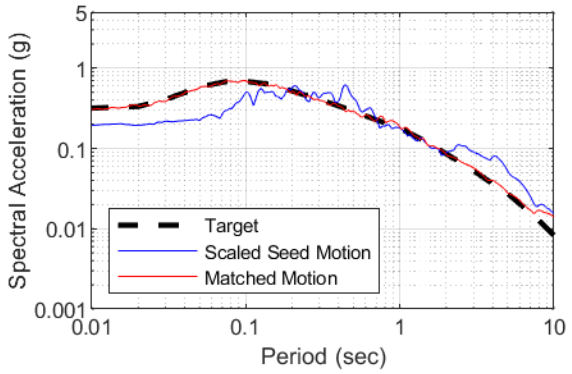

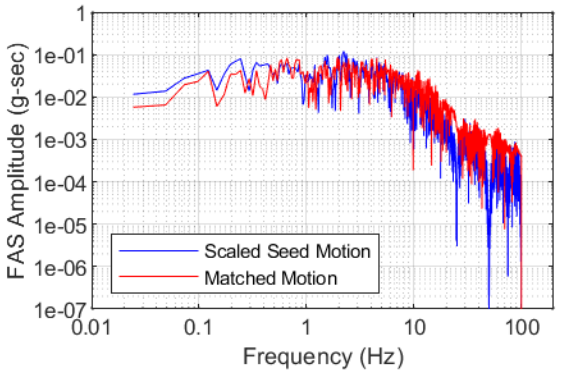

YDTI Site, MCE Median: Set03, RSN6927-H
Set03-RSN6927-H

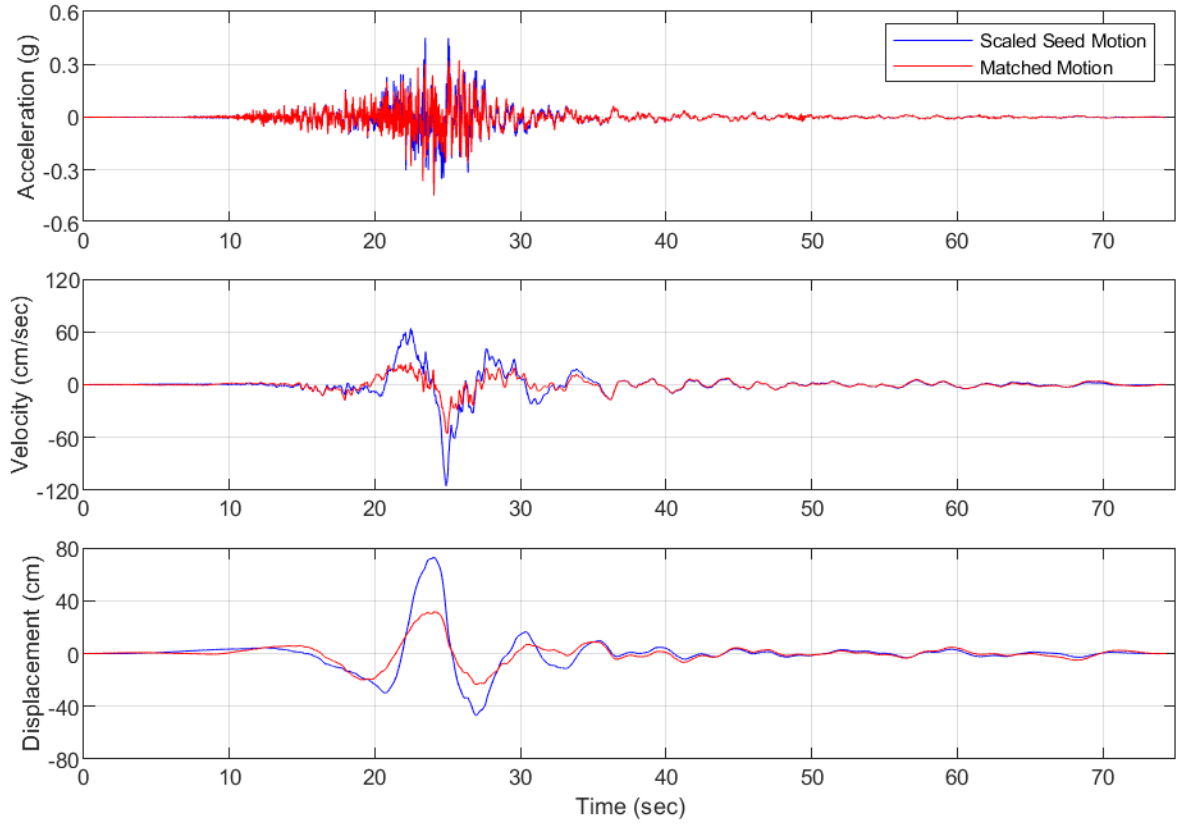

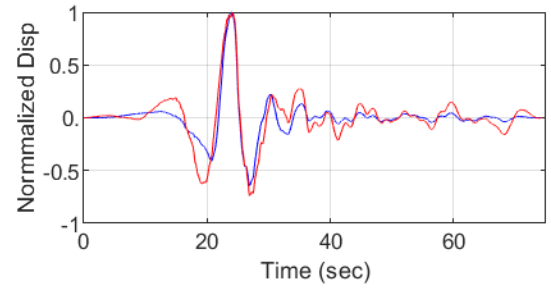

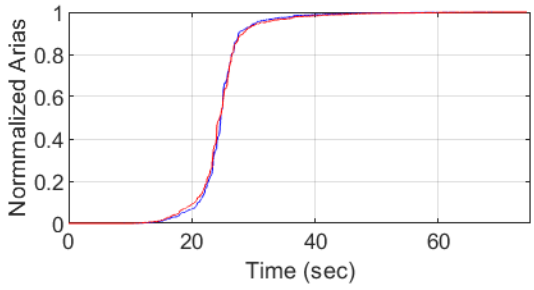

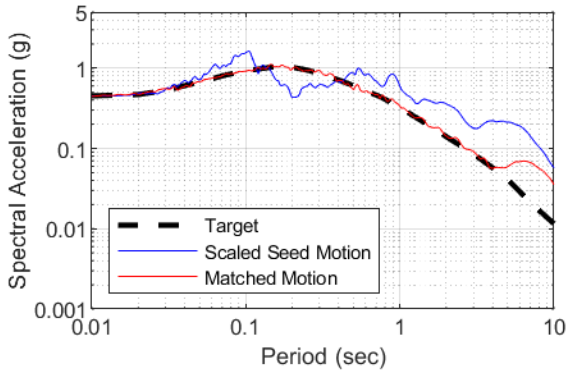

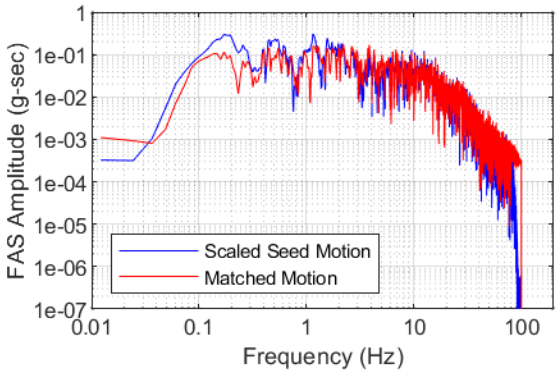

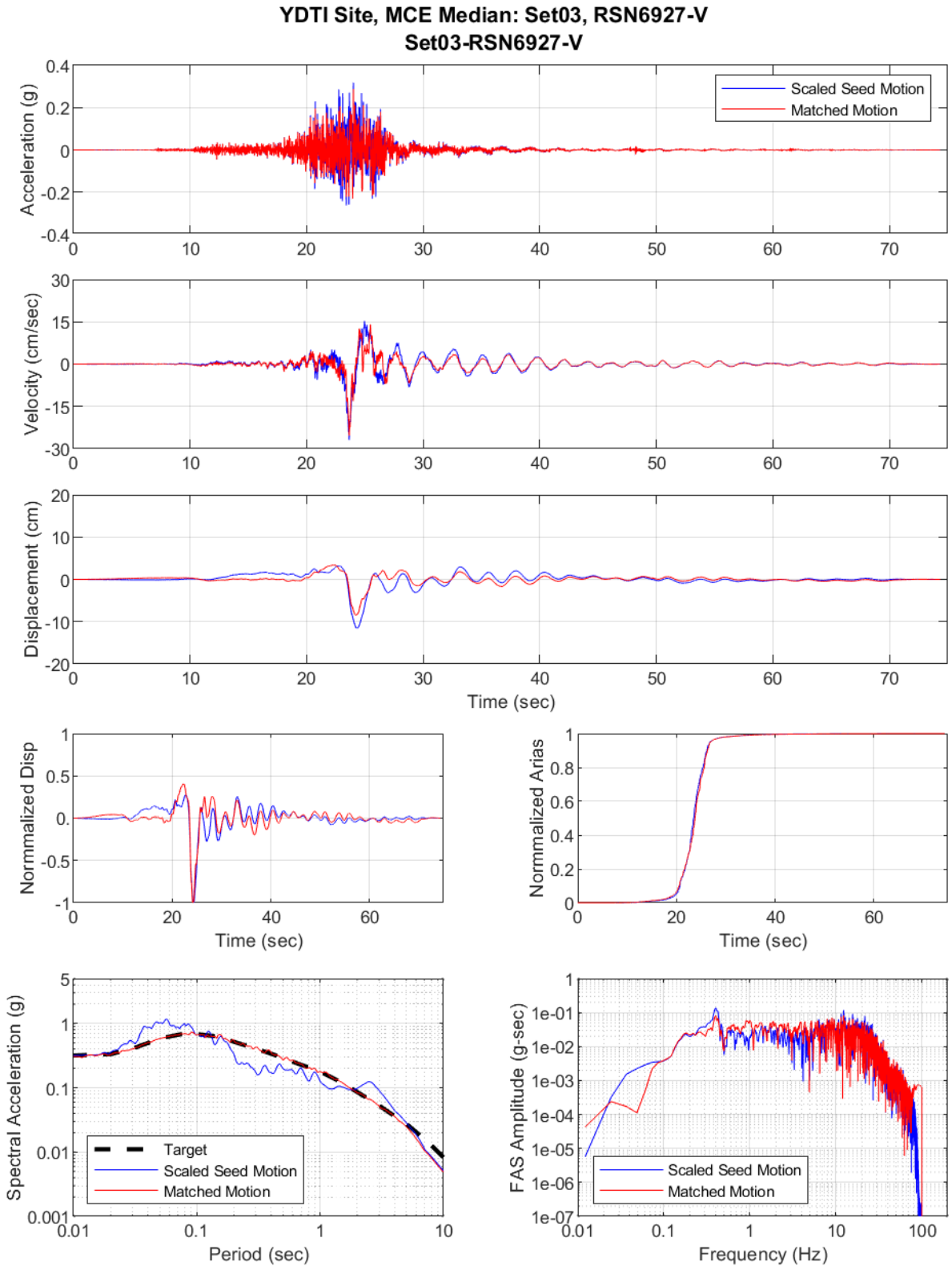
YDTI Site, MCE Median: Set03, RSN6927-V
Set03-RSN6927-V
Scaled Seed Motion
Matched Motion
Acceleration (g)
Velocity (cm/sec)
Displacement (cm)
Time (sec)
Normmalized Disp
Time (sec)
Normmalized Arias
Time (sec)
Spectral Acceleration (g)
Target
Scaled Seed Motion
Matched Motion
Period (sec)
FAS Amplitude (g-sec)
Scaled Seed Motion
Matched Motion
Frequency (Hz)

YDTI Site, MCE Median: Set04, RSN1111-H
Set04-RSN1111-H

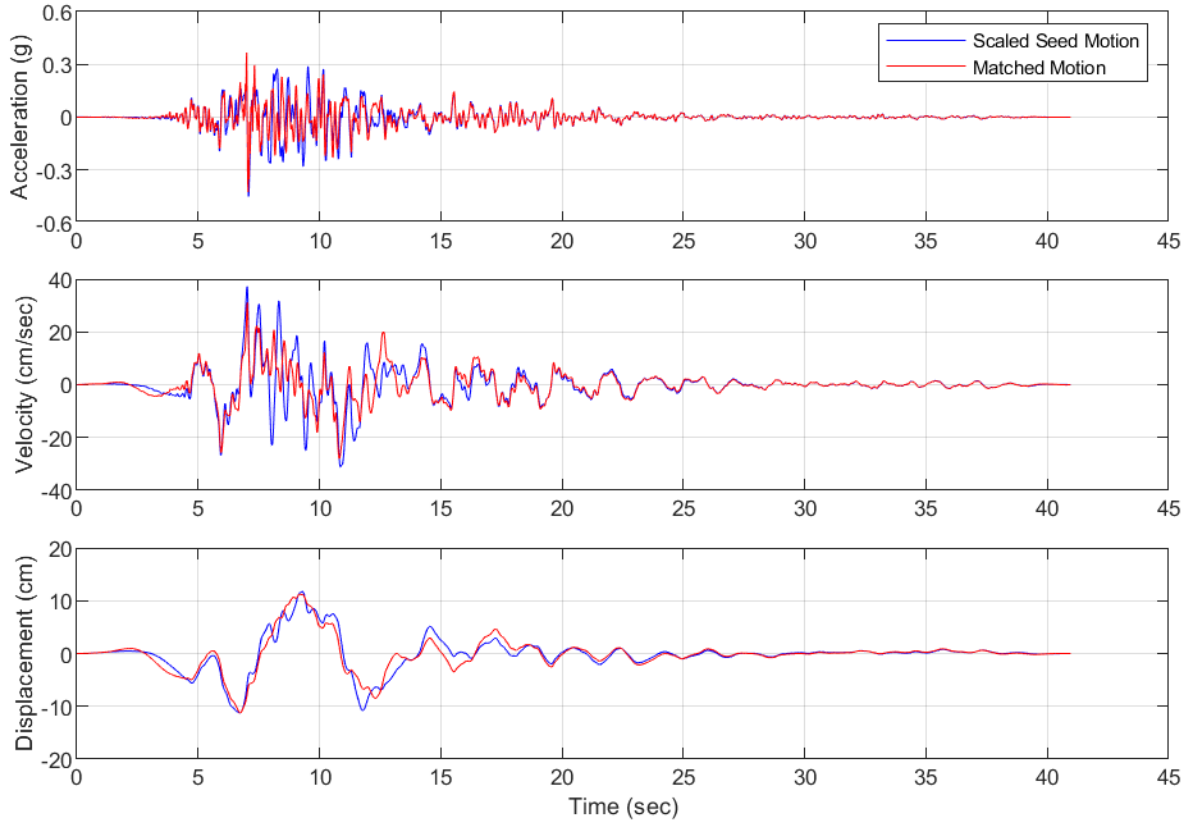

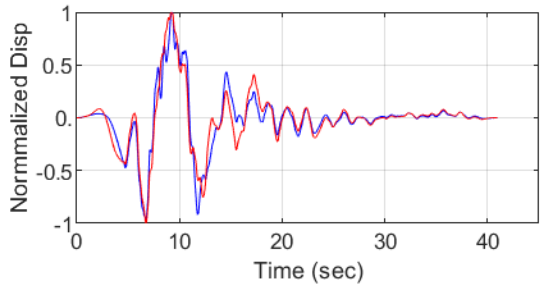

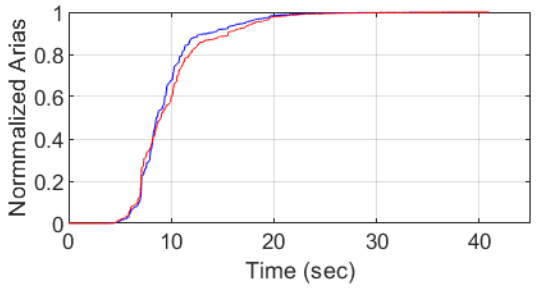

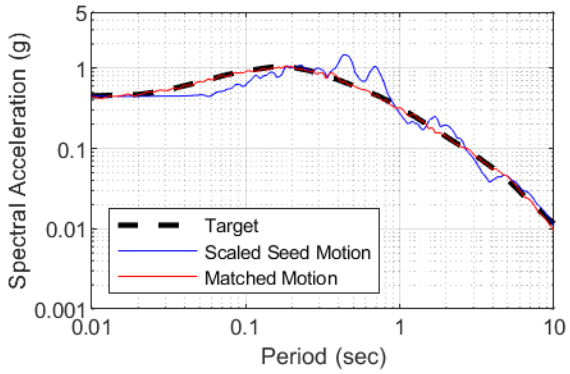

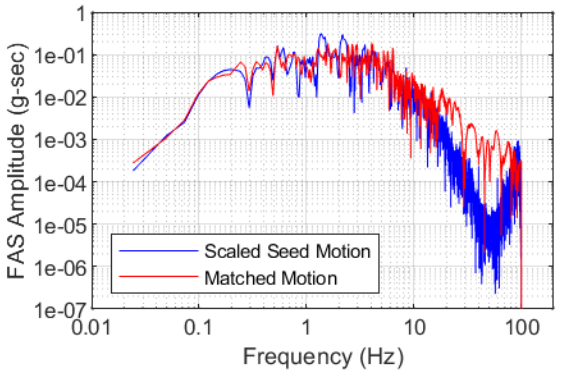

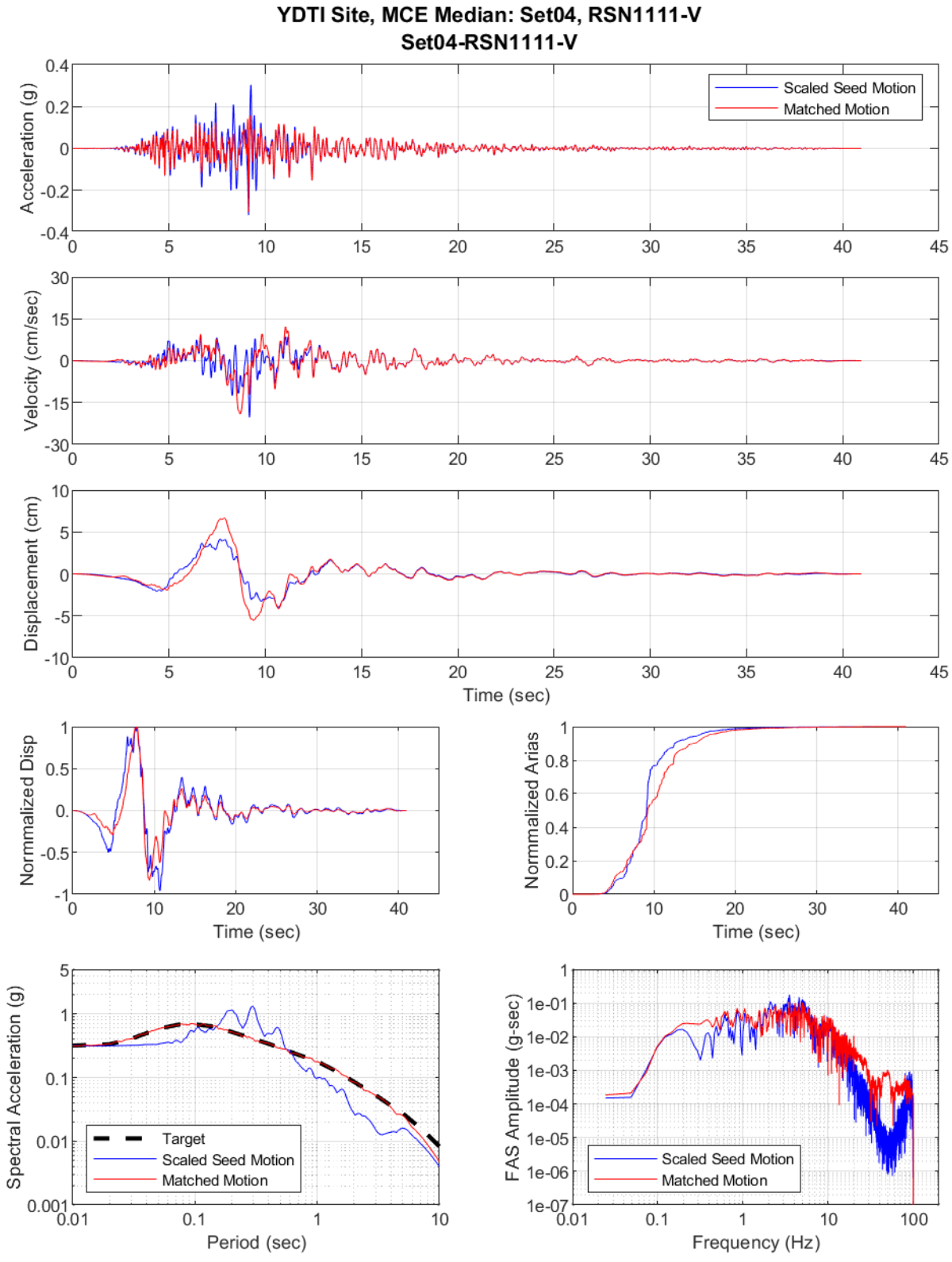
YDTI Site, MCE Median: Set04, RSN1111-V
Set04-RSN1111-V
Scaled Seed Motion
Matched Motion
Acceleration (g)
Velocity (cm/sec)
Displacement (cm)
Time (sec)
Normmalized Disp
Time (sec)
Normmalized Arias
Time (sec)
Spectral Acceleration (g)
Target
Scaled Seed Motion
Matched Motion
Period (sec)
FAS Amplitude (g-sec)
Scaled Seed Motion
Matched Motion
Frequency (Hz)

YDTI Site, MCE Median: Set05, RSN284-H
Set05-RSN284-H

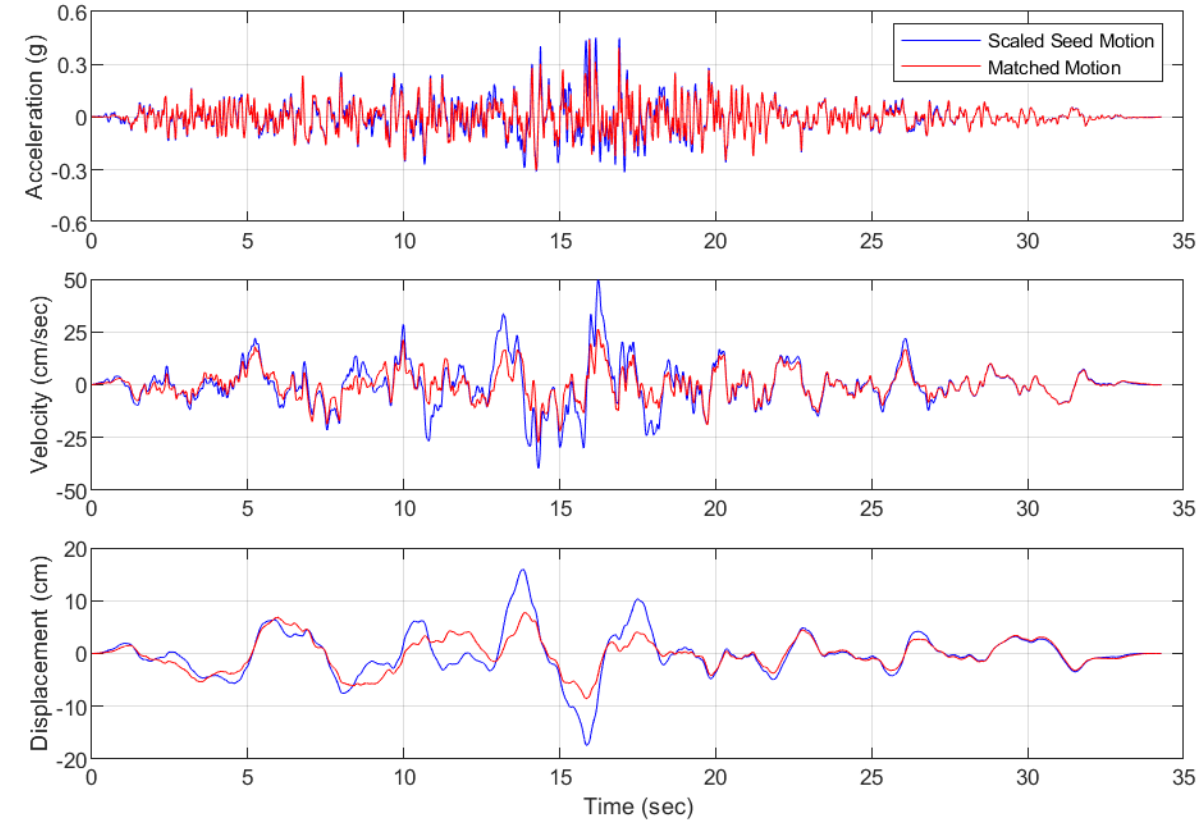

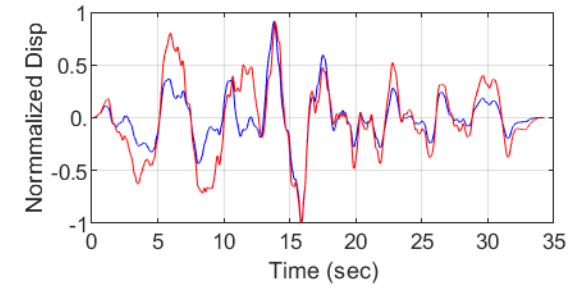

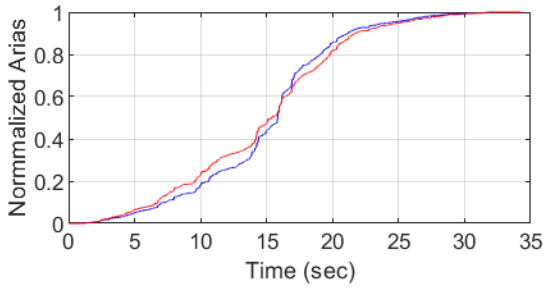

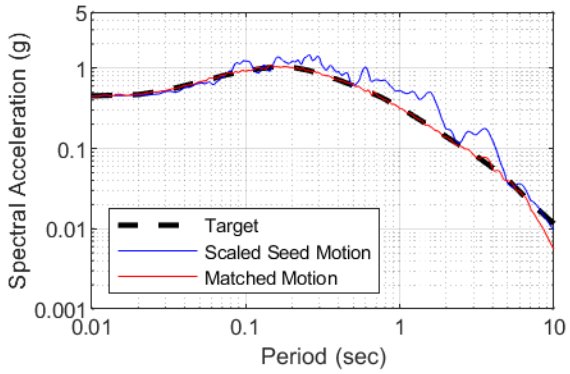

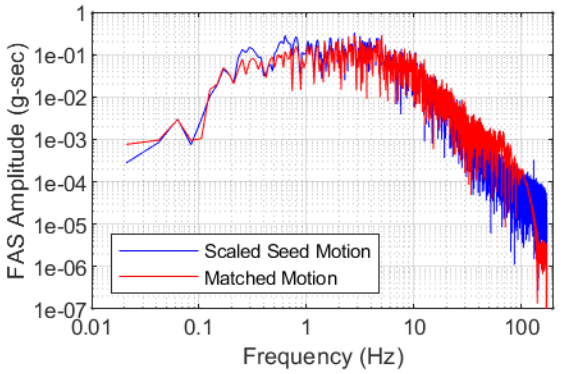

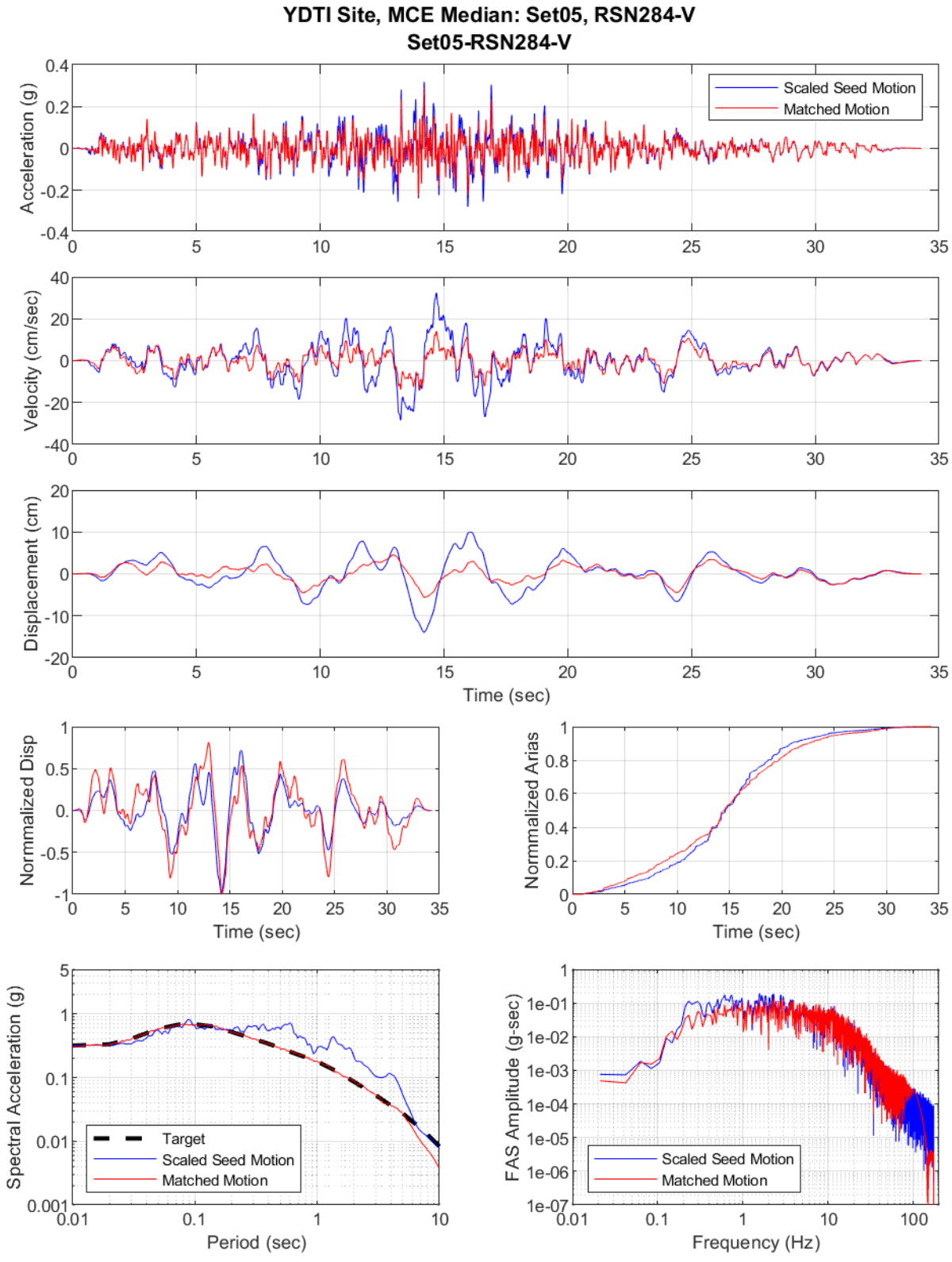
YDTI Site, MCE Median: Set05, RSN284-V
Set05-RSN284-V
Scaled Seed Motion
Matched Motion
Acceleration (g)
Velocity (cm/sec)
Displacement (cm)
Time (sec)
Normmalized Disp
Time (sec)
Normmalized Arias
Time (sec)
Spectral Acceleration (g)
Target
Scaled Seed Motion
Matched Motion
Period (sec)
FAS Amplitude (g-sec)
Scaled Seed Motion
Matched Motion
Frequency (Hz)

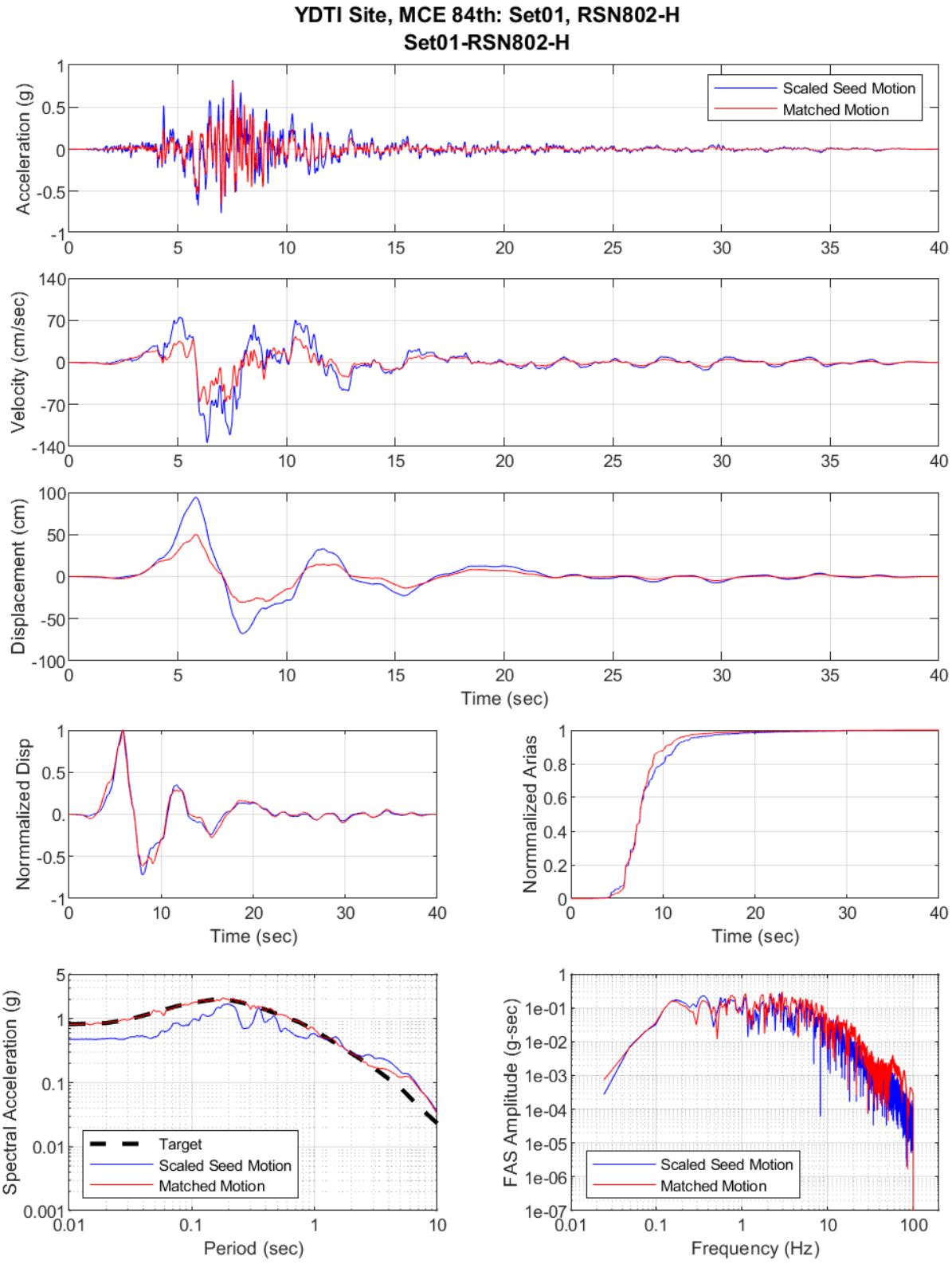
YDTI Site, MCE 84th: Set01, RSN802-H
Set01-RSN802-H
Acceleration (g)
Scaled Seed Motion
Matched Motion
Velocity (cm/sec)
Displacement (cm)
Time (sec)
Normmalized Disp
Time (sec)
Normmalized Arias
Time (sec)
Spectral Acceleration (g)
Target
Scaled Seed Motion
Matched Motion
Period (sec)
FAS Amplitude (g-sec)
Scaled Seed Motion
Matched Motion
Frequency (Hz)

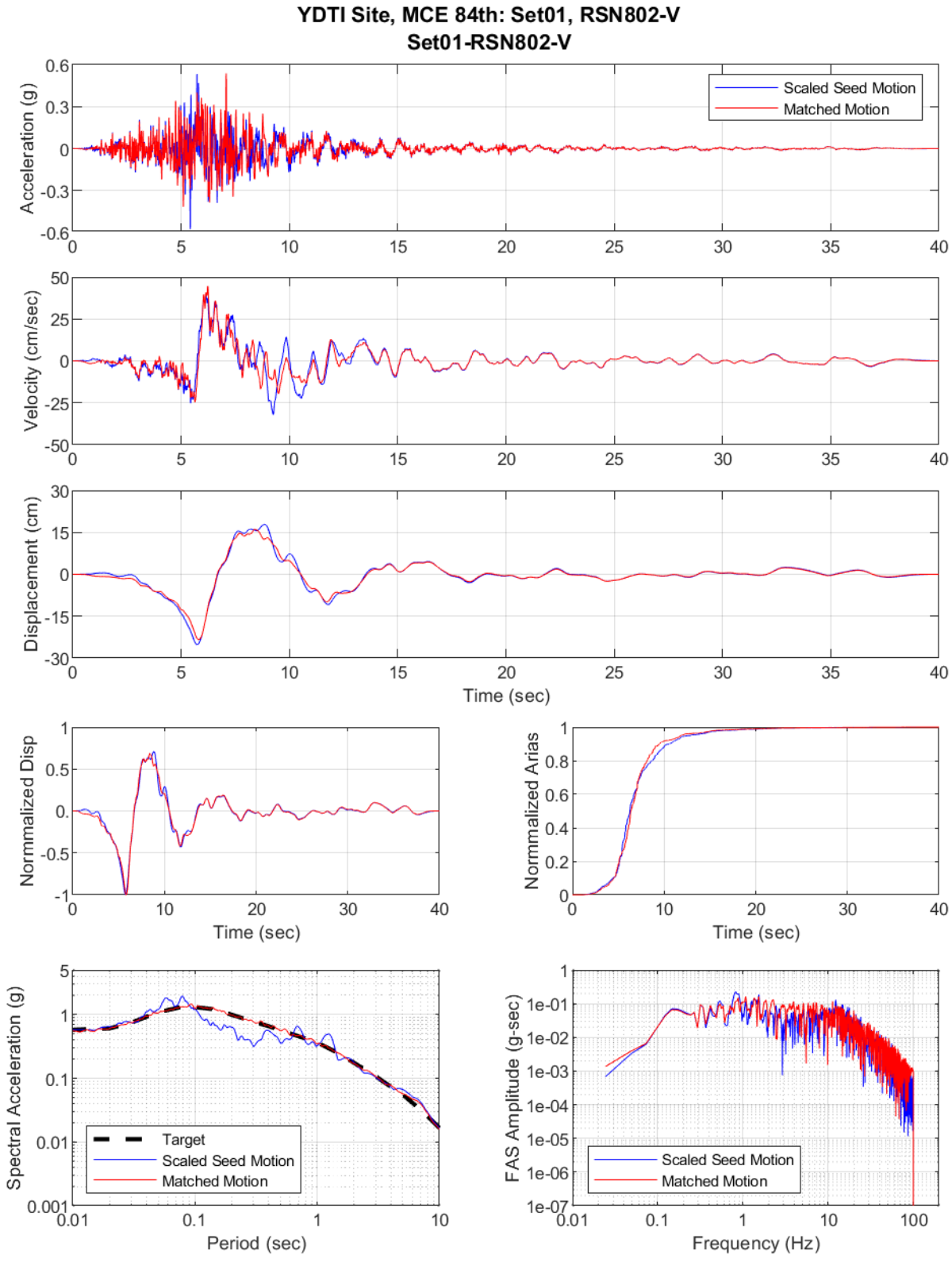
YDTI Site, MCE 84th: Set01, RSN802-V
Set01-RSN802-V
Acceleration (g)
Scaled Seed Motion
Matched Motion
Velocity (cm/sec)
Displacement (cm)
Time (sec)
Normmalized Disp
Time (sec)
Normmalized Arias
Time (sec)
Spectral Acceleration (g)
Target
Scaled Seed Motion
Matched Motion
Period (sec)
FAS Amplitude (g-sec)
Scaled Seed Motion
Matched Motion
Frequency (Hz)

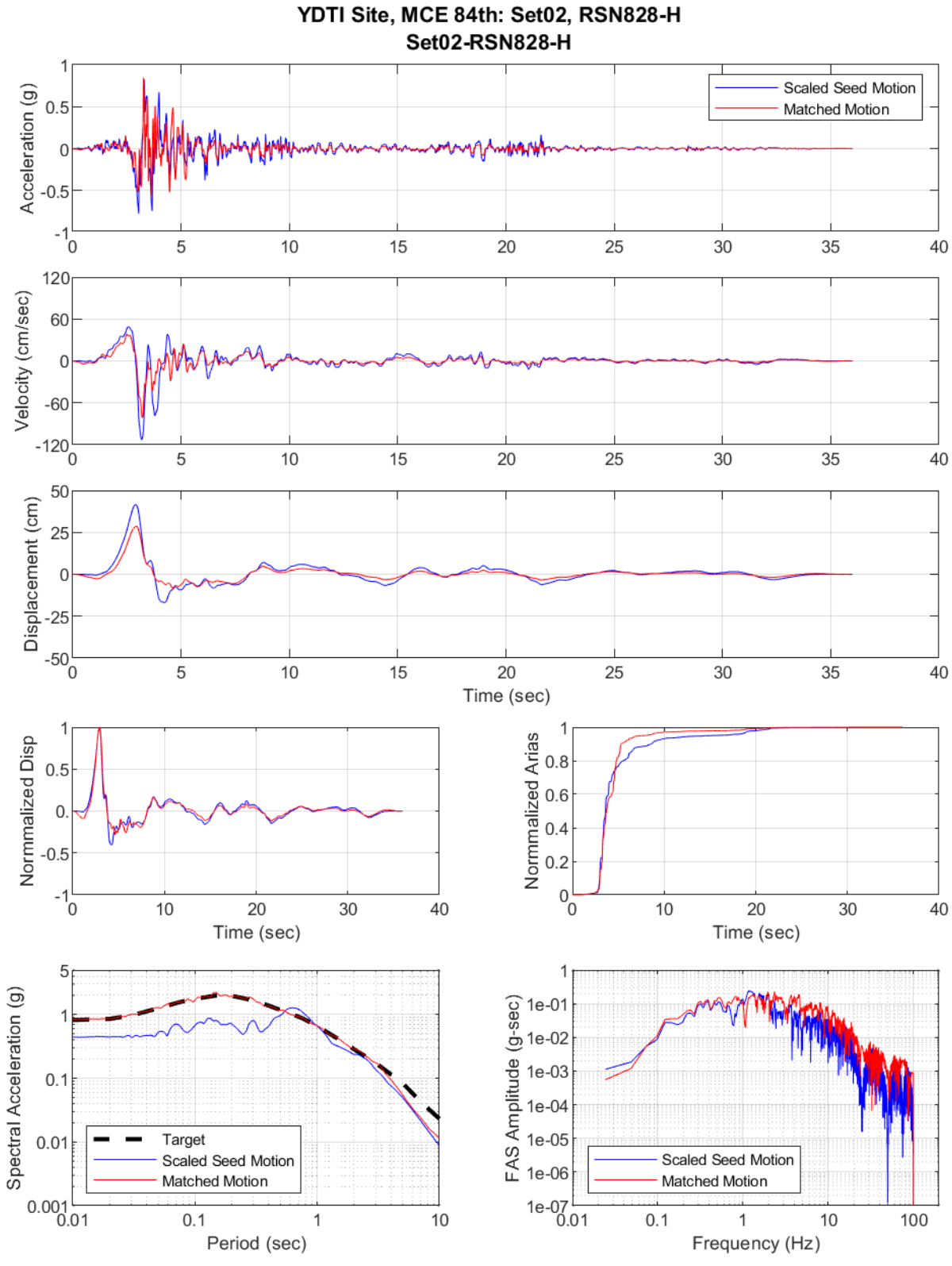
YDTI Site, MCE 84th: Set02, RSN828-H
Set02-RSN828-H
Acceleration (g)
Scaled Seed Motion
Matched Motion
Velocity (cm/sec)
Displacement (cm)
Time (sec)
Normmalized Disp
Time (sec)
Normmalized Arias
Time (sec)
Spectral Acceleration (g)
Target
Scaled Seed Motion
Matched Motion
Period (sec)
FAS Amplitude (g-sec)
Scaled Seed Motion
Matched Motion
Frequency (Hz)

YDTI Site, MCE 84th: Set02, RSN828-V
Set02-RSN828-V

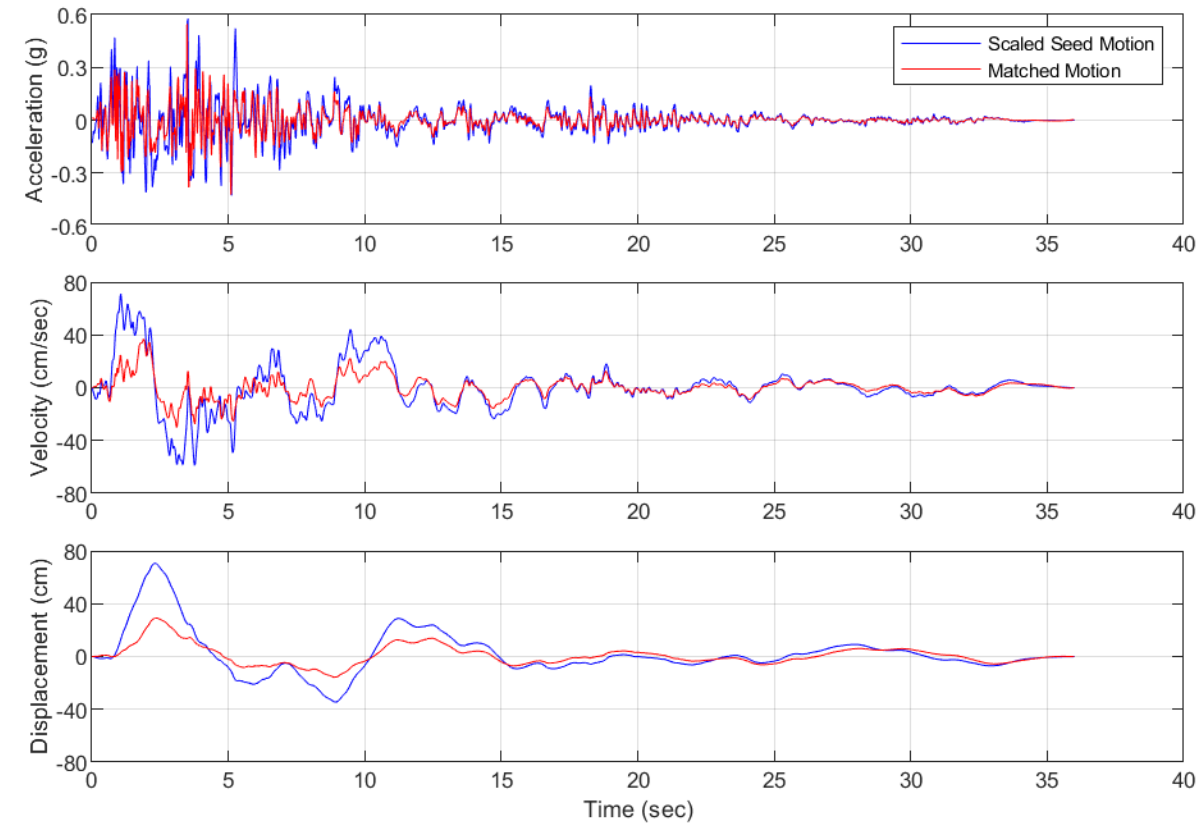

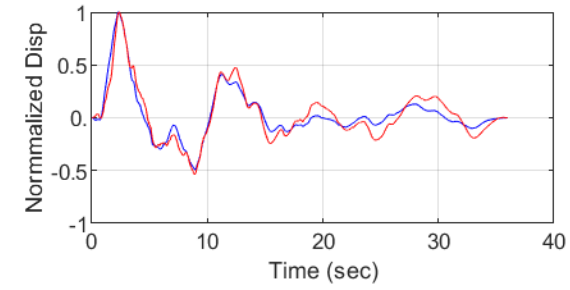

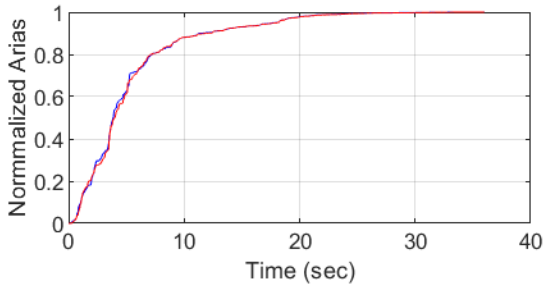

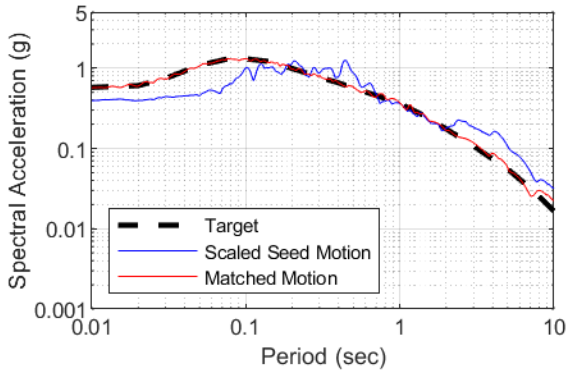

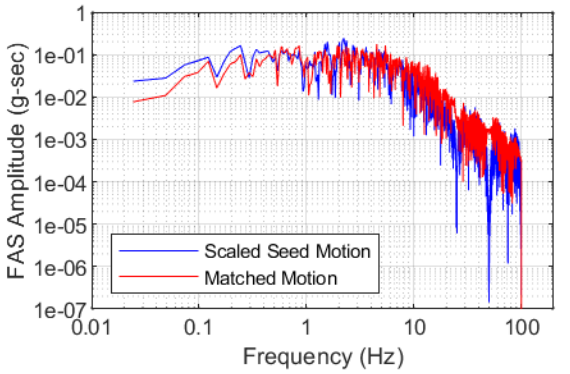

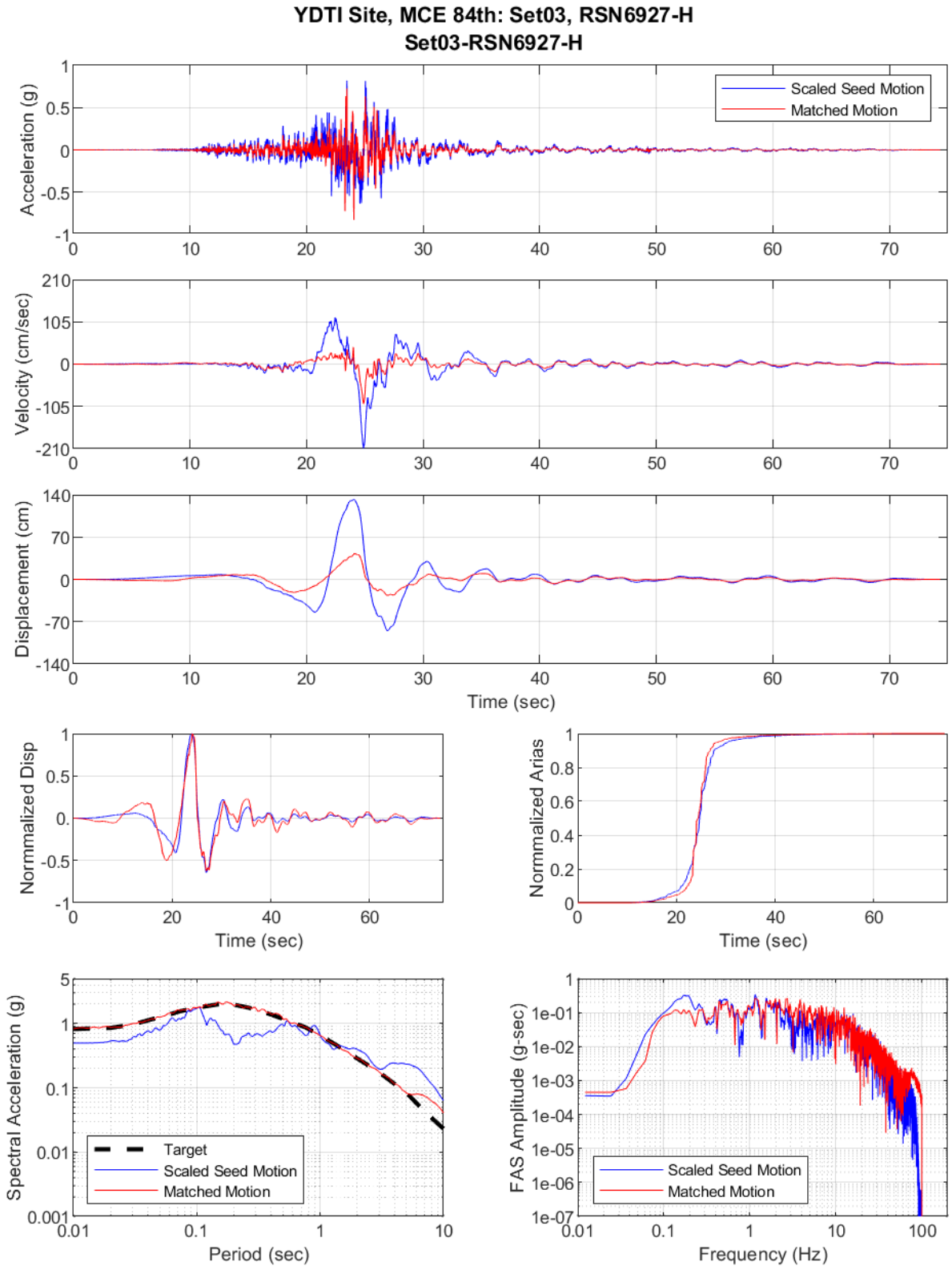
YDTI Site, MCE 84th: Set03, RSN6927-H
Set03-RSN6927-H
Acceleration (g)
Scaled Seed Motion
Matched Motion
Velocity (cm/sec)
Displacement (cm)
Time (sec)
Normmalized Disp
Time (sec)
Normmalized Arias
Time (sec)
Spectral Acceleration (g)
Target
Scaled Seed Motion
Matched Motion
Period (sec)
FAS Amplitude (g-sec)
Scaled Seed Motion
Matched Motion
Frequency (Hz)

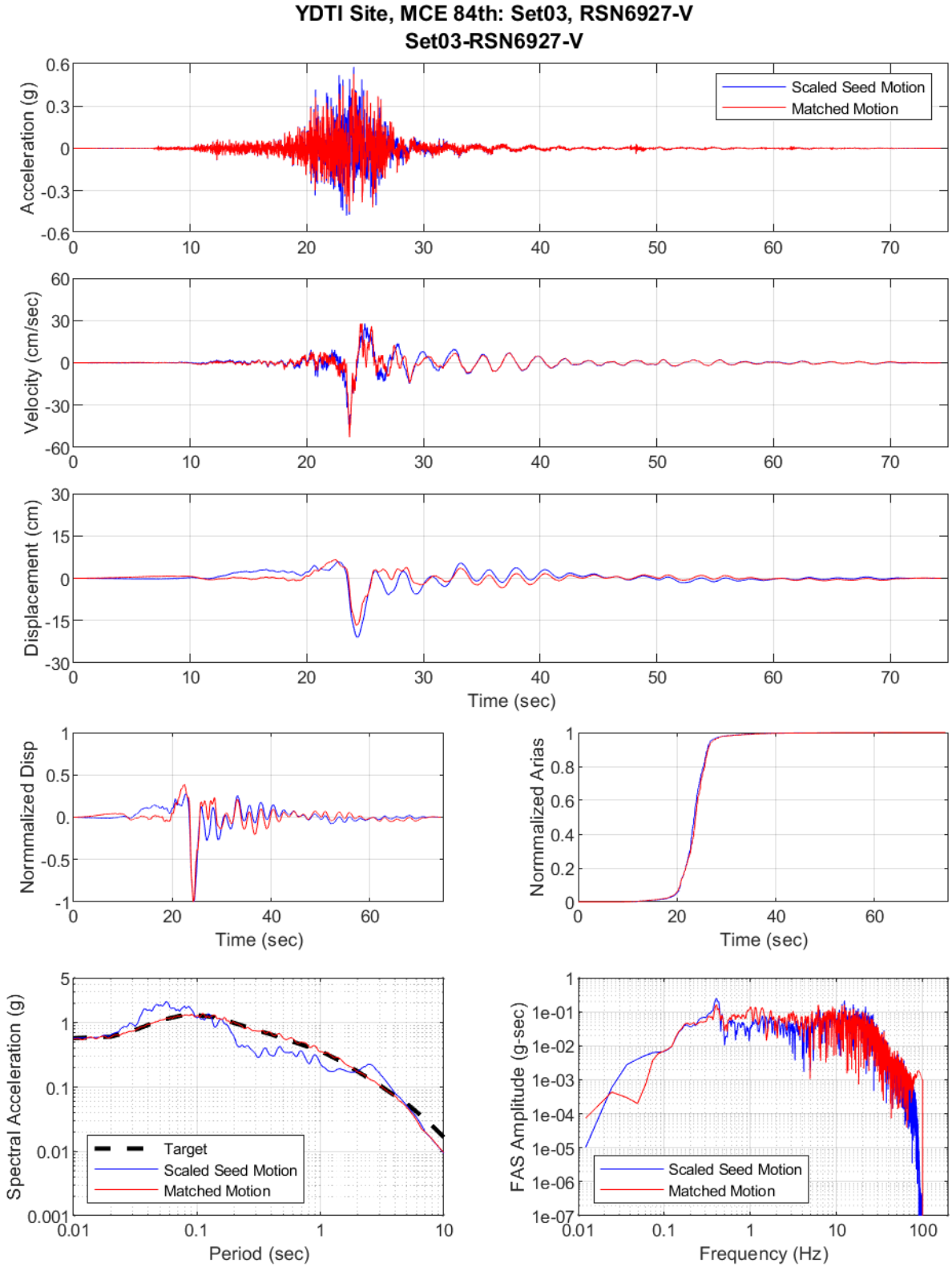
YDTI Site, MCE 84th: Set03, RSN6927-V
Set03-RSN6927-V
Acceleration (g)
Scaled Seed Motion
Matched Motion
Velocity (cm/sec)
Displacement (cm)
Time (sec)
Normmalized Disp
Time (sec)
Normmalized Arias
Time (sec)
Spectral Acceleration (g)
Target
Scaled Seed Motion
Matched Motion
Period (sec)
FAS Amplitude (g-sec)
Scaled Seed Motion
Matched Motion
Frequency (Hz)

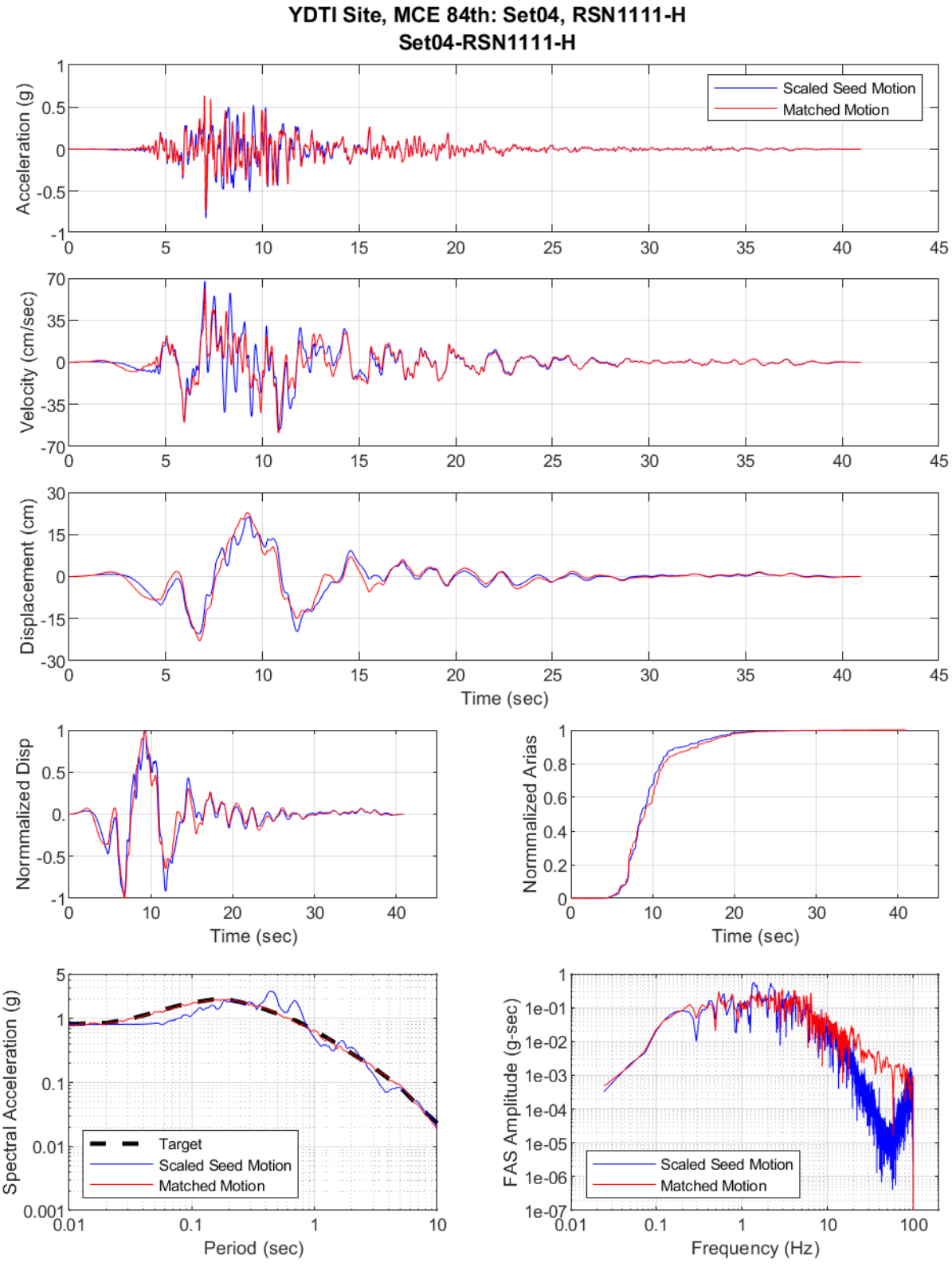
YDTI Site, MCE 84th: Set04, RSN1111-H
Set04-RSN1111-H
Acceleration (g)
Scaled Seed Motion
Matched Motion
Velocity (cm/sec)
Displacement (cm)
Time (sec)
Normmalized Disp
Time (sec)
Normmalized Arias
Time (sec)
Spectral Acceleration (g)
Target
Scaled Seed Motion
Matched Motion
Period (sec)
FAS Amplitude (g-sec)
Scaled Seed Motion
Matched Motion
Frequency (Hz)

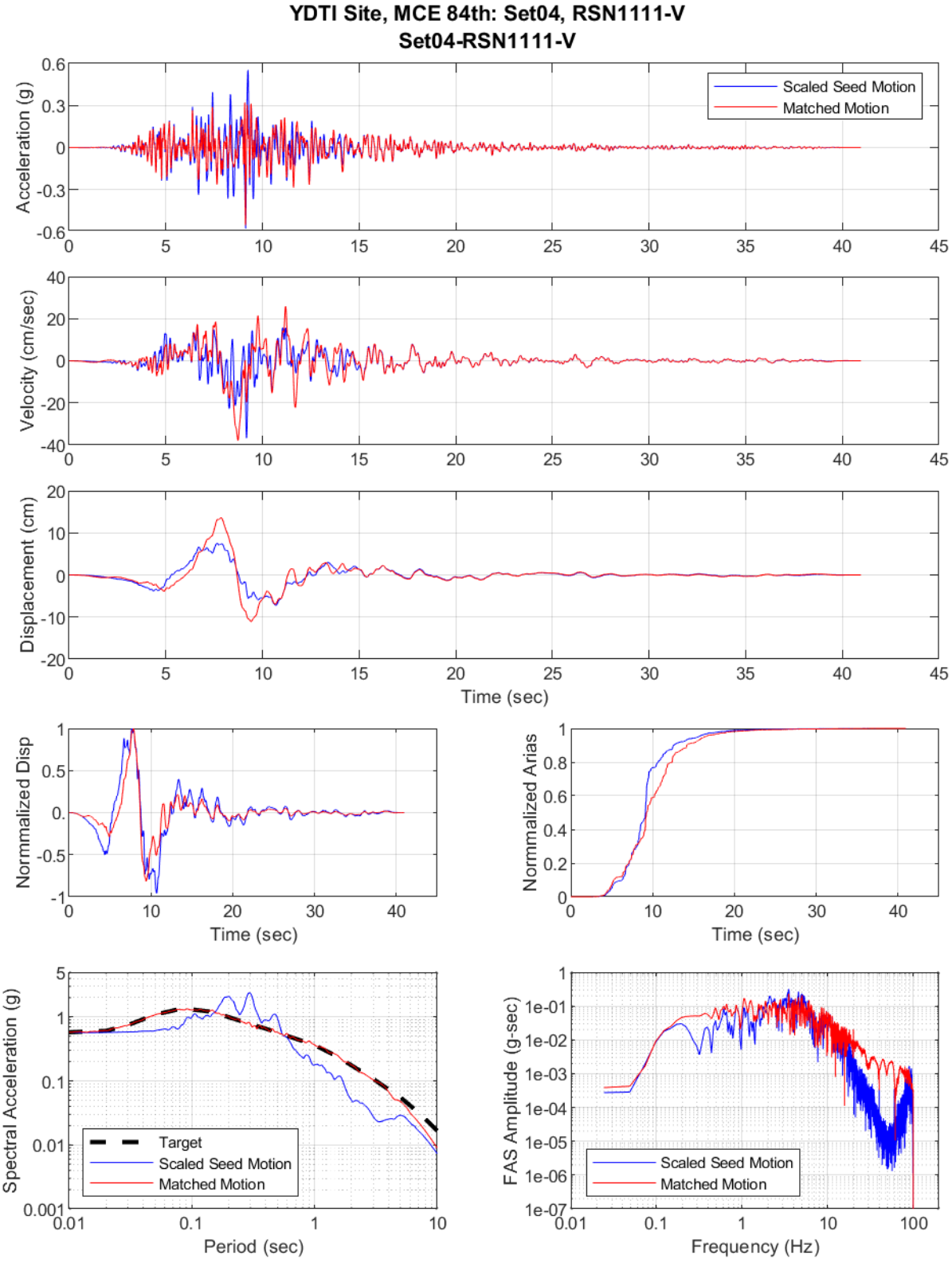
YDTI Site, MCE 84th: Set04, RSN1111-V
Set04-RSN1111-V
Acceleration (g)
Scaled Seed Motion
Matched Motion
Velocity (cm/sec)
Displacement (cm)
Time (sec)
Normmalized Disp
Time (sec)
Normmalized Arias
Time (sec)
Spectral Acceleration (g)
Target
Scaled Seed Motion
Matched Motion
Period (sec)
FAS Amplitude (g-sec)
Scaled Seed Motion
Matched Motion
Frequency (Hz)

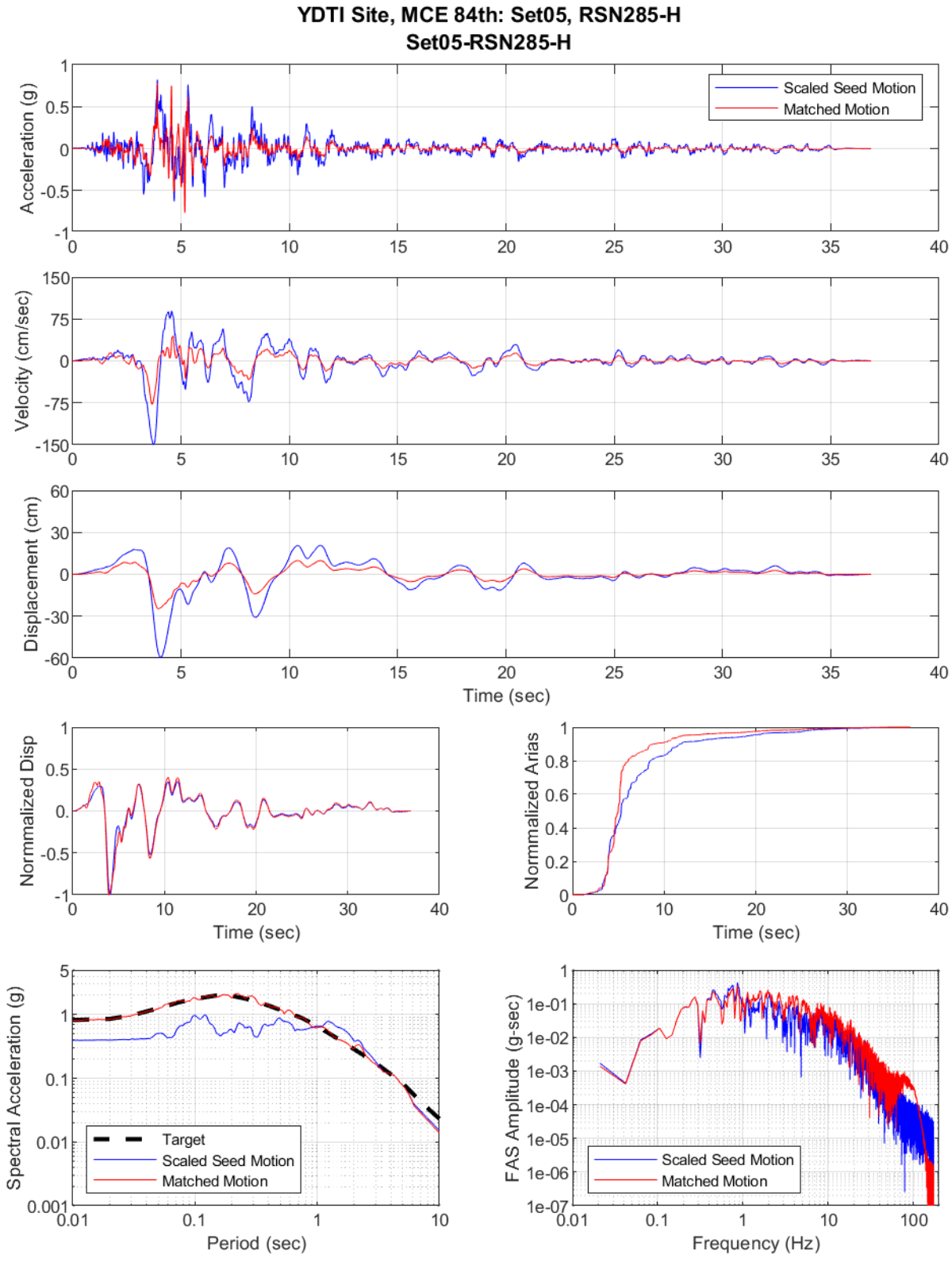
YDTI Site, MCE 84th: Set05, RSN285-H
Set05-RSN285-H
Acceleration (g)
Scaled Seed Motion
Matched Motion
Velocity (cm/sec)
Displacement (cm)
Time (sec)
Normmalized Disp
Time (sec)
Normmalized Arias
Time (sec)
Spectral Acceleration (g)
Target
Scaled Seed Motion
Matched Motion
Period (sec)
FAS Amplitude (g-sec)
Scaled Seed Motion
Matched Motion
Frequency (Hz)

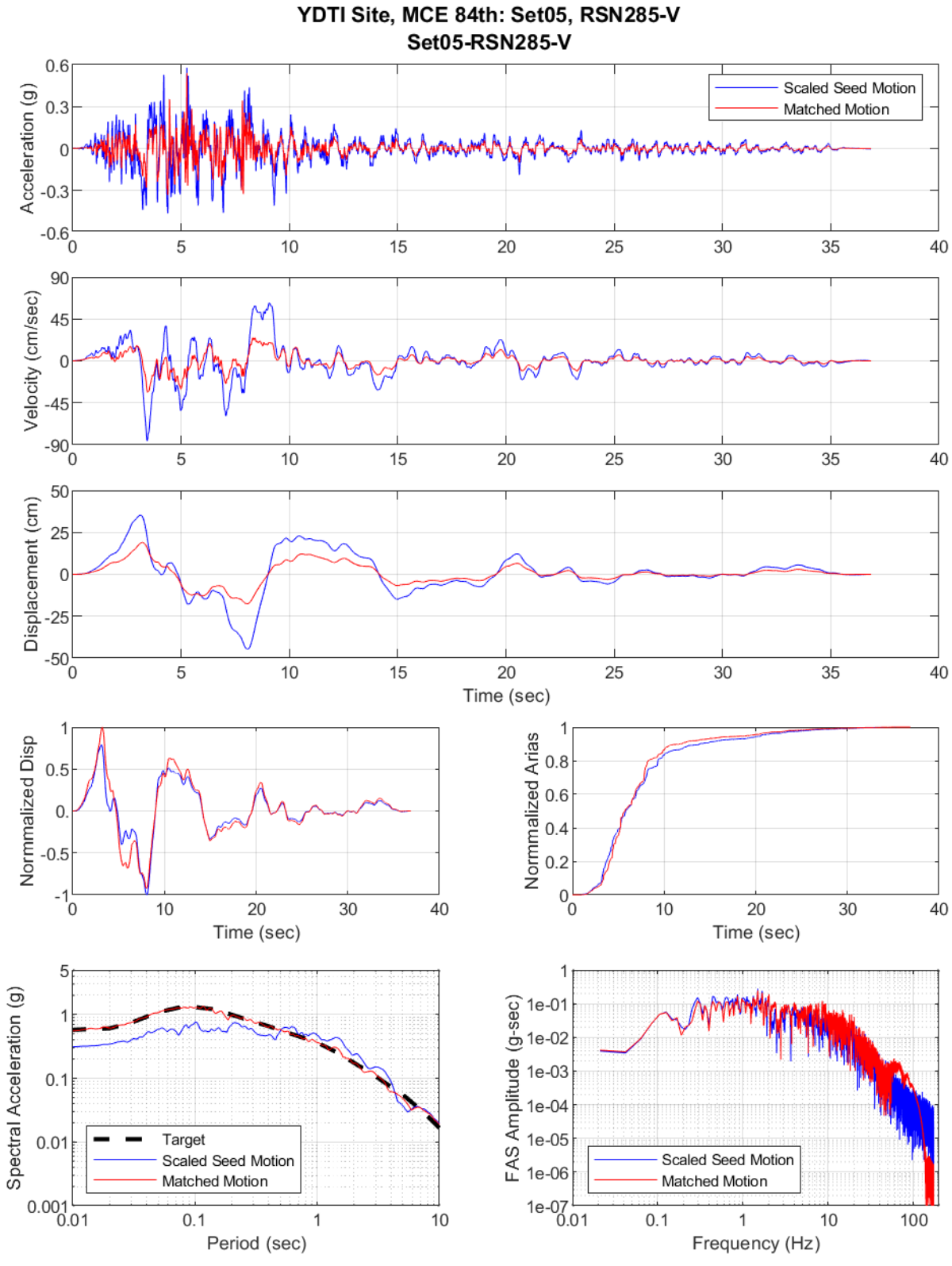
YDTI Site, MCE 84th: Set05, RSN285-V
Set05-RSN285-V
Acceleration (g)
Scaled Seed Motion
Matched Motion
Velocity (cm/sec)
Displacement (cm)
Time (sec)
Normmalized Disp
Time (sec)
Normmalized Arias
Time (sec)
Spectral Acceleration (g)
Target
Scaled Seed Motion
Matched Motion
Period (sec)
FAS Amplitude (g-sec)
Scaled Seed Motion
Matched Motion
Frequency (Hz)

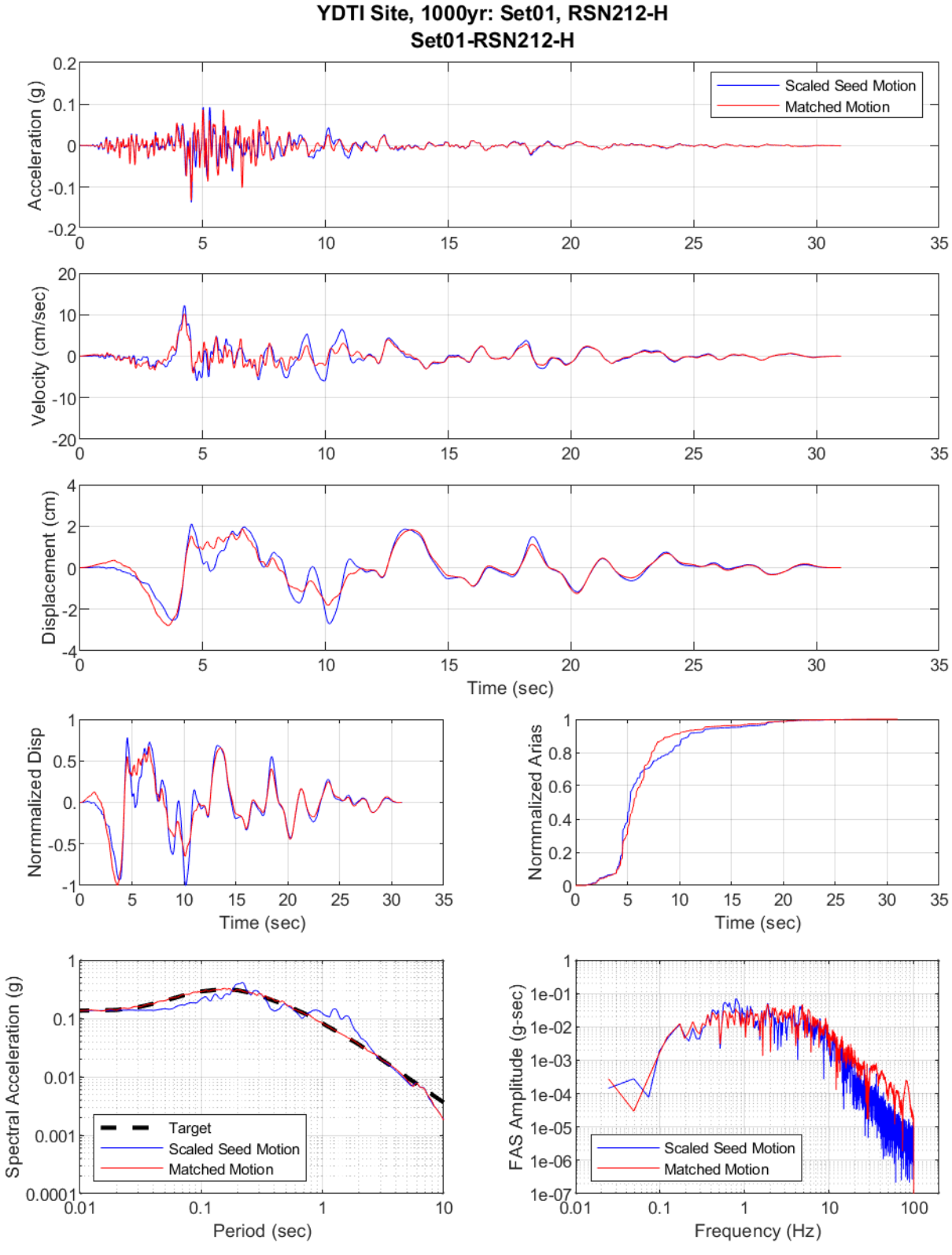
YDTI Site, 1000yr: Set01, RSN212-H
Set01-RSN212-H
Scaled Seed Motion
Matched Motion
Acceleration (g)
Velocity (cm/sec)
Displacement (cm)
Time (sec)
Normmalized Disp
Time (sec)
Normmalized Arias
Time (sec)
Spectral Acceleration (g)
Target
Scaled Seed Motion
Matched Motion
Period (sec)
FAS Amplitude (g-sec)
Scaled Seed Motion
Matched Motion
Frequency (Hz)

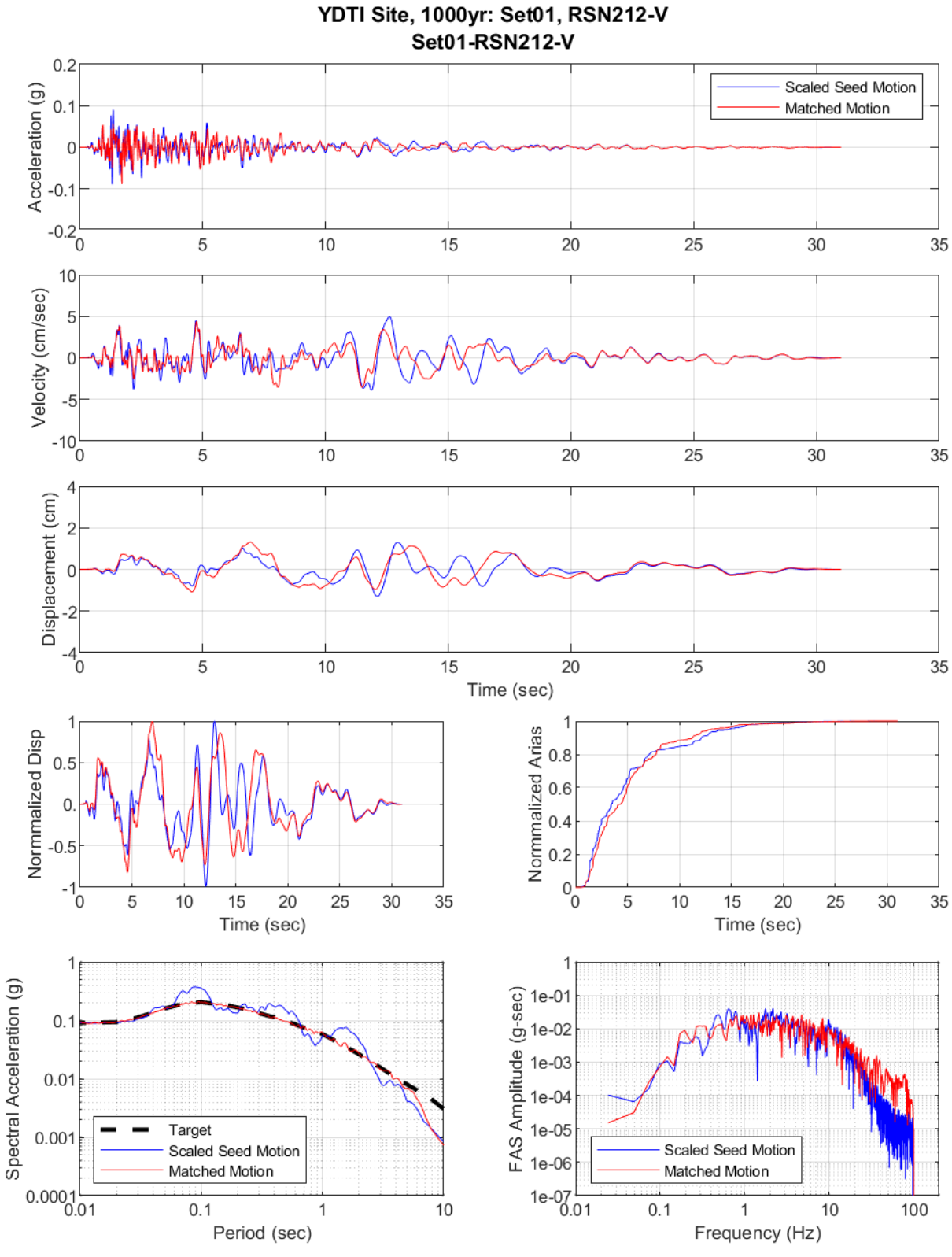
YDTI Site, 1000yr: Set01, RSN212-V
Set01-RSN212-V
Acceleration (g)
Scaled Seed Motion
Matched Motion
Velocity (cm/sec)
Displacement (cm)
Time (sec)
Normmalized Disp
Time (sec)
Normmalized Arias
Time (sec)
Spectral Acceleration (g)
Target
Scaled Seed Motion
Matched Motion
Period (sec)
FAS Amplitude (g-sec)
Scaled Seed Motion
Matched Motion
Frequency (Hz)

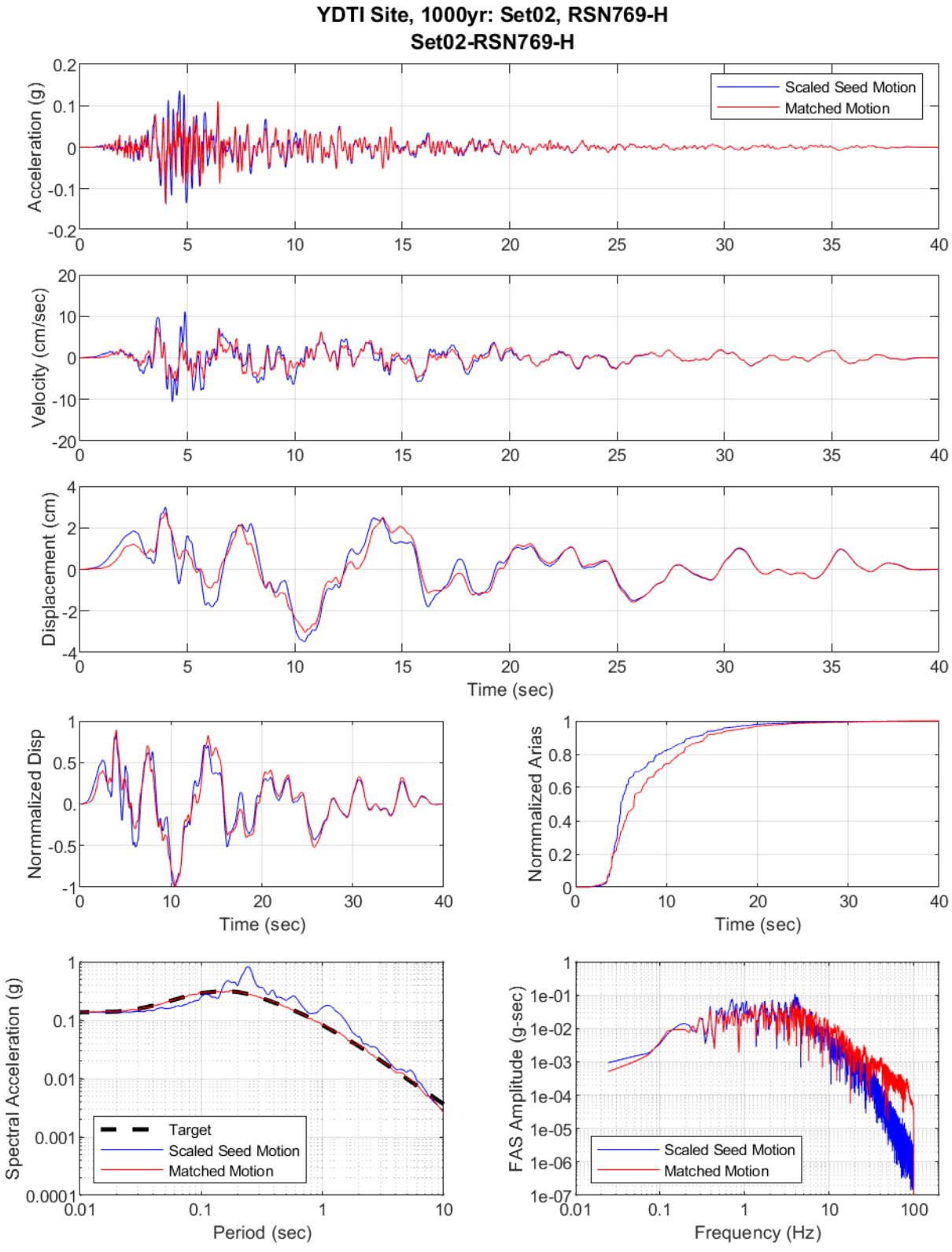
YDTI Site, 1000yr: Set02, RSN769-H
Set02-RSN769-H
Acceleration (g)
Scaled Seed Motion
Matched Motion
Velocity (cm/sec)
Displacement (cm)
Time (sec)
Normmalized Disp
Time (sec)
Normmalized Arias
Time (sec)
Spectral Acceleration (g)
Target
Scaled Seed Motion
Matched Motion
Period (sec)
FAS Amplitude (g-sec)
Scaled Seed Motion
Matched Motion
Frequency (Hz)

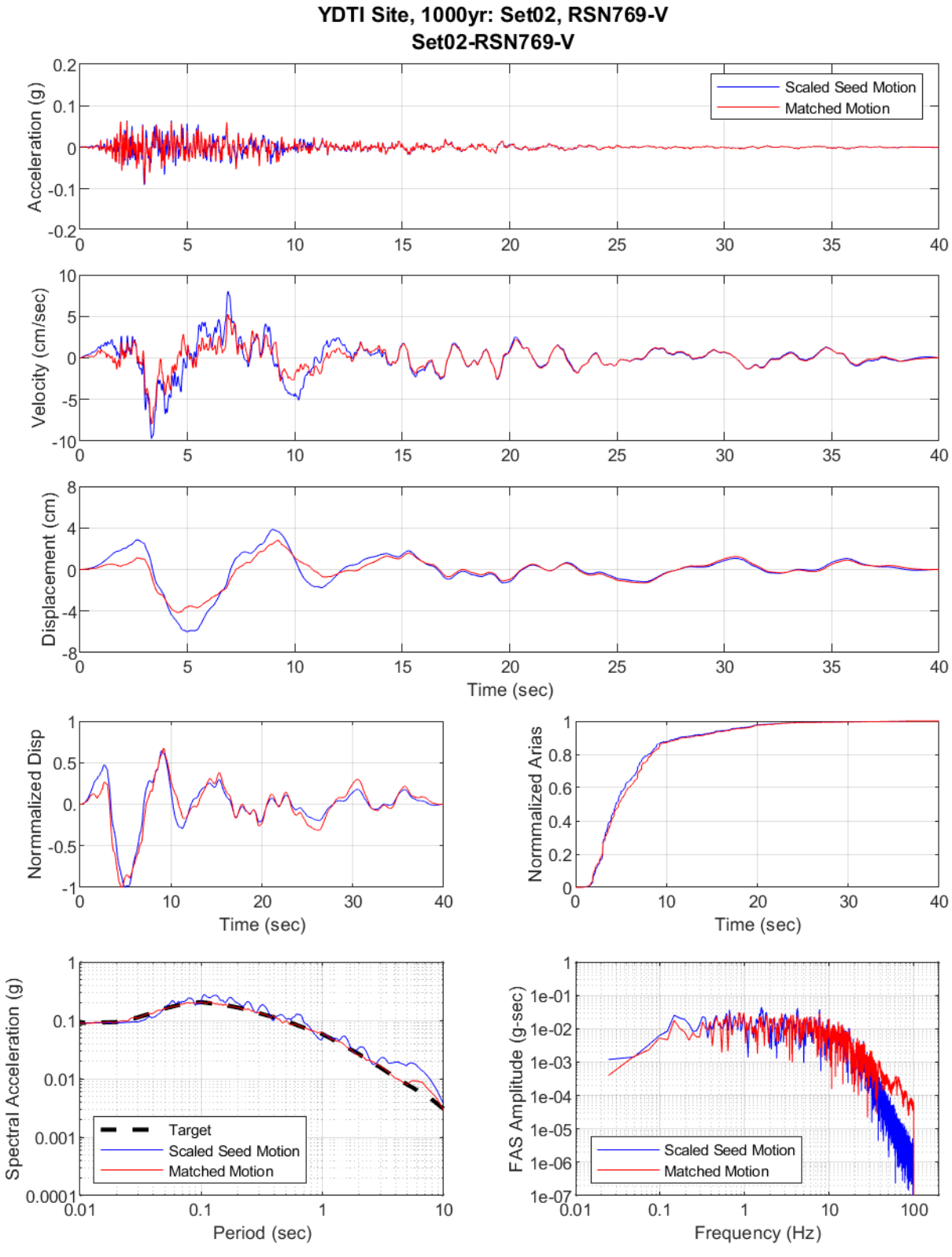
YDTI Site, 1000yr: Set02, RSN769-V
Set02-RSN769-V
Acceleration (g)
Scaled Seed Motion
Matched Motion
Velocity (cm/sec)
Displacement (cm)
Time (sec)
Normmalized Disp
Time (sec)
Normmalized Arias
Time (sec)
Spectral Acceleration (g)
Target
Scaled Seed Motion
Matched Motion
Period (sec)
FAS Amplitude (g-sec)
Scaled Seed Motion
Matched Motion
Frequency (Hz)

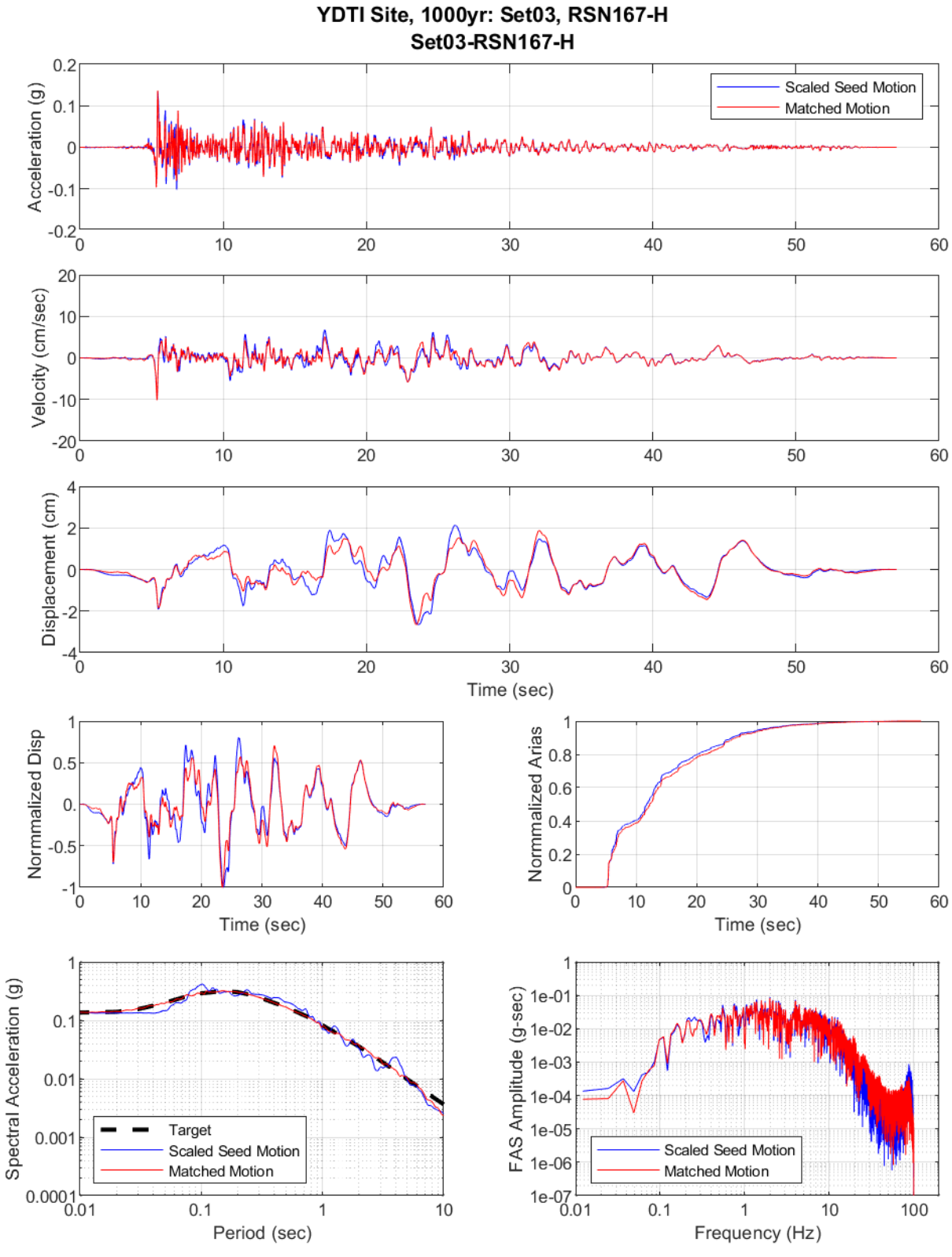
YDTI Site, 1000yr: Set03, RSN167-H
Set03-RSN167-H
Scaled Seed Motion
Matched Motion
Acceleration (g)
Velocity (cm/sec)
Displacement (cm)
Time (sec)
Normmalized Disp
Time (sec)
Normmalized Arias
Time (sec)
Spectral Acceleration (g)
Target
Scaled Seed Motion
Matched Motion
Period (sec)
FAS Amplitude (g-sec)
Scaled Seed Motion
Matched Motion
Frequency (Hz)

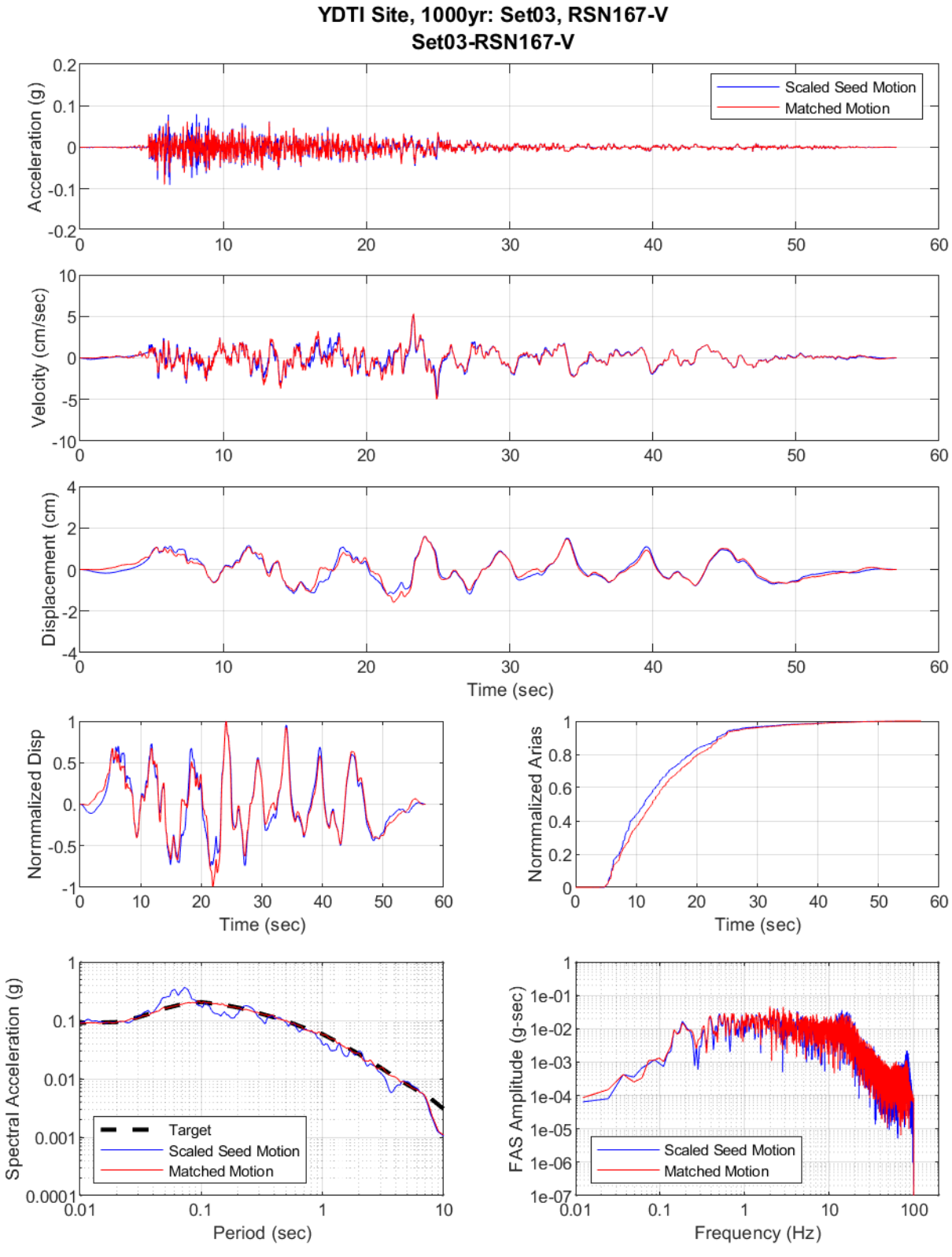
YDTI Site, 1000yr: Set03, RSN167-V
Set03-RSN167-V
Acceleration (g)
Scaled Seed Motion
Matched Motion
Velocity (cm/sec)
Displacement (cm)
Time (sec)
Normmalized Disp
Time (sec)
Normmalized Arias
Time (sec)
Spectral Acceleration (g)
Target
Scaled Seed Motion
Matched Motion
Period (sec)
FAS Amplitude (g-sec)
Scaled Seed Motion
Matched Motion
Frequency (Hz)

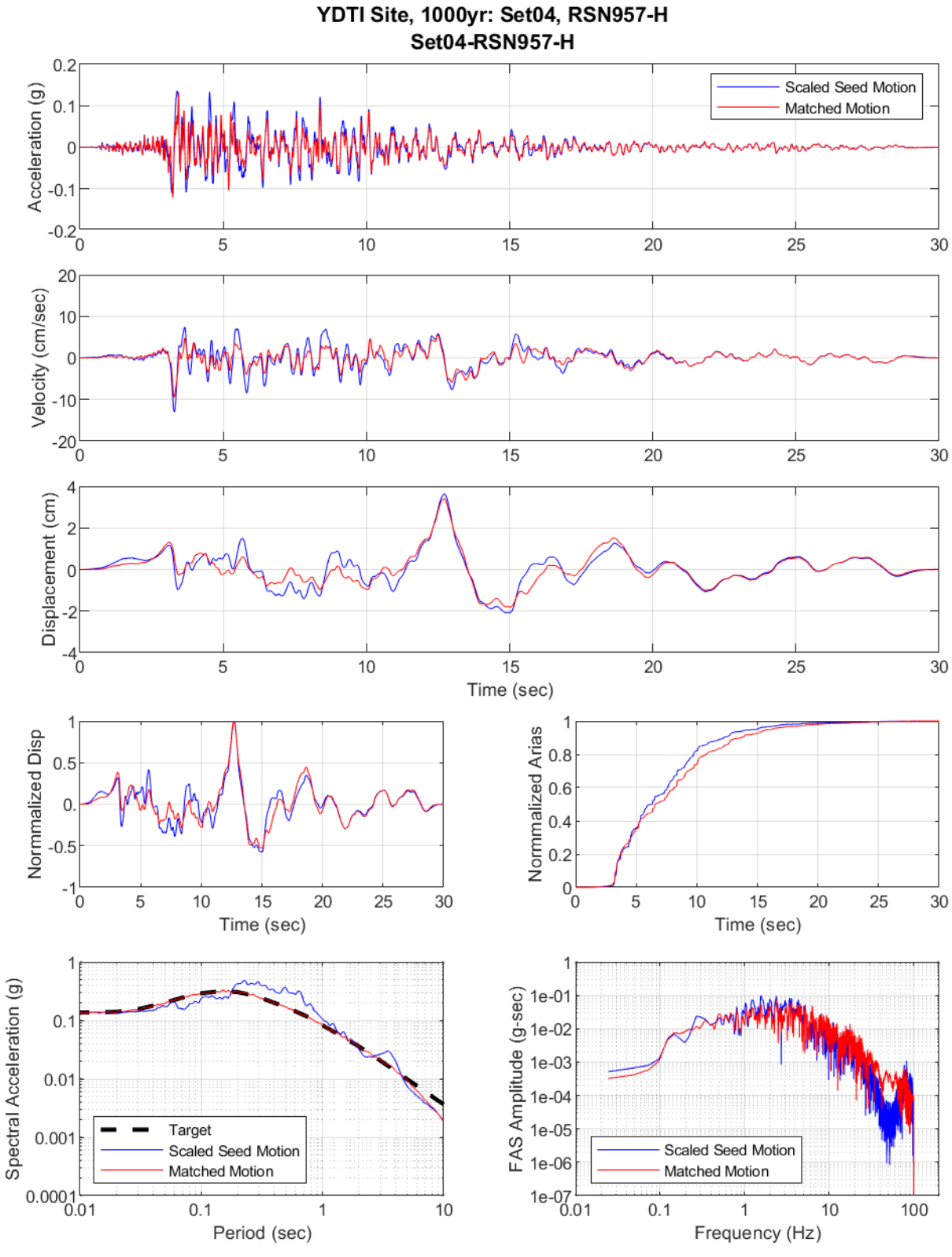
YDTI Site, 1000yr: Set04, RSN957-H
Set04-RSN957-H
Scaled Seed Motion
Matched Motion
Acceleration (g)
Velocity (cm/sec)
Displacement (cm)
Time (sec)
Normmalized Disp
Time (sec)
Normmalized Arias
Time (sec)
Spectral Acceleration (g)
Target
Scaled Seed Motion
Matched Motion
Period (sec)
FAS Amplitude (g-sec)
Scaled Seed Motion
Matched Motion
Frequency (Hz)

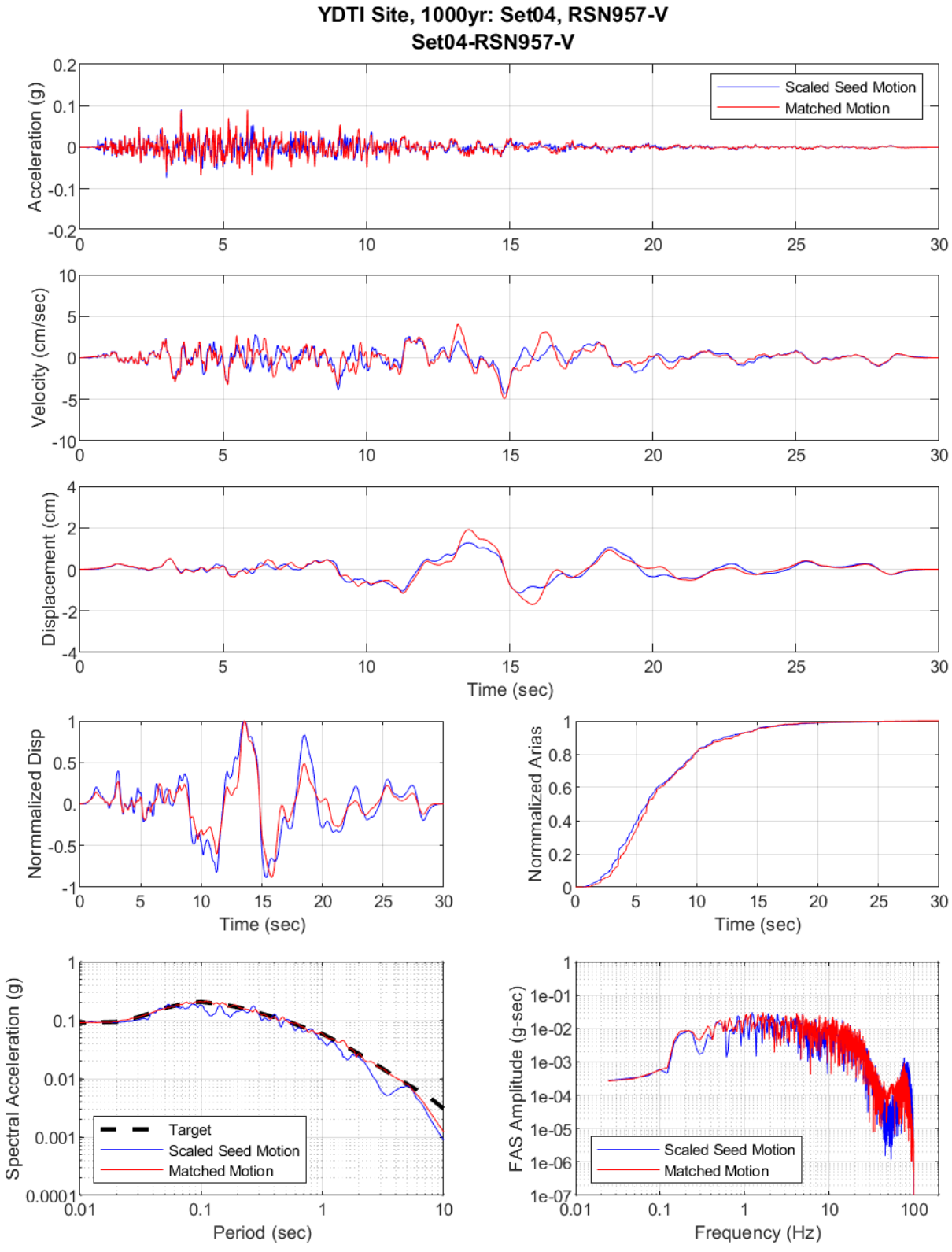
YDTI Site, 1000yr: Set04, RSN957-V
Set04-RSN957-V
Scaled Seed Motion
Matched Motion
Acceleration (g)
Velocity (cm/sec)
Displacement (cm)
Time (sec)
Normmalized Disp
Time (sec)
Normmalized Arias
Time (sec)
Spectral Acceleration (g)
Target
Scaled Seed Motion
Matched Motion
Period (sec)
FAS Amplitude (g-sec)
Scaled Seed Motion
Matched Motion
Frequency (Hz)

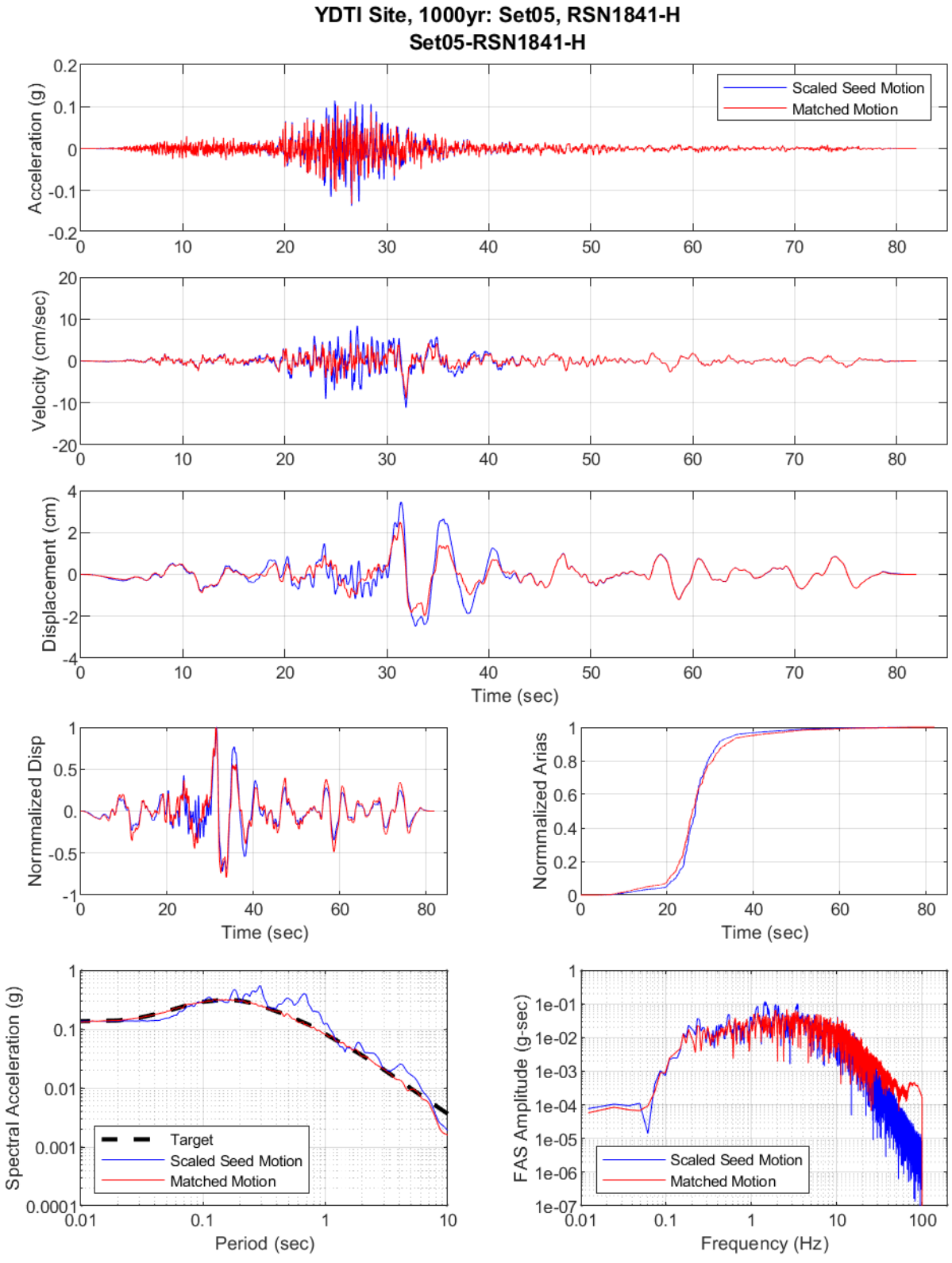
YDTI Site, 1000yr: Set05, RSN1841-H
Set05-RSN1841-H
Acceleration (g)
Scaled Seed Motion
Matched Motion
Velocity (cm/sec)
Displacement (cm)
Time (sec)
Normmalized Disp
Time (sec)
Normmalized Arias
Time (sec)
Spectral Acceleration (g)
Target
Scaled Seed Motion
Matched Motion
Period (sec)
FAS Amplitude (g-sec)
Scaled Seed Motion
Matched Motion
Frequency (Hz)

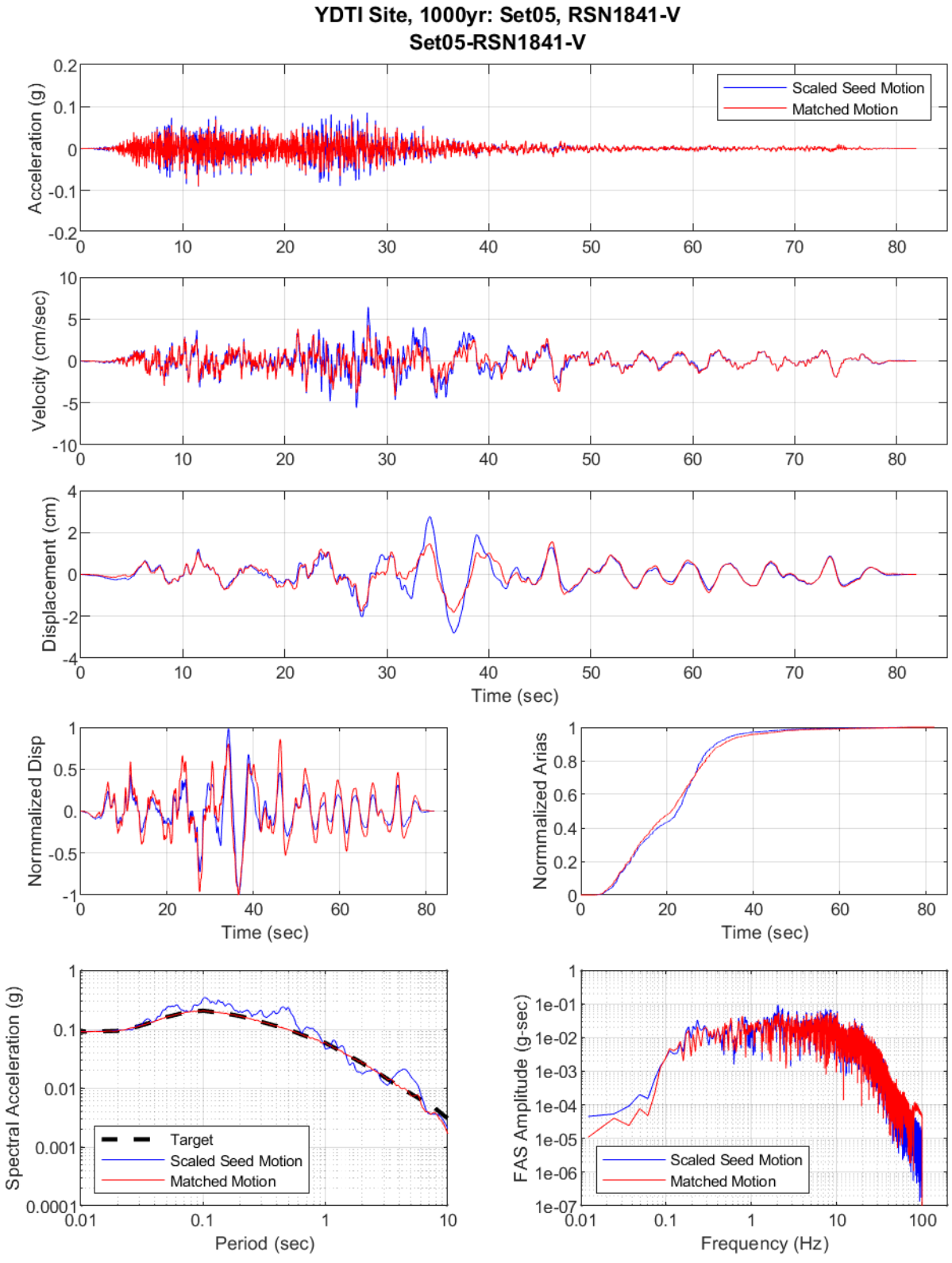
YDTI Site, 1000yr: Set05, RSN1841-V
Set05-RSN1841-V
Acceleration (g)
Scaled Seed Motion
Matched Motion
Velocity (cm/sec)
Displacement (cm)
Time (sec)
Normmalized Disp
Time (sec)
Normmalized Arias
Time (sec)
Spectral Acceleration (g)
Target
Scaled Seed Motion
Matched Motion
Period (sec)
FAS Amplitude (g-sec)
Scaled Seed Motion
Matched Motion
Frequency (Hz)